Biochemical studies on inosine 5′-monophosphate dehydrogenase from the mesophilic protozoan *Plasmodium falciparum* and hyperthermophilic archaeon *Methanocaldococcus jannaschii*

A Thesis Submitted for the Award of the Degree of

Doctor of Philosophy

By

Thota Lakshmi Prasoona

Molecular Biology and Genetics Unit

Jawaharlal Nehru Centre for Advanced Scientific Research (A Deemed University),

Bangalore-560064, India

April 2019

To my dear father and mother.....

DECLARATION

I hereby declare that this thesis entitled **"Biochemical studies on inosine 5'-monophosphate dehydrogenase from the mesophilic protozoan *Plasmodium falciparum* and hyperthermophilic archaeon *Methanocaldococcus jannaschii*"** is an authentic record of the research work carried by me under the supervision of Prof. Hemalatha Balaram at the Molecular Biology and Genetics Unit, Jawaharlal Nehru Centre for Advanced Scientific Research, Bangalore, India and that this work has not been submitted elsewhere for the award of any other degree.

In keeping with the general practice of reporting scientific observations, due acknowledgements have been made wherever the work described has been based on the findings of other investigators. Any omission, which might have occurred by oversight or misjudgment, is regretted.

(Thota Lakshmi Prasoona)

Place:

Date:

Molecular Biology and Genetics Unit
JAWAHARLAL NEHRU CENTRE FOR ADVANCED SCIENTIFIC RESEARCH
Jakkur, Bangalore-560 064, India

Hemalatha Balaram, Ph.D.
Professor

CERTIFICATE

This is to certify that the work described in this thesis entitled **"Biochemical studies on inosine 5'-monophosphate dehydrogenase from the mesophilic protozoan *Plasmodium falciparum* and hyperthermophilic archaeon *Methanocaldococcus jannaschii*"** is the result of investigations carried out by Ms. Thota Lakshmi Prasoona in the Molecular Biology and Genetics Unit, Jawaharlal Nehru Centre for Advanced Scientific Research, Bangalore, India under my supervision, and that the results presented in this thesis have not previously formed the basis for the award of any other diploma, degree or fellowship.

(Hemalatha Balaram)

Place:

Date:

Note of Gratitude

My journey at JNCASR as an MS-PhD student has been a fairly long one and would not have been easier for the transition to the current phase without the care and support from various people. A sincere effort has been attempted in acknowledging each one of them. It is a great pleasure to express my sincere gratitude to my research supervisor, Prof. Hemalatha Balaram. This thesis would certainly not have been possible without her support and guidance. It has been truly an incredible association with her relentless patience, guidance, encouragement, and constructive criticism. I express my earnest thanks to her.

I would like to extend my acknowledgements to former and current chairpersons at the Department of Molecular biology and genetics, Prof. Anuranjan Anand, and Prof. Uday Kumar Ranga, respectively and all the faculty members Prof. Tapas Kumar Kundu, Prof. Maneesha Inamdar, Prof. Namita Surolia, Dr. Kaustav Sanyal, Dr. Ravi Manjithaya, and Dr. James Chellaiah for the critical comments and suggestions throughout the doctoral studies. I also thank Prof. Anjali Karande and Prof. Kondaiah from IISc for evaluation and critical suggestions during my comprehensive examination. I am extremely grateful to Dr. Meher Prakash, Theoretical Sciences unit, JNCASR for all the intricate discussions on the use of computational tools and analysis pertaining to protein engineering.

Prof. KMR Nambiar, Head of the Genetics department at Aurora Degree College, has always been a true source of inspiration, with all his extraordinary enthusiasm and energy. I am fortunate to have had such a dedicated and student-friendly "guru" and very honestly thank him for inculcating scientific attitude and being instrumental in laying the foundation for my career path alongside that of many others.

Work environment has been quite an experience with extremely accommodating and supportive lab members. Special thanks are due to my seniors Dr. Subhra Prakash Chakrabarty, Dr. Javaid Bhat, Dr. Vinay Bulusu, and Dr. Bharath Srinivasan who were instrumental in mentoring me through the initial days of the graduate course. I would also like to thank former members of the lab Dr. Sourav Roy, Dr. Sanjeev Kumar, Dr. Vijay Jayaraman, and Dr. Arpit Shukla for readily extending their support and help. I am thankful to the current crew Lakshmeesha KN, Asutosh B, Santosh S, Arpitha S, Aparna D, Anusha GC, Niveditha P, Neelakshi V, Resmi R, Pavithra K, Rahul M and Rahul CN who are responsible in creating

a vibrant lab space and for all the intense "Tea" sessions. I also thank visiting scholar Dr. Dhanalakshmi for her kindness and care. A very special mention to Dr. Arpit Shukla and Lakshmeesha KN "The technical support team of HB lab" for all the troubleshooting expertise during my experimental work and in thesis writing. I am grateful to Arpitha S, Lakshmeesha KN, and Aparna D for their valuable suggestions and guidance in handling Plasmodial cultures. My honest cheers to Asutosh B for advancing the IMPDH project with his undue skills in X-ray crystallography. I would also like to thank Mr. Balakrishna, lab assistant, for his help.

I am blessed to have friends like Dr. Manjusha Namburi, Dr. Loukya Chowdary, Mr. Ashok Thanikonda and Mr. Rakesh Reddy who are just a call away in time of need. I am also thankful to Mr. Sudarshan, Ms. Koushalya and their adorable kid, Suchinth (Chintoo), for being the friendly neighbors at IISc, and for having created the homely environment.

I thank Mr. Atish Roy Choudhary, MCBL and Ms. Saima Kauser Nasir and Ms. Divya S, The Bio-imaging facility, IISc for their help in understanding and analysis of microscopy images. I would also like to thank the DNA sequencing and the Microscopy facilities at MBGU, JNCASR. I also thank JNCASR Library, Complab, Hostel, Health Centre, Academics, and Administration staff for providing and maintaining all the wonderful facilities. My sincere thanks to JNCASR for providing me with the POBE summer internship and MS-PhD fellowship.

My family has been the utmost strength for me. Words are indeed insufficient to thank my parents. Reaching this far would have been next to impossible without my father (Mr. TV. Satyanarayana) and his endearing motto "hard work, sincerity and willingness to face challenges"- I owe it all to him. I am extremely indebted to my beloved mother (Ms. T. Krishna Kumari) who with her constant hardship and "never-give-up" attitude has brought me to this stage. I am immensely grateful to the biggest critic ever, a great source of inspiration, and philosopher in life, my brother Mr. T. Yashwanth (Babloo). I am indebted to my "in-laws" who are extremely understanding, supportive and caring. Finally, I find words limiting to express gratitude to my dear husband, Krishna Rao Kamisetty, who with his unconditional love, care, limitless support, stands as the backbone for my happiness and success.

Synopsis of the thesis entitled

"Biochemical studies on inosine 5'-monophosphate dehydrogenase from the mesophilic protozoan *Plasmodium falciparum* and hyperthermophilic archaeon *Methanocaldococcus jannaschii*"

Submitted by

Thota Lakshmi Prasoona

Molecular Biology and Genetics Unit,
Jawaharlal Nehru Centre for Advanced Scientific Research, Bangalore, India.

Thesis Supervisor: Prof. Hemalatha Balaram

Guanine nucleotides are indispensable for cell viability. Besides being precursors of nucleic acids (DNA and RNA), GTP forms the energy source for translation and microtubule polymerization. Guanine nucleotides are implied in signal transduction, angiogenesis and axon guidance (Chong CR *et al*., 2006; Long H *et al*., 2006). In addition, they also function as metabolic precursors for a diverse set of metabolites that include tetrahydrobiopterin, folates (vitamin B9) and riboflavin (vitamin B2) (Gross SS and Levi R, 1992; Cossins EA and Chen L,1997; Bacher *A et* al., 2000). It has also been shown that phosphoribosyl pyrophosphate (PRPP) synthetase and ribonucleotide reductase, enzymes involved in nucleotide biosynthesis get stimulated by guanine nucleotides and inhibited by adenine nucleotides (Allison AC *et al*., 1993). Therefore, GMP biosynthesis either through *de novo* route or by salvage of nucleobases stands essential for survival. The purine ring assembled sequentially from biosynthetic precursors of carbohydrate and amino acid metabolism, and from ammonia and carbon dioxide constitute *de novo* purine synthesis (Zalkin H and Dixon JE, 1992) while recycling of preformed nucleobases, nucleosides, and nucleotides forms the salvage pathway (Murray AW, 1971).

Plasmodium falciparum is the most lethal among the five *Plasmodium* species (*P. vivax, P. malariae, P. ovale,* and *P. knowlesi*) that cause human malaria (www.mmv.org). Malaria has a massive impact on human health; it is the world's second biggest killer after tuberculosis (WHO report, 2018). Despite the availability of anti-malarial drugs, the widespread emergence of drug-resistant parasites necessitates a quest for new therapies. Structure- and mechanism-based combinatorial approach for drug design has proved highly productive. The purine salvage pathway of *P. falciparum* is a novel target for antimalarials, as the parasite lacks the *de novo* purine biosynthetic pathway (Gardner MJ *et al.*, 2002) and completely depends on

its host for purine requirements. Hypoxanthine is salvaged by hypoxanthine guanine (xanthine) phosphoribosyltransferase (HG(X)PRT) to form inosine 5'-monophosphate (IMP) which then branches out into either formation of guanosine 5'-monophosphate (GMP) or adenosine 5'-monophosphate (AMP). IMP, on one hand, is converted to xanthine 5'-monophosphate (XMP) and GMP by inosine 5'-monophosphate dehydrogenase (IMPDH) and guanosine 5'-monophosphate synthetase (GMPS), respectively and on the other arm by the sequential action of adenylosuccinate synthetase (ADSS) and adenylosuccinate lyase (ASL) to form AMP.

Genome analysis of *Methanocaldococcus jannaschii* a hyperthermophilic archaeon, reveals that at the molecular level archaea more closely resemble eukaryotes (Bult CJ *et al.*, 1996). The archaeal genome is about 70 % AT-rich while that of the protozoan parasite *P. falciparum* is about 80 % (Bult CJ *et al.*, 1996; Gardner MJ *et al*., 2002). Purine biosynthesis in *M. jannaschii* can occur through the *de novo* route (Bult CJ *et al*., 1996; Selkov E *et al*., 1997; Ownby K *et al*., 2005; Brown AM *et al*., 2011) or by salvage of adenine and guanine (Armenta-Medina D *et al*., 2014; Miller DV *et al*., 2016). However, similar to *P. falciparum*, *M. jannaschii* also lacks adenosine kinase (AK) or adenine phosphoribosyltransferase (APRT) (Armenta-Medina D *et al*., 2014). Therefore, the conversion of adenine to hypoxanthine by adenine deaminase (ADE) followed by IMP synthesis by HGPRT constitutes the purine salvage pathway (Miller DV *et al*., 2016).

The enzyme involved in IMP biosynthesis, HGPRT and the enzymes thereafter (ADSS, ASL, and GMPS) in the purine biosynthesis pathway of *P. falciparum* and *M. jannaschii* have been well characterized from our laboratory and elsewhere (Li CM *et al*., 1999; Ducati RG *et al*., 2017; Bhat JY *et al*., 2008; Bhat JY *et al*., 2011; Raman J *et al*., 2004; Bulusu V *et al*., 2009; Mehrotra S and Balaram H, 2007; Ali R *et al*., 2013; Roy S *et al*., 2015; Roy S *et al*., 2015; Karnawat V *et al*., 2016). PF3D7_0920800 (PfIMPDH) and MJ1616 (MjIMPDH), from *P. falciparum* and *M. jannaschii*, respectively annotated as IMPDH have not been examined thus far. PfIMPDH is one of the essential enzymes present in the parasite as the inhibitor mycophenolic acid (MPA) is lethal for parasite survival (Veletzky L *et al*., 2014). Evidence for expression of PfIMPDH is provided from microarray, RNA sequencing, and proteomic studies by various groups and the data are available in the *Plasmodium* database, PlasmoDB (Bahl A *et al*., 2003). MjIMPDH is similar in polypeptide length (496 amino acids) and is 47 % similar and

34 % identical to the *P. falciparum* protein (510 amino acids). A major focus of our laboratory has been towards understanding nucleotide metabolism of plasmodial species through extensive biochemical, kinetic and structural characterization with a parallel focus on the homologs from the hyperthermophile *M. jannaschii*. The aim of the current study is to identify and characterize the functionality of IMPDH from the mesophilic malarial parasite *P. falciparum* and the thermophilic ortholog *M. jannaschii*.

IMPDH and GMP reductase (GMPR) constitute a family that controls the guanine nucleotide pool and regulates proliferation and many other physiological processes. IMPDH catalyzes the NAD^+ dependent conversion of IMP to XMP. GMPR catalyzes NADPH dependent reductive deamination of GMP to form IMP and is the only route known for conversion of GMP to AMP through IMP. Some organisms (such as *Cryptosporidium parvum, Toxoplasma gondii, Tritrichomonas foetus, Saccharomyces cerevisiae*) lack GMPR alone while few others (*Giardia lamblia, Trichomonas vaginalis, Entamoeba histolytica*) lack IMPDH, GMPS, and GMPR. *Buchnera aphidicola* is one example with no IMPDH and GMPS but has GMPR as this serves as the only source of IMP and thereby, AMP. However, some genomes encode both IMPDH and GMPR (such as *E. coli*, human, kinetoplastids). IMPDH as a potential drug target for immunosuppression, anti-cancer, antimicrobial, anti-parasitic, and antiviral chemotherapy has been realized (Hedstrom L, 2009). Although no extensive literature is available on GMPRs, hGMPR2 is shown to promote the monocytic differentiation of HL-60 leukemia cells (Zhang J *et al*., 2003). Further, hGMPR1, a more abundant isoform in the brain and cerebral cortex, has been identified as a potential therapeutic target for Alzheimer's disease (Liu H *et al*., 2018).

IMPDH (encoded by *guaB* gene) and GMPR (encoded by *guaC* gene) share a high level of sequence identity and similarity (Martinelli LKB *et al*., 2011; Smith S *et al*., 2016) which could lead to misannotation of this family of genes. IMPDH and GMPR have their core catalytic $(\beta/\alpha)_8$ barrel domain arranged in a square planar geometry and are largely known to exist as homotetramers, and homooctamers (Labesse G *et al*., 2015; Buey RM *et al*., 2015; Bessho T *et al*., 2016). Further, polymerization of IMPDH into filaments called cytoophidium that is modulated by the binding of purine nucleotides has also been reported (Keppeke GD *et al*., 2018). Both the enzymes have a cystathionine-β-synthase (first discovered in cystathionine-β-synthase by Bateman, CBS) domain as an insertion within the catalytic $(\beta/\alpha)_8$ domain sequence.

CBS domain occurs across a wide variety of unrelated proteins that include Mg^{2+}-transporters, chloride channels, and protein kinase B. The CBS subdomain in IMPDH regulates adenine and guanine nucleotide pools and is found to interact with various proteins involved in transcription regulation, splicing, and rRNA processing (Lindstrom DL *et al.*, 2003; Ho Y *et al*., 2002; Krogan NJ *et al*., 2004; Stevens SW *et al*., 2002). CBS domain of IMPDH is shown to have no catalytic role in the formation of IMP (Nimmesgern E *et al*., 1999) and modulates activity through nucleotide binding (Labesse G *et al*., 2013; Buey RM *et al*., 2015). Removal of CBS from GMP reductase of *Leishmania donovani* led to growth defects on minimal medium (Smith S *et al*., 2016). Mutations in the CBS subdomain of hIMPDH1 account for 2-3 % of autosomal dominant retinitis pigmentosa (adRP) and are also known to be associated with Leber congenital amaurosis (LCA), a more severe form of hereditary blindness (Bowne SJ *et al*., 2006). The molecular and mechanistic basis of these disorders has not been understood to date.

Both IMPDH and GMPR bind similar ligands with IMP/GMP binding site and nicotinamide portion of the cofactor binding site reported to be similar and highly conserved in both the enzymes while adenosine portions of the cofactors bind to different regions of the barrel domain. However, GMPR and IMPDH possess high substrate specificity and carry out different chemical transformations despite high sequence and structural similarity. Both the enzymes are found to be activated by monovalent cations such as K^+ ions. The hydride transfer by both the enzymes involves nicotinamide cofactor and proceeds through the same covalent intermediate E-XMP*. However, this intermediate reacts with water in the reaction catalyzed by IMPDH which is substituted by ammonia in GMPR. MPA recognized as a potent and IMPDH-specific inhibitor, is now known to inhibit GMPRs from *Leishmania major* and *Trypanosoma congolense* (Digits JA and Hedstrom L, 1999; Smith S *et al*., 2016; Sarwono AEY *et al*., 2017).

This thesis focussed on understanding the functionality of IMPDH from *P. falciparum* and *M. jannaschii* is presented in five chapters. **Chapter 1** provides elaborate literature, reviewing IMP dehydrogenase and GMP reductase from various organisms. This includes biochemical, kinetic and structural features, sub-unit association and modulation of enzyme activity, physiological significance and relevance of the enzyme in the regulation of other cellular processes. Literature in support of IMPDH and GMPR as a valid drug target for a multitude of pathophysiological conditions is also discussed.

Chapter 2 describes *in vivo* studies on PfIMPDH that include subcellular localization in the intraerythrocytic stages of *P. falciparum* and genetic complementation assays using *E. coli* and yeast for examining the functionality. This chapter details the procedure on antibody generation in mouse, purification of antiserum on PVDF membrane adsorbed with the antigen (PfIMPDH), and determination of antibody titre by DOT blot, Western detection, and indirect immunofluorescence microscopy. A single band of PfIMPDH corresponding to the expected molecular mass of 55 kDa was observed through antibody detection on Western blot. PfIMPDH was found to be largely in the cytoplasm with partial nuclear localization in the intraerythrocytic asexual stages of the parasite. Mass spectrometric analysis of *P. falciparum* proteins carried out by two independent research groups (Oehring SC *et al*., 2012; Briquet S *et al*., 2018) identified peptides corresponding to PfIMPDH in the nuclear fractions. These reports serve as additional evidence confirming the partial nuclear localization of PfIMPDH observed through immunofluorescence microscopy.

guaB and *guaC* genes encode for IMPDH and GMPR, respectively. *guaB* (Δ*guaB*^{K} (DE3)) and *guaC* (H1174$^{\Delta guaC}$) deletion strains of *E. coli* were generated following the method of Datsenko and Wanner (Datsenko KA and Wanner BL, 2000). Strains were confirmed through genotyping by diagnostic PCRs and phenotyping by monitoring growth on minimal medium**.** *T. foetus* IMPDH, construct obtained from Prof. Hedstrom, USA, sub-cloned into the desired vector and *E. coli* GMPR were included as positive controls in growth rescue experiments. TfIMPDH and EcGMPR could rescue the growth of *guaB* and *guaC* deletion strains on minimal medium, respectively. However, the presence of expression plasmids for PfIMPDH or PfIMPDH$^{\Delta CBS}$ (catalytic domain alone) in the deletion strains did not complement for loss of function of either IMPDH or GMPR. Various optimizations including co-expression of helper plasmids (coding for chaperones, tRNA synthetases for rare codons), different carbon sources (glucose, malate, and glycerol) and varied temperature (25 ºC, 30 ºC, and 37 ºC) were not successful. Lastly, codon harmonized gene sequence for optimal expression in *E. coli* was custom synthesized however it could not rescue either the growth of *guaB* or *guaC* deletion strain. In all tested conditions, TfIMPDH and EcGMPR were obtained in soluble form while only very small fractions of PfIMPDH and PfIMPDH$^{\Delta CBS}$ were soluble even upon co-expression with chaperones. High levels of soluble and functional protein supported the growth of deletion strain expressing

TfIMPDH or EcGMPR on M9 minimal medium. Non-availability of sufficient soluble and thus functional protein reflects the growth defect of the deletion strains carrying PfIMPDH on minimal medium.

guaB quadrapule deletion strain of yeast (DY891) was obtained from Prof. Daniel Reines, Emory state university, USA. While TfIMPDH which was used as a positive control had rescued the growth of the deletion strain, no growth of DY891 cells carrying PfIMPDH was observed. Although the presence of full-length gene-specific transcripts was confirmed by RT-PCR, expression of PfIMPDH was not evident on the Western blot and hence the growth of yeast cells was not supported.

Chapter 3 describes the efforts channelized towards obtaining the recombinant PfIMPDH protein. The most widely used heterologous expression system, *E. coli* was chosen to serve the purpose of producing recombinant protein. A broad spectrum of strategies including the use of different expression strains of *E. coli*, co-transformed with or without helper plasmids (coding for tRNAs, mesophilic and psychrophilic chaperones), various commercially available solubility enhancing tags and a multitude of expression conditions (varied induction time, temperature, and inducer concentrations) was employed. Despite extensive efforts in increasing the solubility of the expressed protein, PfIMPDH largely remained in inclusion bodies. Attempts made to refold the protein were unsuccessful. Various efforts made at obtaining PfIMPDH protein in soluble form that include approaches like random mutagenesis, site-directed mutagenesis based on solubility prediction tools (PROSO II, Smialowski P *et al.*, 2012) and generation of various fusion constructs were unsuccessful. This stands as a huge impediment for proceeding onto further characterization of the *P. falciparum* IMPDH, a highly promising drug target. It was decided at this point to try *in vitro* translation system. The first *in vitro* translation system used was wheat germ extract procured from Promega, USA. This system was provided with bacterial transcription machinery coupled with eukaryotic wheat germ translation components. The reaction was carried out using circular or linearized DNA construct of PfIMPDH and the synthesized proteins were resolved on SDS-PAGE, electrotransferred onto PVDF membrane, followed by detection using anti-$(His)_6$ antibodies. Examination of the Western blot showed that PfIMPDH was not synthesized.

Although expression in bacteria yielded large amounts of recombinant protein, there were extremely low levels of soluble protein. It was decided that S30 extract from *E. coli* for *in vitro* transcription coupled translation (NEB PURExpress) would be evaluated for production of PfIMPDH protein. As protein expression in *E. coli* from the native *P. falciparum* IMPDH gene was found to be maximal only upon expression of tRNAs for codons that are rare in *E. coli* it was decided to synthesize a codon harmonized PfIMPDH gene. Eugene, an online gene optimization tool was used to re-design PfIMPDH gene for maximal expression in *E. coli* without changing the native amino acid sequence (Gaspar P *et al.,* 2012). The modified gene sequence obtained as output from Eugene was re-analyzed and curated using Genescript codon analysis tool. Codon harmonized PfIMPDH gene sequence, custom synthesized (Biomatik Corporation, Canada) was supplied as a clone in pUC57 vector with multiple restriction sites upstream and downstream of the gene. Expression of harmonized PfIMPDH gene was simultaneously tested in both *in vivo* and *in vitro* systems. In contrast to the native gene whose optimal expression was conditional to co-expression of helper plasmid encoding tRNA genes for rare codons, high level of protein expression was achieved without any tRNA co-expression. Although all the expressed protein was again found to be insoluble *in vivo*, in vitro transcription coupled translation with *E. coli* S30 extract yielded a distinct band of 55 kDa representing PfIMPDH that was soluble. For the first time, we observed soluble protein synthesized in a cell-free reaction on SDS-PAGE stained with Coomassie Brilliant Blue. All components of the transcription and translational machinery provided in the kit were $(His)_6$-tagged recombinant proteins (Shimizu Y *et al*., 2001). Therefore, to enable purification of PfIMPDH, the codon harmonized gene was sub-cloned (with no tag) into the plasmid provided with the kit. Scaling up and purification of PfIMPDH (untagged) using NEB PURExpress system posed its own challenges. Either strong association of PfIMPDH with ribosomes or presence of higher order oligomers probably hindered the purification process. Alternate tagging strategy of PfIMPDH with Strep-tag II was unsuccessful as the *in vitro* reaction yielded insoluble/precipitated protein. In any of the systems mentioned above, crude lysates tested for IMP-specific NAD^+ dependent dehydrogenase activity or NADPH-dependent reductive deamination of GMP by PfIMPDH or $PfIMPDH^{\Delta CBS}$ (CBS deletion) could not be established. Similar studies carried out on *P. berghei*

IMPDH failed to yield soluble protein or complement deficiency in heterologous expression systems.

It has been reported that a large fraction of obligate substrates for GroES-EL assisted protein folding bear $(\beta/\alpha)_8$ barrel structure (Georgescauld F *et al*., 2014). Though our experiments with co-expression of chaperones have yielded some fraction of the protein in the soluble fraction, separation of the soluble fraction from the chaperones could not be achieved. Interestingly, the catalytic domain PfIMPDH$^{\Delta CBS}$ when co-expressed with chaperone KJE7 (DnaK, DnaJ, and grpE) resulted in a moderately good amount of soluble protein (co-transformation of tRNA plasmid was found dispensable) that could not be purified. This probably indicates large hydrophobic patches on the protein surface available for strong interaction with the chaperones and hence, difficult to dissociate. Therefore, an *in-silico* analysis of PfIMPDH sequence was performed with the aim of understanding the protein aspects better and evaluate future directions**.** Gross amino acid composition across different organisms and the β-structure propensity of PfIMPDH were analyzed. An average amino acid percentage across various *Plasmodium* species has been compared with that from other biochemically characterized IMPDH and GMPR sequences. Six (L, W, T, C, M, and K) of the twenty amino acids in the plasmodial group do not significantly differ from their respective averages in the other group that constitutes soluble IMPDHs and GMPRs, while the percentage of occurrence for the rest of the fourteen was found to vary significantly. The significance of such a bias in amino acid composition and associated consequences are yet to be understood. Further, prediction of aggregation-prone regions in unfolded polypeptide chains using TANGO algorithm (Fernandez-Escamilla AM *et al*., 2004; Linding R *et al*., 2004; Rousseau F *et al*., 2006) identified two potential nucleating segments within PfIMPDH$^{\Delta CBS}$ and sequence swapping with MjIMPDH (experimentally found to be highly soluble, discussed in Chapter 5) yielded significantly lowered propensity for β-aggregation. This could form the basis for generating mutants with possibly improved solubility.

Chapter 4 provides the biophysical and biochemical characterization of CBS domain of PfIMPDH. Although PfIMPDH and PfIMPDH$^{\Delta CBS}$ genes expressed in *E. coli* did not yield protein in soluble form, we were fortunate in obtaining the regulatory domain (CBS) of PfIMPDH in soluble form. Codon harmonized PfCBS domain was cloned carrying a C-terminal

$(His)_6$-tag and expressed in *guaB* deletion strain of *E. coli*. It was purified to homogeneity on a Ni-NTA affinity matrix followed by size–exclusion chromatography. The yield of the purified recombinant PfCBS was ~22 mg L^{-1} of induced culture. It was found to exist as a monomer in solution as determined from analytical size-exclusion chromatography. PfCBS, as inferred from far-UV CD measurement, was found to be largely disordered similar to that of the CBS domain from human IMPDH2. All adenine and guanine nucleotides, except GMP, were found to interact with PfCBS domain as detected by a change in intrinsic tyrosine fluorescence. Dissociation constants for PfCBS complexes with the ligands AMP, ADP, ATP, GDP, and GTP as determined through non-linear regression of data fit to the one-site binding equation are in the low micromolar range.

Chapter 5 is focused on understanding the biochemical and kinetic characteristics underlying the functioning of MJ1616 annotated as IMP dehydrogenase from the hyperthermophilic archaeon *Methanocaldococcus jannaschii* (MjIMPDH). The open reading frame of MjIMPDH and the catalytic domain MjIMPDH$^{\Delta CBS}$ were individually cloned with a C-terminal $(His)_6$-tag and expressed in the *guaB* deletion strain of *E. coli.* DNA sequencing of the insert confirmed the clone error-free and identical to the entry in the NCBI gene database. Similar purification procedures were employed for both MjIMPDH and MjIMPDH$^{\Delta CBS}$ proteins that included thermal precipitation for removal of mesophilic *E. coli* proteins, polyethyleneimine (PEI) treatment for elimination of nucleic acids, anion exchange chromatography and finally size-exclusion chromatography. The purity of the proteins was judged by Coomassie Brilliant Blue-stained SDS-PAGE and the identity of the recombinant proteins was assessed by Western blot using anti-$(His)_6$ antibodies. The yield of full-length MjIMPDH and MjIMPDH$^{\Delta CBS}$ proteins was about ~35 mg L^{-1} and ~50 mg L^{-1} of culture, respectively. Interestingly, the recombinant *M. jannaschii* proteins, in the absence or presence β-mercaptoethanol and without prior heating, were found to migrate at molecular weights corresponding to higher order oligomers when resolved on SDS-PAGE. However, they were found to migrate at their respective expected monomer mass (54 kDa and 43 kDa, respectively) upon heat treatment. Far-UV CD spectra of both the enzymes were found to be similar and indicated ordered secondary structure. MjIMPDH exists as octamer and removal of CBS subdomain resulted in a tetramer as determined by analytical size-exclusion chromatography. This subunit assembly of either MjIMPDH or

MjIMPDH$^{\Delta CBS}$ in solution remained unperturbed at varied enzyme concentrations, high salt (1M KCl) or in the presence of ligands (NAD^+ and IMP). Further, higher order oligomers of MjIMPDH were observed during purification on preparative size-exclusion column, the percentage of which varied across different batches of purification. However, they did not further equilibrate to either octamer or tetramer upon dilution.

IMP-specific, NAD^+ dependent dehydrogenase activities of MjIMPDH and MjIMPDH$^{\Delta CBS}$ were monitored as an increase in absorbance at 340 nm due to the formation of NADH. Catalytic properties of the full-length and the CBS deletion mutant were found to be similar reiterating that CBS domain has no role in catalysis. The *M. jannaschii* enzyme exhibited optimal dehydrogenase activity at 70 °C, pH 8.0 and no drop in activity was observed up to 95 °C. However, routine assays were performed at 70 ºC for ease of handling. Enzyme assays using the higher order oligomers of the enzyme from the preparative grade size-exclusion chromatography exhibited either similar or only a minor drop (10-15 %) in specific activity and therefore, not characterized further.

MjIMPDH, unlike other characterized IMPDHs, displayed very weak dependence on monovalent cation for its activity. The absence of K^+ ions in the assay mixture resulted in only a minor drop in activity with the K_m value for NAD^+ lowered by 2.3-fold while the K_m value for IMP remained unchanged. All IMPDHs characterized till date are found to be activated by about 100-fold by K^+ ions and in some cases by other monovalent cations (such as Li^+, Na^+, Rb^+, and Cs^+) (Hedstrom L, 2009). Product inhibition studies identified XMP as a competitive inhibitor of IMP and noncompetitive inhibitor of NAD^+ binding. NADH was found to be noncompetitive with respect to both IMP and NAD^+. Studies on understanding modulation of enzyme activity by the purine nucleotides identified guanine nucleotides to be more potent inhibitors of MjIMPDH than adenine nucleotides and only ATP (up to 5 mM) had no effect on the enzyme activity. Inhibition by the adenine and guanine nucleotides did not require Mg^{2+} ions. Global fit of the inhibition data identified AMP, ADP, GMP, GDP, and GTP as noncompetitive inhibitors of IMP binding. Inhibition by nucleotides is found to be highly effective only in the presence of CBS domain. No nucleotide was found to bind to the active site, while removal of CBS resulted in AMP competing for the IMP binding site albeit with weaker affinity. However, upon of deletion of CBS domain, GMP continued to be a noncompetitive inhibitor of IMP and NAD^+ binding but

with affinity lowered by 100-140 fold. This study highlights the feedback inhibition of MjIMPDH through the regulatory CBS domain by both the purine nucleotides (adenine and guanine) indicating a key role for this domain in the control of metabolic flux balance. MjIMPDH shares high sequence identity with prokaryotic IMPDHs but displays features such as inhibition by guanine nucleotides that is observed only in eukaryotic IMPDHs.

In summary, the current thesis provides subcellular localization of PfIMPDH in the intraerythrocytic stages of *P. falciparum*. Attempts made at understanding the functionality of PfIMPDH using *in vivo* (complementation and expression in *E. coli*, and *S. cerevisiae*) and *in vitro* systems (cell-free protein synthesis) are discussed. Biophysical/biochemical characteristics of CBS domain of PfIMPDH is included. Lastly, MjIMPDH, an ortholog of PfIMPDH identified in *M. jannaschii*, has been successfully cloned, expressed, purified and thorough understanding of biochemical and kinetic characteristics is provided.

References

1. Ali, R. *et al*., *Biochemistry* **52**, 4308–4323 (2013).
2. Allison, A. C. *et al*., *Ann. N. Y. Acad. Sci.* **696**, 63–87 (1993).
3. Armenta-Medina, D. *et al*., *BMC Genomics* **15**, 800-816 (2014).
4. Bacher, A. *et al*., *Annu. Rev. Nutr.* **20**, 153–167 (2000).
5. Bahl, A. *et al*. *Nucleic Acids Res.* **31**, 212–215 (2003).
6. Bessho, T. *et al., PLoS Negl Trop Dis,* **10**, 4339-4358 (2016)
7. Bhat, J. Y. *et al*., *Biochem. J.* **409**, 263–273 (2008).
8. Bhat, J. Y. *et al*., *Biochemistry* **278**, 3756–3768 (2011).
9. Bowne, S. J. *et al. Invest. Ophthalmol. Vis. Sci.* **47**, 34-56 (2006).
10. Briquet, S. *et al*., *PLoS One.* **13**, e0205596-e0205612 (2018)
11. Brown, A. M. *et al*., *Biol. Direct* **6**, 63-84 (2011).
12. Buey, R.M. *et al*., *Nat Commun.* **6**, 8923-8934 (2015).
13. Bult, C. J. *et al*., *Science* **273**, 1058–1073 (1996).
14. Bulusu, V. *et al*., *Biochim. Biophys. Acta* **1794**, 642–54 (2009).
15. Chong, C. R. *et al*., *J. Med. Chem.* **49**, 2677–2680 (2006).
16. Cossins, E. A. and Chen, L. *Phytochemistry* **45**, 437–52 (1997).
17. Datsenko, K. A. and Wanner, B. L. *Proc. Natl. Acad. Sci.* **97**, 6640–6645 (2000).
18. Digits JA and Hedstrom L, *Biochemistry* **38**, 15388-15397 (1999).
19. Ducati RG *et al*., *Biochemistry* **56**, 6368–6376 (2017).
20. Fernandez-Escamilla, A.-M. *et al*., *Nat. Biotechnol.* **22**, 1302–1306 (2004).
21. Gardner, M. J. *et al*., *Nature* **419**, 498–511 (2002).
22. Gaspar, P. *et al*., *Bioinformatics* **28**, 2683–2684 (2012).
23. Georgescauld, F. *et al*., *Cell* **157**, 922–934 (2014).
24. Gross, S. S., and Levi, R. *J. Biol. Chem.* **267**, 25722–9 (1992).
25. Hedstrom, L. *Chem. Rev.* **109**, 2903–2928 (2009).
26. Ho, Y. *et al. Nature* **415**, 180–183 (2002).
27. Karnawat, V. *et al*., *Biochemistry* **55**, 2491-2499 (2016).
28. Keppeke, G. D. *et al. Cell Div.* **13**, 5-23 (2018).
29. Krogan, N. J. *et al. Mol. Cell* **13**, 225–239 (2004).
30. Labesse, G. *et al*., *Structure.* **21**, 975–985 (2013).
31. Li CM *et al., Nat. Struct. Biol.* **6**, 582-587 (1999).

32. Linding, R *et al*., *J. Mol. Biol.* **342**, 345–353 (2004).
33. Lindstrom, D. L. *et al*. *Mol. Cell. Biol.* **23**, 1368–1378 (2003).
34. Liu, H., Luo, K. and Luo, D. *Sci. Rep.* **8**, 2759-2769 (2018).
35. Long, H. *et al*., *Genetics* **172**, 1633–1642 (2006).
36. Martinelli, L.K. *et al*., *Mol. Biosyst.* **7**, 1289–1305 (2011).
37. Mehrotra, S. and Balaram, H. *Biochemistry* **46**, 12821–12832 (2007).
38. Miller, D. V. *et al*., *Proteins* **84**, 828–840 (2016).
39. Murray, A. W. *Annu. Rev. Biochem.* **40**, 811–826 (1971).
40. Nimmesgern, E. *et al*., *Protein Expr Purif.* **17**, 282-289 (1999)
41. Oehring, S.C. *et al*., *Genome Biol.* **13,** R108-R129 (2012).
42. Ownby, K. *et al*., *J. Biol. Chem.* **280**, 10881–10887 (2005).
43. Raman, J. *et al*., *Mol. Biochem. Parasitol.* **138**, 1–8 (2004).
44. Rousseau, F *et al*., *Curr. Opin. Struct. Biol.* **16**, 118–126 (2006).
45. Roy, S. *et al*., *Mol. Biochem. Parasitol.* **204**, 111–120 (2015).
46. Roy, S. *et al*., *Mol. Biosyst.* **11**, 1410–1424 (2015).
47. Sarwono, A. E. Y. *et al*. *Parasitol. Int.* **66**, 537–544 (2017).
48. Selkov, E. *et al*., *Gene* **197**, GC11-26 (1997).
49. Shimizu, Y. *et al*., *Nat. Biotechnol.* **19**, 751–755 (2001).
50. Smialowski, P. *et al*., *FEBS J.* **279**, 2192–2200 (2012).
51. Smith, S. *et al*. *Mol. Microbiol.* **100**, 824–40 (2016).
52. Stevens, S. W. *et al*. *Mol. Cell* **9**, 31–44 (2002).
53. Umejiego, N. N. *et al*., *J. Biol. Chem.* **279**, 40320–40327 (2004).
54. Veletzky, L. *et al*., *Malar. J.* **13**, 476-479 (2014).
55. World Health Organization. (2018). World malaria report 2018. World Health Organization. (http://www.who.int/iris/handle/10665/275867). License: CC BY-NC-SA 3.0 IGO.
56. Zalkin, H. and Dixon, J. E. *Prog. Nucleic Acid Res. Mol. Biol.* **42**, 259–87 (1992).
57. Zhang, J. *et al*. *J. Cancer Res. Clin. Oncol.* **129**, 76–83 (2003).

List of Publications

Publications from this thesis

1. **Thota LP,** Balaram H *et al.*, (2019): Biochemical, Kinetic and Structural characterization of inosine 5'-monophosphate dehydrogenase from hyperthermophilic archaeon, *Methanocaldococcus jannaschii*. **(Manuscript under preparation).**
2. **Thota LP,** Balaram H *et al.*, (2019): Biochemical and functional investigations on PF3D7_0920800 from the protozoan parasite *Plasmodium falciparum*. **(Manuscript under preparation).**

Other publications (MS Thesis)

3. Ballut L, Violot S, Shivakumaraswamy S, **Thota LP**, Sathya M, Kunala J, Dijkstra BW, Terreux R, Haser R, Balaram H, and Aghajari N (2015). Active site coupling in *Plasmodium falciparum* GMP synthetase is triggered by domain rotation. *Nat commun*. *6*: 8930.

List of Abbreviations

ADP	Adenosine 5’-diphosphate
AEC	3-amino-9-ethylcarbazole
AMP	Adenosine 5’-monophosphate
$APAD^+$	Acetyl pyridine adenine dinucleotide (oxidized)
APADH	Acetyl pyridine adenine dinucleotide (reduced)
ATP	Adenosine 5’-triphosphate
BSD	Blasticidin
CBS	Cystathionine-beta-synthase domain
DTT	Dithiothreitol
EDTA	Ethylenediaminetetraacetic acid
GDP	Guanosine 5’-diphosphate
GMP	Guanosine 5’-monophosphate
GMPR	Guanosine 5’-monophosphate reductase
GTP	Guanosine 5’-triphosphate
HRP	Horseradish peroxidase
IMP	Inosine 5’-monophosphate
IMPDH	Inosine 5’-monophosphate dehydrogenase
IPTG	Isopropyl β-D-1-thiogalactopyranoside
MPA	Mycophenolic acid
NAD^+	Nicotinamide adenine dinucleotide (oxidized)
NADH	Nicotinamide adenine dinucleotide (reduced)
$NADP^+$	Nicotinamide adenine dinucleotide phosphate (oxidized)
NADPH	Nicotinamide adenine dinucleotide phosphate (reduced)
NAM	Nicotinamide mononucleotide
Ni-NTA	Nickel-nitrilotriacetic acid
PAGE	Polyacrylamide gel electrophoresis
PBS	Phosphate buffered saline
PCR	Polymerase chain reaction
PEG	Polyethylene glycol
PEI	Polyethyleneimine

PMSF	Phenylmethyl sulfonyl fluoride
PVDF	Polyvinylidene fluoride
SDS	Sodium dodecyl sulfate
SD-Ura	Synthetic defined medium without uracil
TCA	Trichloroacetic acid
TCEP	Tris (2-carboxyethyl) phosphine
XMP	Xanthosine 5'-monophosphate
YPD	Yeast, peptone and dextrose medium
ΔguaB	Deletion of gene that encodes IMPDH
ΔguaC	Deletion of gene that encodes GMPR
RPMI	Roswell Park Memorial Institute medium
DMSO	Dimethyl sulfoxide
TEV	Tobacco etch virus

Table of Contents

Chapter 3. Strategies designed towards obtaining PfIMPDH in soluble form

Chapter 1. Introduction to IMPDH/GMPR family of proteins

Inosine 5'-monophosphate dehydrogenase (IMPDH) and guanosine 5'-monophosphate reductase (GMPR) are the two metabolic enzymes involved in purine nucleotide biosynthesis and together constitute a family. They carry identical catalytic pockets, ligand binding sites and carry out different chemical reactions involving thioimidate intermediate (E-XMP) and result in different metabolic outcomes. They are characterized by the presence of one of the largest represented protein folds referred to as TIM barrel (named after the metabolic enzyme, triose phosphate isomerase), made of eight α-helices and eight parallel β-strands* $(\beta/\alpha)_8$*. The current chapter provides an overall perspective of these enzymes pertaining to their distribution, catalysis, structure, regulation and metabolic significance from the available literature.*

1.1 TIM barrel proteins

Various protein superfamilies are known to carry $(\beta/\alpha)_8$ barrel or TIM barrel as a common structural scaffold which catalyzes over twenty-five different enzymatic reactions like isomerization, condensation, phosphotransfer, hydride transfer etc. (Orengo CA *et al*., 1997; Lo Conte L *et al*., 2002; Nagano N *et al*., 2002; Anantharaman V *et al*., 2003). TIM barrel is believed to have achieved diversification driven by duplication of ancestral genes This led to the development of more efficient and specialized enzymes for a subset of reactions and differ from the ancestral gene that initially was capable of catalyzing multiple distinct reactions (Khersonsky O and Tawfik DS, 2010).

One of superfamily known to be composed of two proteins namely inosine 5'-monophosphate dehydrogenase (IMPDH) and guanosine 5'-monophosphate reductase (GMPR) forms an example for such diversification of the TIM barrel. IMPDH (EC 1.1.1.205) catalyzes the oxidation of inosine 5'-monophosphate (IMP) to xanthosine 5'-monophosphate (XMP) with the concordant reduction of NAD^+ to NADH. The reaction is a branch point between the adenine and guanine nucleotide biosynthesis, and a rate-limiting step of guanosine 5'-monophosphate (GMP) biosynthesis. IMPDH controls the guanine nucleotide pool, which in turn controls the proliferation and many other physiological

processes, making IMPDH an important target for immunosuppressive, cancer, and antiviral chemotherapy (Hedstrom L, 2009). On the other hand, GMP reductase (EC 1.7.1.7) catalyzes NADPH dependent reductive deamination of GMP to IMP and is the only route known for guanine nucleotides to be recycled to adenine nucleotides.

1.2 Inosine 5'-monophosphate dehydrogenase (IMPDH)

1.2.1 Prevalence

IMPDH is known to be present in every organism except protozoan parasites *Giardia lamblia* and *Trypanosoma vaginalis* (Morrison HG *et al*., 2007; Carlton JM *et al*., 2007). A single gene (*guaB*) or multiple genes coding for different isoforms has been reported across various organisms. Humans are identified to carry two distinct cDNAs coding for hIMPDH1 and hIMPDH2 that share 84 % amino acid sequence identity (Natsumeda Y *et al*., 1990; Collart FR and Huberman E, 1988). Expression of hIMPDH2 is found to be specifically up-regulated during neoplastic transformation and lymphocytic activation and down-regulated during cancer cell differentiation making it an important chemotherapeutic target while on the other hand, hIMPDH1 is constitutively expressed in the various states of proliferation and differentiation (Konno Y *et al*., 1991; Collart FR and Huberman E 1990; Collart FR *et al*., 1992; Nagai M *et al*., 1991; Nagai M *et al*., 1992). Similarly, a maximum of four copies has been observed in *Saccharomyces cerevisiae* (IMD1, IMD2, IMD3, and IMD4) that share 83-96 % identity and functional distinctions conferring drug (mycophenolic acid) resistance and guanine prototrophy to yeast are identified (Barton A *et al*., 1997; Wolfe KH and Shields DC 1997; Hyle JW *et al*., 2003). In *Mycobacterium tuberculosis*, three genes encoding IMPDH (annotated as *guaB1*, *guaB2*, and *guaB3*) that are similar to bacterial IMPDHs have been identified while only the activity of *guaB2* stands verified (Cole ST *et al*., 1998; Usha V *et al*., 2011). Zebrafish with three isoforms (IMPDH1a, IMPDH1b, and IMPDH2) forms another example of multiple genes encoding IMPDH isoforms that display varied functional roles and probably regulated by different circadian transcription factors. IMPDH1a was found to contribute to eye development and pigment synthesis, IMPDH2 controls the circadian clock, and lastly, IMPDH1b is reported to be involved in delay of embryonic development, counteracting the function of IMPDH2 (Li Y *et al*., 2015).

1.2.2 General features

Each monomer of most IMPDHs that largely exist as tetramers, contains about 400-500 residues carrying a catalytic domain and a regulatory subdomain (Fig. 1). The subdomain is referred to as Bateman module/CBS domain containing two CBS motifs in IMPDH which were first identified by Alexandre Bateman in cystathionine beta-synthase gene from human (Bateman A, 1997). IMP affinity resin coupled with or without cibacron blue is found to suffice and be efficient in obtaining homogenous preparation of enzyme from various sources (Hedstrom L, 2009). While *Borrelia burgdorferi* and *Cryptosporidium parvum* IMPDHs do not contain the subdomain, removal of CBS motifs from human IMPDH2 was found to be completely active *in vitro* (Sintchak MD *et al*., 1996) and no perturbation in the subunit (tetrameric) organization was observed (Nimmesgern E *et al*., 1999). All IMPDHs reported till date are found to be activated by a monovalent cation (preferably K^+) with optimal activity at pH 8.0 (a few bacterial enzymes were found exceptional with optimal activity at pH 9.0) (Alexandre T *et al*., 2015). Majority of IMPDHs are reported to follow Michaelis-Menten kinetics for IMP and display substrate inhibition by NAD^+ while IMPDHs from *Mycobacterium tuberculosis* and *Pseudomonas aeruginosa* have shown sigmoidal dependence of velocity on IMP concentration (Rostirolla Dc *et al*., 2014; Labesse G *et al*., 2013). Varied allosteric activation by ATP and inhibition by guanine nucleotides (GMP, GDP, and GTP) has also been testified (Labesse G *et al*., 2013; Buey RM *et al*., 2015).

Currently, about 91 X-ray crystal structures of IMPDH are found deposited in PDB, of which, 65 correspond to CBS deletion constructs. However, the CBS domain is found to be completely mapped in only 8 of the total 26 full-length IMPDHs. Protein stoichiometry of homotetramer and further associations leading to a dimer of tetramers (homooctamer) has been identified for IMPDHs from various organisms. A simple tetrameric arrangement has square planar geometry, with the sides of the barrels at the subunit interfaces and the CBS subdomains protrude from the corners of the tetramer (Fig. 1). The junction between the catalytic domain and the CBS subdomain is found to be highly flexible from the various X-ray crystal structures of *Tritrichomonas foetus* IMPDH. The CBS subdomain is found to be

disordered in many of the structures deposited in PDB, and removal of the subdomain is reported to have facilitated crystallization (Hedstrom L, 2009).

1.2.3 Ligand binding pockets and their conservation

IMPDH from *Tritrichomonas foetus* has been well characterized through both kinetic and structural studies and thus serves as a prototype for signifying enzyme features. Substrate binding and catalysis by IMPDH involves five key structural motifs of the enzyme that include catalytic cysteine (Cys) loop, phosphate-binding loop, finger loop, mobile flap, and C-terminal loop (Fig. 1). Catalytic loop carries the active site cysteine and is strictly identical across various enzymes. Adjacent to the active site loop is the phosphate binding region constituting around six residues. Presence of a twisted β-sheet that projects outwards from the carboxy-terminal of the TIM barrel is referred to as "finger domain", a special feature present in all identified IMPDHs with unknown function (Buey RM *et al*., 2015). The interaction of the finger domains from each monomer within IMPDH octamers in AgIMPDH and PaIMDH is identified and has been proposed as a conserved mechanism for regulation of catalytic activity in response to ligand binding to the Bateman domain. This interaction in PaIMPDH is found to be absent/lost upon binding of Mg-ATP or in a mutant enzyme with compromised octamer formation (PaIMPDH$^{\Delta CBS}$). Coupled with mutational studies, the finger domain of IMPDHs is shown to be a key player for transmission of the allosteric signal from the Bateman to the catalytic domain and is essential for catalysis (Buey RM *et al*., 2015). Around ten residues at the distal end of the finger domain constitute the mobile flap that is dynamic to move in and out of the active site during catalysis. The open conformation is projected for dehydrogenase reaction to occur followed by hydrolysis step in a closed conformation. The C-terminal segment couples the active site loop through a monovalent cation. However, coordination of the mobile flap with the catalytic loop and the C-terminal segment is uncertain. The catalytic loop, mobile flap, finger loop and about 20 residues at the C-terminal end are all found highly flexible in the absence of ligands (substrates or products) from X-ray crystal structures of various IMPDHs (Prosise G *et al*. 2002; Hedstrom L, 2009; Morrow CA *et al*. 2012; Rao VA *et al*. 2013; Buey RM *et al*., 2015). IMP binding site is constituted by residues from the catalytic cysteine loop, phosphate

binding motif, and mobile flap. Residues largely from the catalytic loop and mobile flap make up the NAD^+ binding site. Lastly, catalytic cysteine loop and the C-terminal loop together comprise the potassium-binding site. While IMP binding residues are identified as invariant, large divergence has been observed in NAD^+ binding and flap loop (Hedstrom L, 2009)

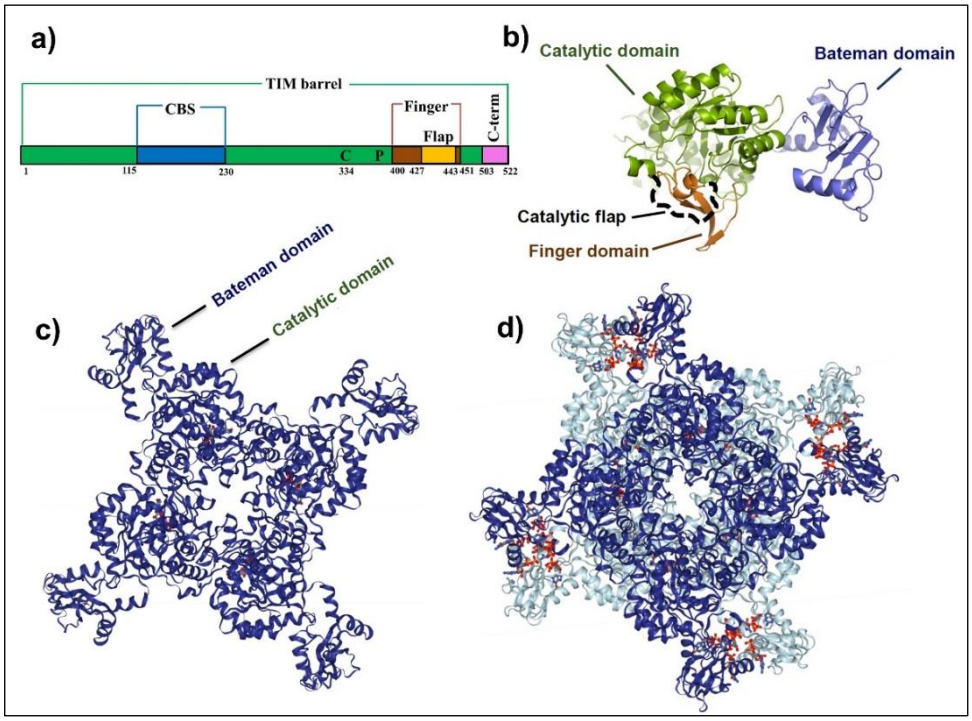

Figure 1. Domain architecture and spatial arrangement of IMPDH. a) Schematic bar representation of AgIMPDH primary sequence with key structural elements and CBS subdomain. *CBS domain inserted within the TIM barrel is indicated in blue (residues 115-230); the catalytic loop (residues –around Cys334; indicated by :C"), phosphate-binding loop (residues 391–395; indicated by "P"), finger loop (residues 400–451; brown), within the finger domain is the flap loop (residues 427–443; yellow) and C-terminal loop (residues 503–522; pink).* ***b) Cartoon representation of AgIMPDH monomer with Bateman (blue) and catalytic domain (green) indicated.*** *The catalytic flap shown as the dashed black line is invisible in the crystal structure of AgIMPDH and finger domain is indicated in brown (PDB 4Z87).* ***c) The tetrameric structure of S. pyogenes IMPDH (PDB 1ZFJ)*** *parallel to the 4-fold axis of symmetry is shown in ribbon diagram. CBS subdomain from each of the subunit points away from the catalytic core.* ***d) The octameric structure of A. gossypium IMPDH (PDB 4Z87)*** *with the two tetramers that pile up tail-to-tail are colored dark blue and sky blue. Bound GMP and GDP molecules are indicated in rainbow color as ball and stick model. Panel b is presented from Buey RM et al., 2017 with copyright permission (http://creativecommons.org/licenses/by/4.0/) while c and d images are rendered using NGL viewer (Rose AS et al., 2018).*

1.2.3.1 IMP binding site

IMP binding site is known to be invariant and most of the residues are highly conserved and SpIMPDH (PDB 1ZFJ) is presented as an example to describe the residues that contact IMP. C310 is the invariant catalytic residue. D343 is observed to form H-bonds with the ribose hydroxyls of IMP. Hydroxyl groups of S308 and Y390 were found to H-bonds with the phosphate group. G345 and G366 interact with the phosphate through main chain amino groups and G394 is seen to H-bond to the purine ring through its amine group and these three residues are invariant. S367 H-bonds with the phosphate while M393 and E421, H-bonds with the purine ring and are found to be highly variable. The variability of E421 is identified to play a key role in catalysis and drug selectivity (Hedstrom L, 2009) (Fig. 2).

1.2.3.2 NAD^+ binding site

NAD^+ site is described using *T. foetus* IMPDH as an example (PDB 1MEW). NAD^+ site and the mobile flap are highly divergent. The carboxyl group of a conserved D261 H-bond with the ribose hydroxyls of the nicotinamide portion of NAD^+. G312 and G314 H-bonds with the carboxamide of NAD^+ and are the only other conserved interactions. The carboxamide H-bonds with the side chain of R322 in *T. foetus* IMPDH, but glutamine and glycine are found as substitutions at this position. The hydroxyls of S262 and S263 interact with the phosphates of NAD^+. Position 262 commonly contains a residue such as threonine or cysteine that preserves the interaction while position 263 is often an alanine and neither of these two residues remain conserved. The residues that interact with the adenine ring are highly varied making it difficult to identify in sequence alignments. The mobile flap is similarly variable, with only the key catalytic residues R418 and Y419 being completely conserved and the presence of insertions and deletions make it difficult to align these two residues in a multiple sequence alignment. Presence of divergence in the cofactor binding site is implicated for the presence of naturally occurring IMPDH inhibitors and intriguingly, in support of this theory, species-selective inhibitors are found to interact with the NAD^+ site (Kohler GA *et al*., 2005; Hedstrom L, 2009) (Fig. 2).

1.2.3.3 Dependence on monovalent cation

All IMPDHs reported till date are found to be activated approximately to a 100-fold by K^+ ions while the specificity of activation varies considerably among different sources. K^+, $CS^{+,}$ and Rb^+ ions are always found to activate, but smaller ions such as Na^+ and Li^+ activate or inhibit or display no effect. K^+ has been found to have no apparent effect on the stability of the IMPDH tetramer, though it is reported to prevent the formation of higher order aggregates in few studies (Zhou X *et al*., 1997; Heyde E and Morrison J 1976; Xiang B *et al*., 1996). Two K^+ binding sites have been identified in X-ray crystal structures of IMPDHs. Site 1 occurs within the catalytic Cys loop (which is frequently disordered) and initially identified only in few X-ray crystal structures of Chinese hamster and *T. foetus* IMPDH (Sintchak MD *et al*., 1996; Prosise GL *et al*., 2002; Gan L *et al*., 2003). However, recent additions to this list include the X-ray crystal structures of *Vibrio cholerae*, *Mycobacterium tuberculosis*, *Campylobacter jejuni*, *Bacillus anthracis*, *Clostridium perfringens,* and *Ashbya gossypium*. Potassium-binding within AgIMPDH (PDB 4Z87) involves six main-chain carbonyls, three in the catalytic Cys loop (G329, G331, and C334) and three in the C-terminal segment from the adjacent subunit (E507′, G508′, and G509′) (Fig. 2). A second K^+ site that is observed only in *T. foetus* IMPDH (PDB 1LRT, Gan L *et al*., 2002; Gan L *et al*., 2003) at the interface between two monomers involves three main chain carbonyls (G20, N460, and F266′), the side chain hydroxyl of S22, and both oxygens of the side chain carboxyl of D264′ which are however are not conserved in IMPDHs from other organisms (Fig. 2). To simplify, the catalytic loop and C-terminal segment together constitute the K^+ binding site of IMPDH with residue conservation at a moderate level and represents one of the highly disordered segments in most of the X-ray crystal structures.

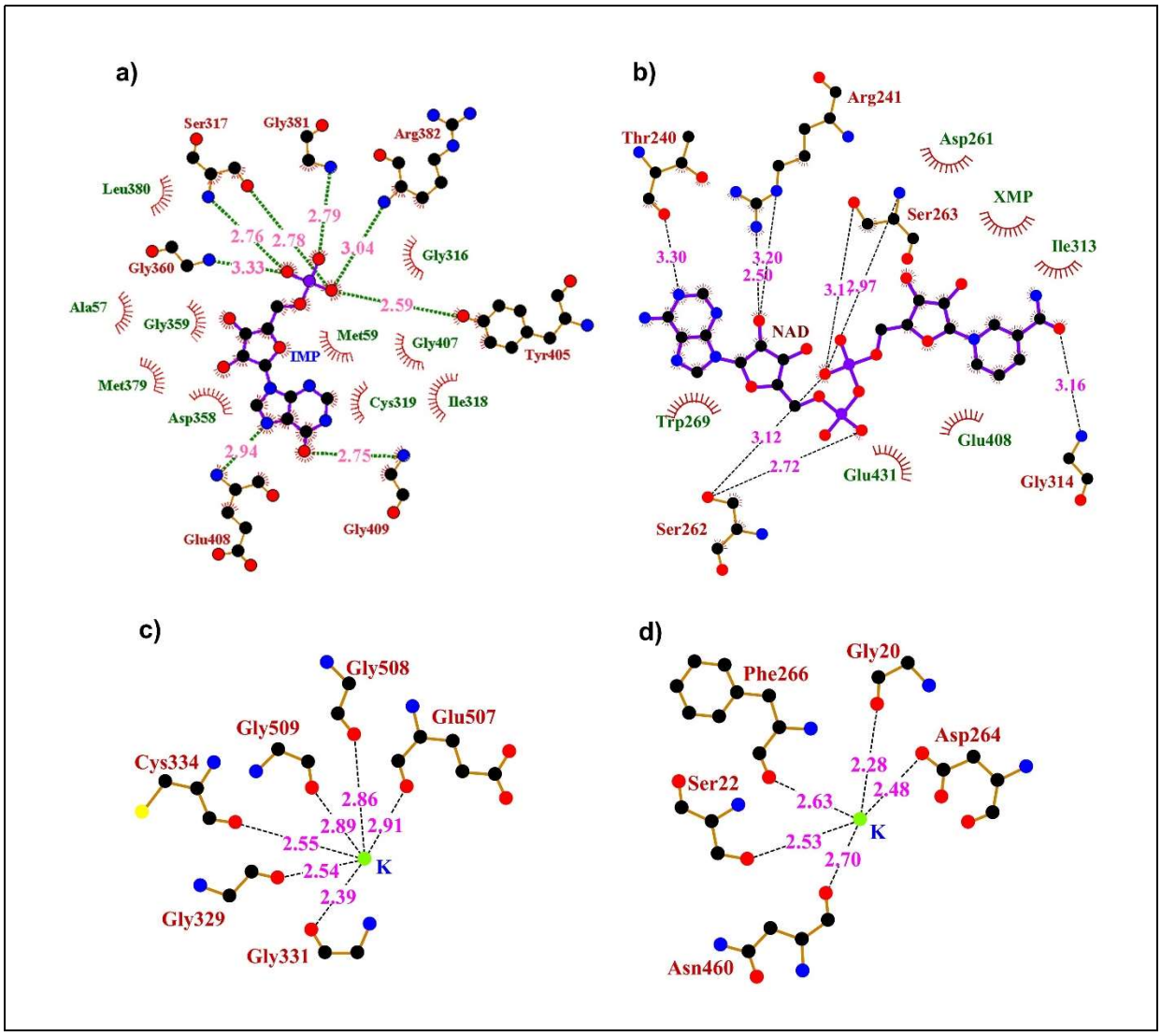

***Figure 2. Schematic diagram of the IMPDH interactions with substrate molecules**. **a) Residues that contact IMP** in the catalytic pocket of T. foetus IMPDH (PDB 1ME9). **b) NAD^+ binding site** from T. foetus IMPDH (PDB 1MEW). **c)** and **d) K^+ binding sites** within A. gossypium (site 1 PDB 4Z87) and T. foetus IMPDH (site 2, PDB 1LRT), respectively. Hydrogen bonds are indicated by dashed black lines between atoms. Residues involved in H-bond formation are indicated in maroon and the bond distances in pink. Hydrophobic contacts are represented by arcs with spokes radiating towards the ligand atoms and the corresponding residues in green. Carbon atoms are indicated as black filled circles, nitrogen in blue, oxygen in red and sulfur in yellow. The figure has been generated using LigPlot+ (Laskowski RA and Swindells MB, 2011).*

1.2.4 Enzyme mechanism

IMPDH carries out two chemical transformations that include a dehydrogenase reaction where the catalytic cysteine attacks C2 of IMP to form the covalent thioimidate intermediate E-XMP* with simultaneous hydride transfer to form NADH followed by a subsequent hydrolase reaction on E-XMP* that yields XMP and free enzyme (Fig. 3). The transition from the dehydrogenase and hydrolase activities is reported to be controlled by the catalytic loop (Josephine HR *et al*., 2010). IMPDH assumes an open conformation that allows NAD^+ to bind during the dehydrogenase reaction while a mobile flap moves into the cofactor binding site during the hydrolase reaction, bringing conserved Arg-Tyr dyad into the active site for Arg to act as a general base catalyst. Hydride transfer is reported to be fast in most IMPDHs. NADH release and E-XMP* hydrolysis have been proposed to be the rate-limiting step for *T. foetus* IMPDH catalysis. On the other hand, hydrolysis of a covalent enzyme intermediate has been proposed to be rate limiting in *C. parvum* IMPDH reaction (Digits JA and Hedstrom L, 1999; Xiang B and Markham GD, 1997; Umejiego NN *et al*., 2004). However, through isotope effects, the conformational change of flap is observed to be fast and hydrolysis as rate-limiting (Riera TV *et al*., 2008). The rate of this flap closure stands as the key variable in the entire catalytic cycle and not the shift in the equilibrium between open and closed conformations. The presence of K^+ is found to increase the rate of association of NAD^+ to the E•IMP complex and accelerate flap closure (Riera TV *et al*., 2011). Various X-ray crystal structures of TfIMPDH complexed with ligands (substrates and inhibitors) and molecular mechanics/quantum mechanics simulations together with mutational studies have identified three key residues R418, Y419, and T321 involved in activation of water with R418 acting as a general base catalyst (Fig. 3). This constitutes two probable channels of activation, one at low pH where a proton relay involving T321 and E431 activates the water while the R418 pathway dominates at high pH. Molecular mechanics simulations performed on the substitution of E431 with glutamine was found to disrupt the T321 pathway (Guillen Schlippe YV and Hedstrom L, 2005; Guillen Schlippe YV *et al*., 2004; Min D *et al*., 2008; Hedstrom L, 2012).

Initially, a partially random rapid equilibrium mechanism inclusive of K^+, IMP, and NAD^+ was described for the enzyme from *Aerobacter aerogenes* (Heyde E *et al*., 1976). In

this mechanism, K^+ and IMP are proposed to bind randomly to the enzyme, whereas NAD^+ binding is conditional to the presence of either K^+ or both K^+ and IMP. Later, a steady-state ordered sequential Bi-Bi mechanism in which IMP binds before NAD^+ and XMP is released after NADH was most commonly used to describe the IMPDH-catalyzed reaction (Carr SF *et al*., 1993). However, identification of E-XMP* intermediate, the measurement of isotope effects and the use of pre-steady-state kinetics revealed that substrates bind randomly, hydride transfer occurs rapidly, and NADH is released prior to the hydrolysis of E-XMP* (Digits JA and Hedstrom L, 1999; Wang W and Hedstrom L, 1997; Xiang B and Markham GD, 1997; Riera TV *et al*., 2008). Substrate inhibition by NAD^+ is reported to be uncompetitive that results from the trap of E-XMP* intermediate by high NAD^+ concentrations and therefore confirm the ordered release of products (Sintchak MD and Nimmesgern E, 2000; Zhou X *et al*., 1997; Kerr KM and Hedstrom L, 1997; Umejiego NN *et al*., 2004). The existence of E-XMP*·NAD^+ complex under physiological conditions (reported K_{ii} for NAD^+ range from 0.6-3 mM) is hypothesized as an alternate mechanism of regulating guanine nucleotide biosynthesis (Hupe D *et al*., 1986). A recent study on initial velocity and product inhibition patterns of *M. tuberculosis* IMPDH suggests a steady-state ordered Bi-Bi kinetic mechanism in which IMP binds first followed by NAD^+ (Rostirolla DC *et al*., 2014).

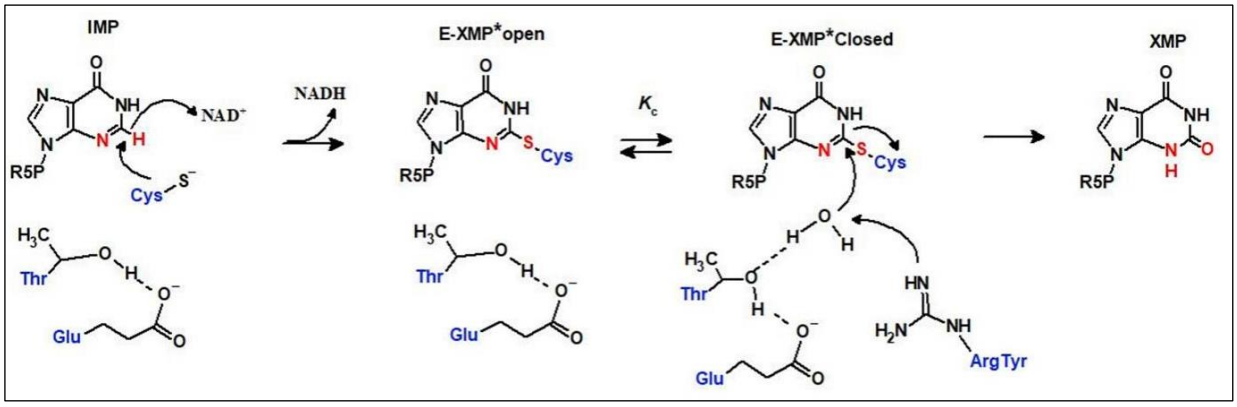

Figure 3. Mechanism of IMPDH reaction. *C2 carbon of IMP is attacked by the nucleophile cysteine from the enzyme followed by hydride transfer and release of NADH. The open conformation of thus formed E-XMP* intermediate goes to the closed state by the movement of flap loop bringing in the Arg-Tyr dyad. H-bonded Thr, Glu activate water followed by hydrolysis with Arg acting as a base catalyst. XMP is released and the enzyme is recycled for the next round of catalysis. K_c is the equilibrium rate constant for open and closed conformations. Active site residues involved in this*

process are indicated in blue while the difference between IMP, E-XMP and XMP in red. The reaction scheme is rendered using ChemSketch tool.*

1.2.5 Subunit organization, a fascinating tale of the tetramer to a cytoophidium

1.2.5.1 Structural aspects

Majority of the IMPDHs exist as tetramers in solution along with varying amounts of higher order multimers earlier misidentified as aggregates (Labesse G *et al*., 2013). Recent reports from *Pseudomonas aeruginosa,* human, *Ashbya gossypium* and class I bacterial enzymes indicate the presence of octamers each variably modulated by purine nucleotides (Labesse G *et al*., 2013; Buey RM *et al*., 2015; Alexandre T *et al.,* 2015; Buey RM *et al*., 2017). The binding of GTP or GDP to the Bateman domain of AgIMPDH was found to induce the formation of octamers with compromised catalytic activity probably the consequence of an alteration of structural dynamics of the finger domain and perturbation in the accessibility of mobile flap to the active site. Presence of octamers within the cells has also been verified in AgIMPDH with haemagglutinin (HA) epitope tagging.

In the apo state, a long and conserved β8-α8 finger loop from each monomer (corresponding to residues 371–427) in the catalytic domain of PaIMPDH is observed to link dimer of tetramers and CBS domains remain disordered. In the MgATP-bound form, the dimer of tetramers is mainly found to be stabilized by interactions between the CBS motifs resulting in ordering of this domain (Labesse G *et al*., 2013). Similar interactions have been identified in the crystal structures of the apo forms of *Streptococcus pyogenes* IMPDH (PDB 1ZFJ) and *Bacillus anthracis* IMPDH (PDB 3TSB). Although the CBS modules in the apo-state were found to be disordered in the X-ray crystal structure, they are evident in the cryo-EM structure (Labesse G *et al*., 2013; Buey RM *et al*., 2015; Alexandre T *et al*., 2015; Buey RM *et al*., 2017). In addition, a study describing the crystal structure of apo-IMPDH from *Pseudomonas aeruginosa* (PDB 6GJV) with completely mapped CBS domains has been reported recently (Alexandre T *et al*., 2019). However, human IMPDH1 (PDB 1JCN) remains an exception with a distinct alternative tetramer interface stabilized by a unique and largely hydrophobic interface with CBS modules isolated and protruded into the solvent. Further, the inclusion of MgATP resulted in the association of octamers into thin fibers ranging from 50 to 200 nm with CBS modules protruding out perpendicular to fiber axis that did not differ in catalytic activity from non-assembled forms (Anthony SA *et al*., 2017). Organization of the finger loop within a tetramer differs from that in an octamer. In a tetramer, the finger loops of each monomer remain ordered pointing out into the solvent and display little or no interaction with the rest of the protein. On the other hand, each finger loop

interacts with an equivalent segment from another monomer protruding from a facing tetramer (Labesse G *et al*., 2015). Most of the residues at the tetramer–tetramer interface are either well conserved (R56, E367, L375, and S383) or invariant (R379 and Y425).

Interactions similar to *P. aeruginosa* enzyme have been reported simultaneously in *A. gossypium* IMPDH. AgIMPDH octamers are found to assemble as dimers of tetramers that stack up tail-to-tail mainly stabilized by the Bateman domains from the upper and the lower tetramers, which associate in an antiparallel arrangement. H-bonds between the backbone atoms of residue R167 and the side chain of Q233 in a monomer with the respective side chains of residues R226 and Q170 in the adjacent Bateman domain, salt bridges between residues D168 and K207, and the hydrophobic packing of residue F171 constitute the interface stabilization. Bateman domains bring the finger domains of each monomer from both tetramers together associating into four pseudo-β-barrels around the fourfold axis of symmetry, thus stabilizing the interface. H-bonds between residues Y403, F405 and D407 in a single chain with residues D522, K518 and K409 in the adjacent monomer, as well as salt bridges between the side chain of residues R406, R410 and E517 and residues E517, D522, and R406, respectively constitute the finger domain association.

1.2.5.2 Cytological aspect

Presence of mycophenolic acid (MPA), an inhibitor of IMPDH was found to induce protein filaments in culture cells (Ji Y *et al*., 2006) which has been also confirmed *in vitro* using purified recombinant protein (Labesse G *et al*., 2013), signifying filament formation as an intrinsic property of IMPDH. Remarkably, these filamentous structures in human cells also referred to as rods and rings, appear very similar to the cytidine triphosphate synthase (CTPS) containing cytoophidium (Carcamo WC *et al*., 2011; Chen K *et al*., 2011). CTPS is a metabolic enzyme involved in the *de novo* synthesis of the nucleotide CTP. Cytoophidium (Greek for “cellular snakes”) was first identified in *Drosophila*, bacteria, and budding yeast carrying CTPS filaments by three independent groups (Liu JL, 2010; Ingerson-Mahar M *et al*., 2010; Noree C *et al*., 2010). The IMPDH cytoophidium is a filamentous structure that contains IMPDH, which may or may not contain CTPS and can be both cytoplasmic and nuclear cytoophidia and filamentation was found to upregulate IMPDH activity (Chang CC

et al., 2015; Carcamo WC *et al*., 2014; Gou KM *et al*., 2014; Shen QJ *et al*; 2016; Zhang J *et al*; 2014; Keppeke GD *et al*., 2015). Apart from MPA, ribavirin, an adjuvant used to treat hepatitis C infection was found to strongly induce IMPDH cytoophidium in patients under treatment (distinct cytoplasmic rods ~3–10 μm in length and rings ~2–5 μm in diameter) while similar structures were observed with 6-Diazo-5-oxo-L-norleucine (DON), a glutamine analog, which blocks CTP and GTP biosynthesis in HEp-2 cells (Table 1) (Carcamo WC *et al*., 2011; Calise SJ *et al*., 2015; Carcamo WC *et al*., 2014; Climent J *et al*., 2016; Keppeke GD *et al*., 2012; Novembrino C *et al*., 2014; Keppeke GD *et al*., 2015).

Cytoophidium is commonly categorized as 'mature' and 'immature' forms based on their appearance. Multiple immature punctate foci and small spicule-shaped cytoophidia occur within a single cell that can further associate by serial fusions resulting in larger and mature cytoophidia. By contrast, only one or a few large linear or ring-shaped mature cytoophidia are reported to be present in one cell in most cases (Fig. 4) (Gou KM *et al*., 2014; Thomas EC *et al*., 2012; Calise SJ *et al*., 2014). The number of IMDPH cytoophidia was found to increase upon CTPS overexpression that might reflect the variations in nucleotide synthesis. In mouse BNL-CL2 cells, inhibition of cell growth, either by serum starvation or by blocking the PI3K-AKT-mTOR pathway was found to trigger disassembly of IMPDH cytoophidia. Moreover, IMPDH cytoophidia have been detected in mouse pancreatic islet cells, with numbers correlating with nutrient uptake by the animal (Chang CC *et al*., 2015). IMP accumulation within the cells was also found to promote cytoophidium assembly while elevated GTP level resulted in disassociation of aggregates. No cytoophidium were formed upon CBS domain deletion from human IMPDH2, indicating the crucial role of CBS in filament formation. A recent report identifies that cytoophidium is highly crucial in maintaining the GTP pool and normal cell proliferation (Keppeke GD *et al*., 2018). Polymers of IMPDH were found to be induced by AICAR and glucose deprivation that disassembled upon guanine nucleotide generation by salvage synthesis regardless of the inducer (Schiavon CR *et al*., 2018). Immune response (T cell activation) is found to trigger reversible filament formation that disassembles with guanosine and inhibits IMPDH activity (Table 1) (Calise SJ *et al*., 2018; Duong-Ly KC *et al*., 2018).

Metabolic enzymes are coordinated and regulated at multiple levels to accomplish critical functions. Compartmentalizing of the metabolic enzymes through filamentation may serve as a novel mechanism for regulation of metabolic processes (Aughey GN *et al*., 2014; Barry RM *et al*., 2014; Noree C *et al*., 2014; Petrovska I *et al*., 2014; Strochlic TI *et al*., 2014). Cytoophidium formation is believed to provide metabolic stabilization, regulated at the transcriptional, translational, and post-translational level and respond to metabolic fluctuations caused by glutamine availability, nutritional stress, and developmental cues. (Liu JL, 2016).

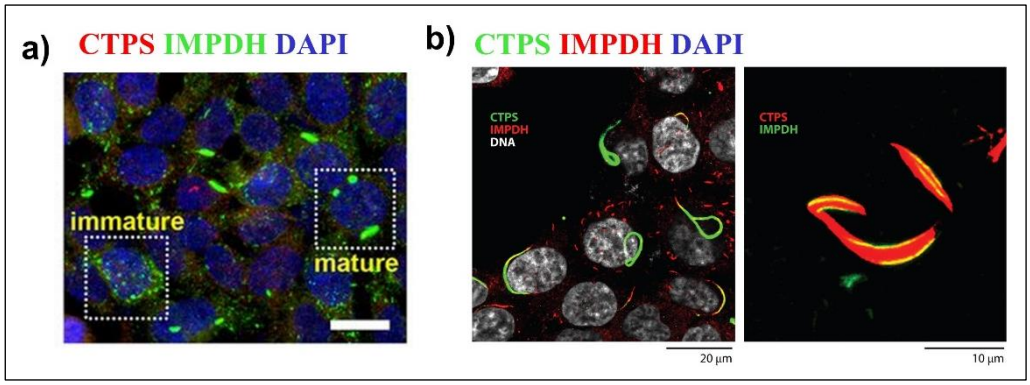

Figure 4. Structure of cytoophidium formed by IMPDH and CTPS in HEK293T cells. *Images have been acquired from Chang CC et al., 2015 and Liu JL, 2016 with copyright permissions (http://creativecommons.org/licenses/by/3.0) a) Indirect immunofluorescence imaging of HEK293T cells cultured in medium containing 100 μM cytidine for 1 h before fixation with antibodies against human enzymes, CTPS and IMPDH. Mature and immature IMPDH cytoophidia are indicated within the dotted square. The nucleus is stained with DAPI in blue while IMPDH and CTPS are shown in green and red, respectively. Scale bar of 20 μm is shown.* ***Panel b*** *represents the microscopy images upon overexpression of CTPS at two different magnifications (scale bars indicated). Here, CTPS is stained green, IMPDH red and DAPI in grey as pseudocolor.*

Table 1. Conditions that regulate the formation of cytoophidium.

Effect	Formation of cytoophidium
Induced	MPA, RVP, DON, overexpression of CTPS, IMP, AICAR, deprivation of glucose and T-cell activation
Disassembled	Inhibition of cell growth by serum starvation or block in the mTOR pathway, elevated GTP levels, deletion of CBS domain, guanine nucleotides generated by salvage pathway regardless of inducer and guanosine.

1.2.6 CBS domains in unrelated protein families - regulation, and disease perspective

CBS domains are found in several structurally and functionally unrelated proteins, including chloride channels (ClC family of proteins), amino acid transporters, and protein kinases along with IMPDH/GMPR family and cystathionine beta-synthase (Janosik M *et al*., 2001; Jamsen J *et al*., 2007; Jentsch TJ *et al*., 2002). They are involved in the maintenance of cellular energy status, metal ion concentration or ionic strength and regulate enzymatic activity (Baykov AA *et al*., 2011; Ereno-Orbea J *et al*., 2013). Structure of CBS domains was first understood from the crystal structure of Chinese hamster IMPDH, which contains two CBS domains in tandem (Sintchak MD *et al*., 1996) with each CBS motif carrying a conserved β1-α1-β2-β3-α2 topology. The overall fold of the CBS domains is conserved across different proteins, while there exists only little sequence identity, yielding the CBS domains that differ in functions (Hedstrom L, 2012).

Cystathionine beta-synthetase enzyme is involved in the cysteine biosynthetic pathway as a regulatory control point for S-adenosyl methionine (AdoMet) binding, thereby activation and protein multimerization (Finkelstein JD, 1998). Mutations that abolish or strongly reduce activation by AdoMet (Kluijtmans LA *et al*., 1996) in the CBS gene result in a genetic disorder referred to as homocystinuria, which is characterized by elevated levels of homocysteine in plasma accompanied by clinical symptoms of mental retardation, lens dislocation, skeletal abnormalities, and endothelial dysfunction (Fig. 5) (Miles EW and Kraus JP, 2004).

An example of CBS domain containing protein, adenosine 5'-monophosphate-activated protein kinase (AMPK) works as a sensor of cellular energy and maintains the ATP balance during periods of metabolic stress (Cheung PC *et al*., 2000). Low ATP and high AMP cause AMPK activation to switch on catabolic pathways like fatty acid oxidation, glycolysis while they switch off anabolic pathways that include fatty acid, cholesterol, and glycogen synthesis by phosphorylating regulatory metabolic enzymes (Hardie DG and Hawley SA, 2001). Hence the role of AMPK activators as new drugs to treat type 2 diabetes, obesity, and metabolic syndrome is being investigated (Winder WW and Hardie DG, 1999; Moller DE, 2001). AMPK is a heterotrimer with a catalytic subunit (α) and two regulatory subunits (β and γ). The γ-subunit comprises four CBS domains which are identified as allosteric binding sites for AMP and ATP

(Daniel T and Carling D, 2002). Each subunit of human AMPK has been identified to be present in various isoforms that include α1, α2, β1, β2, γ1, γ2, and γ3 (Stapleton D *et al*., 1996; Thornton C *et al*., 1998; Cheung PC *et al*., 2000). Mutations in the CBS domains of the AMPK γ2-subunit cause a glycogen storage disease referred to as a familial hypertrophic cardiomyopathy with conduction anomalies (Wolff-Parkinson-White syndrome) (Blair E *et al*., 2001; Gollob MH *et al*., 2001; Gollob MH *et al*., 2001; Arad M *et al*., 2002) while a mutation in the CBS domains of the γ3-subunit in pigs causes an abnormally high glycogen content in skeletal muscle (Milan D *et al*., 2000). Although the functional effect of CBS mutations on AMPK activity is debated between being constitutively active (Hamilton SR *et al*., 2001; Arad M *et al*., 2002) or activity reduction in response to metabolic stress (Fig. 5) (Daniel T and Carling D, 2002).

Another example for CBS domain is the chloride channels of the CLC family that perform a wide variety of cellular functions including membrane excitability, synaptic communication, trans-epithelial transport, cell volume regulation, cell proliferation, and acidification of endosomes and lysosomes (Jentsch TJ *et al*., 2002). CBS domains are found only in eukaryotic CLCs and are not involved in enzyme dimerization (Estevez R *et al*., 2004). The role of CBS domains in the functioning of the CLC channel has been examined and these studies indicate that the binding of nucleotides ATP/ADP/AMP to the CBS domain leads to inhibition of CLC-1, whereas in CLC-5 this potentiates current (Accardi A, 2015). However, it is observed that mutations in CBS domain of human ClC channels ClC-1 (Myotonia), ClC -2 (Idiopathic generalized epilepsy), ClC-5 (Dent's disease), ClC -7 (Osteoporosis) and ClC-Kb (Barter syndrome) result in specific diseases caused by ClC dysfunction (Fig. 5) (Cleiren E *et al*., 2001; Maduke M *et al*., 1999; Kornak U *et al*., 2001; Lloyd SE *et al*., 1997; Pusch M, 2002). Expression studies revealed that CBS2-deficient *Xenopus laevis* oocytes failed to generate the membrane currents and that was restored upon co-expression of CBS2-containing carboxy-terminal fragment (Maduke M *et al*., 1998; Schmidt-Rose T and Jentsch TJ, 1997). Role of CBS pairs as a sensor for cellular energy/ATP and their essentiality for channel gating has been hypothesized. Intriguingly, mutation in the CBS domain of human ClC-2 that include G826D (causing congenital myotonia, Pusch M, 2002), strongly inhibit the ATP binding *in vitro*.

ATP was also found to inhibit ClC-1 by shifting the voltage dependence and that certain mutations in the CBS domains resulted in complete loss or reduction in ATP inhibition (Bennetts B *et al*., 2005).

Most IMPDHs are known to contain two CBS motifs (together CBS module/Bateman domain) in tandem inserted between α2 and β3 of the TIM barrel. Removal of the CBS domains from IMPDH does not perturb enzymatic activity (Sintchak MD *et al*., 1996; Nimmesgern E *et al*., 1999). A repertoire of ligands known to bind CBS motif includes adenine and guanine nucleotides. Deletion of the CBS domains from *E. coli* IMPDH is reported to disrupt the coordinated regulation of the adenine and guanine nucleotide pools, resulting in growth arrest of the bacteria in the presence of inosine and adenosine and further accompanied by a dramatic increase in the adenosine nucleotide pool (Pimkin M and Markham GD, 2008; Pimkin M *et al*., 2009). Increase in adenine nucleotide pools was found to allosterically inhibit PRPP synthetase and ribonucleotide reductase in mammalian cells while guanine nucleotides activate these enzymes (Allison KC *et al*., 1993). Similarly, CBS deletion strain of *A. gossypium* was found to excrete significantly low levels of inosine in comparison to the wild type indicating the regulatory role of Bateman domain in increasing the metabolic flux through the guanine nucleotide pathway (Buey RM *et al*., 2015). Mechanistic basis of such intriguing observations has not been understood yet. Mutations in the CBS domains of human IMPDH1 (that do not affect catalysis) are found to be associated with an autosomal dominant form of retinitis pigmentosa (adRP, RP10), and with Leber congenital amaurosis (LCA), a more severe hereditary blindness both of which are indicative of a critical *in vivo* function of CBS domains (Bowne SJ *et al*., 2002; Kennan A *et al*., 2002; Bowne SJ *et al*., 2006; Wada Y *et al*., 2005). Importantly, retinal hIMPDH1 is identified to associate with polyribosomes translating rhodopsin mRNA and mutations in CBS subdomain were found to comprise the association of the retinal isoforms with polyribosomes (Mortimer SE *et al*., 2008). ATP was observed to bind CBS motifs of hIMPDH2 *in vitro* and display positive cooperativity (Scott JW *et al*., 2004) where binding of the first ATP molecule to a CBS pair causes a conformational change, which further leads to increase in the affinity of ATP for the rest of the CBS pairs. ATP binding and activation were abolished by a single point mutation (R224P) in the second CBS domain of hIMPDH2 which is identified as an

RP10-causing mutation in hIMPDH2 (Bowne SJ *et al.*, 2002). These observations are however reported not to be reproducible by other researchers (Hedstrom L, 2009). Cryo-EM experiments of hIMPDH1 revealed the presence of two types of complementary octamers with 69 % of concave structures (have CBS pointing outward) and 31 % in convex assembly with CBS subdomains involved in tetramer interface. In the presence of MgATP, these complementary octamers pile up into individual fibers. The aggregation of these fibers in the autosomal dominant mutant, D226N of hIMPDH1, probably indicates the onset of the retinopathy autosomal dominant retinitis pigmentosa (adRP) (Fig. 5) (Labesse G *et al.*, 2013).

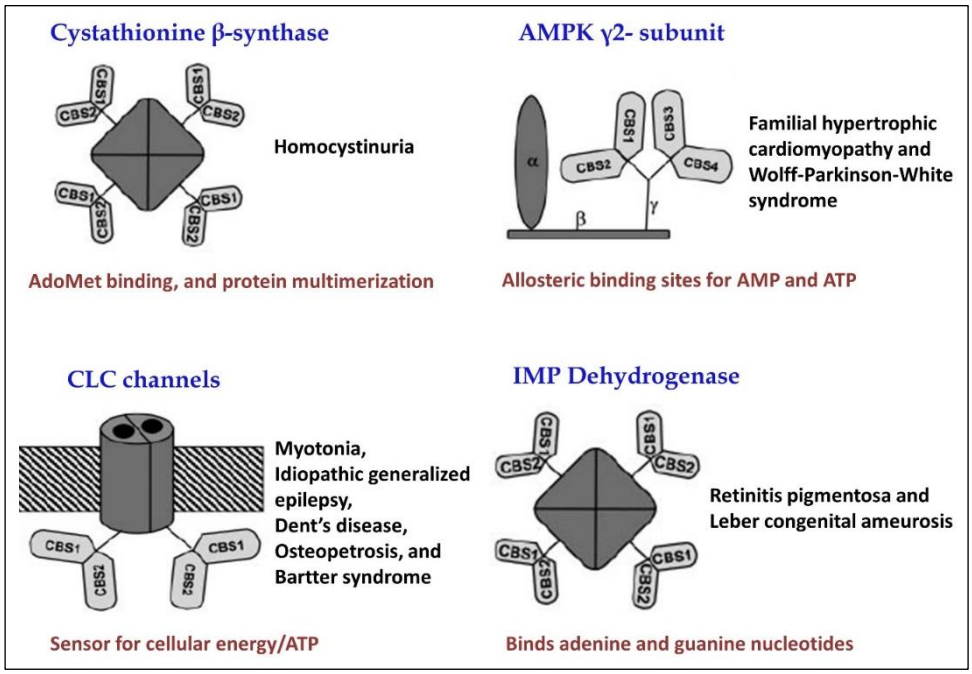

Figure 5. Distribution, regulation, and pathology linked to CBS motifs. *CBS domain is present in various unrelated family of proteins like chloride channels, AMP kinase, Cystathionine β-synthase, and IMPDH. They occur in tandem of two or four copies and carry out varied functions. The topology of such proteins, the role of CBS and associated pathological conditions are indicated. The image is modified and represented with copyright permission from Ignoul S and Eggermont J, 2005 (Copyright © 2005 the American Physiological Society)*

1.2.7 Moonlighting functions

Various reports indicate the additional cellular functions of IMPDH beyond its enzymatic activity. It was found to be essential in maintaining a balance between the adenine and guanine nucleotide pools in *E. coli* (Pimkin M and Markham GD, 2008; Pimkin M *et al*., 2009). Yeast IMPDH was found to be associated with actively transcribed promoters (Park JH and Ahn SH, 2010). Proteins involved in transcription regulation, splicing, and rRNA processing were identified as potential interacting partners through whole-genome screens (Uetz P *et al*., 2000; Lindstrom DL *et al*., 2003; Ho Y *et al*., 2002; Krogan NJ *et al*., 2004; Stevens SW *et al*., 2002; Collins SR *et al*., 2007). Association of IMPDH with polyribosomes, lipid vesicles, and protein kinase B was observed in eukaryotic cells (Mortimer SE *et al*., 2008; Whitehead JP *et al*., 2004; Ingley E and Hemmings BA, 2000). CBS domain-mediated binding of single-stranded nucleic acids with nanomolar affinity has also been reported (Cornuel JF *et al*., 2002; McLean JE *et al*., 2004). Mechanistic basis and the physiological consequences of such interactions have not yet been understood (Fig. 6). Role of CBS domains in the regulation of translation and transcription highlight the non-catalytic functions of IMPDH (Cornuel JF *et al*., 2002; McLean JE *et al*., 2004; Mortimer SE and Hedstrom L, 2005: Bowne SJ *et al*., 2006; Mortimer SE *et al*., 2008; Park JH and Ahn SH, 2010). Cell cycle arrest and apoptosis in human neuroblastoma cell lines were found to be triggered by guanine nucleotide depletion. Intriguingly, the cellular p53 concentration was found to regulate guanine nucleotide biosynthesis through IMPDH (Liu Y *et al*., 1998; Sherley JL *et al*., 1991).

A well-described example of differential regulation includes thymidylate synthase, a key enzyme in pyrimidine biosynthesis which acts as its own translation regulator by binding to its cognate mRNA and repressing translation (Chu E and Allegra CJ, 1996). Presence of substrates causes thymidylate synthase to release mRNA and resume translation. Differential translational regulation exhibited by the parasite and the host resulted in efficient malaria treatment (Zhang K and Rathod PK, 2002). Inhibitors and substrates release translational repression in mammalian cells, yielding more enzyme while neither substrates nor inhibitors relieve translational repression in malaria parasites and thereby succumb to the thymidylate synthase inhibitors. Extensive studies are still awaited to extend such an observation to IMP

dehydrogenase with CBS domain acting as an internal sensor (for small molecules, nucleotides, DNA and RNA, polyribosomes, etc.) (Hedstrom L, 2009)

Also, GMP synthetase (GMPS) an enzyme immediate downstream of IMPDH mediates the conversion of XMP into GMP and comprises the last step in guanine nucleotide biosynthesis. Non-catalytic functions of GMPS from Drosophila and human cells have been identified in the recent past. It is found to associate with and allosterically activate the nuclear ubiquitin-specific protease 7 (USP7) independent of its enzyme activity (van der Knaap JA *et al*., 2005; van der Knaap JA *et al*., 2010; Sarkari F *et al*., 2009; Reddy BA *et al*. 2014; Zhou Z *et al*., 2015; Faesen AC *et al*., 2011). Further, histone H2B deubiquitylation by USP7 in Drosophila and mammalian cells was found to be dependent on the association of USP7-GMPS acting as a transcriptional corepressor (van der Knaap JA *et al*., 2005 van der Knaap JA *et al*., 2010; Sarkari F *et al*., 2009; Frappier L and Verrijzer CP, 2011). GMPS and USP7 together are shown to play a crucial role as a positive mediator of hedgehog signaling (Zhou Z *et al*., 2015). GMPS-USP7 was also identified as a regulator of the p53 tumor suppressor pathway (Reddy BA *et al*., 2014; Bieging KT *et al*., 2014). GMPS is found to be largely in cytoplasm and shuttles to the nucleus in response to the cellular state. Cytoplasmic-nuclear partitioning probably serves as a regulatory mechanism linking metabolic state to transcriptional outcomes (van der Knaap JA and Verrijzer CP, 2016). In the nucleus, GMPS stabilizes p53 through activation of USP7 to restrict aberrant cell proliferation. Therefore, GMPS through its gene regulatory functions (moonlighting) participates in various signaling pathways that couples cell differentiation, growth, and proliferation during development (Fig. 6).

On similar lines to GMPS, a few studies identified the non-enzymatic role of metabolic enzyme IMPDH in gene expression control. Ability to bind RNA and polysomes has a direct implication of the enzyme in selective control of translation (Mortimer SE *et al*., 2008). IMPDH from Drosophila is found to be a sequence-specific DNA-binding transcriptional repressor that binds unwound CT-rich regulatory DNA elements (Kozhevnikova EN *et al*., 2012). IMPDH mostly remains cytoplasmic and was found to accumulate in the nucleus during the G2 phase of the cell cycle or in response to oxidative or replicative stress. Remarkably, IMPDH was found to bind and repress the histone genes and

E2f, the master controller of the G1/S transition (Fig. 6). These studies probably indicate IMPDH together with GMPS aid cell growth and proliferation through their enzymatic function and simultaneously by moonlighting, act as regulators of gene expression preventing aberrant cell proliferation.

The *de novo* purine biosynthetic enzymes are reported to cluster near mitochondria and microtubules, under certain cellular conditions such as high purine demand, to develop into dynamic multienzyme complexes referred to as 'purinosomes'. Purinosome is a novel intracellular organisation of enzymes involved in purine metabolism (Pedley AM and Benkovic SJ, 2017). The enzymes involved in purine nucleotide biosynthesis, adenylosuccinate synthase (ADSS) and inosine monophosphate dehydrogenase (IMPDH), that catalyse reactions downstream of IMP have been shown to be part of the purinosome complex. Live-cell fluorescence microscopy experiments showed the colocalization of IMPDH-GFP and ADSS-GFP with the purinosome marker FGAMS (phosphoribosylformylglycinamidine synthase), confirming their involvement in the purinosome in transiently transfected HeLa cells in purine-depleted medium (Zhao H *et al*., 2015).

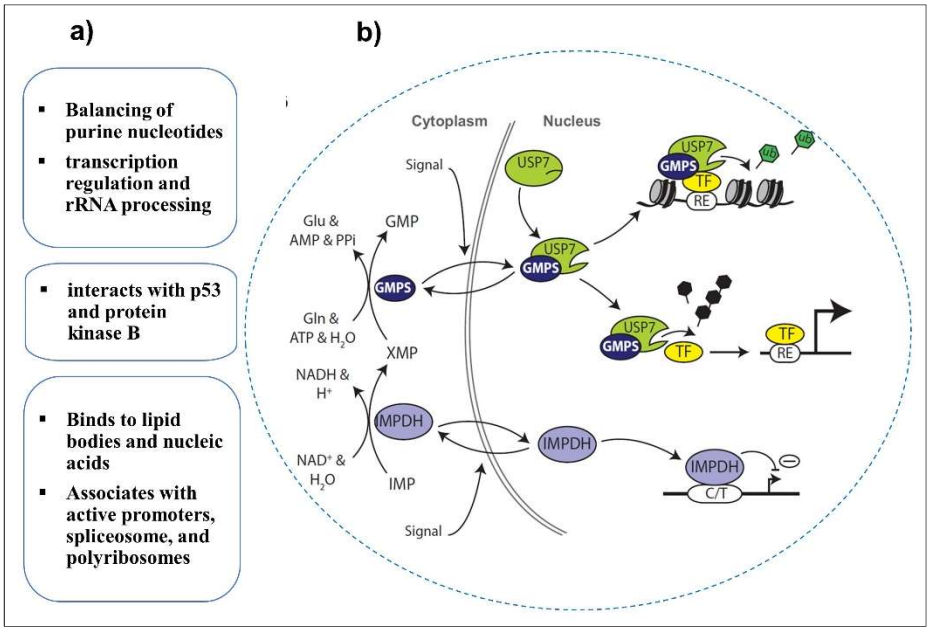

Figure 6. Moonlighting functions of IMPDH. *IMPDH is found to perform non-enzymatic roles in transcription and translation regulation along with the metabolic role of guanine nucleotide biosynthesis.* ***a) Various interactions and functions*** *of IMPDH identified so far in bacteria, yeast, Drosophila, and human are highlighted.* ***b) Schematic of cytoplasmic-nuclear partitioning of IMPDH and GMPS as a part of chromatin and transcription regulation in Drosophila*** *is adapted from van der Knaap JA and Verrijzer CP, 2016 with copyright permission (http://creativecommons.org/licenses/by-nc/4.0/). Both the enzymes mediate biosynthesis of GMP. GMPS translocates to nucleus, binds and activates the deubiquitylating enzyme ubiquitin-specific protease 7 (USP7). This complex further acts as transcriptional corepressor upon recruitment to specific regulatory elements (REs) by gene-selective transcription factors (TFs) through the removal of the active H2B ubiquitylation (H2Bub) mark with ub indicated in green hexagons. Also, GMPS-USP7 complex gets relocated to Polycomb response elements to promote silencing (deubiquitylate) of selective Polycomb group (PcG) proteins resulting in H2Aub. GMPS-USP7 also modulates gene expression through deubiquitylation and stabilization of selective transcription factors like the tumor suppressor p53 and cubitus interruptis, the effector of hedgehog signaling. GMPS largely remains cytoplasmic with continuous shuttling in and out of the nucleus that is driven by the cellular state. IMPDH which is directly upstream of GMPS is known to bind single-stranded CT-rich regulatory DNA elements (C/T) and act as a*

sequence-specific DNA-binding transcriptional repressor. Like GMPS, IMPDH is also found to accumulate in the nucleus in response to oxidative or replicative stress.

1.2.8 IMPDH as a drug target

IMPDH controls the guanine nucleotide pool, which in turn controls the cell proliferation and many other physiological processes, making IMPDH an important target for immunosuppressive, cancer, and antiviral chemotherapy (Hedstrom L, 2009). Amplification of IMPDH in tumors and rapidly proliferating cells initially identified by George Weber formed the basis of initial drug design targeting this enzyme (Weber G, 1983; Jackson R *et al*., 1975). IMPDH has also been identified as a potential drug target for antimicrobial, and antiparasitic infections (Hedstrom L *et al*., 1990; Kohler GA *et al*., 1997; Striepen B *et al*., 2004; Wilson K *et al*., 1991; Wilson K *et al*., 1994; Abraham EP, 1945; Hupe D *et al*., 1986; Webster HK and Whaun JM, 1982; Hedstrom L *et al*., 2011; Gorla SK *et al*., 2012).

1.2.8.1 IMP site-specific reversible inhibitors

Reversible inhibitors of IMPDH that target IMP binding site include ribavirin and bredinin. Ribavirin is a synthetic nucleoside available in various formulations like Copegus, Rebetol, Ribasphere, Vilona, and Virazole and is active as ribavirin 5′-monophosphate (RVP) (Witkowski JT *et al*., 1972; Gish RG, 2006). Ribavirin was used in treating respiratory syncytial virus infection and together with α-interferon, in hepatitis C virus (HCV) (Leyssen P *et al*., 2005). Ribavirin is also found to act as an immunomodulator by enhancing the T-cell response with mechanistic basis unclear (Hultgren C *et al*., 1998). However, ribavirin undergoes further transformation to the triphosphate, which inhibits RNA capping enzymes, polymerases, gets incorporated into RNA and induces lethal mutations (Smith RA and Kirkpatrick W, 1980; Eriksson B *et al*.,1977; Crotty S *et al*., 2001). Bredinin also referred to as mizoribine is a natural product inhibitor of IMPDH used in treating organ allograft rejection, rheumatoid arthritis, primary nephrosis, lupus nephritis, dermatomyositis, and autoimmune dermatoses. It is currently being used as an immunosuppressive agent in Japan (Ishikawa H, 1999). It is an imidazole nucleoside and mizoribine 5'-monophosphate (MZP) constitutes the active form (Fig. 7).

1.2.8.2 Irreversible inhibitors

Several analogs of IMP are reported to form irreversible covalent adducts with the catalytic cysteine residue that include 6-chloro-IMP (6-Cl-IMP), ethynylimidazole carboxamide riboside monophosphate (EICARMP), 2-chloro-methyl-IMP (2-Cl-methyl-IMP), 6-thio-IMP, 2-vinyl-IMP, and 2-fluoro-vinyl-IMP (Gilbert H and Drabble W, 1980; Hampton A, 1963; Brox L and Hampton A, 1968; Matsuda A *et al*., 1988; Zhang HZ *et al*., 1997; Pal S *et al*., 2002; Nair V and Kamboj RC, 2003; Brox LW and Hampton A, 1968). The inhibition reaction of IMPDH by 6-Cl-IMP is the well-defined of all the covalent in-activators. EICAR was found to carry both anti-leukemic and anti-viral activities. Activated forms include mono-, di-, and triphosphates and also the dinucleotide, EAD (Balzarini J *et al*., 1998). IMP is found to protect against inactivation by both 6-Cl-IMP and EICARMP, while NAD^+ displayed no effect (Fig. 7).

1.2.8.3 NAD^+ site-specific reversible inhibitors

Inhibitors that are structural analogs of NAD^+ include benzamide riboside (BR), tiazofurin, selenazofurin and mycophenolic acid (MPA). Adenine dinucleotides constitute the active forms generated through phosphorylation by either adenosine kinase or nicotinamide riboside kinase, or 5′-nucleotidase followed by the action of NMN adenyltransferase (NAD-pyrophosphorylase) and are considered to be reasonably specific inhibitors of IMPDH (Cooney D *et al*., 1982; Kuttan R *et al*., 1982; Saunders PP *et al*., 1990; Fridland A *et al*., 1986; Jayaram HN *et al*., 1992). BR in its active form as benzamide adenine dinucleotide (BAD) is found to be a potent inhibitor of IMPDH although its utility is restricted due to the skeletal muscle toxicity observed in the pre-clinical trials (Gharehbaghi K *et al*., 1994; Jayaram HN *et al*., 2002). Tiazofurin and selenazofurin, are the synthetic nucleosides that are identified with potent antiviral and antitumor activities (Pankiewicz KW *et al*., 2004). Tiazofurin was approved for the treatment of chronic myelogenous leukemia with dose-limiting toxicity of a headache, somnolence, and nausea (Fig. 7).

Mycophenolic acid, a secondary metabolite from the fungus *Penicillium brevicompactum* is a potent inhibitor of mammalian IMPDHs (1000 fold more potent than the bacterial enzymes) and known for its anti-viral, anti-angiogenic and anti-cancer activities

(Fig. 7) (Chong CR *et al*., 2006; Hedstrom L, 2009). Cancer cells are characterized by high levels of glucuronidation of the phenolic oxygen than normal cells leading to the ineffectiveness of MPA as an anticancer agent (Franklin TJ *et al*., 1996). Sodium mycophenolate (Myfortic, Novartis) and a prodrug, mycophenolate mofetil (CellCept, Roche) have been used as an immunosuppressive drug for prevention of transplant rejection. Besides, MPA has also been used in the treatment of psoriasis and also found to induce differentiation or apoptosis of several cancer cell lines, including breast, prostate, melanoma, leukemia, and neuroblastoma (Bacus SS *et al*., 1990; Floryk D and Huberman E, 2006; Floryk D *et al*., 2004; Kiguchi K *et al*., 1990; Kiguchi K *et al*., 1990; Collart FR and Huberman E, 1990; Messina E *et al*., 2004; Messina E *et al*., 2005). Various derivatives known as mycophenolic adenine nucleotide (MAD) compounds targeting the nicotinamide binding site of IMPDH have also been synthesized to combat the dose-limiting gastrointestinal toxicity and unfavorable metabolism of MPA (Lesiak K *et al*.,1998; Rejman D *et al*., 2006; Chen L *et al*., 2008). MPA acts as an uncompetitive inhibitor known to bind E-XMP* and compete with the flap for the vacant NAD^+ binding site (Link JO and Straub KJ, 1996, Sintchak MD *et al*., 1996). Therefore, the equilibrium between the open and closed conformation is identified as a key determinant of drug sensitivity (Digits JA and Hedstrom L, 2000; Kohler GA *et al*., 2005; Riera TV *et al*., 2008). *P. brevicompactum* has two isoforms of IMPDH (A and B) that are 20- and 1000-fold more resistant to MPA, respectively, than the eukaryotic counterparts (Hansen BG *et al*., 2011). While the active site and MPA binding site are completely conserved across, the C-terminal segment that forms part of the K^+ binding site varies widely and swapping this region between MPA sensitive and resistant IMPDHs revealed that this region could account for 7-fold of the resistance. These observations illustrate that the K^+ binding site forms a part of additional "long-range" determinant of drug selectivity and reaction properties that are yet to be identified (Hedstrom L, 2012). However, RVP, MZP, and MPA are currently being used for clinical chemotherapy (Braun-Sand SB and Peetz M, 2010).

Lastly, a combination of IMPDH and histone deacetylase inhibitors (HDAC inhibitors, induce differentiation and apoptosis of tumor cells similar to IMPDH inhibitors) is the new strategy being adopted for anticancer drug development. The hydroxamic acid

analog of MPA (MAHA) forms the prototype for dual function inhibitors targeting both IMPDH and HDAC (Mei S *et al*., 2004; Chen L *et al*., 2007). Parasite-specific inhibitors that compete with tiazofurin for NAD^+ site have been reported only for IMPDH from *Cryptosporidium parvum*, a major causative of diarrhea, malnutrition and a potent biowarfare agent (Umejiego NN *et al*., 2008).

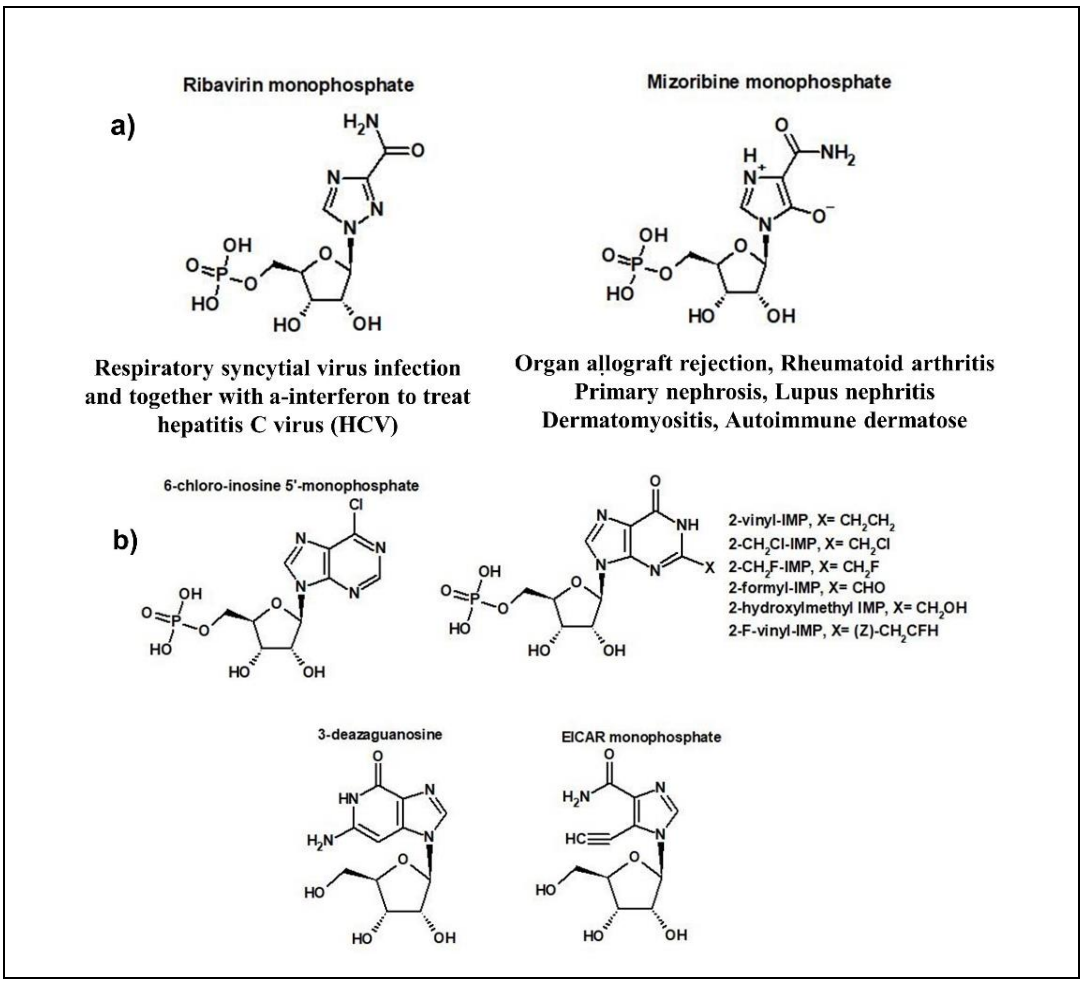

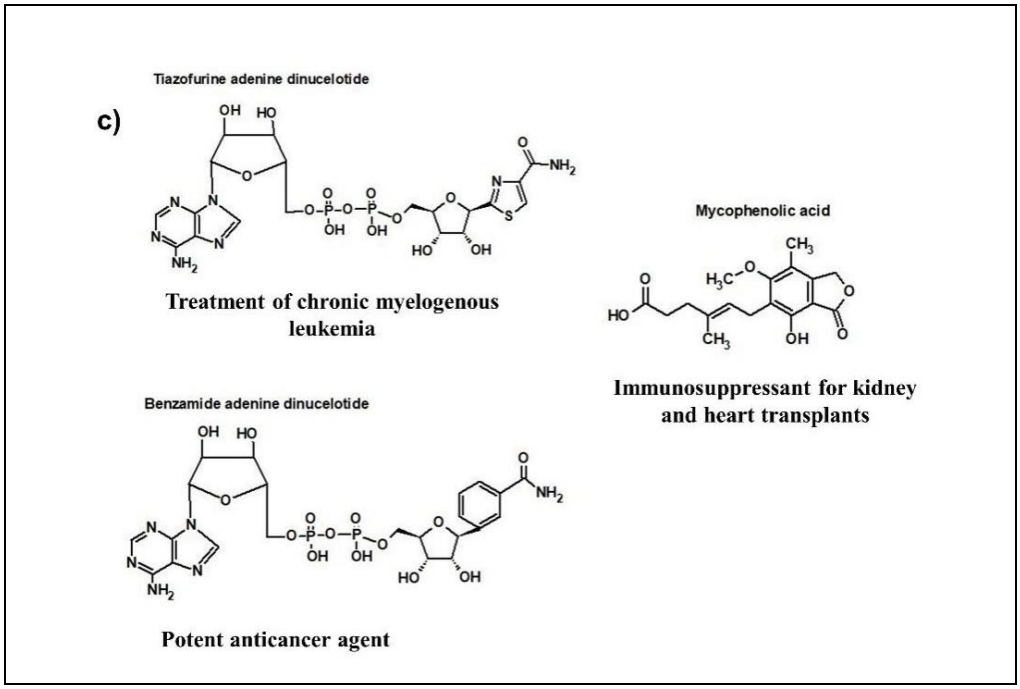

Figure 7. Structures of inhibitors that target IMPDH. a) Reversible IMP-specific inhibitors *that include ribavirin and mizoribine (bredinin). Phosphorylated form constitutes the active metabolite within the cell. Their antiviral and immunosuppressive properties are also indicated.* ***b) Represents the structural analogous of IMP that inhibits IMPDH irreversibly*** *by forming covalent adducts with a cysteine residue in the catalytic pocket.* ***c) Active metabolites of reversible NAD$^+$-specific inhibitors*** *and their role in anticancer and immune suppression are indicated.*

1.3 Guanosine 5'-monophosphate reductase (GMPR)

1.3.1 Occurrence

Guanosine 5'-monophosphate reductase (GMPR) is reported to be absent in *Haemophilus influenzae*, *Mycoplasma genitalium*, *Methanocaldococcus jannaschii*, apicomplexans, *Saccharomyces cerevisiae,* and insects, but has been found in kinetoplastids (*Trypanosoma* and *Leishmania*), and mammals. (Fleischmann RD *et al*., 1995; Fraser CM *et al*., 1995; Bult CJ *et al*., 1996; Becker JL, 1974; Berens RL *et al*., 1995). Reports on enzyme purification from a few sources include *S. typhimurium*, *Aerobacter aerogenes*, human erythrocytes, calf thymus, *Leishmania donovani* and *Artemia salina* (Mager J and Magasanik B, 1960; Brox LW and Hampton A, 1968; Mackenzie J and Sorensen L, 1973; Spector T *et al*., 1979; Stephens RW and Whittaker VK, 1973; Spector T and Jones TE, 1982; Spector T

et al., 1984; Renart MF *et al*., 1976). However, GMPR from only *Homo sapiens, Bos taurus, Escherichia coli, L. donovani, Trypanosoma brucei* and *Trypanosoma congolense* have been cloned, expressed and activity verified (Andrews SC and Guest JR, 1988; Moffat K and Mackinnon G, 1985; Li J *et al*., 2006; Zhang J *et al*., 2003; Deng Y *et al*., 2002; Martinelli LKB *et al*., 2011; Patton GC *et al*., 2011; Smith S *et al*., 2016; Bessho T *et al*., 2016; Sarwono AEY *et al*., 2017). GMPR is coded by the gene *guaC* and like IMPDH is found to exist in multiple copies in human, mouse, and bovine.

1.3.2 Structural elements

The catalytic domain in GMPR constitutes $(\beta/\alpha)_8$ protein fold and is devoid of CBS subdomain in human, *E. coli*, mouse and bovine enzymes. However, recent reports have identified the presence of CBS domain in *L. donovani*, *T. brucei,* and *T. congolense* GMPRs that is an insertion of 90-100 residues in hGMPR2 (Fig 8). Unlike IMPDH, deletion of the CBS domain in LdGMPR was found to disrupt the catalytic activity (Smith S *et al*., 2016). kinetoplastid GMPRs (*L. donovani*, *T. brucei* and *T. congolense*) are shown to express constitutively, appear granular in the cytosol and found to localize in glycosomes like other purine metabolic enzymes.

Solution studies identified homotetramers of EcGMPR by analytical size-exclusion chromatography (Martinelli LKB *et al*., 2011) while quaternary structure changes monitored by rate zonal centrifugation indicate *L. major* GMPR to exist in monomeric and tetrameric forms in apo-state. Presence of saturating amounts of GMP or GTP was found to stabilize the formation of LmGMPR tetramer while ATP caused the enzyme to migrate as monomeric and dimeric forms. This study indicates guanylate and adenylate nucleotides as regulators of subunit association that in turn influences LmGMPR catalytic activity (Smith S *et al*., 2016). Very few X-ray crystal structures are available for GMP reductases that include *B. anthracis* (PDB 1YPF and 2A1Y), Human (PDB 2BLE, 2BWG, 2A7R, 2C6Q, 2BZN), and *T. brucei* (PDB 5X8O). While human and Trypanosoma enzymes are verified for GMPR activity *in vitro*, there exists no record for the *Bacillus* enzyme. Re-analysis of the crystal packing of these structures using PISA server (Krissinel E and Henrick K, 2007) revealed tetrameric

arrangement as the most stable form for all the enzymes except for TbGMPR (complexed with GTP) which was found to be octameric (Fig. 8).

Key catalytic residues of GMPR include cysteine, threonine and glutamic acid and these are highly conserved (Cys186, Thr188, and Glu289 in EcGMPR) and mutation of any one of these residues was found to perturb the enzymatic function *in vivo* (Min D *et al*., 2008; Li J *et al*., 2006). These residues are conserved in both GMPR and IMPDH where C186 reacts to form E-XMP*, T188 and E289 activate the leaving group instead of water and no equivalent exists for the Arg-Tyr dyad of IMPDH. Structural motifs identified from the X-ray crystal structure of hGMPR2 (PDB 2A7R) and sequence analysis, includes the active site loop (residues 179–187 in hGMPR2) to be similar to those of hGMPR1 and IMPDHs with cysteine as the active site residue, the conformation loop (residues 129–133 in hGMPR2) that favors NADPH over NADH and a flexible binding region/flap (residues 268–289 in hGMPR2) (Fig. 8). GMP was found to bind in the catalytic loop and stabilize the flexible binding region while NADPH was observed to interact with the conformational loop (Fig. 9). Active site loops of GMPR and IMPDH carry similar overall topology and are identified to be highly conserved (Fig. 12). Residue S270 within the flap, predicted to interact with the phosphate group of NADPH, may be substituted by glycine in IMPDHs and is reported to be highly flexible and disordered in hGMPR and other IMPDHs (Fig. 12) (Sintchak MD *et al*., 1996; Gan L *et al*., 2002; Gan L *et al*., 2003). Three catalytic site residues found to be involved in binding of the monovalent cation are identical to that of site 1 residues reported for IMPDH in section 1.2.3.3 (Fig. 9).

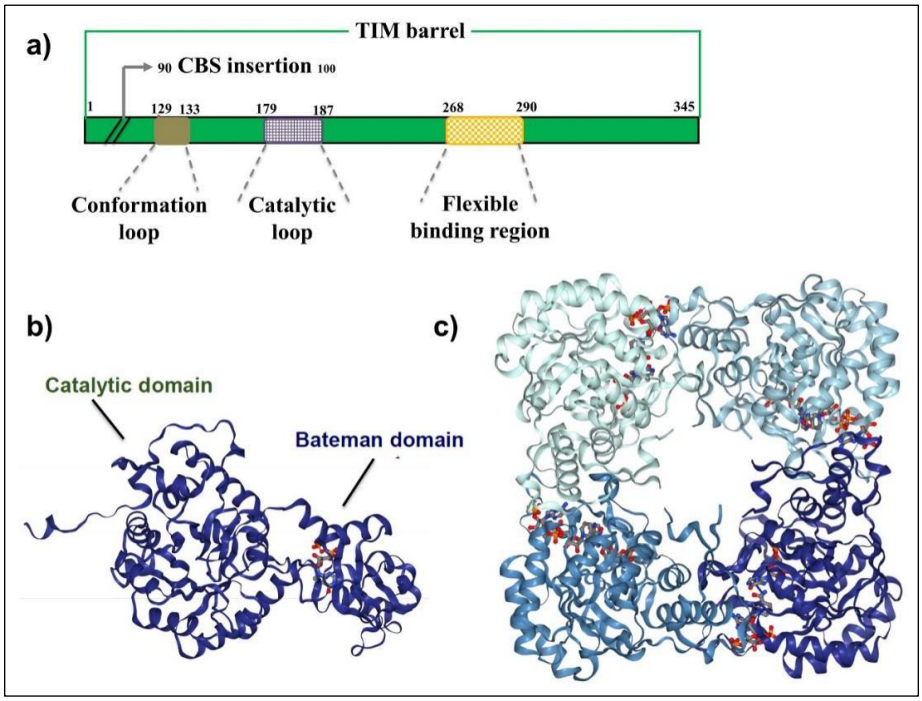

Figure 8. Domain architecture and spatial arrangement of GMPR. a) Schematic bar representation of human GMPR2 primary sequence with key structural elements. *Human, E. coli and bovine GMPR lack CBS domain. CBS domain identified in kinetoplastid GMPR occurs as an insertion within the TIM barrel and aligns between residues 90 and 100 of the human enzyme. The conformational loop (residues 129-133; presented in the grey box); the catalytic loop (residues179-187; indicated in the purple checkbox), adjacent flexible binding loop (residues 268–290; indicated in the yellow checkbox)* ***b) Cartoon representation of GMPR monomer from Trypanosoma brucei.*** *Bateman and catalytic domain are pointed out with GTP bound in the subdomain indicated in rainbow color as a ball and stick model (PDB 5X8O)* ***c) The tetrameric structure of human GMPR2 (PDB 2C6Q)*** *parallel to the 4-fold axis of symmetry is shown in ribbon diagram. Each subunit represented in shades of blue carries a molecule of IMP and NADPH represented in rainbow color as a ball and stick model. X-ray crystal structures are rendered using NGL viewer (Rose AS et al., 2018).*

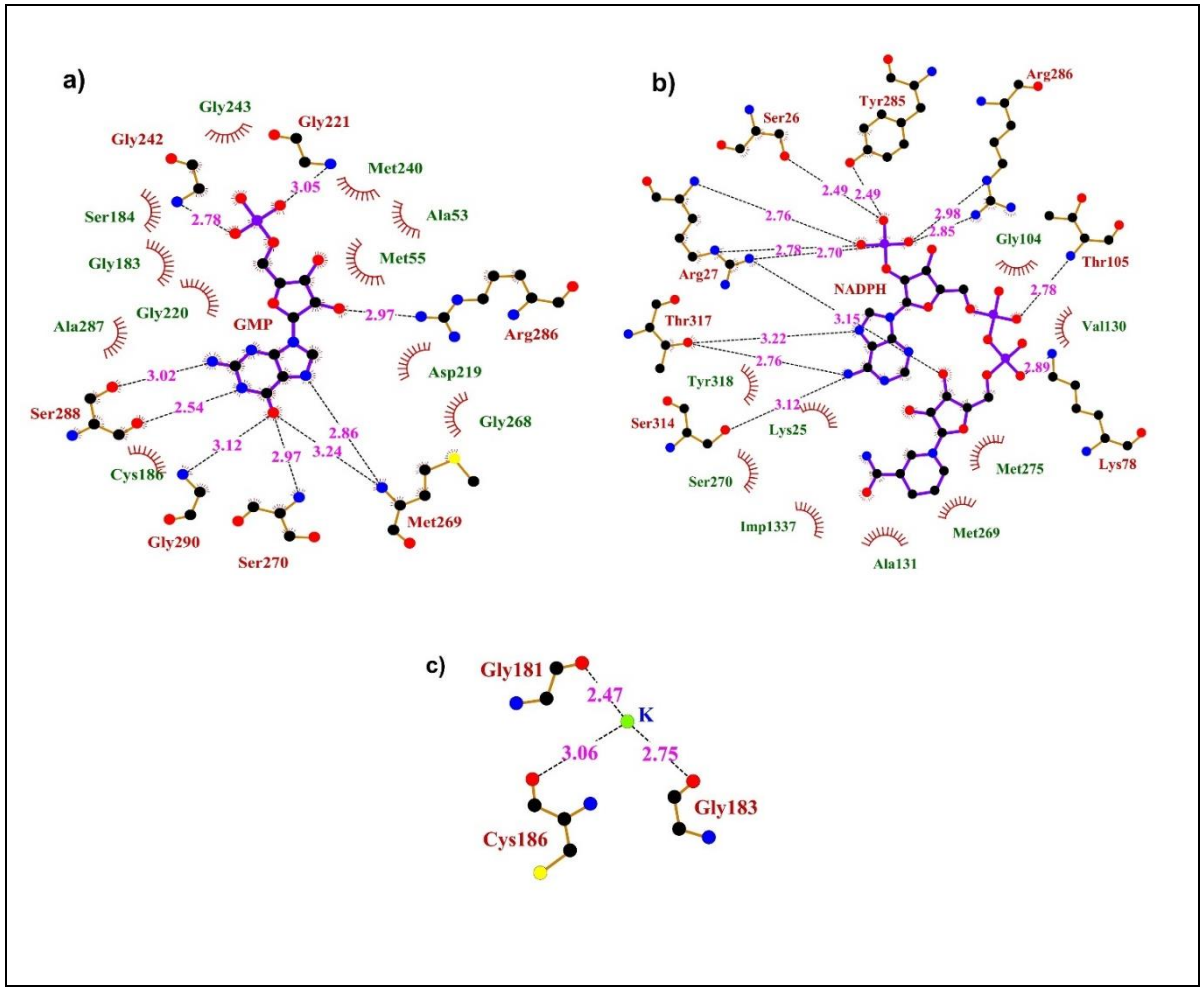

Figure 9. Schematic diagram of GMPR interactions with the substrate molecules. ***a) Residues that contact GMP*** *in the catalytic pocket of human GMPR2 (PDB 2A7R).* ***b) NADPH binding site*** *from human GMPR2 (PDB 2C6Q).* ***c) K^+ binding site found in human GMPR1*** *(PDB 2BWG). Hydrogen bonds are indicated by dashed black lines between atoms. Residues involved in H-bond formation are indicated in maroon and the bond distances in pink. Hydrophobic contacts are represented by arcs with spokes radiating towards the ligand atoms and the corresponding residues in green. Carbon atoms are indicated as black filled circles, nitrogen in blue, oxygen in red and sulfur in yellow. The figure has been generated using LigPlot+ (Laskowski RA and Swindells MB, 2011).*

1.3.3 Catalysis and enzyme mechanism

GMPR stands as the only known enzyme responsible for the conversion of nucleotide derivatives of guanine to the pivotal precursor, IMP necessary for biosynthesis of both adenine and guanine nucleotides (Spector T *et al*., 1979). GMPR, like IMPDH, undergoes two chemical transformations that include a deamination reaction and a hydride transfer. It

catalyzes the irreversible, NADPH dependent, reductive deamination of GMP to yield IMP. In addition to its enzymatic function of the interconversion of purine nucleotides, GMP reductase provides a nitrogen source via its deamination activity. Expression of GMP reductase in *E. coli* was found to be induced by GMP and regulated by cyclic adenosine 5'-monophosphate (cAMP), by the intracellular ratio of purine nucleotides, and by glutamine and its analogs (Roberts RE *et al*., 1988; Benson CE *et al*., 1971; Garber BB *et al*., 1980). It is found to be inhibited by adenosine 5'-triphosphate (ATP) and reactivated by the presence of guanosine 5'-triphosphate (GTP) (Andrews SC and Guest JR, 1988). *E. coli* GMPR was found to display an ordered bi-bi kinetic mechanism that proceeds through the same E-XMP* intermediate as IMPDH, however, this intermediate reacts with ammonia instead of water (Fig. 10). The deamination step is determined to be fast and hydride transfer is rate-limiting. EcGMPR is the only example reported to catalyze the reverse reaction in the presence of NH_4^+ to form GMP from IMP. *L. donovani* GMPR is reported to follow sigmoidal behavior with GMP as substrate (positive cooperativity, n=2.3). ATP was found to inhibit while GTP activated the LdGMPR and further the back conversion of IMP to GMP was found to be highly unfavorable. Mg^{2+} ions have no effect on LdGMPR activity. GMPRs from human, bovine, *T. brucei* and *T. congolense* are found to obey Michaelis–Menten kinetics. ATP displayed no effect on hGMPR2 while GTP, XMP, and all the divalent cations inhibited the human enzyme. Monovalent cation activation has been observed for GMPR from *T. brucei* (K^+ and NH_4^+), *T. congolense* (Na^+, K^+, Cs^+, and NH_4^+) while mammalian GMPRs on the other hand, showed no activation in the presence of K^+, and NH_4^+ in comparison to Na^+ (Deng Y *et al*., 2002; Martinelli LKB *et al*., 2011; Patton GC *et al*., 2011; Smith S *et al*., 2016; Bessho T *et al*., 2016; Sarwono AEY *et al*., 2017).

The presence of cofactor induces a conformational change required for the deamination of GMP and formation of E-XMP* as identified from the X-ray crystal structures of hGMPR (PDB 1BLE, 2C6Q). Two different conformations of the cofactor namely an 'in' conformation poised for hydride transfer and an 'out' conformation where cofactor is 6 Å away from IMP has been observed. Mutagenesis along with substrate and cofactor analog experiments demonstrated the requirement of "out" conformation for the deamination of GMP and found the cofactor as a part of the catalytic machinery that activates

ammonia. The catalytic C186, E289 and the conserved Y285-R286 dyad points away from GMP, folds into the active site, with R286 protecting GMP from the water. Upon cofactor binding, dyad becomes part of the 2'-phosphate binding site and the residues C186, T188 and E289 align for catalysis (Fig. 10) (Spector T *et al*., 1979; Deng Y *et al*., 2002; Li J *et al*., 2006; Martinelli LKB *et al*., 2011; Patton GC *et al*., 2011).

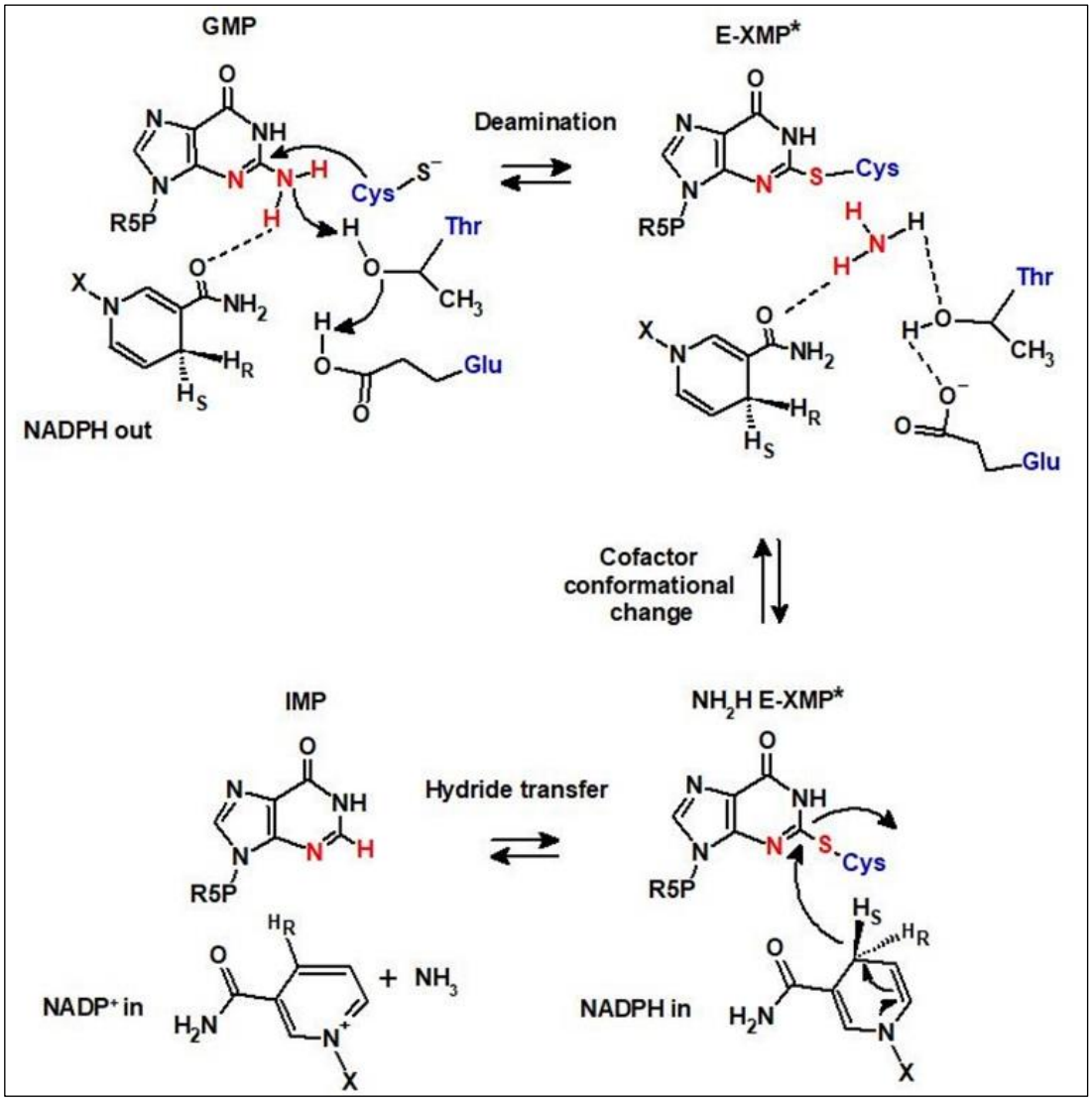

Figure 10. Mechanism of GMPR reaction. *C2 carbon of GMP is attacked by the nucleophile cysteine from the enzyme followed by deamination step. NADPH "out" conformation assisted by the active site residues threonine and glutamate results in E-XMP* intermediate. NAPDH "in" conformation leads to hydride transfer with the release of IMP, $NADP^+$, NH_3, and enzyme is recycled for the next round of catalysis. Active site residues involved in this process are indicated in blue while the difference between GMP, E-XMP* and IMP in red. The reaction scheme is rendered using ChemSketch tool.*

1.3.4 Essentiality and inhibition

No disease has been identified so far linked to GMPR with one of plausible reason could be lack of this enzyme being invariably fatal (Henikoff S and Smith JM, 1989). A significant increase in its expression during cold exposure reveals the critical role of GMP reductase in non-shivering thermogenesis, a process required for the survival of rodents during cold stress (Salvatore D *et al*., 1998). hGMPR2 is shown to promote the monocytic differentiation of HL-60 leukemia cells (Zhang J *et al*., 2003). Role of GMP reductases in various biological functions that include maintenance of purine nucleotides balance, as a possible target for anti-leishmanial, anti-cancer drugs and involvement in human cell differentiation has also been realized (Andrews SC and Guest JR, 1988; Spector T and Jones TE, 1982; Page T *et al*., 1985; Zhang J *et al*., 2003). A recent report attributes hGMPR1 as more abundant isoform in the brain and cerebral cortex and identified it as a potential therapeutic target for Alzheimer's disease (Liu H *et al*., 2018).

GMP reductase is not essential in the presence of intact *de novo* synthesis of purine nucleotides through IMP (Roberts RE *et al*., 1988). However, any block in IMP synthesis results in the essentiality of GMP reductase activity to provide AMP with guanine nucleotides as precursors (Kessler AI and Gots JS, 1985). Further, most of the protozoa are reported to be devoid of *de novo* purine biosynthesis, thus largely rely on the purine salvage pathway making it an attractive chemotherapeutic target (Berg M *et al*., 2010). IMP, XMP, 6-thioGMP, 6-thioIMP, and 6-chloropurine ribonucleotide were found to inactivate GMPR from various sources (Spector T *et al*., 1979; Berens RL *et al*., 1980; Looker DL *et al*., 1986; Deng Y *et al*., 2002; Li J et al., 2006; Patton GC *et al*., 2011). Purine nucleotide analog, ribavirin widely used in the treatment of hepatitis C, in its active form, ribavirin 5'-monophosphate (RVP) was found to inhibit (relative to IMPDH, weak) GMPR from *E. coli* (Patton GC *et al*., 2011), *T. brucei*, and no or little inhibition of human and bovine (Bessho T *et al*., 2016). Mizoribine 5'-monophosphate (MZP), another purine nucleotide analog inhibited the activities of *E. coli*, *T. brucei* and human GMPRs (Bessho T *et al*., 2016). Mycophenolic acid (MPA), a selective nicotinamide-binding site inhibitor of IMPDH, regarded as a potent and IMPDH specific inhibitor, with higher affinity to mammalian

enzymes than to protozoan enzymes was found to inhibit LmGMPR and TcGMPR (Table 2) (Umejiego NN *et al*., 2004; Smith S *et al*., 2016; Sarwono AEY *et al*., 2017).

Table 2. Inhibitors of purine biosynthetic enzymes.

Inhibitor/Mode of inhibition	IMPDH	GMPR	GMPS
Ribavirin/Competitive	+	+[a]	-
Mizoribine/Competitive	+	+	+
IMP analogues/Competitive	+	+	-
Benzamide riboside/Non-competitive	+	n.r	-
Tiazofurin/Non-competitive	+	n.r	-
Mycophenolic acid/Uncompetitive	+	+	-
XMP/Competitive	+	+	-
ATP	*	+[b]	-
GTP	+	+[c]	+

*[a] no effect on Human and bovine enzymes; [b] no effect on human enzyme; [c] Known to activate E. coli and L. donovani enzymes while found to inhibit hGMPR2; * known to either activate IMPDH or has no effect; n.r indicates not reported; + and - indicates presence and absence of inhibition, respectively. (Spector T et al., 1979; Berens RL et al., 1980; Looker DL et al., 1986; Ishikawa H, 1999; Deng Y et al., 2002; Li J et al., 2006; Bhat JY et al., 2008; Patton GC et al., 2011; Bessho T et al., 2016; Umejiego NN et al., 2004; Smith S et al., 2016; Sarwono AEY et al., 2017).*

1.4 Similarities and distinguishing features of GMPR from IMPDH

IMPDH/GMPR family of proteins stand as an example of subtle differences in enzyme structure that dictate the reaction specificity. With the catalytic $(\beta/\alpha)_8$ barrels arranged in a square planar geometry, this family of proteins are largely known to exist as homotetramers with recent studies highlighting octameric and polymeric organization modulated by purine nucleotides. CBS domain within the TIM barrel, as an insertion between α2 and β3, was the feature largely used to distinguish IMPDH from GMPR. However, recent reports identified their presence in kinetoplastid GMPR as well. IMP/GMP binding site and nicotinamide portion of the cofactor binding site are found to be similar and highly conserved in both the enzymes while adenosine portions of the cofactors bind to different regions of the barrel domain in IMPDH and GMPR. Both the enzymes are found to be activated by monovalent cations such as K^+. The active site loop between the β6 and α6 of

a monomer and the C-terminal segment from an adjacent monomer forms the monovalent cation binding site and the residues are not conserved and therefore display variable activation. The hydride transfer by both the enzymes involves nicotinamide cofactor and proceeds through the same covalent intermediate E-XMP*. However, this intermediate reacts with water in IMPDH which is replaced by ammonia in GMPR. The mobile flap between β8 and α8 is another structural segment that varies in both sequence and length and is identified to carry out different roles in each enzyme. In IMPDH, the flap binds in the same site as the cofactor during the hydrolysis reaction and movement of the flap is the conformational change that determines the next step in catalysis. The IMPDH flap is the functional constraint carrying conserved Arg-Tyr dyad that is involved in the activation of water. On the other hand, in GMPR, the flap interacts with the 2′-phosphate of NADPH through a conserved Tyr-Arg dyad and the conformational change is brought about by the movement of cofactor itself. Therefore, differences in protein dynamics controlled by residues neighboring the active site determine the reaction specificities of both the enzymes. Cofactor selectivity, ligand affinity does not determine the metabolic roles of GMPR and IMPDH as they possess high substrate specificity despite high sequence and structural similarity. Deuterium isotope exchange analyzed by NMR spectroscopy indicated the presence of similar placement of substrate and cofactor on GMPR and IMPDH while the rate of the hydride-transfer reaction varied (Hedstrom L, 2009; Patton GC *et al*., 2011; Martinelli LKB *et al*., 2011; Rosenberg MM *et al*., 2018). IMP analogs (MZP and RVP) that inhibit IMPDH are reported to act against GMPR as well although the cellular significance of GMPR inhibition remains to be understood. MPA recognized as a potent and IMPDH specific inhibitor, another demarcating feature of IMPDH from GMPR, is now known to inhibit kinetoplastid GMPRs (Table 3).

Table 3. Comparison of IMPDH *vs* GMPR.

IMPDH *vs* GMPR	**Similarities**
	Identical catalytic pocket binds similar ligands
	Presence/absence of CBS motif
	Monovalent cation activation
	Exists as tetramers, octamers or higher order multimers
	Ribavirin, Mizoribine, and MPA inhibit enzyme activity
	Differences
	Preference of IMPDH for water and GMPR to ammonia
	Interactions of adenine dinucleotide portion of the cofactor

1.5 Evolutionary perspective

Evolutionary implications of IMPDH and GMPR are quite intriguing with phylogenetic analysis provided in a recent article that classifies IMPDHs and GMPRs into different clades (Fig. 11) (Sarwono AEY *et al*., 2017). Although experimental evidence for the enzymatic activity of LdGMPR, TbGMPR, and TcGMPR exists, these enzymes did not classify into the GMPR clade, but to the IMPDH related clade in the phylogenetic tree generated with the neighbor-joining method using MEGA 5.2 software (Fig. 11). Comparison within kinetoplastid GMPR yielded more pronounced similarity along with the presence of cystathionine β-synthase (CBS) pair domain which is only identified in IMPDHs earlier. Like the *Leishmania* enzyme, TbGMPR and TcGMPR showed no enzymatic activity to catalyze IMP to XMP, despite their higher homology towards IMPDHs than to GMPRs of mammals.

Although catalysis in reverse direction has not been observed for GMPR from human, bovine, *L. donovani*, *T. brucei* and *T. congolense,* over-expression of EcGMPR was found to complement bacteria lacking IMPDH and attenuated in GMPS, demonstrating that GMPR is sufficient to support life in ammonia/ammonium-rich environments such as the mammalian gut (Patton GC *et al*., 2011). The aphid symbiont *Buchnera aphidicola* lacks both IMPDH and GMPS but contains a GMPR for GMP utilization (van Ham RC *et al*., 2003). *Buchnera* also uses ammonia to synthesize amino acids (Hansen AK and Moran NA, 2011). About twenty bacteria/archaea are found to have no GMPS, and probably synthesize GMP utilizing

ammonia and IMP. Therefore, it is proposed that ammonia can also serve to synthesize guanine nucleotides (Hedstrom L, 2012). The ability of GMPR to catalyze the conversion between GMP and IMP in both directions and belief for the existence of ammonia-rich reductive environment at the beginning of origin of life might point out the development of IMPDH/GMPR family with GMPR probably being an ancestral enzyme (Zahnle KJ, 2010). However, the opposite reaction by TcGMPR was found to progress very slowly even at high concentrations of enzyme and substrates. It has also been suggested that GMPS came into existence after IMPDH in the phylogeny analysis (Kim HS *et al*., 2006). Down the evolutionary line, IMPDH is proposed to have acquired arginine (R418 in TfIMPDH) for water activation leaving threonine-glutamate (T321-E431 in TfIMPDH) pathway obsolete. In support of this hypothesis, substitution at E431 position by glutamine was found to be tolerated with no loss in catalytic activity (Fig. 12). Conformational changes in IMPDH and co-factor migration in GMPR is found to determine their reaction specificity (Hedstrom L, 2012). The existence of such structural and functional similarities between GMPRs and IMPDHs reported across various organisms probably indicate an evolutionary relationship and further studies could provide detailed vision onto the molecular phylogenetics (Fig. 11) (Sarwono AEY *et al*., 2017).

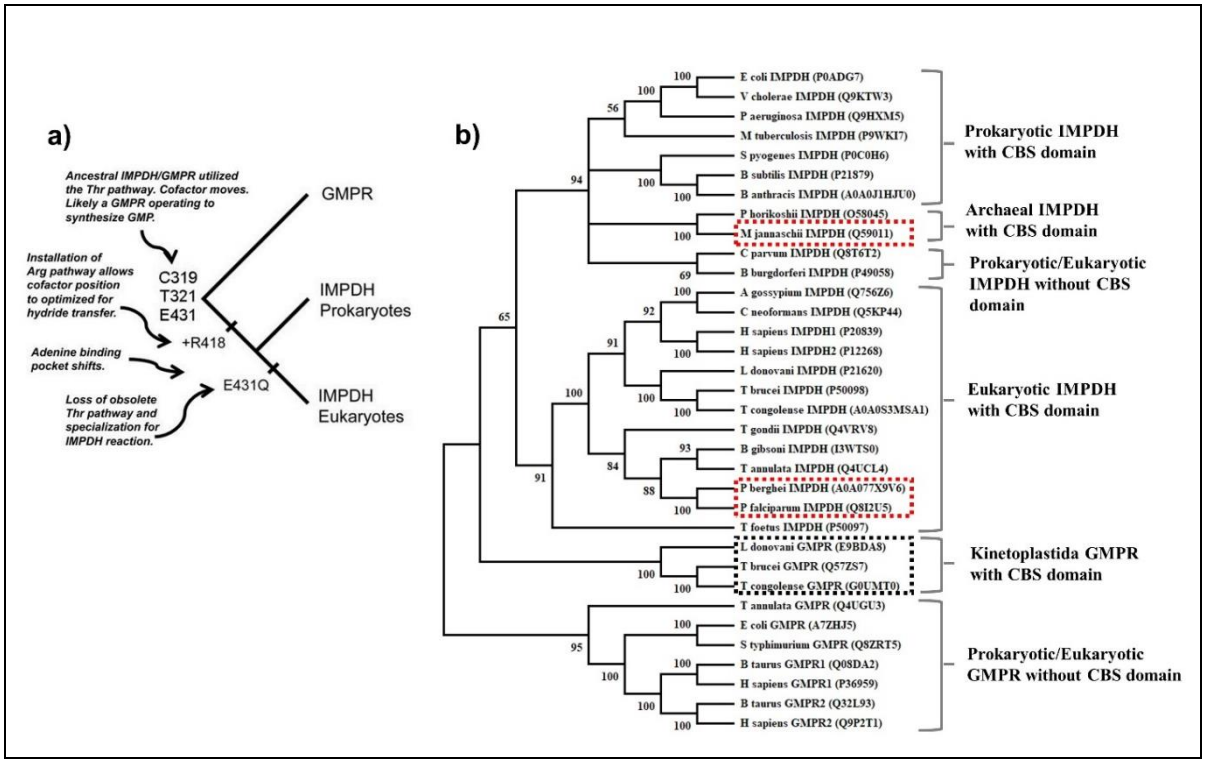

Figure 11. Evolutionary relationship of IMPDH/GMPR family of proteins. a) The evolutionary path for water activation *adapted from Hedstrom L, 2012 with copyright permission (refer to Appendix A). Presence of ancestral enzyme with Thr-Glu dyad for proton relay is followed by the acquisition of arginine that makes the former path obsolete as glutamate to glutamine substitutions are found to have no effect on catalysis.* ***b) Phylogenetic tree generated from the primary sequence of various IMPDHs and GMPRs****. The tree was constructed using the neighbor-joining method in the MEGA 5.2 software (Tamura K et al., 2011). Bootstrap replicate value cutoff as 50 % are shown at the branch points.*

1.6 Discrepancy in the annotation

The incidence of high similarity between GMPR and IMPDH at the primary sequence level leads to misannotation of the enzymes that are identified only by computational gene prediction methods. For example, predicted *L. major* GMPR sequence shares 30–41 % sequence identity with IMPDHs from humans, *E. coli*, and *B. burgdorferi*, but only 24–26 % sequence identity with the *E. coli* and human GMPRs indicating LmGMPR is closer in sequence to IMPDH than GMPR enzymes. All IMPDHs annotated to date share an identical motif "Y-x-G-x-G-S-x-x-A-x" within the mobile flap for IMP binding and residues tyrosine, glycine at indicated position stand invariant (Fig. 12) (Hedstrom L, 2009). Lack of IMPDH

activity in TbGMPR is hypothesized to be associated with the substitution of Tyr and second Gly of this motif to isoleucine and alanine (I398 and A402), respectively. However, tyrosine is often found substituted by an aromatic residue, phenylalanine, and glycine by a serine in other characterized GMPRs (Fig. 12). Lack of extensive structural and functional characterization of GMPRs and existence of high sequence identity among IMPDH and GMPR could lead to misannotation of these genes. Both GMP reductases and IMPDH enzymes contain the IMPDH/GMPR signature motif (identical residues in the catalytic loop) and insertion of CBS subdomain within the catalytic TIM barrel (Fig. 12). Inhibitors against IMPDH also are found to inhibit GMPR. Presence of Arg-Tyr dyad in the flap of IMPDH is reported to tolerate Tyr substitutions (Guillen Schlippe YV *et al*., 2004). Also, Tyr-Arg dyad of GMPR in *E. coli* and human enzymes stands unreliable for identification of a GMPR as it is not found in kinetoplastid GMPRs. Lastly, GMPRs are identified with the presence of glutamate at 431 position in *E. coli* enzyme and substitution with glutamine is associated with IMPDH. However, E289Q mutation in EcGMPR displayed a drop in activity but has not completely abolished it. Therefore, extending the features identified in a few enzymes as a generality cannot be relied upon with confidence and this aspect demands for further studies.

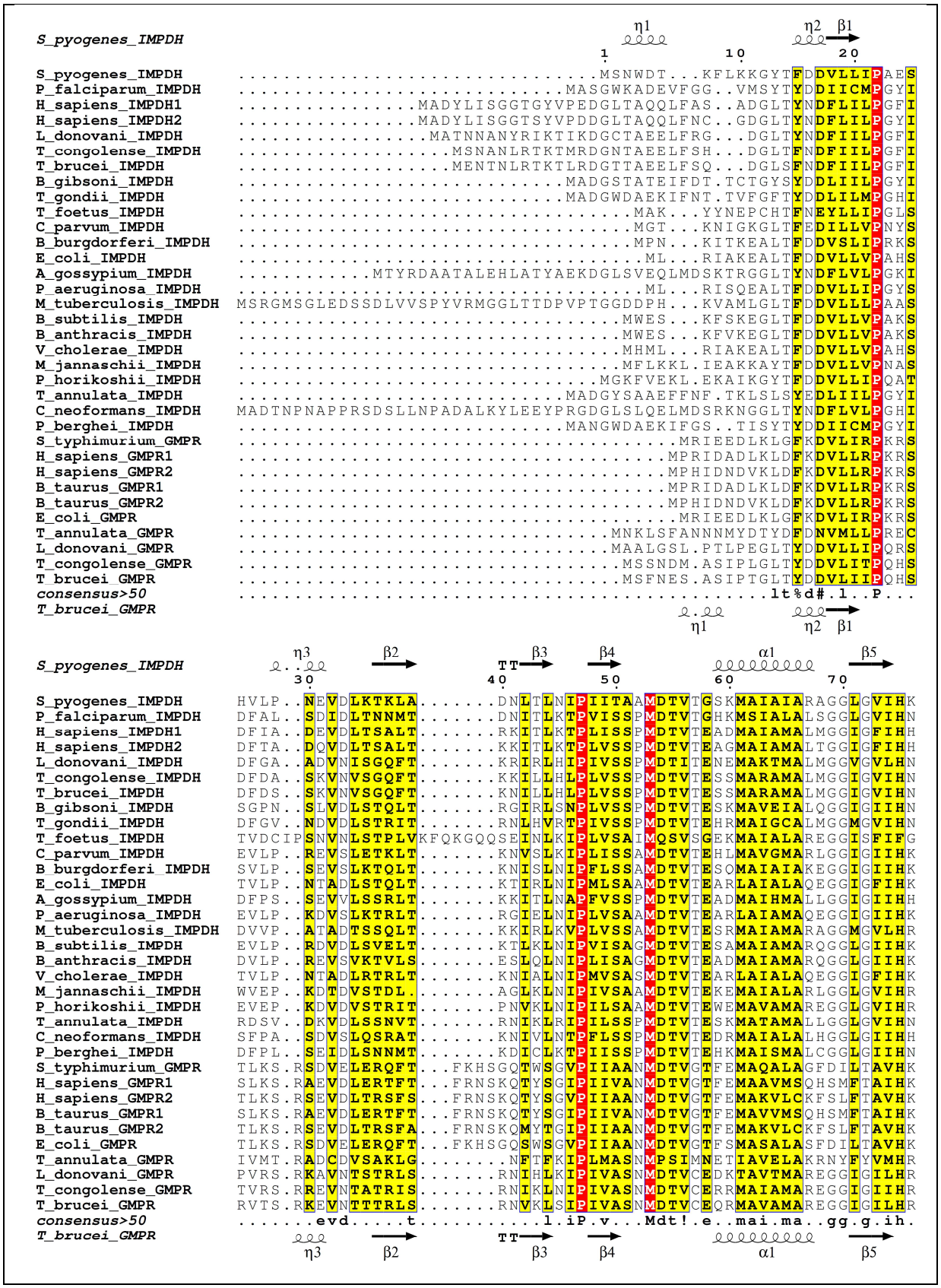
S_pyogenes_IMPDH
S_pyogenes_IMPDH
P_falciparum_IMPDH
H_sapiens_IMPDH1
H_sapiens_IMPDH2
L_donovani_IMPDH
T_congolense_IMPDH
T_brucei_IMPDH
B_gibsoni_IMPDH
T_gondii_IMPDH
T_foetus_IMPDH
C_parvum_IMPDH
B_burgdorferi_IMPDH
E_coli_IMPDH
A_gossypium_IMPDH
P_aeruginosa_IMPDH
M_tuberculosis_IMPDH
B_subtilis_IMPDH
B_anthracis_IMPDH
V_cholerae_IMPDH
M_jannaschii_IMPDH
P_horikoshii_IMPDH
T_annulata_IMPDH
C_neoformans_IMPDH
P_berghei_IMPDH
S_typhimurium_GMPR
H_sapiens_GMPR1
H_sapiens_GMPR2
B_taurus_GMPR1
B_taurus_GMPR2
E_coli_GMPR
T_annulata_GMPR
L_donovani_GMPR
T_congolense_GMPR
T_brucei_GMPR
consensus>50
T_brucei_GMPR
S_pyogenes_IMPDH
S_pyogenes_IMPDH
P_falciparum_IMPDH
H_sapiens_IMPDH1
H_sapiens_IMPDH2
L_donovani_IMPDH
T_congolense_IMPDH
T_brucei_IMPDH
B_gibsoni_IMPDH
T_gondii_IMPDH
T_foetus_IMPDH
C_parvum_IMPDH
B_burgdorferi_IMPDH
E_coli_IMPDH
A_gossypium_IMPDH
P_aeruginosa_IMPDH
M_tuberculosis_IMPDH
B_subtilis_IMPDH
B_anthracis_IMPDH
V_cholerae_IMPDH
M_jannaschii_IMPDH
P_horikoshii_IMPDH
T_annulata_IMPDH
C_neoformans_IMPDH
P_berghei_IMPDH
S_typhimurium_GMPR
H_sapiens_GMPR1
H_sapiens_GMPR2
B_taurus_GMPR1
B_taurus_GMPR2
E_coli_GMPR
T_annulata_GMPR
L_donovani_GMPR
T_congolense_GMPR
T_brucei_GMPR
consensus>50
T_brucei_GMPR

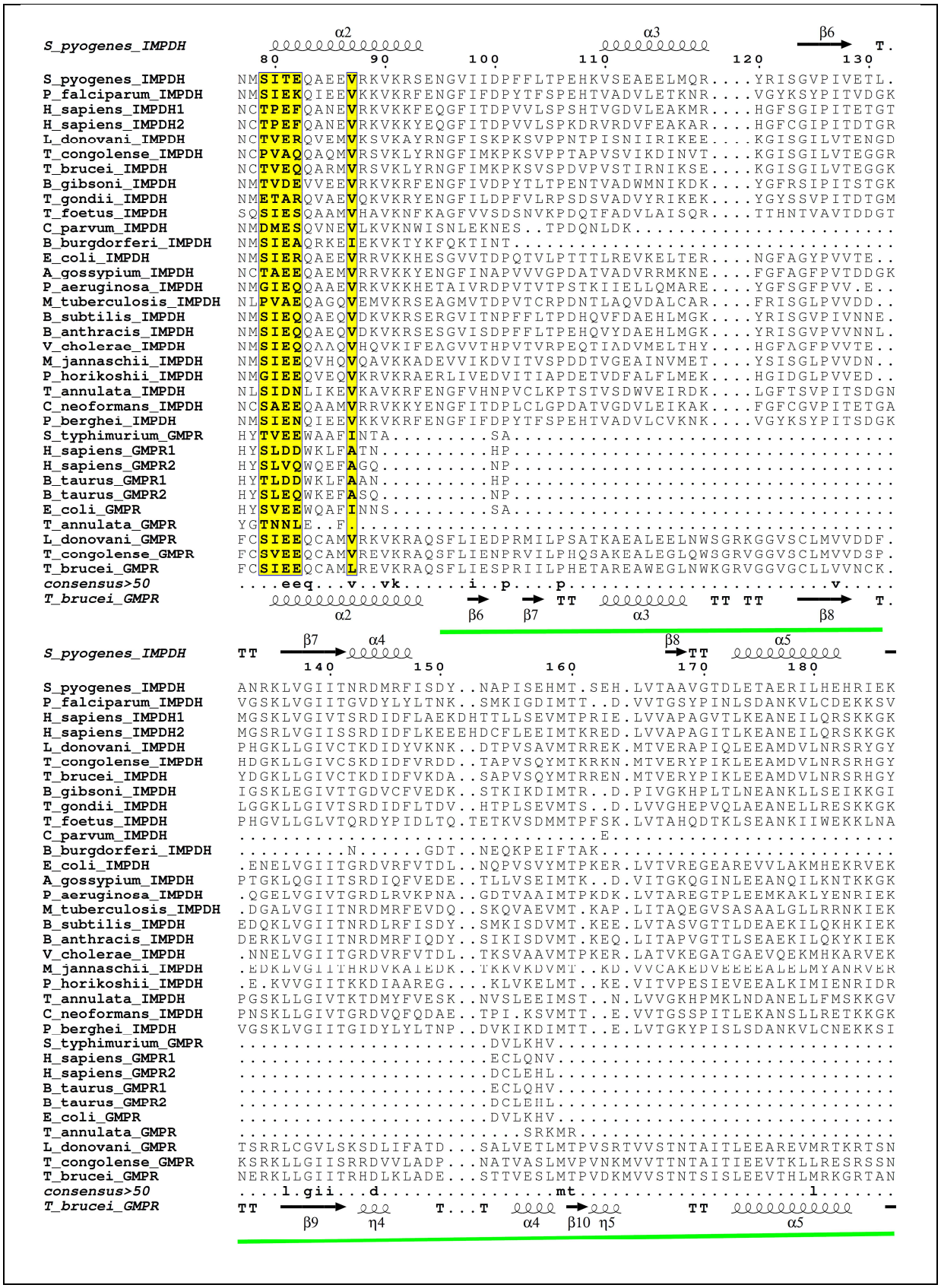
S_pyogenes_IMPDH
S_pyogenes_IMPDH
P_falciparum_IMPDH
H_sapiens_IMPDH1
H_sapiens_IMPDH2
L_donovani_IMPDH
T_congolense_IMPDH
T_brucei_IMPDH
B_gibsoni_IMPDH
T_gondii_IMPDH
T_foetus_IMPDH
C_parvum_IMPDH
B_burgdorferi_IMPDH
E_coli_IMPDH
A_gossypium_IMPDH
P_aeruginosa_IMPDH
M_tuberculosis_IMPDH
B_subtilis_IMPDH
B_anthracis_IMPDH
V_cholerae_IMPDH
M_jannaschii_IMPDH
P_horikoshii_IMPDH
T_annulata_IMPDH
C_neoformans_IMPDH
P_berghei_IMPDH
S_typhimurium_GMPR
H_sapiens_GMPR1
H_sapiens_GMPR2
B_taurus_GMPR1
B_taurus_GMPR2
E_coli_GMPR
T_annulata_GMPR
L_donovani_GMPR
T_congolense_GMPR
T_brucei_GMPR
consensus>50
T_brucei_GMPR
α2
α3
β6
β7
α4
β8
α5
β9
η4
α4
β10
η5
α5

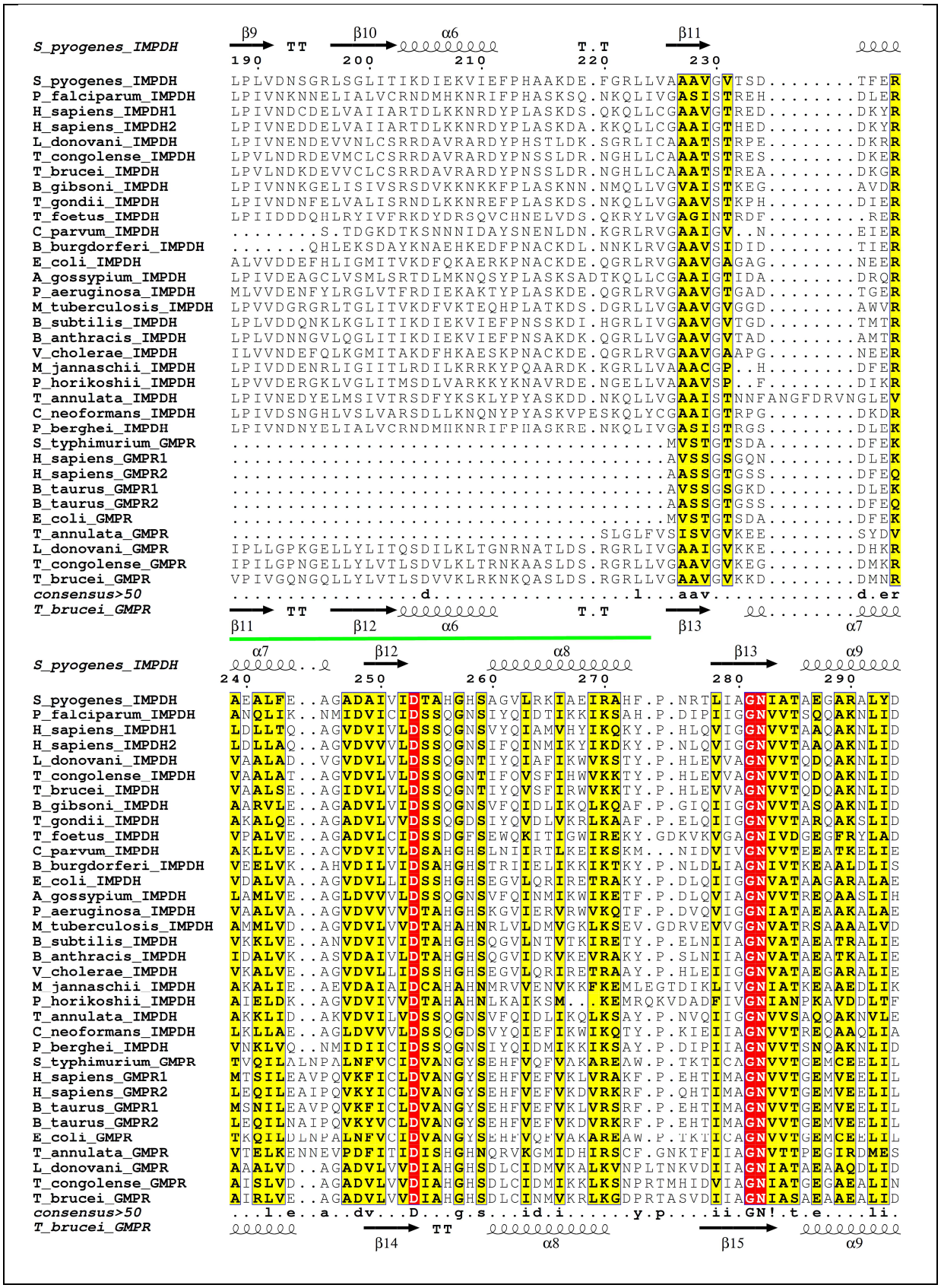
S_pyogenes_IMPDH
S_pyogenes_IMPDH
T_brucei_GMPR

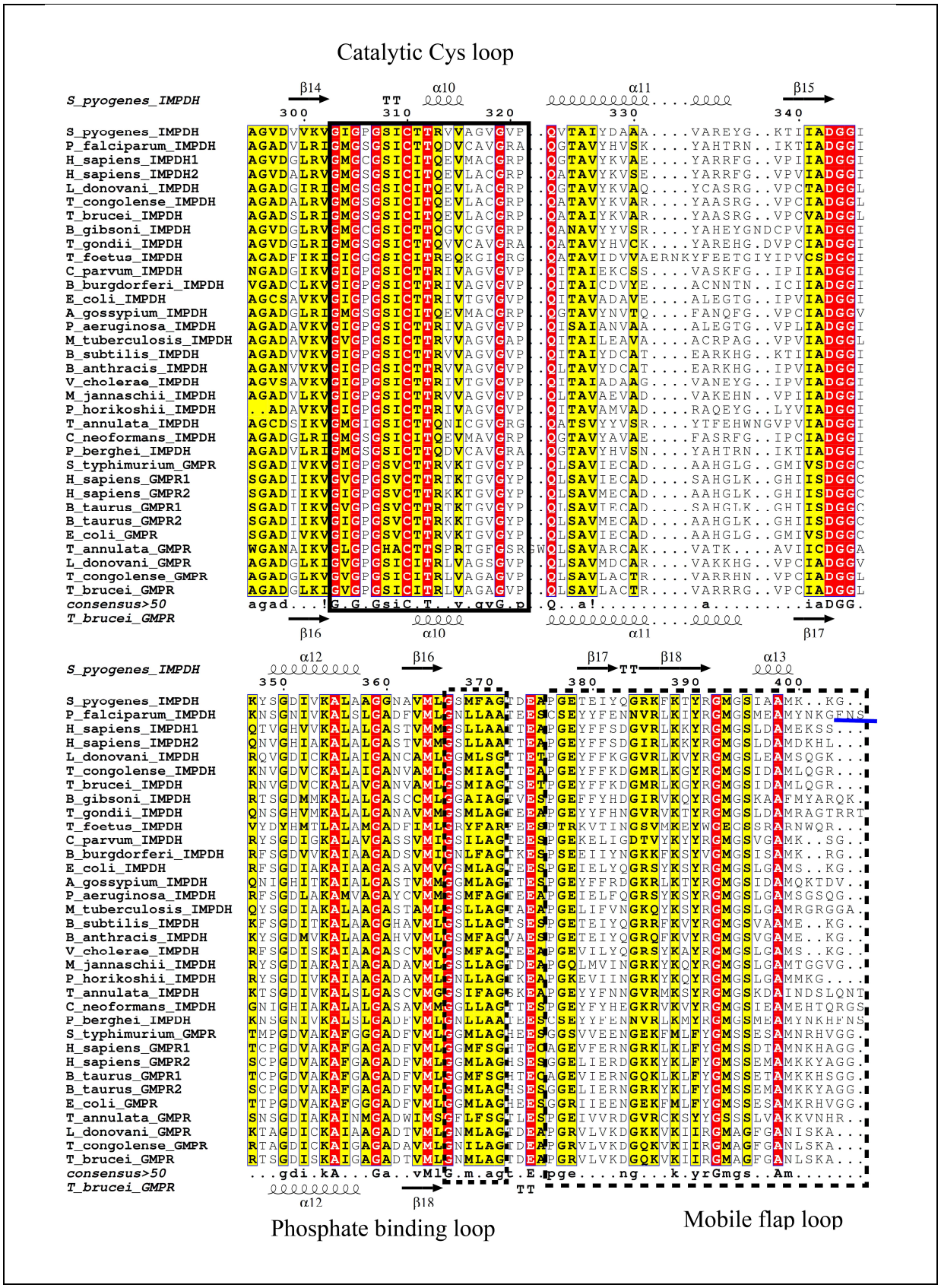
Catalytic Cys loop
Phosphate binding loop
Mobile flap loop

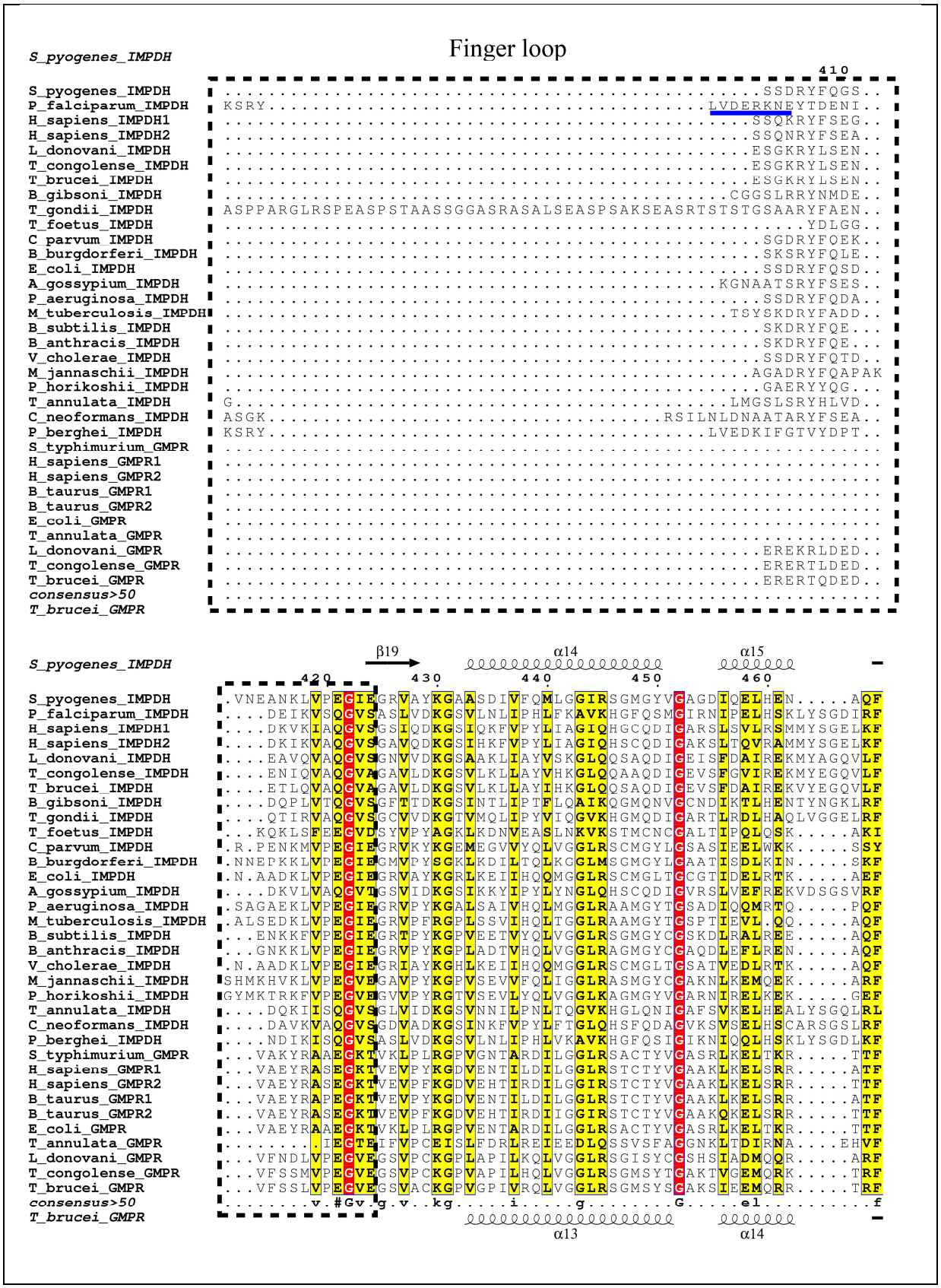
Finger loop
S_pyogenes_IMPDH
410
S_pyogenes_IMPDH
P_falciparum_IMPDH
H_sapiens_IMPDH1
H_sapiens_IMPDH2
L_donovani_IMPDH
T_congolense_IMPDH
T_brucei_IMPDH
B_gibsoni_IMPDH
T_gondii_IMPDH
T_foetus_IMPDH
C_parvum_IMPDH
B_burgdorferi_IMPDH
E_coli_IMPDH
A_gossypium_IMPDH
P_aeruginosa_IMPDH
M_tuberculosis_IMPDH
B_subtilis_IMPDH
B_anthracis_IMPDH
V_cholerae_IMPDH
M_jannaschii_IMPDH
P_horikoshii_IMPDH
T_annulata_IMPDH
C_neoformans_IMPDH
P_berghei_IMPDH
S_typhimurium_GMPR
H_sapiens_GMPR1
H_sapiens_GMPR2
B_taurus_GMPR1
B_taurus_GMPR2
E_coli_GMPR
T_annulata_GMPR
L_donovani_GMPR
T_congolense_GMPR
T_brucei_GMPR
consensus>50
T_brucei_GMPR
β19
α14
α15
S_pyogenes_IMPDH
420
430
440
450
460
α13
α14

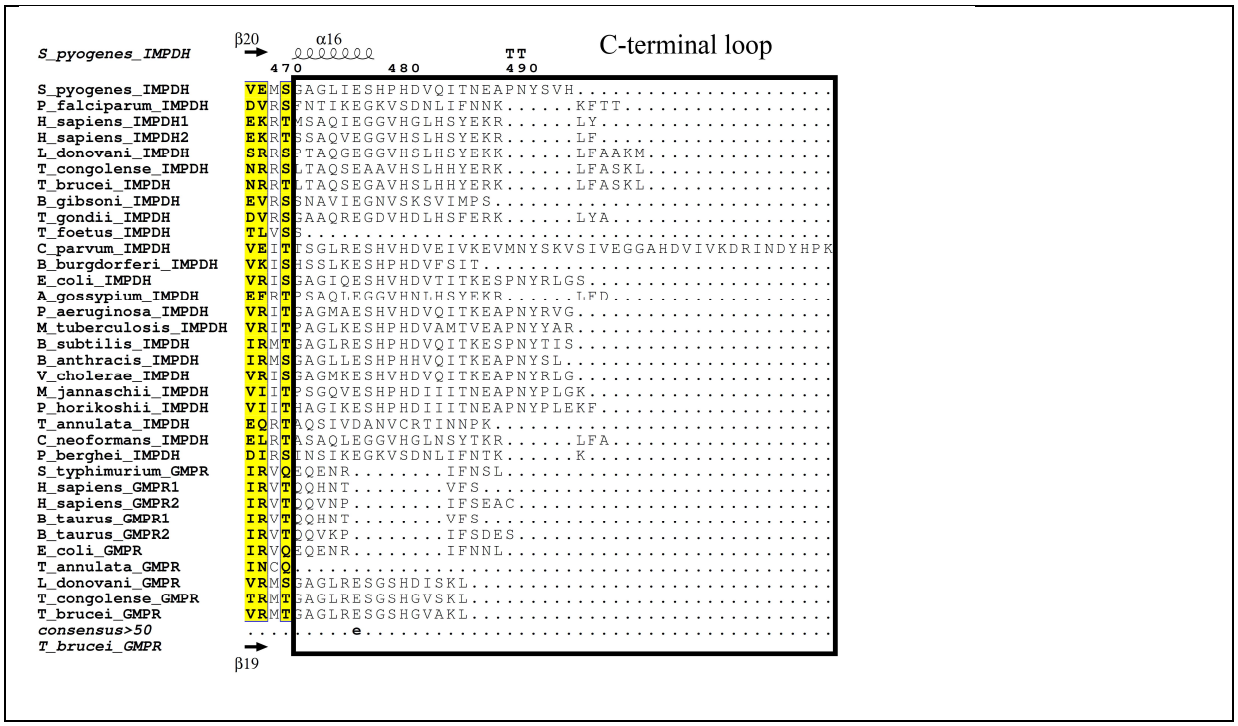

Figure 12. Multiple sequence alignment of IMPDH and GMPR from various organisms. *All the sequences were aligned with Clustal Omega (Sievers F et al., 2011; Sievers F and Higgins DG, 2018) and rendered using ESPRIPT (Robert X and Gouet P, 2014). The consensus of >50 was found across sequences analyzed. The secondary structure of IMPDH and GMPR from a prokaryote, Streptococcus pyogenes (PDB 1ZFJ) and a eukaryote, Trypanosoma brucei (PDB 5X8O) are shown at the top and bottom of the sequence alignment, respectively. α-helices and β-strands are rendered as large squiggles and arrows, respectively. TT and TTT correspond to beta and alpha turns, respectively. The red shaded regions indicate the strictly identical residues while residues highlighted in yellow indicate similarity among the sequences compared. The segments involved in catalysis are enclosed in black boxes which include catalytic cysteine loop, phosphate binding loop, finger loop, mobile flap loop, and the C-terminal loop.*

1.7 GMP biosynthesis in *Plasmodium falciparum* and *Methanocaldococcus jannaschii*

Guanine nucleotides are indispensable for cell viability. Besides being the precursors of nucleic acids (DNA and RNA), they also form the energy source (GTP) for translation and microtubule polymerization, implied in signal transduction, angiogenesis and axon guidance, for a variety of metabolites including tetrahydrobiopterin, GMP as a flavor enhancer, folates (vitamin B9) and riboflavin (vitamin B2) (Chong CR *et al*. 2006; Long H *et al*. 2006; Gross SS and Levi R, 1992; Ledesma-Amaro R *et al*. 2015; Cossins EA and Chen L,1997; Bacher A *et al*. 2000). Metabolic engineering of IMPDH gene from the fungus *A. gossypium* was found to significantly increase the yield of riboflavin (Buey RM *et al*., 2015). In general, there exist two ways of synthesizing purines, a *de novo* synthesis where the purine ring gets assembled sequentially from biosynthetic precursors of carbohydrate and amino acid metabolism and from ammonia and carbon dioxide (Zalkin H and Dixon JE, 1992). Recycling of preformed nucleobases, nucleosides, and nucleotides constitutes the salvage pathway (Murray AW, 1971).

Plasmodium falciparum is the most lethal among the five *Plasmodium* species that cause human malaria. Malaria has a massive impact on human health; it is the world's second biggest killer after tuberculosis. In 2016, an estimated 216 million cases of malaria occurred worldwide. There were an estimated 445,000 deaths from malaria globally (WHO report, 2017). Despite the availability of antimalarial drugs, the widespread emergence of drug-resistant parasites necessitates a quest for new therapies. Structure- and mechanism-based combinatorial approach for drug design has proved highly fruitful. The purine salvage pathway of *P. falciparum* is a novel target for antimalarials, as the parasite lacks the *de novo*

purine biosynthetic pathway (Gardner MJ *et al*., 2002). Hypoxanthine is salvaged by hypoxanthine guanine (xanthine) phosphoribosyl transferase (HG(X)PRT) to form inosine 5'-monophosphate which then branches out into either formation of guanosine 5'-monophosphate (GMP) or adenosine 5'-monophosphate (AMP). IMP, on one hand, is converted to xanthine 5'-monophosphate (XMP) and GMP by coordinated function of inosine 5'-monophosphate dehydrogenase (IMPDH) followed by guanosine 5'-monophosphate synthetase (GMPS) and on the other arm by the concerted action of adenylosuccinate synthetase (ADSS) and adenylosuccinate lyase (ASL) to form AMP (Fig. 13). All the enzymes in the purine biosynthesis pathway from the protozoan parasite have been well characterized from our laboratory as well as others (McConkey GA, 2000; Bhat JY *et al*., 2008; Raman J *et al*., 2004; Bulusu V *et al*., 2009) except PF3D7_0920800 which is annotated as IMPDH based on sequence homology. PfIMPDH is one of the essential enzymes present in the parasite as MPA was found to be lethal for parasite survival (Veletzky L *et al*., 2014) while evidence for expression is provided from RNA sequencing and proteomic studies by various groups in *Plasmodium* database (PlasmoDB) (Bahl A *et al*., 2003).

Genome analysis of *M. jannaschii* reveals that at the molecular level archaea more closely resemble eukaryotes (Bult CJ *et al.,* 1996). The archaeal genome is about 70 % AT-rich while that of the protozoan parasite *P. falciparum* is about 80 % (Bult CJ *et al.,* 1996; Gardner MJ *et al*., 2002). Purine biosynthesis in *M. jannaschii* can occur through the *de novo* route (Bult CJ et al., 1996; Selkov E *et al*., 1997; Ownby K *et al*., 2005; Brown AM *et al*., 2011) or by salvage of adenine and guanine (Fig. 13) (Armenta-Medina D *et al*., 2014; Miller DV *et al*., 2016). MjADSS and MjGMPS have been well characterized earlier from our laboratory (Mehrotra S and Balaram H, 2007; Ali R *et al*., 2012; Ali R *et al*., 2013). MjASL activity has been confirmed while detailed characterization is not available (White RH, 2011). MJ1616 gene of *M. jannaschii* is annotated as IMPDH based on sequence similarity while no report on enzyme activity exists. MjIMPDH from the hyperthermophilic archaeon *M. jannaschii* is similar in polypeptide length (496 amino acids) to that of eukaryotic IMPDH including human (Isoform I and II), *Tritrichomonas foetus* and *P. falciparum* which are 514,

503 and 510, respectively and is 47 % similar and 35 % identical to the *P. falciparum* IMPDH (Fig. 12).

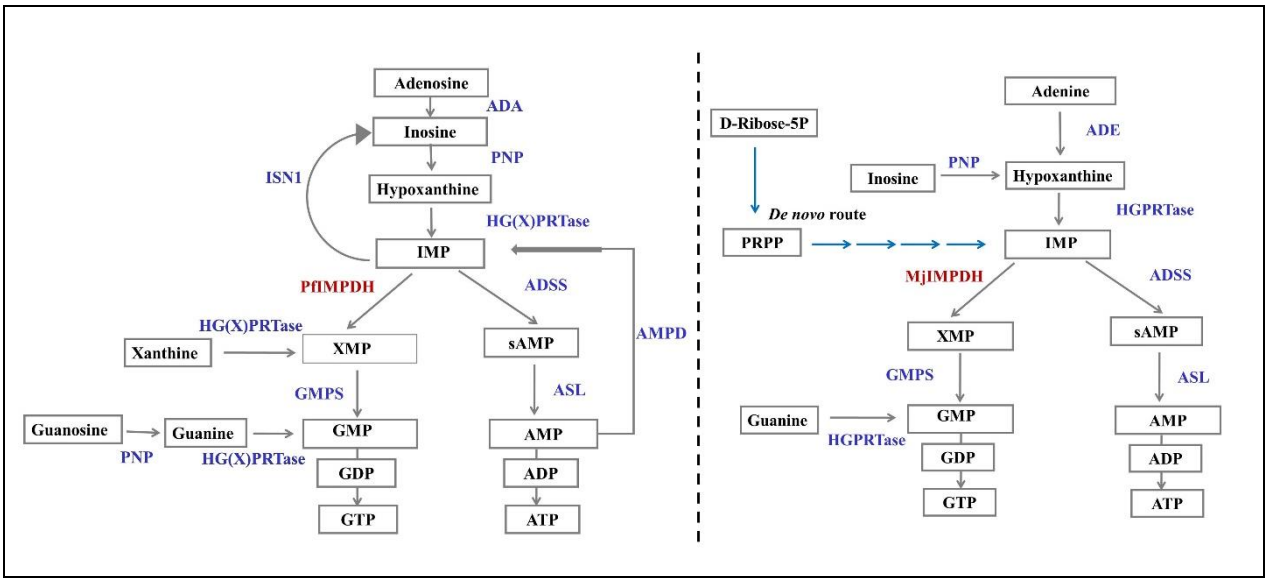

Figure 13. Purine nucleotide biosynthesis in P. falciparum (left) and M. jannaschii (right). *Purine salvage alone operates in the protozoan parasite while both de novo and salvage routes are found in the archaeon. All the enzymes involved in purine nucleotide biosynthesis are indicated in blue except the enzymes in the study are highlighted in red. PF3D7_0920800 and MJ1616 based on sequence homology are inferred as IMPDH. Left panel -conversion of adenosine to inosine followed by inosine to hypoxanthine occurs by the concerted action of adenosine deaminase (ADA) and purine nucleoside phosphorylase (PNP), respectively. Hypoxanthine is further acted upon by hypoxanthine guanine (xanthine) phosphoribosyltransferase (HG(X)PRTase) to yield inosine 5'-monophosphate (IMP). IMP is further acted upon by the downstream enzymes to yield adenosine 5'-monophosphate (AMP) and guanosine 5'-monophosphate (GMP) or could be broken down to inosine by the enzyme IMP-specific nucleotidase (ISN1). IMP dehydrogenase (IMPDH) and GMP synthetase (GMPS) on one arm yield GMP while on the other by the concerted action of adenylosuccinate synthetase (ADSS) and adenylosuccinate lyase (ASL) forms AMP. AMP is deaminated to IMP by the enzyme AMP deaminase (AMPD). Salvage of guanosine to guanine occurs by the action of PNP. HG(X)PRTase could directly phosphoribosylate guanine and xanthine to yield GMP and XMP, respectively. Right panel -Adenine is salvaged to form hypoxanthine by the action of adenine deaminase (ADE). The conversion of D-ribose-5-phosphate to PRPP includes the first step in the de novo path and subsequent steps are indicated in blue arrows to yield IMP. Subsequent steps are similar to that of parasite nucleotide metabolism in the left panel.*

1.8 Focus of the current study

We have examined the gene PF3D7_0920800 annotated as IMPDH from the mesophilic malarial parasite *Plasmodium falciparum* for its functionality. MJ1616 gene from a hyperthermophilic archaeon, *Methanocaldococcus jannaschii* is established as a bonafide IMPDH. Experimental work performed is presented in four chapters. Chapter 2 highlights the *in vivo* studies on PfIMPDH which includes an examination of cellular localization in the parasite during erythrocytic stages of the life cycle and the assessment of function through complementation assay using *E. coli* and *S. cerevisiae* as expression systems. Chapter 3 summarizes the various efforts employed in obtaining recombinant PfIMPDH protein in soluble form and the associated difficulties. Chapter 4 describes the biophysical parameters of the CBS subdomain from PfIMPDH. Chapter 5 includes biochemical and kinetic characterization of MjIMPDH. Lastly, a note on conclusions from the current study and future directions are indicated.

Chapter 2. Subcellular localization and functional complementation assay of PfIMPDH

Examination of cellular localization and functionality of the gene PF3D7_0920800 annotated as inosine 5'-monophosphate dehydrogenase (IMPDH) from the parasite Plasmodium falciparum is discussed in this chapter. Cytoplasmic and partial nuclear localization of the endogenous protein within the parasite was observed through indirect immunofluorescence microscopy using in-house generated mouse anti-PfIMPDH antibody. The generation of impdh deletion strain of E. coli, ΔguaB^{K}(DE3) along with genetic complementation assay and protein expression profile in bacterial and yeast systems is also presented. Expression of PfIMPDH in ΔguaB^{K}(DE3) strain did not functionally complement the growth deficiency on M9 minimal medium. The codon harmonized PfIMPDH gene sequence for optimal expression in E. coli also could not rescue the growth of ΔguaB^{K}(DE3) strain in minimal medium. Lastly, the functional capability of PfIMPDH enzyme to catalyze GMP reductase reaction was also examined through genetic complementation assay using gmpr deletion strain of E. coli (H1174$^{\Delta guaC}$).

2.1 Introduction

PF3D7_0920800 (previously referred as PFI1020c) from the human malarial parasite *P. falciparum*, strain 3D7, is annotated as inosine 5'-monophosphate dehydrogenase (IMPDH) in *Plasmodium* database (PlasmoDB) (Bahl A *et al*., 2003; Aurrecoechea C *et al.*, 2009). Protein inferred from homology is found to have cystathionine-beta-synthase domain (CBS) insertion within the catalytic core and predicted to be involved in the oxidation-reduction process in the purine nucleotide metabolism. It is an intron-less protein-coding gene present on chromosome 9 with a transcript length of 1533 bp and protein length of 510 amino acid residues (Hall N *et al*., 2002). No signal peptide (DeepLoc-1.0 server) (Almagro Armenteros JJ *et al*., 2017) or transmembrane regions are predicted (TMHMM server v. 2.0) (Krogh A *et al*., 2001). The functional interactome of *P. falciparum*, PlasmoMap (Date SV & Stoeckert CJ Jr, 2006) predicts top 3 over-represented gene ontology (GO) (out of 191 total)

and Kyoto Encyclopedia of Genes and Genomes (KEGG) (out of 21 total) categories of proteins linked to PfIMPDH that includes RNA metabolism, RNA processing, transcription and RNA polymerase, aminoacyl-tRNA biosynthesis, pentose phosphate pathway, respectively.

2.1.1 PfIMPDH as a drug target

Mycophenolic acid (MPA) and bredinin, known inhibitors of IMPDH were found to inhibit *Plasmodium growth* (Webster HK and Whaun JM, 1982; Queen SA *et al*., 1988; Queen SA *et al*., 1990; Veletzky L *et al*., 2014). Presence of the PfIMPDH gene transcript was observed in multiple studies focused on data mining of the transcriptome and has been identified as a potential drug target (Yeh I and Altman RB, 2006; Bozdech Z, Ginsburg H, 2005; Bozdech Z and Ginsburg H, 2004). Computational analysis of the metabolism of *Plasmodium falciparum* and knock out simulations also predicted PfIMPDH as a potential antimalarial drug target (Huthmacher C *et al*., 2010). Genetic modification attempt of IMPDH was not successful in the rodent malarial parasite, *P. berghei* (Bushell E *et al*., 2017). Essentiality of *P. falciparum* gene in the asexual stage of the parasite life cycle is established by high throughput *piggyBac* transposon insertional mutagenesis (Zhang M *et al*., 2018).

2.1.2 Evidence for expression

Evidence for expression comes from microarray, RNA seq, and proteomics data. Microarray studies available from blood stages, gametocytes, invasion pathway knockouts, Sir2 knockouts and different clonal strains found transcripts for PfIMPDH gene (Bozdech Z *et al*., 2003; Linas M *et al*., 2006; Le Roch KG *et al*., 2003; Young JA *et al*., 2005; Pelle KG *et al*., 2015; Stubbs J *et al*., 2005; Jiang H *et al*., 2008; Tonkin CJ *et al*., 2009; Rovira-Graells N *et al*., 2012). RNA sequencing data is available from various studies focused on blood stages, gametocytes, oocyst and sporozoite (mosquito stages) (Lasonder E *et al*., 2016; Otto TD *et al*., 2010; Bartfai R *et al*., 2010; Vignali M *et al*., 2011; Lopez-barragan MJ *et al*., 2011; Zanghi G *et al*., 2018). Transcriptome and translatome of the asexual cell cycle and ribosome profiling of blood stages were also determined by RNA sequencing (Bunnik EM *et al*., 2013; Caro F *et al*., 2014).

A total proteomic view of the parasite was reported by Florens L *et al*., 2002. Thereafter, multiple mass spectrometry-based proteomic studies on blood stage (Treeck M *et al*., 2011; Pease BN *et al*., 2013), gametocyte (Silvestrini F *et al*., 2010; Lasonder E *et al*., 2016), surface proteins of infected erythrocytes (Florens L *et al*., 2004) and salivary gland sporozoites (Lasonder E *et al*., 2008; Swearingen KE *et al*., 2016; Swearingen KE *et al*., 2017; El-Manzalawy Y *et al*., 2016; Lindner SE *et al*., 2013) have identified peptides matching PfIMPDH protein. Presence of PfIMPDH in both cytoplasmic and nuclear fraction of the blood stage parasites was reported (Oehring SC *et al*., 2012). Study on clinical proteomics from malaria-infected patient samples also has identified the presence of peptides from PfIMPDH (Acharya P *et al*., 2009). Protein microarrays hybridized with plasma samples from human malaria patients identified PfIMPDH as one of the protein targets for antibodies found in response to *P. falciparum* infection (Crompton PD *et al*., 2010).

2.1.3 Post-translational modifications

Phosphorylation of S399 is reported from phosphoproteome analysis by various research groups (Treeck M *et al*., 2011; Solyakov L *et al*., 2011; Lasonder E *et al*., 2012; Pease BN *et al*., 2013; Collins MO *et al*., 2014; Lasonder E *et al*., 2015). Palmitome of *Plasmodium falciparum* was examined and modified peptides corresponding to PfIMPDH is reported (Jones ML *et al*., 2012). Peptides corresponding to PfIMPDH with S-glutathionylation and S-nitrosothiol modifications were also observed in a total proteome study (Kehr S *et al*., 2011; Wang L *et al*., 2014). It was recently identified as one among the parasite proteins that undergo lysine acetylation (Cobbold SA *et al*., 2016). Further confirmatory validation and significance of these modifications in the cellular context are yet to be understood.

2.1.4 Genetic variations

A total of 14 single nucleotide polymorphisms (SNPs) have been detected in about ~200 different isolates of *P. falciparum* 3D7 strain through genome sequencing studies, of which, 5 are non-synonymous (results in amino acid change), and 9 are synonymous (no amino acid change). The gene sequence used in the current study was confirmed to be

identical to the PlasmoDB entry except for the presence of a non-synonymous SNP at nucleotide position 851 and a synonymous SNP at 231 (Table 1).

Table 1. Single nucleotide polymorphisms identified in the gene PfIMPDH through genome sequencing studies are retrieved from PlasmoDB. Non-synonymous SNP leads to amino acid change while synonymous SNP has no effect. CDS refers to coding sequencing. A, T, G, C constitute the nucleobases. The frequency of occurrence for major and minor alleles is provided in parenthesis. Standard single letter code for amino acid residues encoded as a result of either major or minor allele is specified. Highlighted in red are the SNPs found in PfIMPDH gene sequence used in the current study.

Phenotype	Position in protein	Position in CDS	Major allele	Minor allele	Major residue	Minor residue
Non-synonymous	496	1488	A (1)	T (0)	K	N
	471	1411	C (1)	G (0)	P	A
	284	**851**	**C (0.9)**	G (0.1)	**A**	G
	400	1200	G (0.99)	T (0)	M	I
	6	16	A (0.99)	G (0.01)	K	E
Synonymous	413	1239	A (1)	G (0)	R	
	408	1224	C (1)	T (0)	F	
	389	1167	C (1)	T (0)	V	
	306	918	T (1)	C (0)	I	
	132	396	A (1)	G (0)	T	
	123	369	T (1)	C (0)	R	
	77	**231**	G (0.98)	**A (0.02)**	**V**	
	71	213	G (0.99)	A (0.01)	L	
	58	174	T (1)	C (0)	D	

2.1.5 Gene annotation

PF3D7_0920800 is annotated as inosine 5'-monophosphate dehydrogenase based on sequence homology (PlasmoDB). *P. falciparum* enzyme shares ~50 % identity with eukaryotic IMPDHs and ~35 % with the archaeal and prokaryotic counterparts (Table 2). IMPDH together with guanosine 5'-monophosphate reductase (GMPR) constitutes a family

A very few GMPRs are characterized to date and share an identity of ~ 30 % with PfIMPDH protein (Table 2). Presence of the CBS domain and mycophenolic acid (MPA) binding site were believed to be the major differentiating factors of IMPDH from a GMPR (Hedstrom L, 2012). However, identification of *L. donovani* GMPR (Smith S *et al.,* 2016) followed by characterization of *T. brucei* and *T. congolense* GMPR carrying CBS domains and also inhibited by MPA (Bessho T *et al.,* 2016; Sarwono AEY *et al.,* 2017) strongly suggest the possibility of misannotation due to the presence of identical catalytic site residues, substantial sequence similarity and structural features. *In silico* sequence analysis and *in vitro* protein expression studies of PfIMPDH are presented in Chapter 3.

Table 2. Identity matrix of protein sequences among various IMP dehydrogenases and GMP reductases. Multiple sequence alignment was performed, and percent identity was calculated using Clustal Omega (Sievers F *et al*., 2011; Sievers F and Higgins DG, 2017).

Source	PfIMPDH *vs.* GMPR		PfIMPDH *vs.* IMPDH	
	FL	**ΔCBS**	**FL**	**ΔCBS**
E. coli	29	29	35	37
Human I	27	28	50	51
Human II	27	27	49	51
Bovine I	27	27	50	51
Bovine II	27	28	50	51
****L. donovani***	32	34	43	47
****T. brucei***	31	32	33	33
****T. congolense***	33	34	34	34

*Percent identity of PfIMPDH with other IMPDHs and GMPRs is indicated. FL- full-length protein, Δ*CBS*- core catalytic domain without CBS domain. * GMPR from these organisms has a CBS subdomain.*

2.2 Chemicals and reagents

Restriction enzymes, Phusion DNA polymerase, and T4 DNA ligase were from NEB and were used according to the manufacturer's instructions. Primers were custom synthesized

at Sigma-Aldrich, India. All chemical reagents were of high quality and obtained from Sigma-Aldrich or Merck India. Media components were from HiMedia Laboratories, India. Expression plasmid carrying the gene for *T. foetus* IMPDH, pTf1 was a kind gift from Prof. Hedstrom L, Brandies University, USA. DY891 strain of yeast with deletion of all four isoforms of IMPDH, was a generous gift obtained from Prof. Reines D, Emory state university, USA. pFCENv2 an episomally maintained centromeric plasmid expressing GFP was a generous gift from Dr. Iwanaga S, Mie University, Japan. The H1174 strain of *E. coli* was procured from the Coli genetic stock center, USA.

2.3 Experimental procedure

2.3.1 Purification of PfIMPDH under denaturing conditions

The inclusion bodies of PfIMPDH obtained after the lysis were solubilized in buffer containing 6 M guanidine hydrochloride (GdnHCl) followed by Ni-NTA affinity chromatography. The bound protein was washed with lysis buffer and eluted using 0.1 M EDTA in 6 M GdnHCl buffer. The eluate was ethanol precipitated and separated on 12 % SDS-PAGE, protein band cut from the gel and the gel piece was minced into fine pieces. This was subjected to electro-elution using 25 mM Tris HCl, 192 mM glycine, 0.1 % SDS (SDS-PAGE buffer), followed by electrodialysis using 15 mM ammonium bicarbonate buffer containing 0.0125 % SDS. The obtained sample was lyophilized, resuspended in 1X PBS and quantified by Coomassie-stained SDS-PAGE.

2.3.2 Antibody generation in mice

Electroeluted recombinant PfIMPDH protein was used as an antigen to immunize BALB/C Mice to generate antibodies. The immunization schedule was as follows – pre-immune serum collection on day 0, primary injection on day 1 (30 µg antigen with Freund's complete adjuvant), 1st booster on day 25 (30 µg antigen with Freund's incomplete adjuvant), 2nd booster on day 40 (30 µg antigen with Freund's incomplete adjuvant), 3rd booster on day 55 (30 µg antigen with Freund's incomplete adjuvant), test bleed on day 61, and major bleed on day 62. Blood collected from the mouse was allowed to clot overnight at 4 ℃. Later it was centrifuged and the supernatant consisting of antiserum was collected and stored in aliquots at -20 ℃.

2.3.3 Determination of antibody titer

2 µg of antigen was spotted on the nitrocellulose membrane and allowed to dry for 15 min. The nitrocellulose membrane was blocked with 5 % skimmed milk in 1X PBS for 1 h on a rocker at room temperature. Primary antibody was added and further incubated on a rocker for 1 h at room temperature. The blots were washed for 15 min in 1X PBS containing 0.1 % Tween 20. 5 % skimmed milk containing 1:4500 dilution of secondary antibody was added and kept on a rocker for 1 h at room temperature. Blots were again washed for 15 min in 1X PBS containing 0.1 % Tween 20. Blots were developed using coloring reagent aminoethylcarbazole.

2.3.4 Antibody purification

PfIMPDH was purified from the inclusion bodies in denaturating conditions (6 M GdnHCl buffer) and resolved by electrophoresis on a 12 % polyacrylamide gel, which was then electroblotted onto PVDF membrane using semi-dry transfer apparatus (Bio-Rad Laboratories, USA). Antiserum of mice was diluted 2-fold in 1X PBS. The diluted antiserum was kept for binding with the electroblotted PVDF membrane at 4 ˚C with continuous tumbling overnight. The unbound antiserum was removed, and the membrane was washed with 1X PBS followed by antibody elution using 0.2 M glycine, pH 2.8. The fractions were immediately neutralized with 20 mM Tris HCl, pH 8.5. The protein concentration of eluates was estimated by the method of Bradford (Bradford MM, 1976). PVDF blot was regenerated by washing with low pH and high pH wash buffer (50 mM Glycine pH 3.5, 1 M NaCl and 50 mM Tris HCl, pH 8.0, 1 M NaCl) alternately for four times and was stored in 1X PBS containing 0.01 % sodium azide at 4 ˚C.

2.3.5 Parasite culture maintenance

O+ve blood was collected from volunteers and stored in the acid-citrate-dextrose solution (anticoagulant) at 4℃ overnight. Plasma was separated and discarded. The erythrocytes were washed with 1X PBS two times, followed by a wash with incomplete RPMI medium containing 25 mM HEPES and stored as 50 % hematocrit in the same medium containing gentamycin 2.5 µg mL^{-1}. Parasites were grown at 37 ℃ in complete RPMI medium (20 mM glucose, 0.2 % sodium bicarbonate, 0.5 % Albumax and 50 µM

hypoxanthine) with hematocrit at 5 % under micro-aerophilic conditions using a candle-jar setup. Parasitemia was checked regularly by making Giemsa stained smears. 5-10 % parasitemia was maintained and media change was given every day.

2.3.6 Isolation of erythrocyte-free parasites

Treatment of infected RBC with saponin, a mild detergent, renders the erythrocyte and parasitophorous vacuolar membrane permeable to macromolecules but leaves the parasite plasma membrane intact (Saliba KJ *et al.*, 1998). Parasites were isolated from the host erythrocytes by treating parasitized erythrocytes with saponin following the procedure reported earlier (Hsiao LL *et al*., 1991) with slight modification in the conditions. The parasitized culture was centrifuged at 2000g for 10 min and the spent medium was removed. To one volume of cell pellet, two volumes of 0.15 % saponin solution in 1X PBS was added. Components were mixed gently and incubated at room temperature for 5 min. The culture was centrifuged at 2000g for 40 min and the supernatant was removed. The pellet containing the parasites were washed twice with 1X PBS, flash frozen in liquid nitrogen and stored at -80 ˚C.

2.3.7 Western detection

Lysate of saponin-released parasites from 10 ml of culture was separated on 12 % SDS-PAGE and transferred on to PVDF membrane pre-activated in 100 % methanol for 2 min. The transfer was done for 1 h at 50 V and 400 mA. The success of transfer was checked by staining the membrane with Ponceau S dye for 5 min. The membrane was washed extensively to remove the stain followed by incubation with 5 % skimmed milk in 1X PBS for 1 h at room temperature. Thereafter the membrane was washed with PBST (phosphate buffered saline with 0.1 % Tween20) and incubated with the primary antibody, anti-PfIMPDH raised in mice (used at 1:2500 dilution) for 1 h at room temperature. The membrane was washed with PBST to remove excess unbound primary antibody and then incubated with secondary antibody anti-mouse IgG raised in goat (HRP conjugated from Sigma Chemical Co., used at 1:4500 dilution) for 1 h at room temperature. This was then developed using the coloring reagent aminoethylcarbazole.

2.3.8 Indirect immunofluorescence

0.5 ml of parasite culture was washed with 1X PBS and fixed with 4 % paraformaldehyde and 0.0075 % glutaraldehyde for 30 min at room temperature. Following a wash with 1X PBS, the culture was permeabilized with 0.08 % TritonX-100 in 1X PBS for 9 min. The cells were again washed with 1X PBS and blocked with 3 % BSA in 1X PBS for 1 h at room temperature with continuous tumbling. Primary antibody at a dilution of 1:200 in 3 % BSA in 1X PBS was added to the cells and incubated for 1 h at room temperature. After a thorough wash with 1X PBS, secondary antibody at a dilution of 1:500 in 3 % BSA in 1X PBS was added and incubated for 1 h at room temperature. This was again followed by an extensive wash with 1X PBS. Thereafter, DAPI (1 μg ml^{-1}) was added and incubated for 15 min in order to stain the parasite nucleus. Cells were resuspended in 70 % glycerol after extensive wash with 1X PBS. Cells were mounted on a glass slide using the poly L-lysine coated coverslips. They were sealed using transparent nail polish and stored at 4 °C without exposing to light. Confocal images were acquired on an LSM 510 META microscope. Stack mode with a stack size of 0.38 μm and multibeam splitter, HFT KP 700/488 was used. DAPI was excited at 358 nm and visualized at 461 nm and the secondary antibody conjugated to Alexa 488 fluorophore was excited at 488 nm and emission imaged at 525 nm.

2.3.9 Episomal expression of GFP-tagged PfIMPDH

PfIMPDH gene was PCR amplified with primers having *AvrII* and *KpnI* restriction sites (Table 3) and the pGlux plasmid (Tran PN *et al*., 2014) was restriction digested with *KpnI* and *AflII* to release a fragment of DNA bearing GFP. The ligation reaction was set up with PCR amplified PfIMPDH and the released GFP fragment. Second PCR with PfIMPDH forward primer and GFP specific reverse primer was carried out on the ligated product to amplify PfIMPDH-GFP fusion (Table 3). Thus, obtained PfIMPDH-GFP amplicon and the PFCENv2 vector was double digested with *AvrII* and *AflII* and ligated to obtain the GFP-tagged IMPDH construct. The clone was confirmed by DNA sequencing.

Table 3. Primers used to introduce a C-terminal GFP tag.

S. No.	Primer	Sequence
1)	Pf_For	5'CTACGAGCTCCCTAGGATGGCTAGCGGATGGAAAGC3'
2)	Pf_Rev	5'CCGCGGTACCTGTAGTAAACTTTTTGTTGTTGAATATTAAATTATCACT3'
3)	GFP_Rev	5'TCGCCTTAAGTTATTTGTATAGTTCATCCATGCCATGTG3'

2.3.10 Transfection of *P. falciparum*

Parasites were synchronized with 5 % sorbitol according to a standard protocol (Lambros C and Vanderberg JP, 1979) and 70 % percoll was used to enrich schizonts (Rivadeneira EM *et al.,* 1983). Following the protocol of Deitsch K *et al*., 2000, uninfected RBCs were suspended in 400 µl of cytomix containing 65 µg of plasmid DNA. Electroporation was performed in 0.2 cm cuvettes using Bio-Rad Gene Pulser set at 0.32 kV, 950 µF. Electroporated cells were washed once with complete media and then infected with percoll enriched schizonts in 5 ml culture under standard conditions. The medium was changed every 24 h and drug selection of the transgenic parasites was initiated 48 h after the electroporation using blasticidin (2.5 µg ml^{-1}). Parasitized erythrocytes were monitored through microscopic examination of Giemsa stained thin smear once in every four days post drug selection.

2.3.11 Generation of IMPDH deletion strain of *E. coli*

Amplification of the kanamycin resistance cassette (Kan-cassette) with primers that include 50 nucleotide homology regions on either side of the gene to be knocked out and 20 nucleotide priming sequences for pKD13 (used as a template for Kan-cassette) was performed (Table 4). BL21(DE3) strain of *E. coli* was transformed with Red helper plasmid pKD46 which codes for Red recombinase. Cultures were grown in 0.1 mg ml^{-1} ampicillin and 1 mM arabinose at 30 °C to an A_{600nm} of 0.6 to make electrocompetent cells. The amplified Kan-cassette with the homology arms was gel purified, DpnI digested and re-purified. Electrocompetent *E. coli* cells containing pKD46 plasmid were transformed with the PCR product and selected for kanamycin-resistant colonies. After the primary selection, the bacterial cells were maintained on no antibiotic plate for one generation followed by two cycles grown at 42 °C and tested for the loss of pKD46 plasmid (Datsenko KA and Wanner

BL, 2000). The thus obtained deletion strain was confirmed for the loss of gene using a set of confirmatory primers listed in Table 5.

Table 4. List of primers used for deletion of *impdh* gene from BL21(DE3) strain of *E. coli.*

S. No.	Primer	Sequence
1)	H1P1	5'AAGTGAAACAGATAATATAAATCGCCCGACATGAAGTCGGGC GAAGAGAAGTGTAGGCTGGAGCTGCTTC3'
2)	H2P4	5'GTATAATGCCGCGGCAATATTTATTAACCACTCTGGTCGAGAT ATTGCCCCTGTCAAACATGAGAATTAATTCCG3'

Table 5. List of primers used to confirm the deletion of *impdh* gene in *E. coli.*

S. No.	Primer	Sequence
1)	EcGMPS_F	GGTGCTGGCTACGGTGATGAAGTCGGACGG
2)	EcXseA_R	CACACCAACGCAATGCGCAGGGGAGGGAAG
3)	Kan_Int_F	CAGGTAGCCGGATCAAGCGTATGCAGCCGC
4)	Kan_Int_R	GCGGCTGCATACGCTTGATCCGGCTACCTG
5)	Ec_Int_R	GCGGTGCGGGCATTCAGGAAAGCCACGTTC

2.3.12 Cloning of *Tritrichomonas foetus* IMPDH (TfIMPDH)

pTf1 plasmid containing *T. foetus* IMPDH was used as a template to PCR amplify the gene with a C-terminal $(His)_6$-tag. Set of forward and reverse primers (Table 6) were used to amplify and clone the gene into the pET21b+ vector between *NdeI* and *XhoI*. The clone was confirmed through DNA sequencing.

Table 6. Primers used for amplification of *T. foetus* IMPDH.

S.No.	Primer	Sequence
1)	Tf_F	5'GTC*CATATG*GCAAAATACTACAACGAACCATGC3'
2)	Tf_R	5'GTA*CTCGAG*TTTTGGGTGATAGTCGTTAATCCTGTCC3'

2.3.13 Functional complementation assay using *guaB* deletion strain of *E. coli*

M9 minimal medium containing 1X M9 salts, 0.4 % glucose or 0.4 % malate, 0.5 % casaminoacids, 0.1 % thiamine, 0.1 mg ml^{-1} tryptophan, 0.01 mg ml^{-1} biotin, 2 mM $MgSO_4$, 0.1 mM $CaCl_2$, 1X trace elements and appropriate antibiotics was used for complementation assay. The minimal medium was either supplemented with 0.1 mM IPTG or 20 µg ml^{-1} guanosine or 20 µg ml^{-1} xanthine. *ΔguaB*^{K}(DE3) strain of *E. coli* was transformed with

pET21b+ vector carrying either PfIMPDH (native or harmonized) or PfIMPDH$^{\Delta CBS}$ (catalytic domain, native or harmonized), TfIMPDH (positive control) and PbIMPDH (from *P. berghei*) along with helper plasmid coding for tRNA synthetases from the Arctic express strain of *E. coli* (Agilent Technologies, USA.) and chaperone plasmid pKJE7 (Takara Bio, Japan). The transformants were grown overnight in LB medium containing appropriate antibiotics. Overnight grown cells (A_{600nm} =1) were washed twice with 1X minimal medium, serial diluted and spotted on the minimal medium plate containing 100 µM IPTG.

2.3.14 Cloning and expression of PfIMPDH in *Saccharomyces cerevisiae*

A bacterial expression vector carrying PfIMPDH was used as a template to PCR amplify the gene of interest using a set of primers (Table 7) introducing *BamHI* and *XhoI* as cloning sites. The yeast expression vector, pYES2CT, and PCR amplicon were double digested, spin-column purified and used for the ligation reaction. Clones obtained were confirmed by DNA sequencing.

Table 7. Primers used for cloning PfIMPDH into the yeast expression vector, pYES2CT.

S.No.	Primer	Sequence
1)	pY_F	5'TCA***GGATCC***ATGGCTAGCGGATGGAAAGCT3'
2)	pY_R	5'TCA***CTCGAG***TGTACTAAACTTTTTGTTGTTG3'

2.3.15 Functional complementation assay in yeast

guaB deletion strain of yeast, DY891 was transformed with pY_PfIMPDH or pY_PfIMPDH$^{\Delta CBS}$, plated on synthetically defined medium lacking uracil (SD-Ura) plates with 50 µg ml^{-1} G418 and 0.5 mM guanine, and incubated at 30 °C for 24 h. Single colonies were re-grown in SD-Ura broth supplemented with guanine at 30 °C for 24 h. Cells were harvested at A_{600nm} =1 per ml and washed twice with sterile water. Serial dilutions were performed and 2 µl of each dilution was spotted on SD-Ura agar plates supplemented with 50 µg ml^{-1} G418 in the presence or absence of guanine and incubated at 30 °C.

2.3.16 cDNA synthesis and RT-PCR

Total RNA was extracted from the yeast transformants following the Trizol method adapted from Rio DC *et al*., 2010. Isolated RNA samples were treated with DNase I followed by cDNA synthesis through reverse transcription reaction using the revertaid reverse

transcriptase enzyme (genetically modified MMLV, Thermo-Scientific, USA) and random hexamers as primers. The thus obtained cDNA was used as a template for PCR amplification with gene-specific primers.

2.3.17 Deletion of the *guaC* gene from H1174 strain (H1174$^{\Delta guaC}$)

A similar methodology described in section 2.3.11 was employed in the deletion of the *guaC* gene that encodes GMPR in H1174 strain of *E. coli* and was replaced by kanamycin antibiotic selection marker using primers in Table 8 and confirmed using primers in Table 9. Further, kanamycin resistant cells were selected and transformed with plasmid pCP20 (selected on 50 µg ml^{-1} ampicillin and 34 µg ml^{-1} chloramphenicol) expressing yeast FLP recombinase which recognizes FRT sites present as overhangs of Kan-cassette and performs the excision of the antibiotic resistance gene. Transformants were then grown at 42 °C to cure them off pCP20. *guaC* knockout bacterial cells (H1174$^{\Delta guaC}$) were tested for their sensitivity towards ampicillin, chloramphenicol and kanamycin and further genotyped through PCR for confirmation of gene deletion. Thereafter, H1174$^{\Delta guaC}$ was tested for its ability to grow on M9 minimal medium with or without 100 µM adenine or 300 µM guanine or 300 µM guanosine. For the functional complementation assay, a similar procedure was employed as provided in section 2.3.13, except that cells were supplemented with 0.3 mM IPTG and either 0.1 mM adenine or 0.3 mM guanosine/ 0.3 mM guanine in the M9 minimal medium agar plates.

Table 8. Primers used for generating the *guaC* knockout strain of H1174$^{\Delta guaC}$.

S.No.	Primer	Sequence
1)	EcGMP_H1P1	5'ACTGGAGTTGCGCTCTTACCCTTATAGCCATTAACCCCAGGA ATCCGCACGTGTAGGCTGGAGCTGCTTC3'
2)	EcGMP_H2P4	5'GAGTGGGATGGGATAACGCTGGCGTGTTGCTCCACGCCAGCG TTGGGAGACTGTCAAACATGAGAATTAATTCCG3'

Table 9. Primers used for genotyping H1174$^{\Delta guaC}$ strain of *E. coli*.

S.No.	Primer	Sequence
1)	Ec_CoaE_F	5'CCAGCAATGGCACAACCCACAGTACATAGG3'
2)	Ec_HofC_R	5'GTGGCGAATGGAGCTGGCTGCTGGTGTTG3'
3)	Kan_Int_R	5'GCGGCTGCATACGCTTGATCCGGCTACCTG3'
4)	EcGMPR_F	5'GTACCATGGCACGTATTGAAGAAGATCTGAAGTTAGG3'

2.3.18 Cloning of *E. coli* GMPR (EcGMPR)

Genomic DNA from XL1 blue strain of *E. coli* was used as a template to PCR amplify the EcGMPR with a C-terminal $(His)_6$-tag. Set of forward and reverse primers (Table 10) were used to amplify and clone the gene into the pTrc99a vector between *NcoI* and *PstI*. The clone was confirmed through DNA sequencing.

Table 10. Primers used for cloning GMPR from *E. coli*.

S.No.	Primer	Sequence
1)	EcGMPR_F	5'GTA***CCATGG***CACGTATTGAAGAAGATCTGAAGTTAGG3'
2)	EcGMPR_R	5'GTA***CTGCAG***TTAGTGGTGGTGGTGGTGGTGCTCGAGCAGGTTGTTGAAGATGCGG3'

2.3.19 Generation of active site mutants of PfIMPDH

PfIMPDH (native and codon harmonized genes) was subcloned into the pTrc99a expression vector. With codon harmonized PfIMPDH in pTrc99a expression vector as a template, a set of primers were used to introduce mutations at active site residues (C314A, T316A, and Q435E) through overlapping PCR (Table 11). All the clones obtained were confirmed by DNA sequencing.

Table 11. Primers used for generating active site mutations of PfIMPDH.

S.No.	Primer	Sequence
1)	pTrc99a_F	5'GTTTTTTGCGCCGACATCATAACGG3'
2)	pTrc99a_R	5'CGCCAGGCAAATTCTGTTTTATCAGACC3'

3)	Pf_C314A_F	5'GGGCAGCGGCAGCATTGCGACCACCCAGGATGTGTGCGCGGTGG GCCGCGCGCAGGGCACCGCGGTGT3'
4)	Pf_C314A_R	5'ACACCGCGGTGCCCTGCGCGCGGCCCACCGCGCACACATCCTGGG TGGTCGCAATGCTGCCGCTGCCC3'
5)	Pf_T316A_F	5'GGGCAGCGGCAGCATTTGCACCGCGCAGGATGTGTGCGCGGTGG GCCGCGCGCAGGGCACCGCGGTGT3'
6)	Pf_T316A_R	5'ACACCGCGGTGCCCTGCGCGCGGCCCACCGCGCACACATCCTGCG CGGTGCAAATGCTGCCGCTGCCC3'
7)	Pf_Q435E_F	5'CATCGATGAAATTAAAGTAAGCGAAGGTGTGAGCGCCAGCCTGGT GG3'
8)	Pf_Q435E_R	5'CCACCAGGCTGGCGCTCACACCTTCGCTTACTTTAATTTCATCGAT G3'

2.3.20 Functional complementation assay in H1174$^{\Delta guaC}$ strain

A similar procedure was employed as provided in section 2.3.13, except that cells were supplemented with 0.3 mM IPTG and either 0.1 mM adenine or 0.3 mM guanosine/ 0.3 mM guanine in the M9 minimal medium agar plates.

2.4 Results and discussion

2.4.1 Detection of IMPDH from the parasite lysate

Recombinant PfIMPDH was found to be insoluble when expressed in *E. coli*, a detailed description of this is provided in Chapter 3. C-terminal $(His)_6$-tagged PfIMPDH was denatured in 6 M GdnHCl and purified by Ni-NTA affinity chromatography. The purity of the eluted protein as accessed by SDS-PAGE was greater than 95 % (Fig. 1). Using this as an antigen, anti-PfIMPDH antibodies were generated in mice and the antibody titer determined on a dot blot was found to be effective up to 1: 25000 dilution (Fig. 1). The purified protein was electro-blotted onto the PVDF membrane and used as a matrix to purify PfIMPDH antibody from the mice antisera. The purified antibody was quantified by the method of Bradford (Bradford MM, 1976).

Purified anti-sera were used to probe the presence of IMPDH in the parasite lysate through Western blotting. Saponin treatment of infected erythrocytes (mixed asexual stages) released RBC membrane leaving parasites intact. Several cycles of freeze-thawing lysed the

parasites and the lysate was resolved on SDS-PAGE and electrotransferred on to PVDF membrane. Western blot developed using HRP conjugated secondary anti-mouse antibody yielded a single band at 55 kDa confirming the expression of PfIMPDH in the parasite while no protein band was detected in the RBC lysate used as a negative control (Fig. 1). This further supports the evidence for expression reported earlier through microarray analysis, RNA sequencing and proteomics data. Recombinant PfCBS protein corresponding to a molecular weight of 14 kDa (discussed in Chapter 4) served as a positive control for anti-PfIMPDH antibody detection.

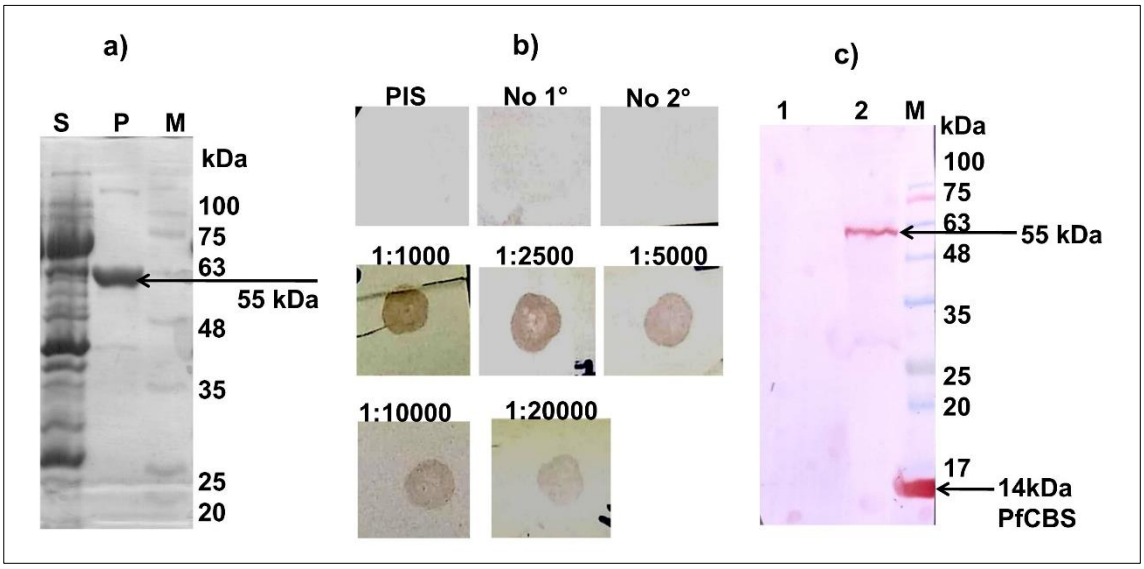

Figure 1. IMPDH purification under denaturing conditions, antibody generation in mice and Western detection. a) Expression profile of recombinant PfIMPDH in E. coli. *Lane S and P represent soluble and insoluble fractions, respectively; M, pre-stained protein molecular weight ladder (Abcam, USA). PfIMPDH (55 kDa) is indicated by an arrow.* ***b) Determination of antibody titre by dot blot.*** *2 µg of antigen was spotted on the nitrocellulose membrane and probed with varying concentration of anti-PfIMPDH antibody. Dilutions are indicated on top of each blot. PIS corresponds to pre-immune serum control. No primary and no secondary antibody controls are labeled as No 1º and No 2º, respectively.* ***c) Detection of IMPDH in parasite lysate by Western blotting using anti-PfIMPDH antibody.*** *Lane 1, uninfected erythrocytes; Lane 2, lysate from 10 ml of saponin released P. falciparum from a culture of 7 % - 8 % parasitemia. anti-PfIMPDH antibody raised in the mouse was used at 1:2500 dilution and the blot was developed with HRP conjugated goat anti-mouse antibodies (Sigma-Aldrich, USA). Recombinant PfCBS (14 kDa) was used as a positive control for Western detection.*

2.4.2 Indirect immunofluorescence microscopy

Life cycle of *Plasmodium falciparum* involves two hosts. During a blood meal, *Plasmodium*-infected female Anopheles mosquito injects sporozoites into the human host. Sporozoites infect liver cells and mature into schizonts, which rupture and release merozoites. After this initial replication in the liver (exo-erythrocytic schizogony), the parasites undergo asexual multiplication in the erythrocytes (erythrocytic schizogony). Merozoites infect red blood cells resulting in rings that are the intra-erythrocytic asexual stage of the parasites. The ring stages develop into trophozoites that further matures into schizonts. Schizont rupture leads to the release of merozoites into the blood stream. Some parasites differentiate into sexual erythrocytic stages (gametocytes).

Blood stage parasites are responsible for the clinical manifestations of the disease. The gametocytes, male (microgametocytes) and female (macrogametocytes), are ingested by an Anopheles mosquito during a blood meal. The parasites' multiplication in the mosquito is known as the sporogonic cycle. While in the mosquito's stomach, the microgametes fuse with the macrogametes generating zygotes. The zygotes in turn become motile and elongated (ookinetes) which invade the midgut wall of the mosquito where they develop into oocysts. The oocysts grow, rupture, and release sporozoites, which make their way to the mosquito's salivary glands. Infection of the sporozoites into a new human host perpetuates the malaria life cycle.

All the intra-erythrocytic stages of the parasite stained positive for the presence of IMPDH in the cytoplasm as examined by indirect immunofluorescence microscopy (Fig. 2). Fluorescence signals were not observed in uninfected erythrocytes, in controls probed with either pre-immune sera (PIS) or lacking primary or secondary antibody confirming the specificity of the fluorescence detection (Fig. 2). Further, partial nuclear staining was also observed throughout all the intra-erythrocytic asexual stages of the parasite (Fig. 2). Mass spectrometric analysis of *P. falciparum* proteins carried out by two independent research groups (Oehring SC *et al*., 2012; Briquet S *et al*., 2018) identified 11 unique peptides corresponding to PfIMPDH (Table 12) in the nuclear fractions. These reports serve as additional evidence confirming the partial nuclear localization of PfIMPDH observed through immunofluorescence microscopy. Percentage nuclear localization of PfIMPDH has been calculated using the colocalization analysis tool on Zen 2.1 SP2 version of Carl Zeiss Microscopy GmbH (Fig. 2)

The most useful of the colocalization measurements for standard biology applications are the colocalization coefficients derived by Manders (Manders EMM *et al*., 1993). The colocalization coefficients can be measured for each channel (refers to a color) in a dual color image. Manders colocalization coefficient for one of the channels colocalizing with the other in an image, is defined as the ratio of the "summed intensities of the colocalizing pixels from one channel for which the corresponding intensities of the pixels in the other channel are above zero"

to the "total intensity in the channel being analyzed". The colocalization coefficient values will range from 0 to 1 where the former corresponds to non-overlapping channels and the latter indicates 100% co-localisation between the two channels of an image being examined. Manders colocalization coefficient could be determined even for an image where both the channels differ in their intensities.

The images were analyzed by choosing a region of interest to avoid the background noise and the colocalized pixels are false-colored (white) for the ease of viewing (Fig. 2). The extent of overlap of the green signal corresponding to PfIMPDH with that of the DAPI stained nucleus in the region of interest was found to be 0.3 to 0.4 (Fig. 2). A total number of 50 parasites were examined. Determination of colocalization using JACoP tool (Just Another Co-localization Plugin) (Bolte S and Cordelières FP, 2006) on Fiji image processing program (Schindelin J *et al*., 2012) also confirmed the partial nuclear localization of PfIMPDH (Appendix B at the end of the thesis provides parasite images). Also, similar to immature cytoophidia of human IMPDH (Chang CC *et al*., 2015), small distinct foci of PfIMPDH have been observed across various stages of the parasite (Fig. 2). However, the significance for the presence of such structures in *P. falciparum* in a metabolic context needs further studies.

Most of the IMPDHs are known to be largely cytosolic while nuclear localization is reported for *Drosophila* and human enzymes (Kozhevnikova EN *et al*., 2012; MCLean JE *et al*., 2004). In addition to the catalytic function, IMPDH is also implicated in the binding of RNA, polyribosomes, and also involved in regulation of translation and transcription (Mortimer SE *et al*., 2008; Hedstrom L, 2009). Accumulation of IMPDH in the nucleus during the G2 phase of the cell cycle has been observed under oxidative or replicative stress in *Drosophila* (Kozhevnikova EN *et al*., 2012). In the nucleus, it was identified to bind to C/T sequence of the regulatory DNA elements and subsequently, leads to the transcriptional repression of histone genes and E2f, a regulator of the G1/S transition (Van der Knaap JA and Verrijzer CP, 2016). Guanosine 5'-monophosphate synthetase (GMPS), an enzyme downstream of IMPDH in GMP biosynthesis pathway was shown to associate, allosterically activate nuclear ubiquitin-specific protease 7 (USP7) and aid in deubiquitylation of histone H2B in *Drosophila* and mammalian cells. GMPS was also found to stabilize p53 through activation of USP7 (Van der Knaap JA *et al*., 2005; Van der Knaap JA *et al*., 2010; Sarkari F *et al*., 2009; Reddy BA *et al*., 2014; Zhou Z *et al*.,.2015; Faesen AC *et al*. 2011; Frappier L and Verrijzer CP, 2011). These observations indicate the role of IMPDH together with GMPS not only in the biosynthesis of purine nucleotides but also as regulators of cell proliferation (Van der Knaap JA and Verrijzer CP, 2016).

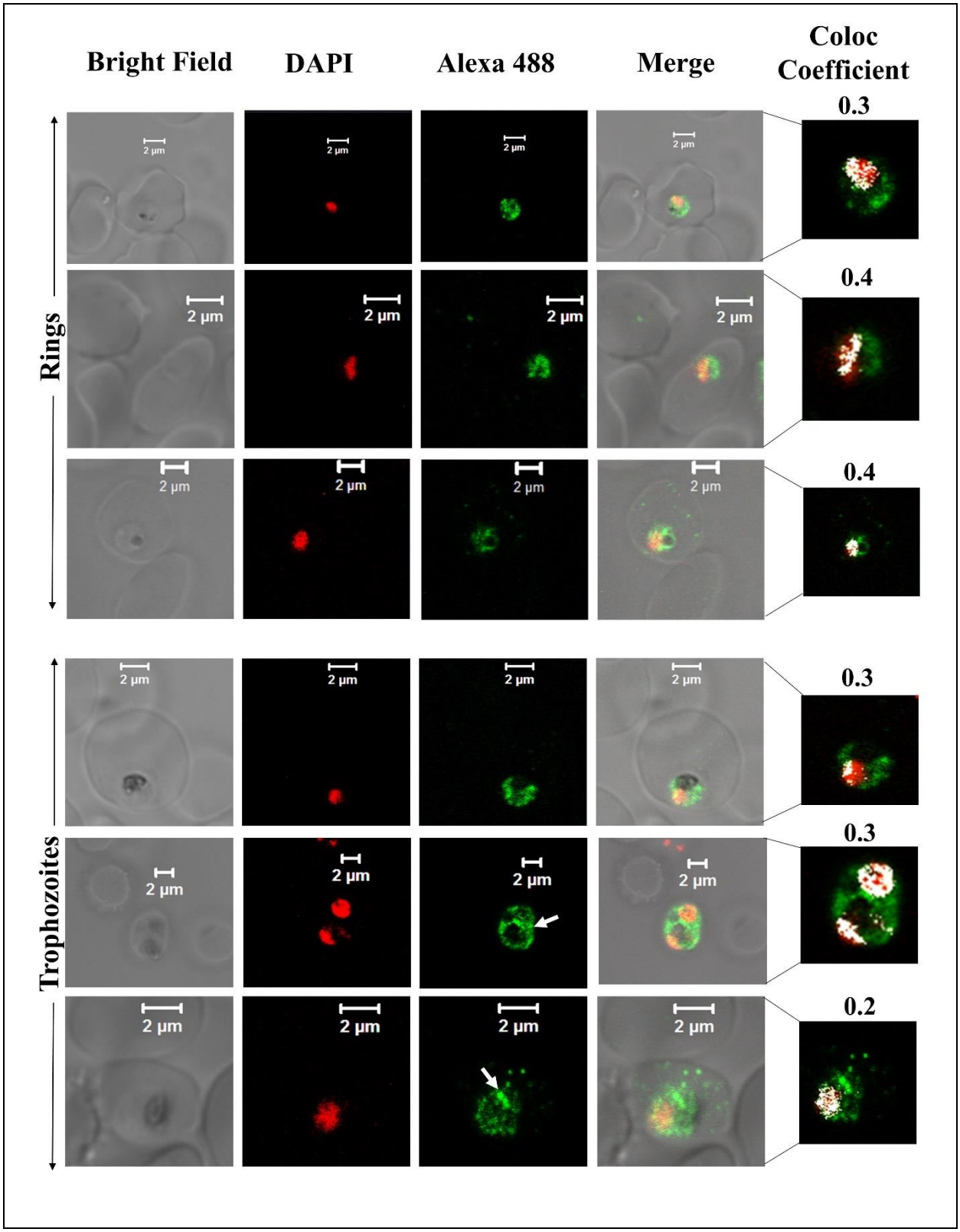
Bright Field
DAPI
Alexa 488
Merge
Coloc Coefficient
Rings
Trophozoites
2 µm
0.3
0.4
0.4
0.3
0.3
0.2

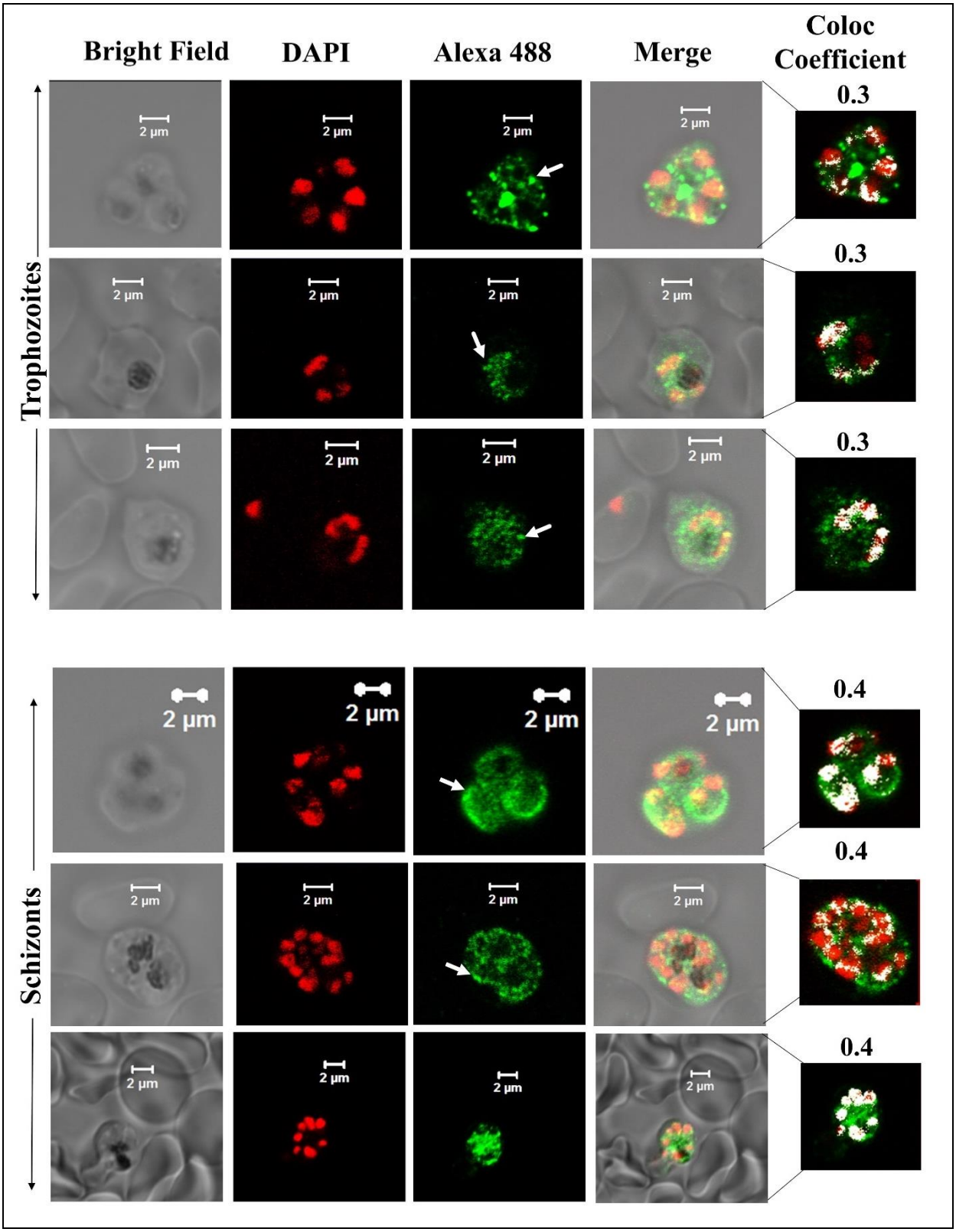
Bright Field
DAPI
Alexa 488
Merge
Coloc Coefficient
Trophozoites
Schizonts
2 µm
0.3
0.3
0.3
0.4
0.4
0.4

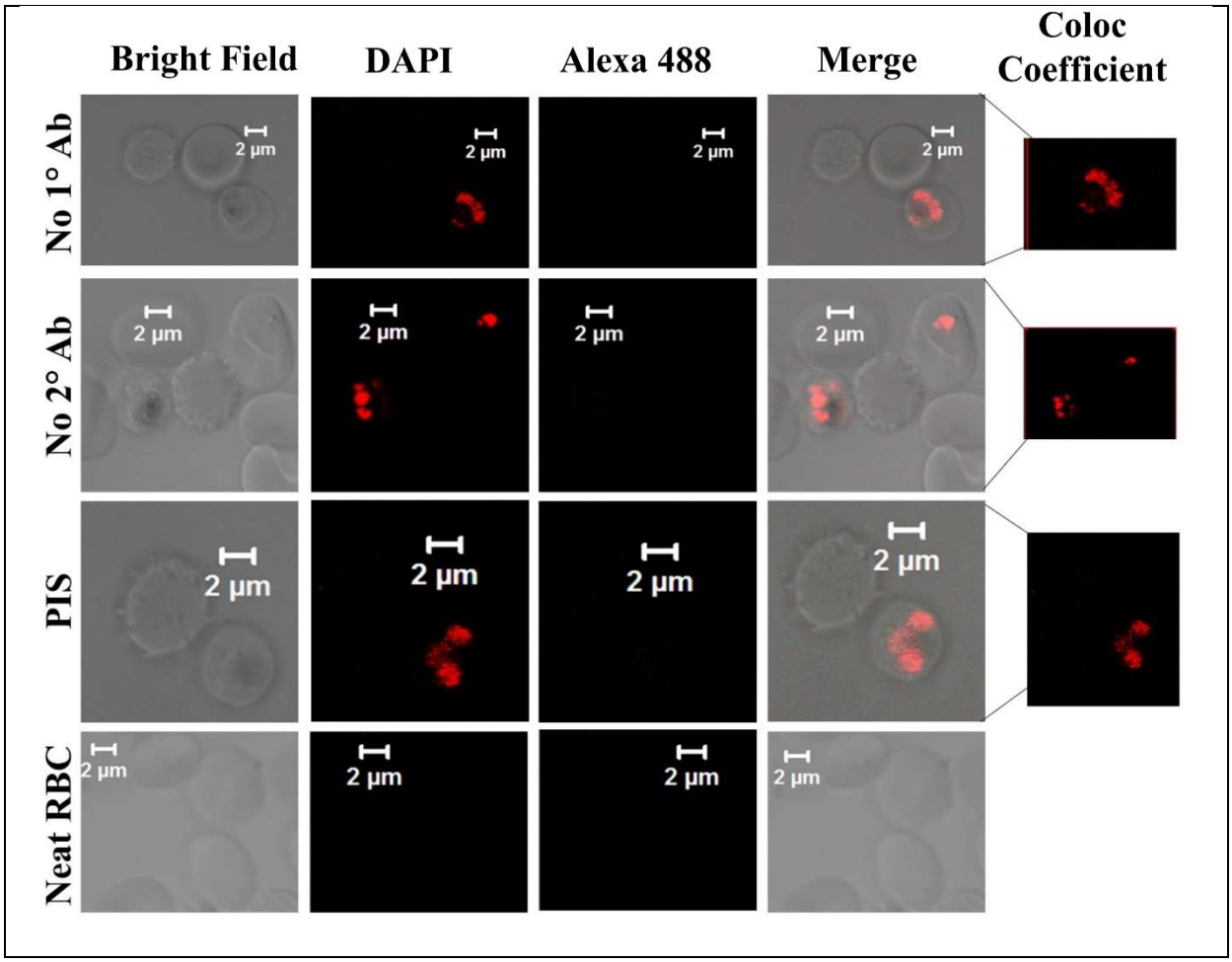

Figure 2. Subcellular localization of IMPDH in P. falciparum. *LSM 510 META microscope was used for the confocal studies. Stack mode was used with a stack size of 0.38 µm. Multibeam splitter – HFT KP 700/488 was used. Primary antibody raised in the mouse was strip-affinity purified against PfIMPDH electro-blotted on PVDF membrane and used at 1:200 ratio. Secondary anti-mice IgG antibody conjugated with Alexa 488 chromophore was used at a ratio of 1:400. DAPI was used to stain the nucleus and is false-colored red. For permeabilization, 0.08 % Triton X-100 was used. Each panel shows cytoplasmic localization of IMPDH along with partial nuclear signal in various intra-erythrocytic asexual stages of the parasite. Pre-immune serum (PIS), no primary and no secondary antibody controls confirm the specificity of the generated antibodies. The region of interest was manually selected using the freehand tool and image analysis was performed on the Zen 2.1 SP2 version. Manders colocalization coefficients for the extent of overlap of green channel (corresponding to PfIMPDH antibody staining) with the nucleus stained with DAPI (false-colored red) has been indicated. Also, multiple foci similar in appearance to that of immature cytoophidia of human IMPDH observed across various stages of the parasite are highlighted with white arrows.*

Table 12. Peptide sequences of PfIMPDH identified from the mass-spectrometry studies on nuclear fractions of *Plasmodium falciparum* (Oehring SC *et al*., 2012; Briquet S *et al*., 2018).

11 unique peptides of PfIMPDH	K.RFENGFIFDPYTFSPEHTVADVLETK.N
	R.AQGTAVYHVSK.Y
	K.SAHPDIPIIGGNVVTSQQAK.N
	K.VSDNLIFNNK.K
	K.HGFQSMGIR.N
	K.VSQGVSASLVDK.G
	K.TPVISSPMDTVTGHK.M
	K.GSVLNLIPHLFK.A
	K.NEYTDENIDEIK.V
	R.GMGSMEAMYNK.G
	K.NLIDAGADVLR.I

2.4.3 Episomal expression of GFP-tagged PfIMPDH

PFCENv2, an episomally maintained centromeric plasmid expressing GFP was a generous gift from Dr. Iwanaga S, Japan (Iwanaga S *et al.,* 2012). The pFCENv2_IMPDH_GFP construct was generated to further examine the localization of PfIMPDH within the parasite (Fig. 3). The clone was confirmed error-free by DNA sequencing. Uninfected RBCs were pre-loaded with PFCENv2_IMPDH_GFP plasmid and infected with percoll enriched schizonts. 48 h post-transfection, upon examination of Giemsa stained smears healthy parasites at a parasitemia of 3-4 % was observed and blasticidin was introduced as a selection pressure for the transfectants. Complete disappearance of parasites after the introduction of drug pressure was observed by the 5^{th}-day post-transfection. However, no transfectants have appeared till 45 days post-transfection. This experiment stands unsuccessful and has been done only once.

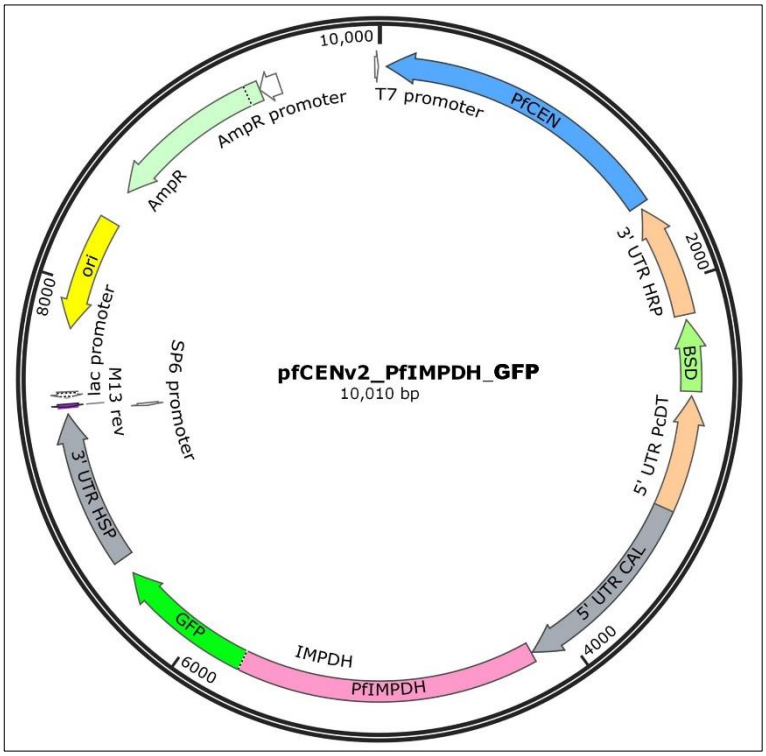

Figure 3. Schematic of construct for episomally expressing PfIMPDH-GFP fusion in P. falciparum. *The PFCENv2_PfIMPDH_GFP construct was generated in order to examine the localization of IMPDH within the parasite. Calmodulin promoter drives the expression of the gene. Blasticidin serves as a drug selection marker.*

2.4.4 Generation of *impdh* deletion strain of *E. coli*

Following the protocol of Datsenko KA and Wanner BL, 2000 to delete the chromosomal genes in *E. coli*, pKD13 plasmid bearing kanamycin cassette was amplified with primers having 50 nucleotide overhangs homologous to regions flanking to the gene of interest (IMPDH) to be disrupted. pKD46, a temperature sensitive plasmid confers ampicillin resistant to bacteria and encodes for Red recombinase under arabinose promoter. The gene coding for IMPDH in *E. coli*, *guaB* was disrupted by transforming the wild-type BL21(DE3) strain with DpnI treated, purified PCR product followed by induction of Red recombinase by addition of arabinose (Fig. 4). Bacterial colonies which were integrants for Kan-cassette and devoid of the IMPDH gene survived on kanamycin selection. Single colonies that had appeared on LB agar plate supplemented with ampicillin and kanamycin were further re-

grown on a plate lacking ampicillin at 42 °C for two generations to eliminate pKD46 plasmid and thereby ampicillin selection. The thus obtained strain was verified as a knockout of the *guaB* gene by its ability to grow on kanamycin selection (Δ*guaB*^{K}(DE3)) (Fig. 5) and further confirmed through PCR using confirmatory primers (Table 5, and Fig. 5). Δ*guaB*^{K}(DE3) strain was confirmed auxotrophic for guanine nucleotide as it was unable to grow on M9 minimal medium without supplementation of either guanosine or xanthine (Fig. 6). On supplementation, guanosine can be phosphorylated to GMP by guanosine kinase (Mori H *et al*., 1995) and xanthine can be phosphoribosylated by XPRT/HG(X)PRT (Vos S *et al*., 1997 and Guddat LW *et al*., 2002) to XMP which can be further utilized by GMP synthetase to form GMP (Tiedeman AA *et al*., 1985).

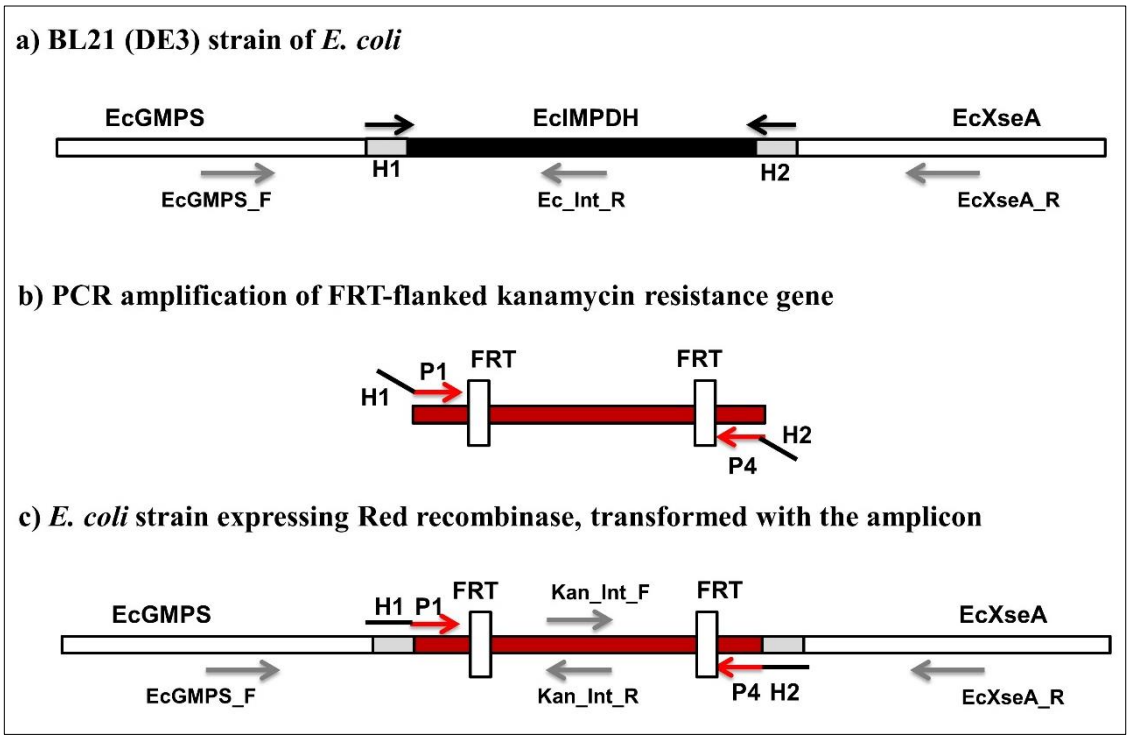

Figure 4. Schematic of the strategy used for knockout of IMPDH in E. coli using Red recombinase. a) Genetic organization *of BL21(DE3) strain of E. coli with EcIMPDH gene flanked on either side by EcGMPS (Guanosine 5'-monophosphate synthetase) and EcXse A (Exonuclease A). 50 nucleotide homology arms (H1 and H2) flanking EcIMPDH are in grey boxes with black arrows highlighting the primers.* ***b) Amplification of FRT-flanked antibiotic selection cassette from the pKD13 plasmid.*** *Priming sites (P1 and P4) of kanamycin cassette followed by homology arms (H1 and H2) are indicated in red and black arrows, respectively.* ***c) Homologous recombination aided by***

Red recombinase expressed from the plasmid pKD46 *replaced EcIMPDH with Kan cassette resulting in impdh deletion strain. Shown in grey arrows are the various oligonucleotides used for confirming deletion of EcIMPDH through PCR (Datsenko KA and Wanner BL, 2000).*

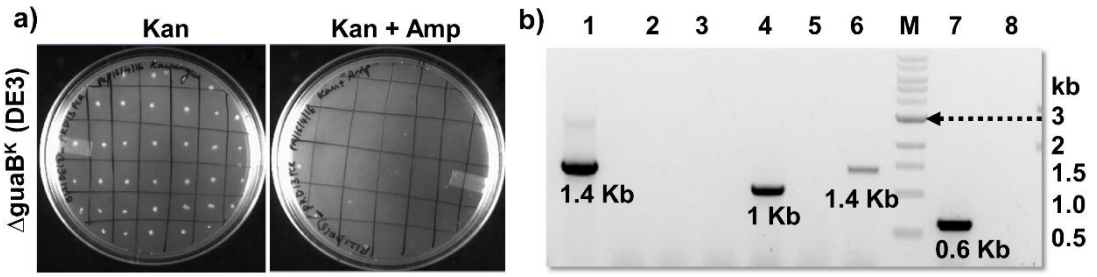

c)

Primer set used	Expected size of amplicon	
	BL21 (DE3)	ΔguaB^K (DE3)
H1P1/H2P4 (set 1)	-	+ (1423 bp)
EcGMPS_F/Ec_Int_R (set 2)	+ (628 bp)	-
EcGMPS_F/Kan_Int_R (set 3)	-	+ (1061 bp)
Kan_Int_F/EcXseA_R (set 4)	-	+ (1433 bp)

Figure 5. Confirmation of loss of pKD46 plasmid and genotyping of the knockout strain. a) loss of pKD46 plasmid confers ampicillin sensitivity. *Isolated colonies were replica spotted on LB agar plates containing either kanamycin alone or kanamycin and ampicillin. Replacement of EcIMPDH with Kan-cassette confers the knockout strain kanamycin resistance. Temperature sensitive pKD46 plasmid gets cleared from the cell after two rounds of growth at elevated temperature (42 °C) resulting in no growth phenotype upon ampicillin selection.* ***b) PCR verification of guaB deletion strain of E. coli.*** *Lane 1, 4, 6 and 8 correspond to PCR performed with DNA from ΔguaB^K(DE3) strain as a template while Lane 2, 3, 5 and 7 correspond to DNA from wild-type strain being used as a template. Lane 1, 2 represent PCR performed with primer set 1 (1.4 kb amplicon expected from deletion strain); lane 3, 4 with primer set 3 (1.0 kb amplicon expected from deletion strain); lane 5, 6 with primer set 4 (1.4 kb amplicon expected from deletion strain) and lane 7, 8 with primer set 2 (0.6 kb amplicon expected from wild-type strain). M, 1 kb DNA molecular weight ladder, NEB.* ***c) Tabulation of confirmatory primers used to verify the deletion strain*** *by PCR and expected amplicon size. Sequences of the primers used are mentioned in Table 5. Primer set (1), (3), and (4) were used for positive confirmatory PCR of the deletion strain and expected amplicons correspond to 1.4 kb, 1.0 kb, and 1.4 kb, respectively. Primer set (2) was designed as a negative PCR control for knockout and positive for wild-type with 0.6 kb amplicon.*

2.4.5 Functional complementation assay with *ΔguaB*^{K}(DE3) strain of *E. coli*

IMP dehydrogenase from a protozoan parasite *Tritrichomans foetus* has been extensively studied and thoroughly characterized (Hedstrom L, 2009). An expression vector carrying *T. foetus* IMPDH gene, pTf1 was a kind gift from Prof. Hedstrom L, Brandeis University, USA (Digits JA and Hedstrom L, 1999). TfIMPDH was cloned into pET21b+ vector yielding a C-terminal $(His)_6$-tag to be able to incorporate it as a positive control in the growth rescue experiments of Δ*guaB*^{K}(DE3) strain of *E. coli*. The *impdh* deletion strain was transformed with pET21b+ plasmids carrying the gene for IMPDH from *T. foetus, P. falciparum* (full length, PfIMPDH, and catalytic domain alone, PfIMPDH$^{\Delta CBS}$) and *P. berghei* to test the ability of these enzymes to complement the function of the lost gene.

Various conditions including co-transformation of helper plasmids (coding for a chaperone and tRNA synthetases for rare codons), different carbon sources (glucose, malate, and glycerol) and temperatures (25 °C, 37 °C) have been tested. The M9 minimal medium was supplemented with 0.1 mM IPTG for the induction of T7 RNA polymerase that would, in turn, drive the expression of the gene under the T7 promoter. However, only TfIMPDH was able to rescue the growth of Δ*guaB*^{K}(DE3) strain on minimal medium with no guanosine supplementation (Fig. 6). In addition, the PfIMPDH gene sequence, codon harmonized for optimal expression in *E. coli* (discussed in Chapter 3) was also found to be unable to complement the growth deficiency.

Expression of the recombinant proteins from all the transformants was analyzed on SDS-PAGE followed by Western blot probed with anti-$(His)_6$ antibodies. Hyperexpression of TfIMPDH was achieved without co-expression of any helper plasmid, while the presence of either chaperon KJE7 or tRNA helper plasmid or both was essential for the expression of native *P. falciparum* IMPDH. However, codon harmonized PfIMPDH yielded hyper expression without co-expression of tRNA helper plasmid. While, in all tested conditions, TfIMPDH was obtained in high yields in soluble form, the catalytic domain and PfIMPDH were found to be completely insoluble. Although low levels of soluble PfIMPDH and PfIMPDH$^{\Delta CBS}$ were obtained with co-expression of chaperones (discussed in Chapter 3), no

rescue of the purine auxotroph was observed. A representative gel image of expression and solubility from codon harmonized PfIMPDH and PfIMPDH$^{\Delta CBS}$ is shown in Fig. 6. High levels of soluble and functional protein supported the growth of *impdh* deletion strain expressing TfIMPDH on M9 minimal medium. Non-availability of sufficient soluble and thus functional protein might probably reflect the growth defect of Δ*guaB*^{K}(DE3) strain carrying PfIMPDH on minimal medium with no supplementation. A detailed description of various conditions, constructs generated, expression and solubility analysis of native and codon harmonized PfIMPDH and PfIMPDH$^{\Delta CBS}$ are provided in Chapter 3.

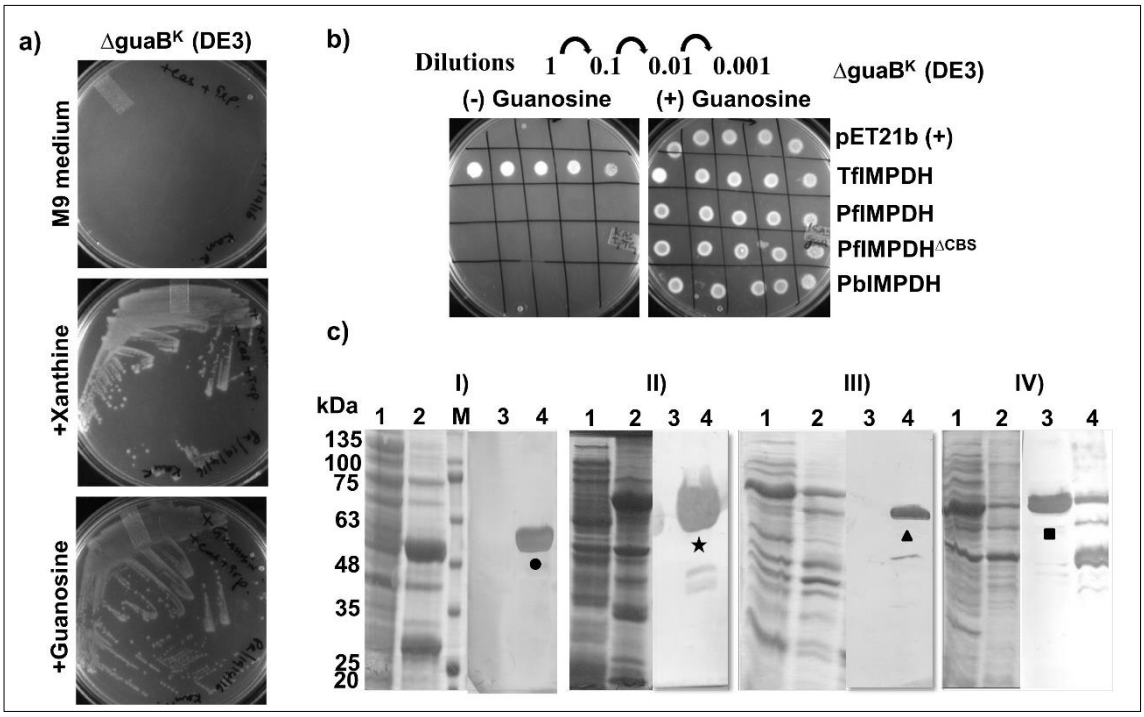

Figure 6. The phenotype of the Δ*guaB*^{K}(DE3) strain, complementation assay, and expression analysis. a) Guanine auxotrophy of the impdh deletion strain. *Δ*guaB*^{K}(DE3) strain of E. coli was streaked on M9 minimal medium containing 50 µg ml^{-1} kanamycin alone or supplemented with either 20 µg ml^{-1} xanthine or 20 µg ml^{-1} guanosine. Bacterial growth was supported by the presence of either xanthine or guanosine. Cell revival on xanthine indicates the presence of functional GMP synthetase (guaA).* ***b) Functional complementation assay.*** *Δ*guaB*^{K}(DE3) strain was transformed with pET21b+ vector carrying either TfIMPDH or PfIMPDH or PfIMPDH$^{\Delta CBS}$ or PbIMPDH and grown overnight in LB medium containing appropriate antibiotics. One A_{600nm} of cells were washed with M9 minimal medium twice, serially diluted and spotted on M9 plates supplemented with either 0.1 mM IPTG or 20 µg ml^{-1} guanosine. 0.2 % glucose or 0.2 % malate served as a carbon source. Co-*

transformation of the impdh deletion strain with chaperone expressing plasmids (Takara, Japan) or helper plasmid expressing tRNA synthetases for rare E. coli codons or both did not rescue growth of transformants carrying either PfIMPDH or PfIMPDH$^{\Delta CBS}$ or PbIMPDH on minimal medium. The M9 agar plates were incubated at either 37 °C or 25 °C. PfIMPDH gene sequence codon harmonized for optimal expression in E. coli was also tested for its ability to complement the growth deficiency. However, in all tested conditions, only TfIMPDH was able to functionally complement the growth deficiency of Δ*guaB*^{K}*(DE3) strain.* ***c) Expression and solubility.*** *All the transformants were grown in LB medium and induced with 0.1 mM IPTG at 25 °C for 12 h. I, II, III, and IV represent lysates from* Δ*guaB*^{K}*(DE3) strain expressing PfIMPDH*$^{\Delta CBS}$*, PfIMPDH, PbIMPDH, and TfIMPDH, respectively. Lane 1, 2 correspond to the soluble and insoluble fraction detected by Coomassie blue staining, while Lane 3, 4 confirm the expression by Western blot. PfIMPDH*$^{\Delta CBS}$*, PfIMPDH, PbIMPDH, and TfIMPDH proteins were found to be insoluble shown by a sphere, asterisk, triangle, and square, respectively. All the lysates were electrotransferred onto PVDF membrane and probed using anti-(His)*$_6$ *antibodies (Sigma-Aldrich, USA); M-pre-stained protein molecular weight marker (Abcam, USA).*

2.4.6 Functional complementation assay in yeast, DY891

The yeast expression vector, pYES2/CT carrying either full-length *P. falciparum* IMPDH (pY_PfIMPDH) or the catalytic domain (pY_PfIMPDH$^{\Delta CBS}$) or *P. berghei* IMPDH (pY_PbIMPDH) or *T. foetus* IMPDH (pY_TfIMPDH) under galactose promoter was constructed and confirmed error-free by DNA sequencing. *S. cerevisiae* contains four isoforms of IMPDH gene which were deleted to yield DY891 strain *(BY4741; MATα; his3Δ1; leu2Δ0; ura3Δ0; MET15; lys2Δ0; Δimd1::HIS3; Δimd2::LEU2; Δimd3::kanMX4; Δimd4::LYS2*) (McPhillips CC *et al*., 2004). DY891 strain of yeast transformed with all the above-mentioned IMPDH expression constructs and the transformants were selected on SD-Ura plates containing 50 µg ml^{-1} G418 and 0.5 mM guanine.

Functional complementation assay was performed using yeast transformants at A_{600nm} =1 per ml on SD-Ura containing 50 µg ml^{-1} G418 in the presence or absence of guanine. Upon incubation at 30 °C, all the transformants were found to grow on the plate supplemented with guanine (Fig. 7). TfIMPDH used as a positive control had rescued the growth of *impdh* deletion strain, while no growth of DY891 cells carrying either *P. falciparum* or *P. berghei* IMPDH was observed on the minimal medium plate lacking guanine (Fig 7). All the yeast transformants that appeared on guanine containing plate were found to be positive for the presence of the gene of interest upon PCR amplification.

However, except for cells carrying TfIMPDH, all other transformants were found to lack expression of the respective recombinant proteins confirmed by Western blot (Fig. 7). Therefore, lack of expression of *P. falciparum* and *P. berghei* IMPDHs in the DY891 yeast cells could be the cause for no growth phenotype on minimal medium plate lacking guanine. Further, RT-PCR performed on the cDNA prepared from all the transformants was found to be positive indicating the presence of mRNA (gene transcript) encoding IMPDH from *T. foetus*, *P. falciparum* and *P. berghei* (Fig. 7). Both PfIMPDH and PbIMPDH gene sequences yielded a codon adaptability index (CAI value) of 0.82 and 0.63 when expressed in yeast, respectively (ideal value to be > 0.8-1.0, Genscript analysis, discussed in Chapter 3). They also are found to contain negative CIS elements (22 and 3, respectively) which are known to negatively regulate the gene expression at the transcription or translation level. Although TfIMPDH gene sequence yielded a low CAI value of 0.65 with 2 negative CIS elements, it was found to be translated to protein and thus could rescue the guanine auxotrophic yeast. Therefore, a block at the mRNA translation for plasmodial protein synthesis, together with other unknown complexities plausibly lead to no growth phenotype of DY891 cells on minimal medium agar plates.

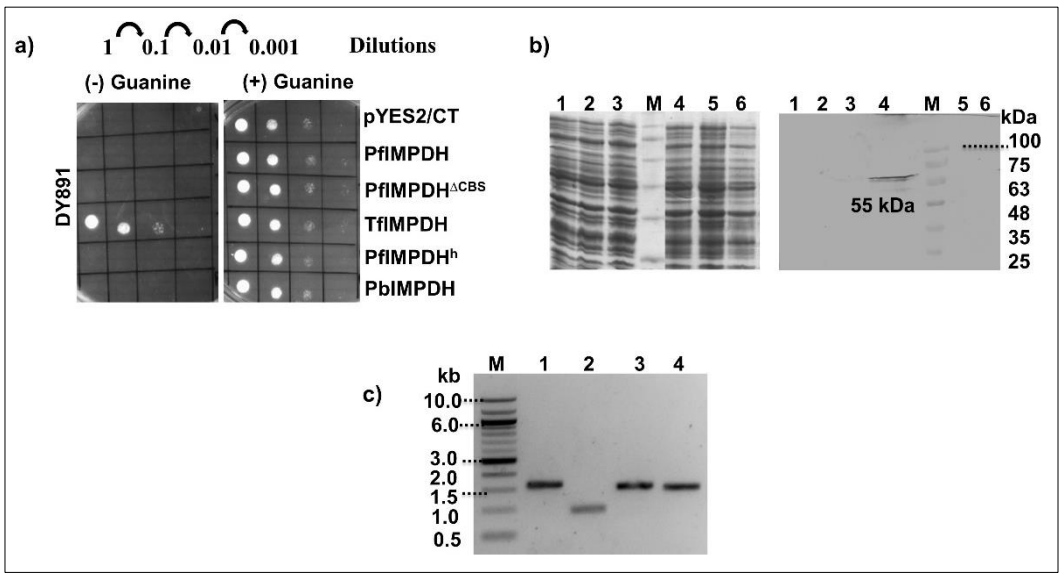

Figure 7. Functional complementation assay and expression analysis in yeast impdh knockout strain, DY891. a) Growth assay. *1 ml of yeast cells were harvested at A_{600nm} =1 and washed twice with sterile water. Serial dilutions were performed and 2 µl of each dilution was spotted on agar plates containing synthetically defined medium lacking uracil (SD-Ura) containing 50 µg ml^{-1} G418, 0.5 mM hypoxanthine, 2 % galactose supplemented with or without 0.5 mM guanine and incubated at 30 °C. All the transformants grew in the presence of guanine while only TfIMPDH was found to rescue growth in the minimal medium lacking guanine. pYES2/CT represents a neat vector (used as a negative control); PfIMPDH and $PfIMPDH^{\Delta CBS}$ correspond to the full length and CBS deletion constructs of P. falciparum IMPDH, respectively; $PfIMPDH^{h}$ corresponds to P. falciparum IMPDH gene codon harmonized for expression in E. coli; PbIMPDH corresponds to P. berghei IMPDH, and TfIMPDH is T. foetus IMPDH (used as a positive control).* ***b) Western detection.*** *The left panel shows Coomassie-stained yeast lysates resolved on 12 % SDS-PAGE and the right panel corresponds to detection of expression by Western blot using anti-$(His)_6$ antibodies (Sigma-Aldrich, USA). Lanes 1 to 6 correspond to lysates from yeast cells carrying pYES2/CT, and pYES2/CT carrying PfIMPDH, $PfIMPDH^{\Delta CBS,}$ TfIMPDH, $PfIMPDH^{h,}$ and PbIMPDH, respectively. M, pre-stained protein molecular weight marker (Abcam, USA). A Western positive signal for protein expression was observed only for TfIMPDH.* ***c) RT-PCR to detect gene transcript.*** *The trizol method was employed for total RNA extraction from the yeast transformants. cDNA was prepared using revertaid reverse transcriptase (Thermo-Scientific, USA) and PCR was carried out to detect the presence of the gene transcript of interest. Lane 1, 2, 3, and 4 represent RT-PCR products of PfIMPDH (1.5 kb), $PfIMPDH^{\Delta CBS}$ (1.2 kb) PbIMPDH (1.5 kb), and TfIMPDH (1.5 kb) respectively. Presence of Plasmodial IMPDH gene transcripts but lack of protein expression indicates a probable block in translation and therefore no growth rescue of the knockout strain on minimal medium.*

2.4.7 Generation of *gmpr* deletion strain of *E. coli*, H1174$^{\Delta guaC}$

A bacterial system as a model to examine the GMPR functionality of the *P. falciparum* gene was attempted using H1174 strain of *E. coli*, obtained from Coli Genetic Stock Centre, Yale, USA. H1174 strain (*thr-20*, guaC*23*, *fhuA2::IS2*, *proA35*, *lacY1*, *tsx-70*, *glnX44*(AS), *gal-6*, *λ*$^{-}$, *trpC45*, *his-68*, *tyrA2*, *rpsL125*(strR), *malT1*(λ^{R}), *xyl-7*, *mtlA2*, *thiE1*, *purH57*, *ilv-635)* carries mutant version of the genes, *purH* and *guaC* and is reported to have a block at *de novo* IMP synthesis and also to lack a functional GMP reductase (De Haan PG *et al*., 1969). The growth of H1174 strain on M9 minimal medium is therefore conditional to the presence of adenine or IMP. However, the strain was found to sustain on minimal medium supplemented with guanine or guanosine (Fig. 9) (although the growth rate was found to be significantly lower than that of adenine). This could be due to

the presence of mutant *guaC* gene supporting the cell survival (presence of the *guaC* gene in H1174 was confirmed through gene-specific primers mentioned in Table 9).

Therefore, H1174 strain lacking the *guaC* gene, $H1174^{\Delta guaC}$ was generated and verified as described in section 2.4.4 (Fig. 8 and Fig. 9). Further, the antibiotic selection cassette that replaced *guaC* gene was excised out using a plasmid expressing flippase (FLP). pCP20 (expressing FLP), like pKD46 (expressing Red recombinase), contains temperature sensitive origin of replication and cells grown at 42 °C for 2 cycles were cured off these plasmids. Thus, generated *gmpr* deletion strain was verified for its resistance towards streptomycin and sensitivity towards ampicillin, kanamycin, and chloramphenicol. Thereafter, the genotype of the *guaC* deletion strain was verified and compared with H1174 through PCR using confirmatory primers (Table 8, Table 9, Fig. 9). $H1174^{\Delta guaC}$ strain was found to grow on minimal medium agar plates supplemented with adenine while the presence of either guanine or guanosine did not support its growth, confirming the phenotype of the generated knockout (Fig. 9).

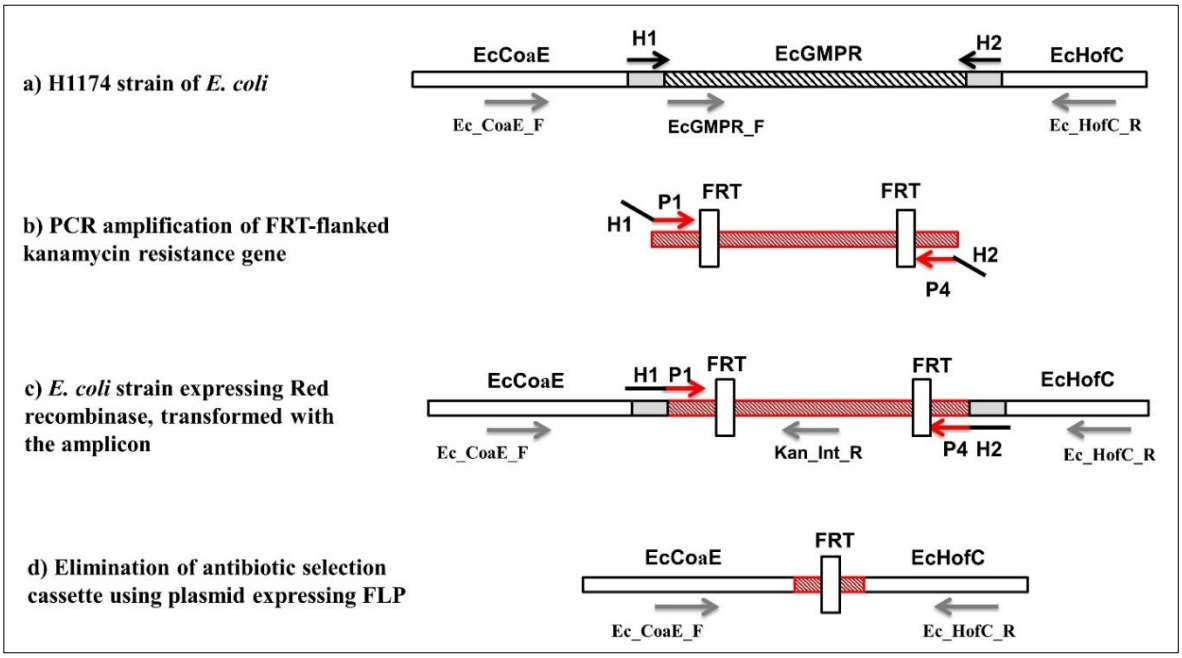

Figure 8. Schematic of the strategy used for knockout of GMPR in H1174 strain of E. coli using Red recombinase. a) Genetic organization *of H1174 strain with EcGMPR gene flanked on either side by EcCoaE (Dephospho-CoA Kinase) and EcHofC (host function of plasmid maintenance). 50 nucleotide homology arms (H1 and H2) flanking EcGMPR are in grey boxes with black arrows*

highlighting the primers. ***b) Amplification of FRT-flanked antibiotic selection cassette from the pKD13 plasmid.*** *Priming sites (P1 and P4) of kanamycin cassette followed by homology arms (H1 and H2) of EcGMPR, respectively are indicated.* ***c) Homologous recombination aided by Red recombinase expressed from the plasmid pKD46*** *replaced EcGMPR with Kan cassette in the knockout strain.* ***d) Excision of the antibiotic selection cassette aided by flippase expressed from the plasmid pCP20.*** *Shown in grey arrows are the various oligonucleotides used for confirming deletion of EcGMPR through PCR (Datsenko KA and Wanner BL, 2000).*

a)

Primer set used	Expected size of amplicon	
	H1174	H1174$^{\Delta guaC}$
EcGMP_H1P1/EcGMP_H2P4 (set 1)	-	+ (1423 bp)
Ec_CoaE_F/Ec_HofC_R (set 2)	+ (2214 bp)	+ (2493 bp)
Ec_CoaE_F/Kan_Int_R (set 3)	-	+ (1083 bp)
EcGMPR_F/Ec_HofC_R (set 4)	+ (1644 bp)	-

b)

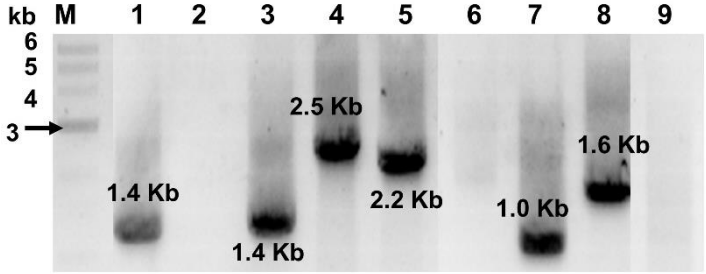

c)

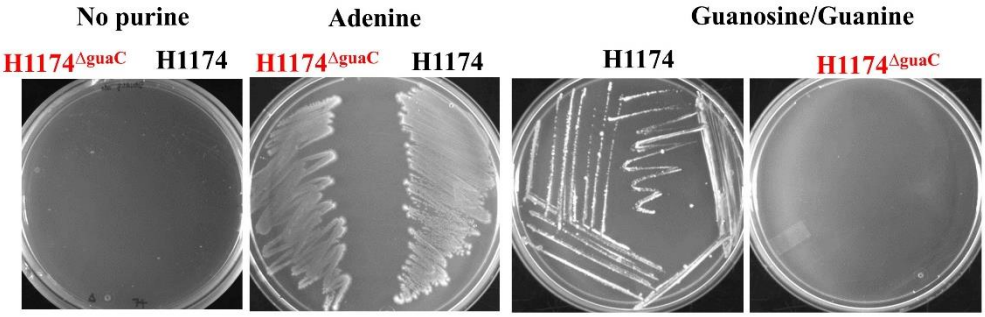

Figure 9. Genotyping and phenotyping of H1174$^{\Delta guaC}$ strain of E. coli. a) Tabulation of confirmatory primers used to verify the deletion strain *by PCR and expected amplicon size (refer Table 8, and Table 9 for oligonucleotide sequences). Primer set (1), and (3) were used for positive confirmatory PCR of the deletion strain and expected amplicons correspond to 1.4 kb, and 1.0 kb, respectively. Primer set (2) yields a positive PCR for both the strains with a 0.3 kb difference. Primer set (4) was designed as a negative PCR control for knockout and positive for H1174 with 1.6 kb amplicon.* ***b) PCR verification of guaC deletion strain of E. coli.*** *Lane 1 is PCR positive control with pKD13 as a template using primer set 1. Lane 3, 4, 9 and 7 correspond to PCR performed with DNA from H1174$^{\Delta guaC}$ strain as a template while Lane 2, 5, 8, and 6 correspond to DNA from H1174 strain being used as a template. Lane 2, 3 represent PCR performed with primer set 1 (1.4 kb amplicon expected from deletion strain); lane 4, 5 with primer set 2 (2.2 kb and 2.5 kb amplicon expected from H1174 and deletion strain, respectively); lane 6, 7 with primer set 3 (1.0 kb amplicon expected from deletion strain) and lane 8, 9 with primer set 4 (1.6 kb amplicon expected from H1174 strain). M, 1 kb DNA molecular weight marker, NEB.* ***c) Dependence of H1174 and H1174$^{\Delta guaC}$ on purines for survival on M9 minimal medium.*** *H1174 and H1174$^{\Delta guaC}$ cells were streaked on M9 minimal medium agar plates containing 50 µg ml^{-1} streptomycin supplemented with no purine or with either 100 µM adenine, or 300 µM guanine/guanosine. Presence of adenine supports the growth of both strains while the lack of purine supplementation resulted in no growth. Plates containing guanine or guanosine led to the growth of H1174 but not H1174$^{\Delta guaC}$, indicating the complete loss of the guaC gene in the later.*

2.4.8 Complementation assay with H1174$^{\Delta guaC}$ strain of *E. coli*

H1174$^{\Delta guaC}$ strain of *E. coli* was transformed with a pTrc99a expression vector carrying the gene for PfIMPDH or PbIMPDH. Multiple constructs of *P. falciparum* gene were examined in the growth rescue assay that expresses native and codon-harmonized full-length and CBS deletion proteins. Based on multiple sequence alignments discussed in Chapter 1 and Chapter 3, catalytic site mutants (C314A, T316A, and Q435E) were generated and tested for their effect on the phenotype of *gmpr* deletion strain in M9 minimal medium. EcGMPR cloned into the pTrc99a vector was used as a positive control.

EcGMPR was found to rescue the growth of H1174$^{\Delta guaC}$ on minimal medium agar plates supplemented with either guanine or guanosine while no growth was observed with any construct of *Plasmodium* species (Fig. 10). As expression levels were found to be extremely low under "Trc" promoter (provided in Chapter 3) all the constructs were further subcloned into pET21b+ expression vector to be able to achieve high levels of protein expression under the strong T7 promoter. H1174$^{\Delta guaC}$ strain was co-transformed with

pACT7, a plasmid expressing T7 RNA polymerase. The bacterial cells were also co-transformed with helper plasmid pKJE7, that codes for a chaperone and/or pLysS plasmid expressing tRNA synthetases for rare codon. The dependence of EcGMPR activity on the key catalytic residues (C186, T188, and E289) was reported using genetic complementation assay in *E. coli* (Min D *et al*., 2008). Complete compromise in bacterial growth was observed with the presence of C186A and T188A mutations while a moderate growth was observed with E289Q mutation. Multiple sequence alignments (presented in Chapter 1 and Chapter 3) revealed that C186 and T188 residues are identical across various IMPDH/GMPR family of proteins while E289 is found replaced by glutamine in PfIMPDH, and PbIMPDH among few others. Therefore, the corresponding amino acid positions in PfIMPDH were mutated (C314A, T316A, and Q435E) and examined for their effect on the growth phenotype of $H1174^{\Delta guaC}$. However, no growth rescue of the *guaC* deletion strain carrying plasmodial genes was observed in any tested condition (Fig. 10). Similar to the observations made in section 2.4.5, various constructs of PfIMPDH expressed in $H1174^{\Delta guaC}$ strain yielded no soluble protein while EcGMPR (positive control) was found to be soluble (data not shown). Hence, genetic complementation assays could not functionally establish PF3D7_0920800 and PBANKA_0821700 genes (annotated as PfIMPDH and PbIMPDH, respectively) as an IMPDH or a GMPR plausibly due to an insufficient soluble and functional protein.

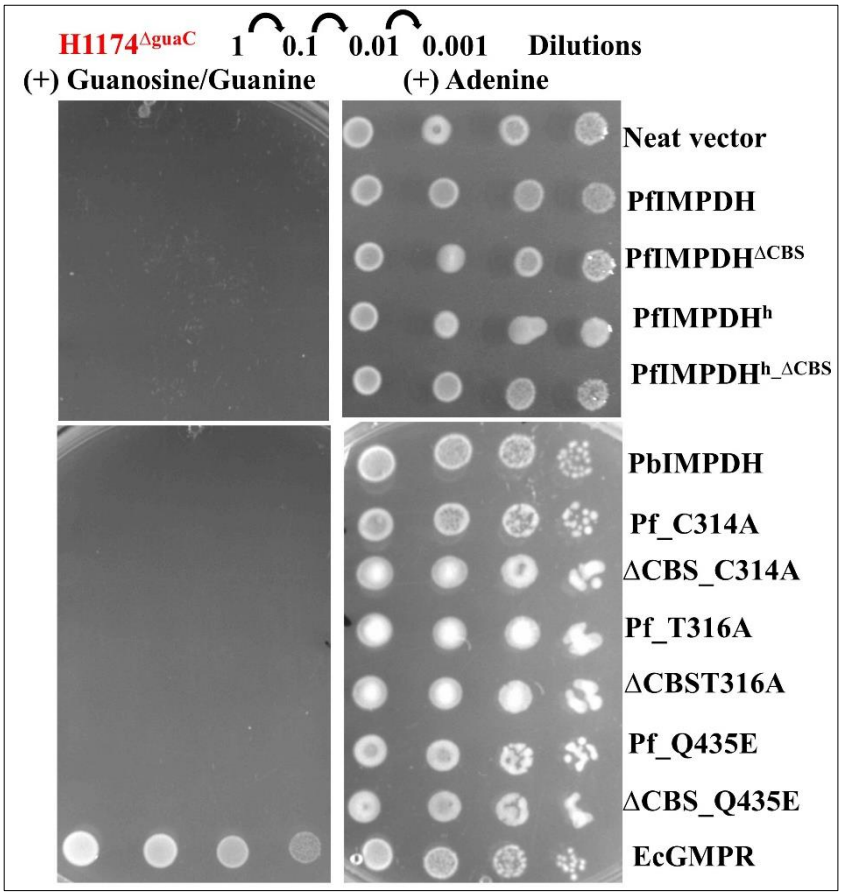

Figure 10. Functional complementation assay of PfIMPDH and PbIMPDH for GMPR activity. *H1174$^{\Delta guaC}$ strain was transformed with pTrc99a or pET21b+ vector carrying either EcGMPR or PbIMPDH or PfIMPDH or PfIMPDH$^{\Delta CBS}$ (both native and codon-harmonized genes) or catalytic site mutants of PfIMPDH and grown overnight in LB medium containing appropriate antibiotics. A_{600nm} =1 of cells were washed with M9 minimal medium twice, serially diluted and spotted on M9 plates containing 0.3 mM IPTG and supplemented with either 100 µM adenine or 300 µM guanosine or guanine. 0.2 % glucose served as a carbon source. All the transformants also contain pACT7 plasmid expressing T7 RNA polymerase. Co-transformation of the deletion strain with chaperone expressing plasmids (Takara, Japan) or helper plasmid expressing tRNA synthetases for rare E. coli codons or both did not rescue growth of transformants carrying PfIMPDH or PbIMPDH on minimal medium. The M9 agar plates were incubated at either 37 °C or 25 °C. However, in all tested conditions, only EcGMPR was able to functionally complement the growth deficiency of H1174$^{\Delta guaC}$ strain.*

2.5 Conclusion

Presence of IMPDH protein in *P. falciparum* was confirmed through antibody detection and found to be localized in the cytoplasm and nucleus (partial) of the parasite. Plasmodial proteins could not complement for loss of IMPDH/GMPR function in *E. coli and S. cerevisiae*. There was no detectable amount of soluble protein on Western blot despite codon harmonization of the gene for expression in *E. coli*. Lack of protein expression despite the presence of gene transcript (RT-PCR) in yeast cells resulted in no growth phenotype of the *guaB* deletion strain on minimal medium. However, the *T. foetus* IMPDH and *E. coli* GMPR used as positive controls were found to functionally complement the deficiency of *guaB* and *guaC*, respectively. Therefore, the insolubility feature of the plasmodial proteins makes it difficult to establish PF3D7_0920800 and PBANKA_0821700 (annotated as IMPDHs) as a bonafide IMPDH or a GMPR.

Chapter 3. Strategies designed towards obtaining PfIMPDH in soluble form

Inosine 5'-monophosphate dehydrogenase (IMPDH) catalyzes the rate-limiting step of guanine nucleotide biosynthesis. IMPDH consists of two domains in the Plasmodium falciparum (Pf) enzyme: core catalytic domain with a $(\beta/\alpha)_8$ barrel and cystathionine beta-synthase (CBS) or Bateman domain. This is the only enzyme which stands uncharacterized till date from purine salvage pathway of P. falciparum. Present work is focused on understanding this enzyme from the parasite. The intron less gene of IMPDH and core catalytic domain, $IMPDH^{\Delta CBS}$ of P. falciparum were cloned into E. coli expression system earlier in the laboratory. Standardization of conditions optimal for over-expression and purification of recombinant PfIMPDH protein in the host stands as a pre-requisite for any further characterization studies.

Various efforts including solubility enhancing tags, generation of various fusion constructs, random mutagenesis, in vitro refolding and codon harmonization stand unsuccessful in obtaining PfIMPDH and $PfIMPDH^{\Delta CBS}$ proteins in the soluble form. Co-expression of tRNA synthetase for the rare codons was always found essential for hyperexpression of the native gene while the presence of chaperones yielded low levels of PfIMPDH and $PfIMPDH^{\Delta CBS}$ in soluble form. However, tight binding of chaperone proteins led to difficulties in purification. Based on protein interactome prediction on STRING, co-expression of PfIMPDH with guanosine 5'-monophosphate synthetase (PfGMPS), an enzyme downstream of IMPDH involved in purine nucleotide biosynthesis was examined. Solubility enhancing mutants predicted using PROSO II were also found to be unsuccessful. Attempts with cell-free protein synthesis using a wheat germ system were not fruitful while E. coli S-30 extract has yielded PfIMPDH in soluble form. However, purification of PfIMPDH from the invitro transcription coupled translation reaction still remains a roadblock. Lastly, sequence analysis among various characterized IMPDH/GMPR family of proteins, with emphasis on the bias in amino acid composition among IMPDHs from plasmodial species and β-aggregation propensity of PfIMPDH is presented.

3.1 Purine nucleotide biosynthesis in *Plasmodium falciparum*

Purines are essential for informational molecules (DNA and RNA), required for energy sources (ATP and GTP), for signaling molecules and also for co-factors. In general, there exist two ways of synthesizing them: *de novo* route and by salvage pathway. However, only the salvage pathway is found to operate in *P. falciparum* (Gardner MJ *et al*., 2002). *Plasmodium falciparum* is most lethal among the five *Plasmodium* species that cause human malaria that includes *P. vivax*, *P. malariae*, *P. ovale,* and *P. knowlesi (www.mmv.org)*. Malaria has a massive impact on human health; it is the world's second biggest killer after tuberculosis. In 2016, an estimated 216 million cases of malaria occurred worldwide. There were an estimated 445,000 deaths from malaria globally (WHO report, 2018). Despite the availability of anti-malarial drugs, the widespread emergence of drug-resistant parasites necessitates a quest for new therapies. Structure and mechanism-based combinatorial approach for drug design have proved highly fruitful. The purine salvage pathway of *P. falciparum* is a novel target for antimalarials, as the parasite lacks the *de novo* purine biosynthetic pathway (Gardner MJ *et al.*, 2002) and completely depends on its host for purine requirements.

In the erythrocytic stages, nucleobases (inosine, hypoxanthine, xanthine, and guanine), nucleosides (adenosine and guanosine) and nucleotides (adenosine 5' monophosphate, AMP) get transported from erythrocytes to the parasite (Cassera MB *et al*., 2011). Hypoxanthine is the major purine source available in the erythrocyte. Hypoxanthine can also be formed from adenosine or inosine by the sequential action of adenosine deaminase (ADA) and purine nucleoside phosphorylase (PNP). Formation of inosine 5'-monophosphate (IMP) from hypoxanthine by the action of hypoxanthine (guanine or xanthine) phosphoribosyl transferase (HG(X)PRTase) stands as a branch point between adenosine 5' monophosphate (AMP) or guanosine 5'-monophosphate (GMP) biosynthesis. IMP, on one hand, is converted to xanthine 5'-monophosphate (XMP) and GMP by sequential action of inosine 5'-monophosphate dehydrogenase (IMPDH) followed by guanosine 5'-monophosphate synthetase (GMPS) and on the other arm by the successive action of adenylosuccinate synthetase (ADSS) and adenylosuccinate lyase (ASL) to form AMP. The parasite has not retained either adenosine or guanosine kinase to be able to

phosphorylate nucleobases (adenosine and guanosine) to AMP and GMP, respectively. Xanthine or guanine could be phosphorylated by HG(X)PRTase to form the final product GMP. However, the extremely low level of these molecules in the red blood cell (RBC) makes the flux through this path insignificant. Lastly, under excess concentrations of adenine or adenosine in the erythrocyte compartment, human adenine phosphoribosyltransferase (hAPRT) or adenosine kinase (hAK) can make AMP available for uptake by the parasite (Cassera MB *et al*., 2008). Thus, salvage of hypoxanthine stands as a major route for purine biosynthesis of the parasite making enzymes involved in the catalysis of IMP to AMP or GMP potential candidates for malarial drug target (Fig. 1).

Inosine 5'-monophosphate dehydrogenase (IMPDH, EC 1.1.1.205) catalyzes the oxidation of inosine 5'-monophosphate (IMP) to xanthosine 5'-monophosphate (XMP) with the concordant reduction of nicotinamide adenine dinucleotide (NAD^+) to NADH. The reaction is a branch point between the adenine and guanine nucleotide biosynthesis, and a rate-limiting step of guanosine 5'-monophosphate (GMP) biosynthesis. Guanine moieties not only serve as building blocks of DNA and RNA synthesis but are also essential for translation, glycosylation, synthesis of tetrahydrobiopterin, and are co-factors for G-proteins and signaling molecules. Further, they also are key allosteric regulators in the cell (Allison AC and Eugui EM, 2000). It has also been shown that PRPP synthetase and ribonucleotide reductase, enzymes involved in nucleotide biosynthesis get stimulated by guanine molecules and inhibited by adenine nucleotides (Allison AC *et al*., 1993). IMPDH, therefore, controls the guanine nucleotide pool which in turn controls the proliferation and many other physiological processes, making IMPDH a potential target for immunosuppression, cancer, antimicrobial, and anti-parasitic infections, and antiviral chemotherapy (Hedstrom L *et al*., 1990; Kohler GA *et al*., 1997; Striepen B *et al*., 2004; Wilson K *et al*., 1991; Wilson K *et al*., 1994; Webster HK and Whaun JM, 1982; Hedstrom L, 2009; Hedstrom L *et al*., 2011; Gorla *et al*., 2012).

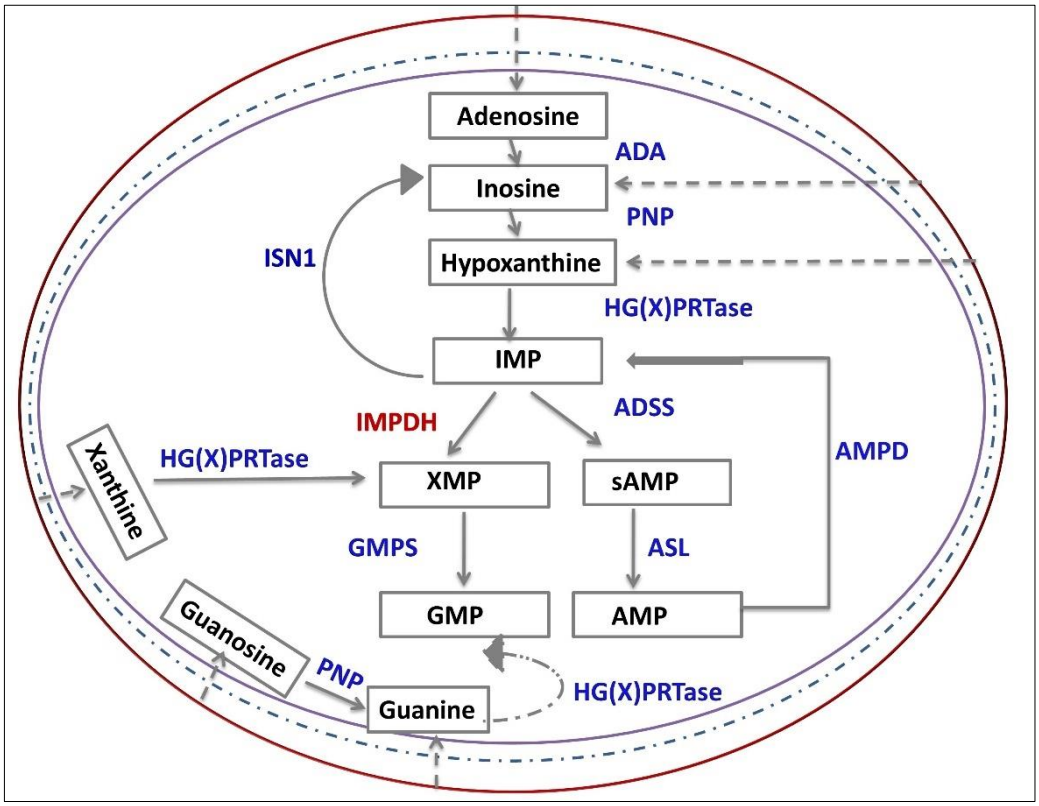

Figure 1. Purine nucleotide synthesis in Plasmodium falciparum. *Adenosine, inosine, hypoxanthine, xanthine, guanosine, and guanine that are salvaged by the parasite from the erythrocyte compartment are indicated in dotted grey arrows. Conversion of adenosine to inosine followed by inosine to hypoxanthine occurs by the sequential action of adenosine deaminase (ADA) and purine nucleoside phosphorylase (PNP). Hypoxanthine is acted upon by hypoxanthine guanine (xanthine) phosphoribosyltransferase (HG(X)PRTase) to yield inosine 5'-monophosphate (IMP). IMP is then acted upon by the downstream enzymes to yield adenosine 5'-monophosphate (AMP) and guanosine 5'-monophosphate (GMP) or could be broken down to inosine by the enzyme IMP-specific nucleotidase (ISN1). IMP dehydrogenase (IMPDH) and GMP synthetase (GMPS) on one arm yields GMP while on the other by the sequential action of adenylosuccinate synthetase (ADSS) and adenylosuccinate lyase (ASL) AMP is formed. AMP is deaminated to IMP by the enzyme AMP deaminase (AMPD). Conversion of salvaged guanosine to guanine occurs by the action of PNP. HG(X)PRTase could directly phosphoribosylate guanine and xanthine to yield GMP and XMP, respectively. The enzyme under study, IMPDH is highlighted in red while all other enzymes are indicated in blue. The red circle is indicative of erythrocyte membrane, while grey dotted and grey circles represent parasitophorous vacuole and parasite plasma membranes, respectively.*

3.2 An overview of procedures employed in obtaining a recombinant protein

A general strategy followed in obtaining a recombinant protein includes cloning of the gene of interest in an expression vector. Choosing bacteria as host is by large advantageous due to its cost-effectiveness and the time required for high yields of cell density. However, protein obtained in such a way would be devoid of post-translational modifications. Optimization of gene expression conditions, solubility assessment followed by protein purification forms a prerequisite for any enzyme characterization. Depending on the availability of a tag and biochemical properties of protein under study, methods employed in purification could vary (Fig. 2). For the purpose of obtaining recombinant PfIMPDH protein, expression profile under different conditions in various strains of *E. coli* (Fig. 3 and Fig. 4) and *S. cerevisiae* were examined. No expression of the protein was found in *S. cerevisiae* (presented in Chapter 2). Episomal expression within human malarial parasite *P. falciparum* (presented in Chapter 2) and rodent parasite *P. berghei* (refer to appendix D at the end of the thesis) were also attempted. Lastly, cell-free protein synthesis was carried out using two commercially available sources that include wheat germ and *E. coli* S30 extracts (Fig. 3).

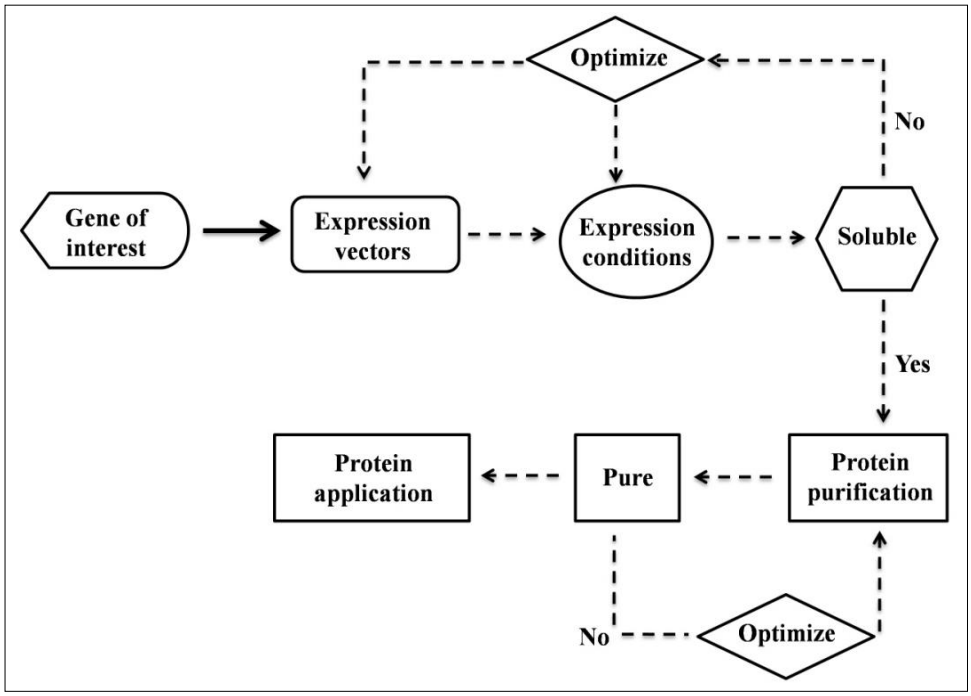

Figure 2. A flow chart describing the steps involved in the characterization of a protein. *The first prerequisite is cloning of the desired gene into expression vectors carrying a suitable tag (solubility tags, affinity tags, and signal sequences). Next step involves the selection of appropriate expression strain with optimal conditions for expression of the protein (temperature, inducer, and presence of helper plasmids). Protein once obtained in soluble form is taken through purification procedures, while insoluble form demands optimization at each step. Further, at the level of purification various chromatographic techniques, buffers and pH conditions need to be standardized. Pure protein obtained is lastly taken forward for downstream applications (structural and kinetic assessment).*

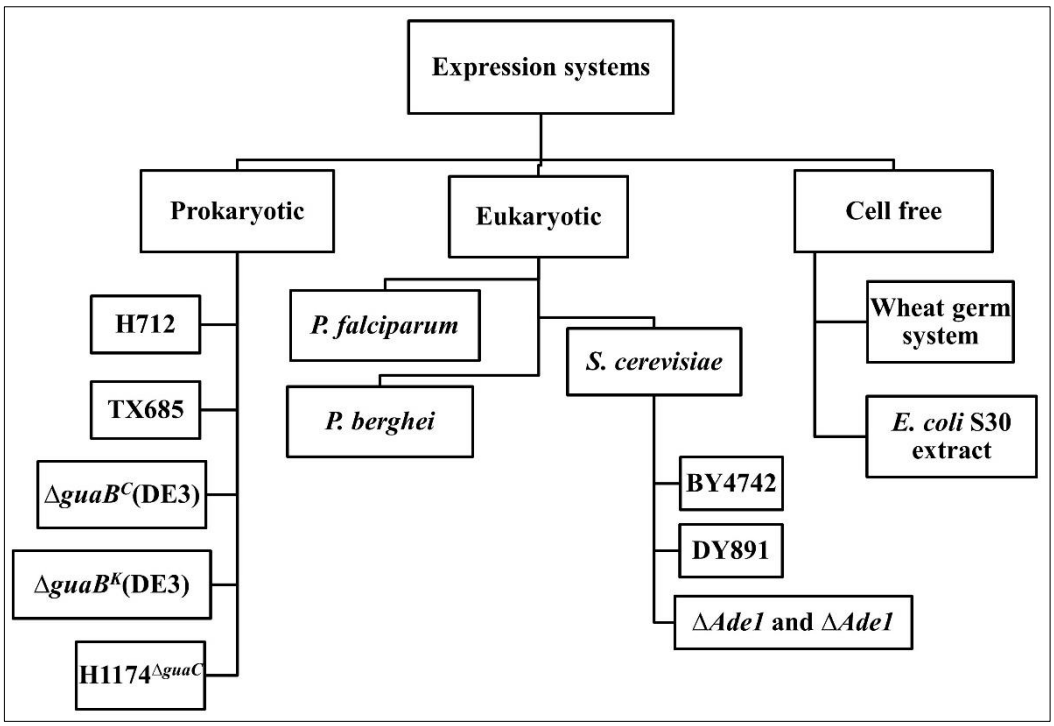

Figure 3. Schematic of various expression systems and the cell types used in the current study. *guaB and guaC are the genes that encode for IMPDH and GMPR, respectively. H712, TX685, and Δ$guaB^C$(DE3) are the impdh deletion strain of E. coli procured from Prof. Hedstrom L, Brandeis University, USA. H712 and TX685 are E. coli K-12 strains while Δ$guaB^C$ is a BL21(DE3) derivative carrying the gene for chloramphenicol resistance. Δ$guaB^K$ is the impdh deletion strain of BL21(DE3) generated in the current study where the endogenous gene was replaced with* neomycin *phosphotransferase II (kanamycin resistance marker). H1174, obtained from Coli genetic stock center, USA is an E. coli K-12 strain with a block in de novo purine synthesis and carries a mutant GMP reductase. P. falciparum 3D7 and P. berghei ANKA strains were used for episomal expression studies. Wild-type (BY4742) and deletion mutants (Δade1 and Δade2) of S. cerevisiae were procured from EUROSCARF, Germany. DY891 is the quadruple impdh deletion strain of yeast obtained from Prof. Reines D, Emory University, USA. Wheat germ and E. coli S30 extracts were purchased from Promega Corporation, USA and New England Biolabs, USA, respectively.*

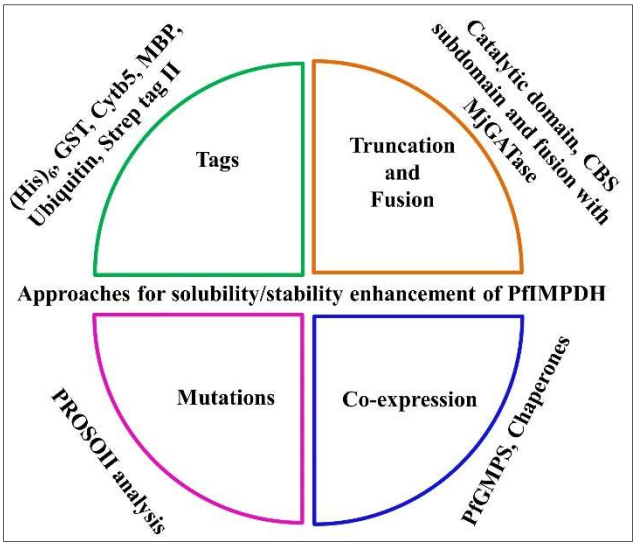

Figure 4. Schematic of the multiple approaches attempted to obtain a stable and soluble form of PF3D7_0920800 annotated as IMPDH in PlasmoDB using E. coli as an expression host. *Various tags to enhance stability and solubility of PfIMPDH were examined that includes glutathione S-transferase (GST), cytochrome b5 (Cytb5), maltose binding protein (MBP), ubiquitin, $(His)_6$-tag and Strep-tag II. Core catalytic domain and the CBS subdomain have been individually cloned and expressed. Glutamine amidotransferase from the hyperthermophilic archaeon, Methanocaldococcus jannaschii (MjGATase) was used as a solubility enhancer fusion tag. Various point mutations were generated using PROSO II solubility predictions. Guanosine 5'-monophosphate synthetase from Plasmodium falciparum (PfGMPS), a downstream enzyme in the purine nucleotide biosynthesis was found to be one of the closely associated proteins of PfIMPDH as determined by STRING analysis and therefore was co-expressed.* ***Also, PfIMPDH gene sequence was codon harmonized for optimal expression in E. coli to enable protein production in the soluble form.***

3.3 Chemicals and reagents

Restriction enzymes, Phusion DNA polymerase, and T4 DNA ligase were from New England Biolabs and were used according to the manufacturer's instructions. Primers were custom synthesized at Sigma-Aldrich, India. All chemical reagents were of high quality and obtained from Sigma-Aldrich, India or Merck, India. Media components were from HiMedia Laboratories, India. IMP, NAD^+ and other biochemicals were of the highest quality available from Sigma-Aldrich, USA. H712, TX685, and Δ*guaB*^{C}(DE3) are the *impdh* deletion strains of *E. coli* procured from Prof. Hedstrom L, Brandeis University, USA. pHUE plasmid was a kind gift obtained from Prof. Baker R, The Australian National University, Australia. Plasmids carrying Strep-tag II (pST50Trc4-STRDHFR and pST50Trc4-DHFRSTR) were purchased from Addgene, USA (Addgene plasmids # 63991 and #64004) (deposited by Dr. Tan S, The Pennsylvania State University, USA). Wheat germ, and.

E. coli S 30 extracts were purchased from Promega Corporation, USA and New England Biolabs, USA, respectively.

3.4 Experimental procedure

3.4.1 Expression analysis

Sequences of primers for PCR amplification and expression vectors used are provided in the Appendix C at the end of the thesis. Clones were confirmed error-free by DNA sequencing. Depending on the expression vector and the promoter, the appropriate strain of *E. coli* was used for protein production that includes TX685, H712, *ΔguaB*^{C} (DE3), *ΔguaB*^{K} (DE3) and H1174$^{\Delta guaC}$ strain of *E. coli.* Helper plasmids used were tRNA synthetases (pLysS from Rosetta(DE3) or pRIL from Arctic Express(DE3)) and chaperone expressing plasmids (pKJE7, pG-KJE8, pGro7, pG-Tf2, and pTf16) from TAKARA, Japan. Transformants were grown at 37 °C prior to induction with various concentrations of IPTG at an A_{600nm} of 0.5-0.6 followed by lowering of growth temperature to either 25 °C or 18 °C. Cells were harvested 8 h-12 h post-induction, resuspended in lysis buffer containing 50 mM Tris HCl, 10 % glycerol, 2 mM DTT, 0.1 mM PMSF and 0.25 mM KCl. A thorough pH screen was performed to obtain PfIMPDH in soluble form, amenable for purification. (Details of various tags, molecular weight, pI values and pH screening are given in the Appendix C at the end of the thesis). In brief, different buffers with pH values ranging from 5.5 to 12.0 were used as lysis buffer to obtain recombinant PfIMPDH in soluble form. Multiple attempts with varying pH, salt concentration, buffer type, and ionic strength (in all possible permutations and combinations) were carried out and these are summarized in TableC3. Co-expression of chaperone plasmids was achieved with transformants grown at 30 °C till an A_{600nm} of 0.7-1.0 in the presence of 0.5 mg ml^{-1} arabinose before induction with 0.1 mM IPTG at 25 °C for 12 h. Antibiotics were used at a final concentration of 50 µg ml^{-1} kanamycin, 100 µg ml^{-1} ampicillin, 34 µg ml^{-1} chloramphenicol and 20 µg ml^{-1} streptomycin. Cell disruption was achieved by ultrasonication or by subjecting the lysate to a pressure of 1000 psi using a French press. Cell debris was separated by centrifugation at 30000g for 30 min at 4 °C. Lysates were resolved on 12 % SDS-PAGE followed by Western blotting probed using protein-specific antibodies raised in mouse or anti-$(His)_6$ antibodies (Sigma-Aldrich, USA).

Transformants expressing PfIMPDH with pelB sequence (periplasmic localization signal) were subjected to osmotic shock immediately after harvest. Briefly, 2 ml of culture was centrifuged and re-suspended in 0.02 ml of culture medium. 0.02 ml of chloroform was added to the cells and incubated at room temperature for 15 min with intermittent vortexing. 0.2 ml of 10 mM Tris HCl, pH 8.0 was added to stop the reaction followed by centrifugation

at 6000g for 20 min. The supernatant thus obtained was treated as osmotic shock fluid and examined for the presence of PfIMPDH by Western detection.

3.4.2 Solubility predictions

PROSO II (Smialowski P *et al.*, 2012), an online solubility predictor for the proteins expressed in *E. coli* was used to check the solubility index of PfIMPDH. Global alignments of several IMPDH sequences were generated with Clustal Omega (Sievers F *et al*., 2011) and rendered using ESPIRPT 3.0 (Robert X and Gouet P, 2014). These alignments were carefully examined for plausible residues that could be mutated to obtain protein in soluble form. Primers were designed to introduce the point mutations using overlapping PCR strategy (Appendix C at the end of the thesis provides primer sequences). Further, a fusion of PfIMPDH with highly soluble protein, glutamine amidotransferase from *Methanocaldococcus jannaschii* (MjGATase) yielded high solubility scores on PROSO II.

3.4.3 Dehydrogenase assay

For the activity measurements, reaction mix containing 50 mM Tris HCl, pH 8.0, 100 mM KCl, 3 mM EDTA, 1 mM DTT, 0.1 mM IMP and 0.2 mM NAD^+ in a volume of 250 µl was used. All the assays were carried out at 37 °C on a Hitachi-U 2010 spectrophotometer fitted with water circulated cell holder. The temperature was maintained using an external water bath. The enzymatic activity of PfIMPDH was measured by an increase in absorbance at 340 nm with the formation of NADH as a function of time (ε= 6.22 mM^{-1} cm^{-1}). The data were analyzed using GraphPad Prism, version 5 (GraphPad Software Inc., San Diego, CA).

3.4.4 Codon harmonization

Re-designing of PfIMPDH gene sequence suitable for heterologous expression in *E. coli* was carried out using the software Eugene (Gaspar P *et al.*, 2012). The obtained output was checked on Genescript rare codon analysis tool for parameters such as codon adaptation index (CAI) and presence of negative CIS elements [(GGTAAG), (GGTGAT), (AATAAA), (AAAAAA), (ATTTA), (TTTTTT), (AAAAAAA)] that could hinder expression in *E. coli*. Manual curation of the negative CIS elements was done, checked for inclusion of any restriction site or STOP codon during the process of re-design. Lastly, the codon harmonized gene sequence was represented graphically on a graphical codon usage analysis tool, GCUA (Fuhrmann M *et al.*, 2004). Gene sequence codon harmonized for expression in *E. coli*

system was custom synthesized at Biomatik Co-operation, Canada. This was further sub-cloned into the desired expression vector.

3.4.5 Cell-free protein synthesis

3.4.5.1 Wheat germ extract

In vitro protein synthesis was performed by transcription coupled to translation using wheat germ extract as per manufacturer's guidelines (Promega Corporation, USA). Briefly, 1 µg of template DNA was used per 50 µl reaction containing 25 µl wheat germ extract, 2 µl reaction buffer, 1 µl T7 RNA polymerase, 1 mM amino acid mixture, 1 µl murine ribonuclease inhibitor (New England Biolabs, USA) and volume made up using nuclease-free water. The reaction was incubated at 30 °C for 2.5 h followed by detection on Western blot using anti-$(His)_6$ antibody (Sigma-Aldrich, USA).

3.4.5.2 *E. coli* S30 extract

In vitro protein synthesis was performed using *E. coli* S-30 extract from NEB PURExpress system as per the manufacturer's guidelines (PURExpress, New England Biolabs, USA). Briefly, 125 ng of template DNA was used per 12.5 µl reaction containing 5 µl of solution A, 3.75 µl of solution B, 0.25 µl murine ribonuclease inhibitor (New England Biolabs, USA) and volume made up using nuclease-free water. The reaction was incubated at 37 °C for 2.5 h followed by detection on Western blot using an *in-house* generated anti-PfIMPDH antibody. Reaction volumes were either scaled up or down accordingly as per the experimental requirement.

The reaction volume was scaled up to 0.05 ml and incubated at 37 °C for 2.5 h. Post-incubation, reaction volume was made up to 150 µl using a buffer containing 50 mM HEPES-KOH, pH 7.6, 0.3 M KCl and 10 mM magnesium acetate. The reaction sample was then loaded on 1000 kDa cutoff 0.5 ml centrifugal filter units (Vivaspin 500, Sartorius, Germany), centrifuged at 4 °C till about 30 µl was retained in the upper chamber. Approximately 120 µl of flow through was collected and applied onto Ni-NTA matrix (Thermo-Scientific, USA) for 30 min at 4 °C. Unbound fraction was separated from the matrix. Ni-NTA matrix with bound protein was directly analyzed on 12 % SDS-PAGE and detected by Western blotting probed with anti-PfIMPDH antibody generated in mouse.

3.4.6 *In silico* examinations on amino acid sequence of PfIMPDH

Amino acid composition of all the biochemically characterized IMPDHs and GMPRs till date has been calculated using the web server (http://protcalc.sourceforge.net/). An average representation of each amino acid across these soluble IMPDHs and GMPRs is calculated and compared with amino acid content of IMPDH from various plasmodial species. The β-aggregation propensity of PfIMPDH$^{\Delta CBS}$ and identification of potential residues to be altered to accomplish protein in soluble form have been carried out using the online tool, TANGO (Linding R *et al*., 2004; Fernandez-Escamilla AM *et al*., 2004). The input parameters were set at pH 7.0, 277.15 K, 50 mM ionic strength, and PfIMPDH$^{\Delta CBS}$ protein concentration at 10 µM with no protection at N- and C- termini.

3.5 Results and discussion

3.5.1 Initial observations from expression studies

PfIMPDH and PfIMPDH$^{\Delta CBS}$ were cloned into the bacterial or yeast expression vectors to yield either untagged or tagged recombinant proteins. Multiple tags cloned either on N- or C-terminus were tested to be able to achieve stable and soluble protein which includes glutathione S-transferase (GST), cytochrome b5 (Cytb5), maltose binding protein (MBP), ubiquitin, $(His)_6$-tag and Strep-tag II. Co-transformation of a plasmid expressing tRNA synthetases (pLysS or pRIL) for rare codons was essential for hyperexpression of native PfIMPDH gene.

Bacterial expression vector pTrc99a carrying PfIMPDH with no tag had been cloned earlier in the laboratory (pTrc_PfIMPDH). As the expression of PfIMPDH was found to require helper plasmid encoding tRNA synthetases (pLysS from Rosetta(DE3) or pRIL from Arctic Express(DE3)) for codons that are under-represented in *E. coli*, these plasmids were always included. Expression of PfIMPDH was found to be extremely low under Trc promoter (Fig. 5). Maltose binding protein (MBP) was reported to be a preferred fusion partner due to its remarkable ability to enhance the solubility of its fusion partners (Kapust RB & Waugh DS, 1999). The ubiquitin tag was also reported to be an enhancer of solubility (Catanzariti AM *et al*., 2004). Expression of PfIMPDH from pMal_(MBP)PfIMPDH was found to yield a low level of soluble protein. However, it was observed to be extremely unstable and no protein band corresponding to PfIMPDH was detected after treatment with Factor Xa (to cleave MBP) on silver stained SDS-PAGE (Fig. 5). Expression of PfIMPDH

from pHUE_(His_6-Ub)PfIMPDH construct was also found to be low, associated with degradation and yielded insoluble form of protein (Fig. 5) Fusion of cytochrome b5 (Cytb5) (pET21b_(Cytb5)PfIMPDH) and glutathione S-transferase to PfIMPDH (pGEX_(GST)PfIMPDH) also could not yield protein in soluble form (data not shown). Expression studies carried out in various strains of *E. coli* that include TX685, H712, BL21(DE3) or Rosetta(DE3) pLysS also yielded similar results. A summary of the expression host, protein tag and solubility are provided in Table 1.

Subcloning of PfIMPDH under T7 promoter with an N- or C-terminal $(His)_6$-tag (pET15b_PfIMPDH$(His)_6$ or pET28b_PfIMPDH$(His)_6$) yielded hyperexpression of recombinant PfIMPDH as compared to expression under weak promoters such as "Trc" and "Tac"; however, no protein was detected in the soluble form (Fig. 5). According to a report by San-Miguel T (San-Miguel T *et al.,* 2013), a high yield of active soluble proteins were obtained by combining early-log phase cultures and low temperatures for protein induction. When IPTG was added at an A_{600nm} of 0.1 and cultures were maintained at 4 °C for 48-72 h, the soluble protein yield was 3 fold higher than that obtained in the mid-log phase (A_{600nm} of 0.6). Besides, it was reported that the target protein expression increased and the endogenous bacterial proteins reduced, thus making the protein purification process easier and more efficient. PfIMPDH was always found to yield inclusion bodies when expressed in *E. coli* at 18 ˚C. Hence, an attempt was made to induce the recombinant PfIMPDH at 0.1 A_{600nm} with 0.3 mM IPTG followed by incubation at 6 ˚C for 4 days. Intriguingly, hyperexpression of PfIMPDH was not hindered at such low temperatures however, the induced protein was found to remain insoluble. Efforts to solubilize the inclusion body of PfIMPDH using 1 % Triton X-100 which is a non-ionic detergent or 100 mM zwitterionic CHAPS buffer or alkali treatment with 100 mM sodium carbonate (Na_2CO_3) remained unsuccessful. The inclusion bodies obtained after the lysis were solubilized in lysis buffer containing 6 M guanidine hydrochloride (GdnHCl) and purified under denaturing conditions. On-column refolding or drop dilution or dialysis were not successful in obtaining a refolded and functional PfIMPDH protein. However, purified recombinant PfIMPDH under denaturing conditions was used for the generation of antibody in mouse (presented in Chapter 2).

Table 1. Various expression constructs of native PfIMPDH gene.

Expression Vector	Expression construct	Expression host	Observations
pTrc99a Untagged	pTrc_PfIMPDH	TX685, H712, H1174$^{\Delta guaC}$	low level of expression upon tRNA supplementation, completely insoluble
pMal-p2x N-term MBP tag	pMal_(MBP)PfIMPDH	Rosetta (DE3) pLysS, BL21(DE3)	low level of expression, completely insoluble
Cytb5_pET21b N-term Cytb5 tag	pET21b_(Cytb5)PfIMPDH	Rosetta(DE3) pLysS, BL21(DE3)	low level of expression, completely insoluble
pGEX-6p-3 N-term GST tag	pGEX_(GST)PfIMPDH	Rosetta(DE3) pLysS, BL21(DE3)	low level of expression, completely insoluble
pHUE N-term ubiquitin tag	pHUE_(His_6-Ub)PfIMPDH	Rosetta(DE3) pLysS	low level of expression, completely insoluble and degraded
pET15b N-term $(His)_6$ tag	pET15b_$(His)_6$PfIMPDH	Rosetta(DE3) pLysS, BL21(DE3)	hyperexpression, completely insoluble
pET28b/pET21b C-term $(His)_6$ tag	pET28b_PfIMPDH$(His)_6$ pET21b_PfIMPDH$(His)_6$	Rossetta(DE3) pLysS, BL21 (DE3), C41 (DE3), C43 (DE3), LEMO, Δ*guaB*^{C}(DE3)	hyperexpression, largely insoluble, minor amount of soluble protein upon supplementation with pKJE7
pET23d Untagged catalytic core	pET23d_PfIMPDH$^{\Delta CBS}$	Rosetta(DE3) pLysS, BL21(DE3)	hyperexpression, completely insoluble
pET28b/pET21b catalytic core C-term $(His)_6$ tag	pET28b_PfIMPDH$^{\Delta CBS}(His)_6$ pET21b_PfIMPDH$^{\Delta CBS}(His)_6$	Rosetta(DE3) pLysS, BL21(DE3), Δ*guaB*^{C}(DE3)	hyperexpression, largely insoluble, a significant increase in soluble protein level upon supplementation with pKJE7

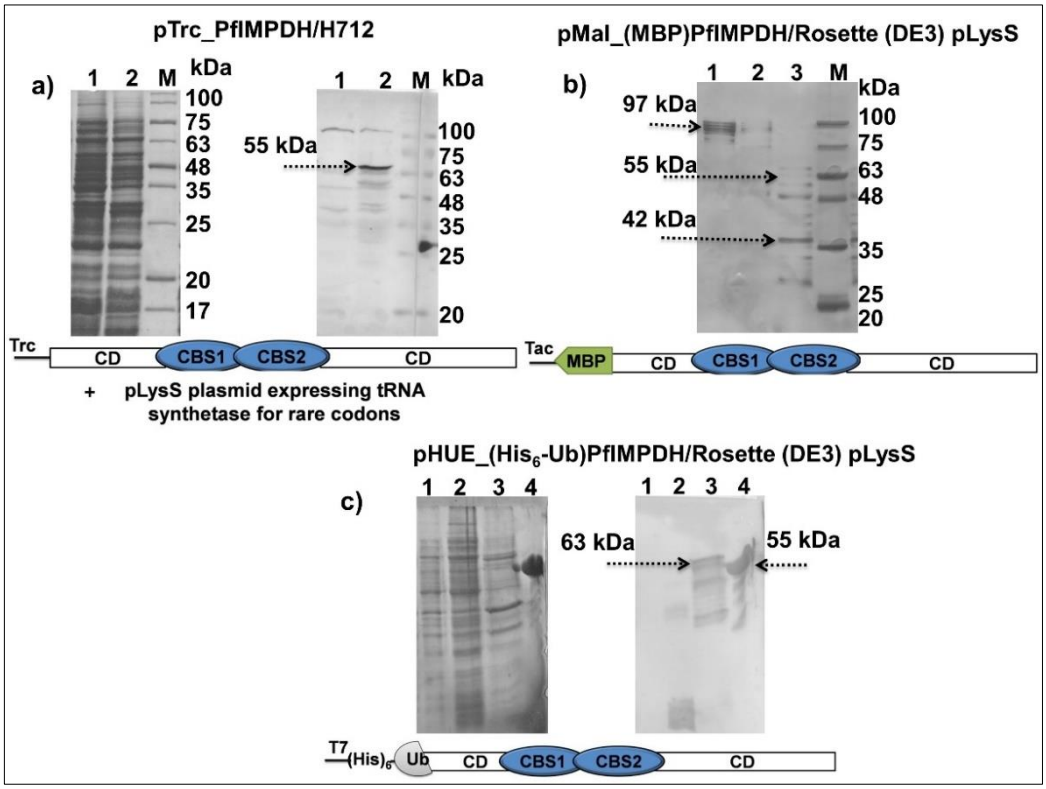

Figure 5. Expression and solubility check by SDS-PAGE of various constructs of PfIMPDH. a) Expression of un-tagged PfIMPDH using pTrc_PfIMPDH construct in H712 co-transformed with the helper plasmid pLysS, expressing tRNA synthetases for codons under-represented in E. coli. *Left and right panel correspond to Coomassie blue stained SDS-PAGE and Western blot, respectively. Lane 1, pTrc99a neat vector; lane 2, PfIMPDH, the molecular weight of 55 kDa highlighted with a black arrow (0.6 A_{600nm} culture incubated with 0.5 mM IPTG at 27 ˚C for 18 h).* ***b) Silver-stained SDS-PAGE of maltose binding protein cleaved from MBP-PfIMPDH fusion protein using Factor Xa.*** *Expression was performed in Rosetta(DE3) pLysS strain of E. coli. Lane 1, uncut MBP-IMPDH; lane 2, MBP-IMPDH mock digestion (protein was found unstable); lane 3, 4 h digestion; Black arrows (42 kDa, and 97 kDa) point out protein bands corresponding to MBP, and the MBP_PfIMPDH fusion, respectively. However, arrow at 55 kDa indicates absence of PfIMPDH.* ***c) Solubility check of (His_6-Ub)PfIMPDH expressed in Rosetta(DE3) pLysS strain of E. coli.*** *Left and right panel correspond to Coomassie Blue stained SDS-PAGE and Western blot, respectively. Lane 1, cells containing pHUE neat vector; lanes 2 and 3, soluble and insoluble fractions of induced pHUE_(His_6-Ub)PfIMPDH containing cells, respectively; lane 4, protein sample used as positive control for antibody detection. The molecular weight of (His_6-Ub)PfIMPDH is 63 kDa highlighted by the black arrow. M, pre-stained protein molecular weight marker (Abcam, USA). Western blot was probed using anti-PfIMPDH antibody (1:2500) raised mouse. Secondary anti-mouse antibody (1:4500) conjugated to HRP was purchased from Sigma Aldrich, USA.* AEC *(3-amino-9-ethylcarbazole) was used as a substrate for HRP yielding a colored precipitate on the membrane. Schematic of each vector expressing PfIMPDH is represented below the respective expression profiles where CD refers to the catalytic domain.*

3.5.2 Co-expression of PfIMPDH with PfGMPS or pKJE7

STRING is a platform for known and predicted protein interactions (Snel B *et al.*, 2000; Szklarczyk D *et al.,* 2017). Based on the parameters of co-existence, neighborhood, gene fusion, co-expression, experimental evidence, databases, and text mining the associations of various proteins are mapped out. With PfIMPDH protein sequence as input, STRING analyzer listed the functional partners of PfIMPDH in decreasing order of their relevance (Table 2). Guanosine 5'-monophosphate synthetase (PfGMPS), the enzyme downstream of PfIMPDH in the guanosine nucleotide biosynthesis was found to have the highest score of 0.999 among various others. The proximity of their occurrence and sequential enzyme action forms the basis for attempting co-expression of these two genes with the possibility of obtaining PfIMPDH in the soluble fraction. This further could be extrapolated to study the effect of enzyme associations on the protein folding and thereby improved yield of soluble fraction.

Thus, genes involved in GMP biosynthesis, PfIMPDH (*guaB*) and PfGMPS (*guaA*) were cloned tandemly into pETDuet expression vector (pET_PfIMPDH$(His)_6$_PfGMPS) under T7 promoter for co-expression. *ΔguaB*^{C}(DE3), an *E. coli* strain deficient of endogenous IMPDH and partially disrupted GMPS (Macpherson IS *et al*., 2010) was transformed with the pET_PfIMPDH$(His)_6$_PfGMPS and helper plasmid for tRNA synthetases for rare codons in *E. coli* (pRIL plasmid from Arctic Express (DE3)). PfGMPS was found to be soluble as reported earlier from the laboratory (Bhat JY *et al*., 2008) while PfIMPDH formed inclusion bodies under all tested induction and growth conditions. Also, the degradation of both the proteins was evident from Western blot under any tested growth condition (Fig. 6).

Hyper expression of PfIMPDH$(His)_6$ was observed under T7 promoter but no Western detectable soluble form. Therefore, co-expression of chaperones for obtaining proper folded and thereby soluble PfIMPDH was tested. Out of the five commercially available chaperone expressing plasmids (TAKARA, Japan), pKJE7 composed of DnaK (70 kDa), DnaJ (40 kDa) and GrpE (22 kDa) was found to yield for the first-time antibody detectable soluble recombinant PfIMPDH (Fig. 6). The total protein content, however, is reduced due to lower cell density caused by quadruple antibiotic selection pressure. The

supernatant was applied onto Ni-NTA matrix, washed with 10 column volumes of lysis buffer followed by 2 column volumes of lysis buffer containing 0.5 M $MgCl_2$-25 mM ATP. Bound protein was eluted in lysis buffer containing 0.1 M EDTA. Amount of PfIMPDH protein bound to Ni-NTA matrix as assessed by SDS-PAGE followed by Western blot using anti-PfIMPDH antibody was found to be extremely low and most of it was observed in the unbound fraction. Further, the three chaperon proteins DnaK (70 kDa), DnaJ (40 kDa) or GrpE (25 kDa) always co-purified along with PfIMPDH despite a wash step with lysis buffer containing 25 mM Mg-ATP (Fig. 6). *In silico* modeling of PfIMPDH has predicted the protein to be an octamer. Further, IMPDH from various other sources is known to possess an intrinsic property of aggregation with the evidence for the formation of higher-order oligomers' (Hedstrom L, 2009, Labesse G *et al*., 2003). A large fraction of soluble protein being unbound to Ni-NTA matrix could be attributed to its oligomeric state occluding the $(His)_6$-tag from binding. Purification profile was found to be similar even upon the inclusion of 0.1 % Triton X-100 with no further improvement in levels of soluble recombinant PfIMPDH protein.

Table 2. The predicted associations of PfIMPDH on String database.

PlasmoDB Id	Protein	Score
PF3D7_1012600	Guanosine 5'-monophospahte synthetase (PfGMPS)	0.999
PF3D7_1410200	Cytidine triphosphate synthetase (PfCTPS)	0.993
PF3D7_0720800	Pyrophosphatase, putative (PfPPase)	0.992
PF3D7_0206700	Adenylosuccinate synthetase (PfADSS)	0.989
PF3D7_1012400	Hypoxanthine guanine (xanthine) phosphoribosyl transferase (PfHG(X)PRTase)	0.988
PF3D7_1329400	Adenosine 5'-monophosphate deaminase, putative (PfAMPD)	0.976

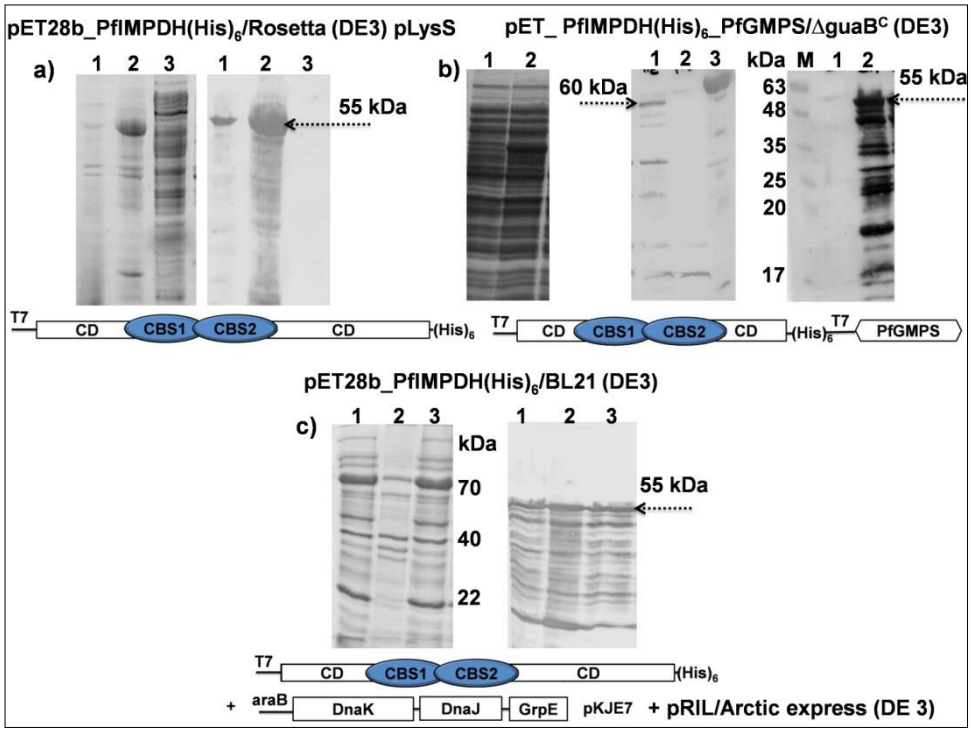

Figure 6. Expression and solubility check on SDS-PAGE of PfIMPDH expressed from a T7 promoter. a) Expression of PfIMPDH(His)$_6$ in Rosetta(DE3)pLysS strain of E. coli. *Left and right panel correspond to Coomassie Blue stained SDS-PAGE and Western blot, respectively. Lane 1, protein sample used as positive control for antibody detection; lanes 2 and 3 are insoluble and soluble fractions (0.6 A_{600nm} with 0.25 mM IPTG at 27 ˚C for 18 h). The molecular weight of PfIMPDH is 55 kDa indicated by the black arrow.* ***b) Co-expression of PfIMPDH and PfGMPS in Δ$guaB^C$(DE3) strain of E. coli.*** *Left panel corresponds to Coomassie Blue stained SDS-PAGE where lanes 1 and 2 are uninduced and induced samples of PfIMPDH(His)$_6$_PfGMPS (induced at 0.6 A_{600nm} with 0.25 mM IPTG at 27 ˚C for 18 h). The middle panel is Western detection using anti-PfGMPS antibody raised in rabbit where lanes 1 and 2 contain soluble and insoluble fractions, respectively; lane 3, protein sample used as positive control for antibody detection. The right panel is Western confirmation of PfIMPDH, where lanes 1 and 2 correspond to soluble and insoluble fractions, respectively. M, pre-stained protein molecular weight marker (Abcam, USA). Expression of PfGMPS (60 kDa) and PfIMPDH (55 kDa) are highlighted by black arrows. Secondary anti-rabbit/anti-mouse antibody conjugated to HRP was purchased from Sigma-Aldrich, USA.* AEC *(3-amino-9-ethylcarbazole) was used as a substrate for HRP yielding a colored precipitate on the membrane.* ***c) Co-expression of PfIMPDH(His)$_6$ with chaperone expressing plasmid, pKJE7 in BL21(DE3) strain of E. coli****. Lanes 1, 2, and 3 indicate soluble, insoluble and Ni-NTA flow-through fractions, respectively. DnaK (70 kDa), DnaJ (40 kDa) and grpE (22 kDa) from pKJE7 constitute the chaperone system expressed under inducible arabinose promoter. Schematic of each construct is represented below the respective expression profiles where CD refers to the catalytic domain.*

3.5.3 PROSO II analysis

PROSO II (**Pro**tein **so**lubility evaluator) is a public web server which predicts the solubility of a given protein based on a classifier exploiting subtle differences between soluble proteins from target registration database (TargetDB), protein data bank (PDB) and insoluble proteins from TargetDB. It does not include the membrane-bound and transmembrane proteins. On a scale of 0-1, a default threshold of ≥0.6 was set to categorize soluble proteins. PfIMPDH inherently gave a score of 0.446 on PROSO II indicating the insolubility feature which was evident from various expression and purification attempts in the current study. Various permutations and combinations with different fusion tags on PfIMPDH and PfIMPDH$^{\Delta CBS}$ were given as input to predict a construct with high solubility score. The generated fusion proteins and their solubility index are listed in Table 3 and Table 4.

3.5.3.1 MjGATase as a solubility enhancer

The glutamine amidotransferase gene involved in purine biosynthesis from *M. jannaschii,* a hyperthermophilic archaeon (MjGATase) was characterized from our laboratory and found to be highly soluble when expressed in *E. coli* (Table 4) (Ali R *et al*., 2012; Ali R *et al*., 2013). Owing to the solubility, stability, and foldability, MjGATase was fused to PfIMPDH (MjGATase-PfIMPDH(His)$_6$) and PfIMPDH$^{\Delta CBS}$ (MjGATase-PfIMPDH$^{\Delta CBS}$(His)$_6$). TEV protease cleavage site was introduced between MjGATase and PfIMPDH that could be used to separate the two proteins. A (His)$_6$-tagged construct of TEV protease generated by Prof. Waugh D, National Cancer Institute, USA was obtained from Addgene, USA. No expression of MjGATase-PfIMPDH(His)$_6$ fusion gene was detectable (79 kDa) on Western blot while MjGATase-PfIMPDH$^{\Delta CBS}$(His)$_6$ was largely found to be in insoluble fraction (65 kDa) when expressed in Rosetta(DE3) pLysS strain of *E. coli* (Fig. 7, Table 5). The very low level in the soluble fraction precluded purification.

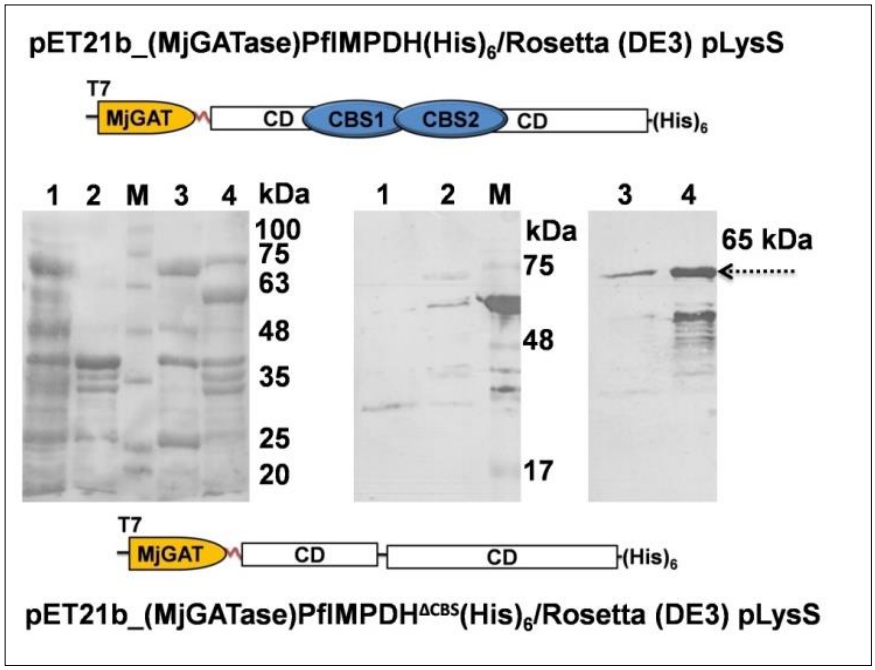

Figure 7. Expression and solubility check by SDS-PAGE of *MjGATase-PfIMPDH(His)$_6$* ***and*** *MjGATase-PfIMPDH$^{\Delta CBS}$(His)$_6$* ***in Rosetta(DE3) pLysS strain of E. coli.*** *Glutamine amidotransferase from the hyperthermophilic archaeon M. jannaschii (MjGATase) is a highly soluble and stable protein previously characterized in the laboratory. Using this as a solubility enhancer, fusion constructs were generated. Left panel represents the Ponceau S stained electro-transferred PVDF membrane. Middle and the right panel correspond to antibody detection of the fusion constructs. Lanes 1 and 2 contain soluble and insoluble fractions of cells expressing the fusion protein MjGATase-PfIMPDH(His)$_6$, respectively. Lanes 3 and 4 have soluble and insoluble fractions of cells expressing the fusion protein MjGATase-PfIMPDH$^{\Delta CBS}$(His)$_6$, respectively. M, pre-stained protein molecular weight marker (Abcam, USA) along with a protein (55 kDa) used as a positive control for Western detection. PfIMPDH full-length fusion protein was undetectable (79 kDa) on the Western blot. A faint band corresponding to MjGATase-PfIMPDH$^{\Delta CBS}$(His)$_6$ was observed in the soluble fraction (65 kDa, indicated with a black arrow). Western blot was probed using mouse anti-(His)$_6$ antibody (Sigma Aldrich, USA). Secondary anti-mouse antibody conjugated to HRP was also purchased from Sigma-Aldrich, USA.* AEC *(3-amino-9-ethylcarbazole) was used as a substrate for HRP yielding a colored precipitate on the membrane. Schematic of each construct is indicated below the respective expression profiles where CD refers to the catalytic domain.*

3.5.3.2 Mutations based on PROSO II analysis

A study on expression analysis of about a thousand open reading frames from *P. falciparum* using *E. coli* as a heterologous expression system was published by structural genomics consortium (Mehlin C *et al*., 2006). The study reports that the expression of a significantly large number of the target genes could not be achieved while one-third of the

targets (337) express, but remain in inclusion bodies and only a few (63) of the total targets yielded soluble protein. A list of features like high molecular weight, more basic isoelectric point (pI) and less homology to *E. coli* proteins were independently correlated with difficulties in expression. Of these, pI of the protein strongly correlates to the determination of the expressed protein being soluble or insoluble. The isoelectric point of PfIMPDH was found to be 7.8 as determined by the tool ProtParam on the Expasy server (Wilkins MR *et al.,* 1999). The solubility index was found to be 0.4 which was below the threshold of 0.6 for a protein to be soluble when expressed in *E. coli* as predicted by PROSO II. The PROSO II score and pI value strongly correlate to the insolubility of PfIMPDH in *E. coli* expression system. Designing minimal changes in the amino acid composition without perturbing any key residues involved in either catalysis or holding essential interactions was carried out manually. The multiple sequence alignments generated were carefully examined for the variable and conserved regions of IMPDH across organisms, specifically among *Plasmodium* species. The amino acids in PfIMPDH sequence were replaced by corresponding residues from PbIMPDH. Multiple iterations with curated protein sequences were analyzed for the solubility score and pI value using PROSO II and ProtParam, respectively. The list of minimal mutations which yielded solubility index of 0.76 and pI value of 6.8 was generated (Table 3 and Table 4). The mutations were incorporated into PfIMPDH using overlap PCR strategy. The clones obtained were confirmed for the presence of designed residue changes by DNA sequencing.

Δ*guaB*^{K}(DE3) strain of *E. coli* was transformed with pET21b_PfIMPDH(His)$_6$(m_I) (K86D, S172H, H218K_K221H, S310G, A325G, and K420V) or pET21b_PfIMPDH(His)$_6$(m_II) (K86D, S172H, H218K_K221H, S310G, and K420V) along with helper plasmids (pKJE7, plasmid expressing chaperone and pRIL from Arctic Express(DE3) expressing tRNA synthetases for rare codons). PfIMPDH(His)$_6$(m_I) carrying seven mutations was found to be highly unstable and degraded while, stable full-length protein expression of PfIMPDH(His)$_6$(m_II) was found to be largely in the insoluble form (Fig. 8). However, the minor fraction of the soluble form of PfIMPDH(His)$_6$(m_II) detected on Western blot, similar to PfIMPDH(His)$_6$ did not efficiently bind the Ni-NTA affinity matrix. This demonstrates that the in-silico analysis is not fruitful, and predictions are

difficult to implicate for such proteins. Ability of IMPDHs to multimerize and form fibrils could possibly contribute to the insolubility feature of the recombinant PfIMPDH (literature on high order oligomers and fibril formation is provided in Chapter 1).

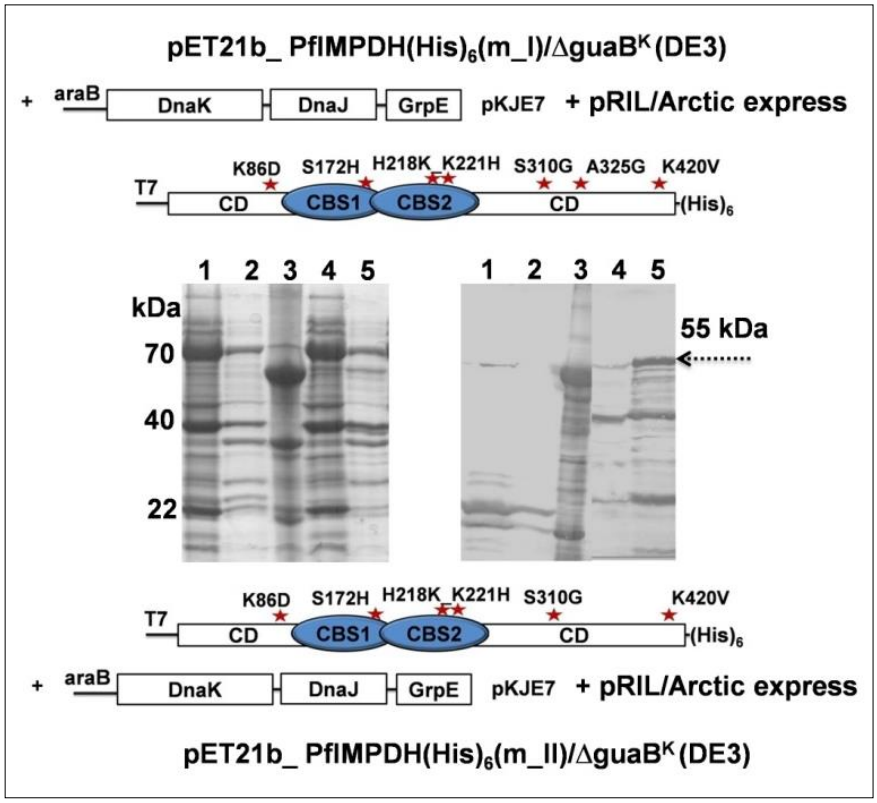

Figure 8. Solubility check of *PfIMPDH(His)$_6$(m_I) and PfIMPDH(His)$_6$(m_II)* ***expressed in ΔguaB^K (DE3) strain of E. coli.*** *Left and right panel corresponds to Coomassie-stained SDS-PAGE and Western blot, respectively. PfIMPDH(His)$_6$(m_I) and PfIMPDH(His)$_6$(m_II) carry a set of single point mutations (**K86D, S172H, H218K_K221H, S310G, A325G, and K420V**) and (**K86D, S172H, H218K_K221H, S310G, and K420V**), respectively, that were generated based on solubility predictions by PROSO II, an online solubility prediction server (**Smialowski P. et al, 2012**). Both the mutant proteins were tested for expression and solubility in the impdh deletion strain with 0.5 mM IPTG at 25 °C, co-transformed with chaperone expressing plasmid, pKJE7 (Dnak 70 kDa, DnaJ 40, grpE 22 kDa) and pRIL, helper plasmid expressing tRNA synthetases for rare codons in E. coli (isolated from Arctic Express(DE3) strain of E. coli (Stratagene, USA)). Lanes 1 and 2 correspond to the soluble and insoluble fraction of cells expressing PfIMPDH(His)$_6$(m_I); lanes 4 and 5 correspond to the soluble and insoluble fraction of cells expressing PfIMPDH(His)$_6$(m_II); Back arrow points to PfIMPDH(His)$_6$(m_II) in the insoluble fraction, while an extremely faint band corresponding to PfIMPDH(His)$_6$(m_I) was observed; lane 3 corresponds to a protein sample (55 kDa) used as a positive control for antibody detection. Western blot was probed using anti-PfIMPDH antibody raised in mouse. Secondary anti-mouse antibody conjugated to HRP was purchased from Sigma Aldrich, USA.* AEC *(3-amino-9-ethylcarbazole) was used as a substrate for HRP yielding a colored*

precipitate on the membrane. Schematic of each construct is indicated below the respective expression profiles where CD stands for the catalytic domain and the point mutations generated are indicated in red asterisks.

Table 3. Solubility index of various IMPDHs calculated using PROSO II solubility prediction algorithm (Smialowski P *et al.*, 2012). Sequences from various species of *Plasmodium* which share an identity of 84 % and similarity of 89 % are compared with *Tritrichomans foetus* and *M. jannaschii* IMPDHs both of which are highly soluble when expressed in *E. coli*.

Source	Predicted class	Solubility score
P. falciparum	Insoluble	0.446
P. berghei	Insoluble	0.555
P. chaubudi	Insoluble	0.425
P. vivax	Insoluble	0.519
P. knowlesi	Insoluble	0.521
P. yoelii	Insoluble	0.458
T. foetus	Soluble	0.717
M. jannaschii	Soluble	0.684

Table 4. Solubility predictions of fusion, deletion and mutant constructs of *P. falciparum* and *P. berghei* IMPDH using PROSO II web server (Smialowski P *et al.*, 2012). MjGATase refers to glutamine amidotransferase from *M. jannaschii*, a highly soluble protein. TEV (tobacco etch virus) protease cleavage site aids in separation of the tag from the protein. M_I and M_II refer to the mutant constructs of PfIMPDH generated using predictions of PROSO II. The amino acids in PfIMPDH sequence were replaced by corresponding residues from PbIMPDH.

	Predicted class and score	Fusion construct or mutation	Predicted class and modified score
PfIMPDH	Insoluble; 0.446	pET21b_PfIMPDH(His)$_6$	Insoluble; 0.505
PfIMPDH	Insoluble; 0.446	pET21b_(MjGATase)PfIMPDH(His)$_6$	Soluble; 0.647
PfIMPDH$^{\Delta CBS}$	Insoluble; 0.547	pET21b_PfIMPDH$^{\Delta CBS}$(His)$_6$	Soluble; 0.619
PfIMPDH$^{\Delta CBS}$	Insoluble; 0.547	pET21b_(MjGATase)PfIMPDH$^{\Delta CBS}$(His)$_6$	Soluble; 0.757
[a]PfCBS	Insoluble; 0.364	pNEB_PfCBS(His)$_6$	Soluble; 0.645
MjGATase	Soluble; 0.873	pET21b_(His)$_6$MjGATase	Soluble; 0.901
[b]PbIMPDH	Insoluble; 0.555	pET21b_PbIMPDH(His)$_6$	Soluble; 0.605
PbIMPDH	Insoluble; 0.555	pET21b_(MjGATase)PbIMPDH(His)$_6$	Soluble; 0.738
M_I	Insoluble; 0.446	pET21b_ PfIMPDH(His)$_6$(m_I)	Soluble; 0.76
M_II	Insoluble; 0.446	pET21b_ PfIMPDH(His)$_6$(m_II)	Soluble; 0.75

[a] *Provided in Chapter 4;* [b] *Appendix D at the end of the thesis*.

Table 5. Summary of gene expression from various constructs generated based on STRING and PROSO II predictions.

Expression vector	Expression construct	Expression host	Observations
pET21b N-term MjGATase and C-term $(His)_6$ tag	pET21b_(MjGATase)PfIMPDH$(His)_6$	Rosetta(DE3) pLysS	No expression
pET21b N-term MjGATase and C-term $(His)_6$ tag	pET21b_(MjGATase)PfIMPDH$^{\Delta CBS}(His)_6$	Rosetta(DE3) pLysS	low level of expression and largely insoluble
pETDUET IMPDH C-term $(His)_6$ tag and untagged GMPS	pET_ PfIMPDH$(His)_6$_PfGMPS	Δ*guaB*^{C}(DE3)	low level of expression, high degradation seen in both GMPS and IMPDH.
pET21b K86D, S172H, H218K_K221H, S310G, A325G, and K420V with C-term $(His)_6$ tag	pET21b_ PfIMPDH$(His)_6$(m_I)	Δ*guaB*^{K}(DE3)	Largely degraded, a faint protein band was observed
pET21b K86D, S172H, H218K_K221H, S310G and K420V with C-term $(His)_6$ tag	pET21b_ PfIMPDH$(His)_6$(m_II)	Δ*guaB*^{K}(DE3)	Moderate level of degradation, a minor amount of soluble protein

3.5.3.3 Expression analysis of PfIMPDH$^{\Delta CBS}$

PfIMPDH$^{\Delta CBS}$ cloned into the pET23d expression vector (pET23d_PfIMPDH$^{\Delta CBS}$) earlier in the laboratory yielded completely insoluble protein with gene expression conditional to the presence of pLysS helper plasmid (Fig. 9). Based on the results obtained from PROSO II solubility predictions (Table 4) a C-terminal $(His)_6$-tagged core catalytic domain was constructed (PfIMPDH$^{\Delta CBS}(His)_6$). Rosetta(DE3) pLysS strain of *E. coli* transformed with pET28b_PfIMPDH$^{\Delta CBS}(His)_6$ yielded PfIMPDH$^{\Delta CBS}$ for the first time in a soluble form (Fig. 9). Similar to the full-length PfIMPDH, the presence of pKJE7 chaperone plasmid significantly improved the yield of soluble protein intriguingly in the absence of a helper plasmid expressing tRNA synthetases for rare codons in *E. coli*. However, the

majority of the soluble PfIMPDH$^{\Delta CBS}$ did not bind to the Ni-NTA matrix but remained in the flow-through and always found to co-exist with the chaperone proteins (despite an extensive wash with 25 mM Mg-ATP).

Polyethyleneimine (PEI) treatment was performed to enable separation of the contaminating chaperones (DnaK, 40 kDa and grpE, 22 kDa) which are highly negatively charged at pH 7.6 (Table 6). PEI precipitation depends on two factors, pH and ionic strength and it preferentially precipitates DNA along with highly negatively charged proteins at an ionic strength of 0.1-1 M KCl (Zillig W *et al.*, 1970 and Burgess RR and Jendrisak JJ, 1975). However, the nucleic acid-protein pellet was found to have a very large proportion of the soluble PfIMPDH$^{\Delta CBS}$ co-precipitated with chaperone proteins. Attempts were unsuccessful in improving the yield of the soluble fraction and purity of the recombinant proteins (PfIMPDH and PfIMPDH$^{\Delta CBS}$) because of the co-purification of any or all of the three chaperone proteins DnaK, DnaJ or grpE.

Table 6. Physico-chemical properties of chaperone proteins and PfIMPDH$^{\Delta CBS}$. Protein sequences were obtained from the Universal Protein Resource repository (UniProt). Physico-chemical properties were determined using an online tool, Protein Calculator v3.4 (http://protcalc.sourceforge.net/).

Protein	Molecular weight	pI	Charge at pH 7.6
DnaK	70 kDa	4.83	Highly negative
DnaJ	40 kDa	7.98	Positive
GrpE	22 kDa	4.68	Highly negative
pET28b_PfIMPDH$^{\Delta CBS}$(His)$_6$	43 kDa	6.95	Negative

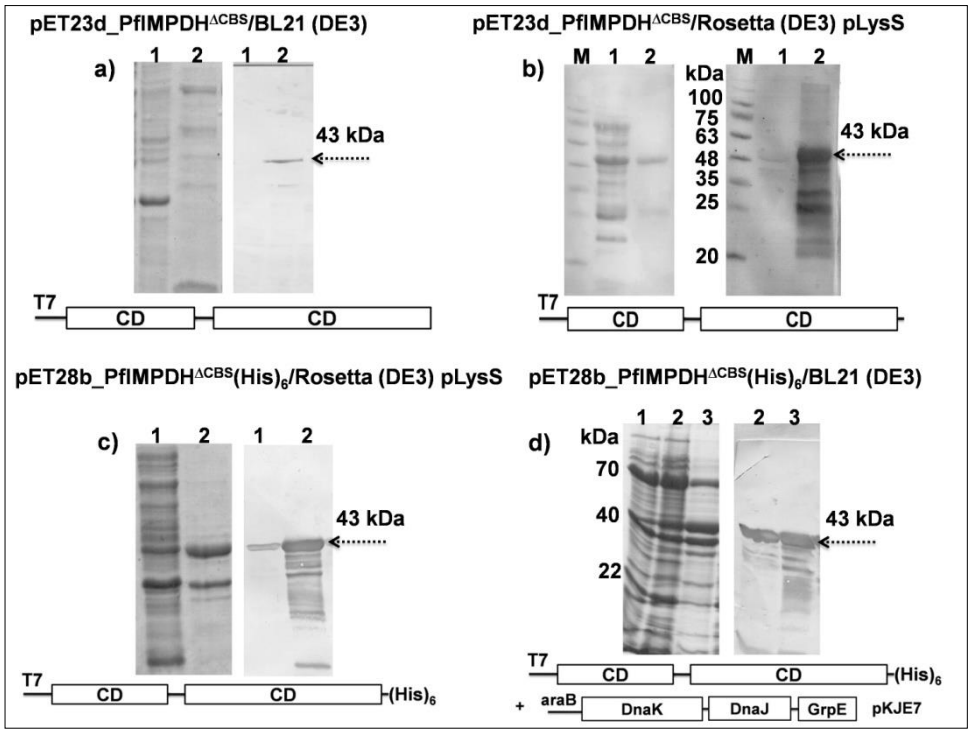

Figure 9. Solubility check of various PfIMPDH$^{\Delta CBS}$ expression constructs. *In each image left and right panel corresponds to Coomassie-stained SDS-PAGE and Western blot, respectively.* ***a)*** *Expression of* ***PfIMPDH$^{\Delta CBS}$ in BL21(DE3) strain of E. coli****. Lanes 1 and 2 are the soluble and insoluble fractions.* ***b)*** *Expression of* ***PfIMPDH$^{\Delta CBS}$ in Rosetta(DE3) pLysS strain of E. coli.*** *Presence of helper plasmid carrying genes for tRNA synthetases for rare codons increased the expression level of PfIMPDH$^{\Delta CBS}$. Lanes 1 and 2 are the soluble and insoluble fractions.* ***c)*** *Expression of* ***PfIMPDH$^{\Delta CBS}$(His)$_6$ in Rosetta(DE3) pLysS strain of E. coli****. The inclusion of C-terminal (His)$_6$ tag has yielded a small fraction of soluble protein. Lanes 1 and 2 are the soluble and insoluble fractions.* ***d)*** *Expression of* ***PfIMPDH$^{\Delta CBS}$(His)$_6$ in BL21(DE3)****. Co-expression of plasmid, pKJE7 carrying DnaK (70 kDa), DnaJ (40 kDa) and grpE (22 kDa) chaperone system has resulted in increased levels of soluble protein without the supplementation of helper plasmid for tRNA synthetases. Lane 1, neat pET28b/pKJE7 vectors; lanes 2 and 3 correspond to soluble and insoluble fractions; M, pre-stained protein molecular weight marker (Abcam, USA). Western blot was probed using anti-PfIMPDH antibody raised in mouse. Secondary anti-mouse antibody conjugated to HRP was purchased from Sigma Aldrich, USA.* AEC *(3-amino-9-ethylcarbazole) was used as a substrate for HRP yielding a colored precipitate on the membrane. Schematic of each construct is indicated below the respective expression profiles where CD refers to the catalytic domain.*

3.5.4 Activity measurements

Lysates corresponding to 3.2 ml of *ΔguaB*^{K}(DE3) strain of *E. coli* carrying pET21b neat vector, pET21b_PfIMPDH(His)$_6$, pET21b_PfIMPDH$^{\Delta CBS}$(His)$_6$, pET21b_ PfIMPDH(His)$_6$(m_I) and pET21b_ PfIMPDH(His)$_6$(m_II) co-transformed with both pRIL and pKJE7 were examined for IMP dehydrogenase activity. The NAD^+ dependent dehydrogenase activity of PfIMPDH/PfIMPDH$^{\Delta CBS}$ was monitored at 340 nm as the formation of NADH from NAD^+ with an absorption coefficient of 6.22 mM^{-1} cm^{-1}. As compared to neat vector control, all other bacterial lysates displayed similar activity of NAD^+ to NADH conversion with no significant increase in NADH production upon addition of IMP to the assay mix (Fig. 10). Activity measurements of the MjIMPDH enzyme (Chapter 5) monitored in the presence of any of these bacterial lysates was found to be significantly inhibited indicating the presence of contaminants in the protein preparation (soluble lysate) inhibiting IMP dependent dehydrogenase activity (Fig. 10). Dehydrogenase activity measurements in the presence of Mg-ATP (in order to dislodge the bound chaperon molecules) and higher concentrations of substrates (1 mM NAD^+ and 1 mM IMP to relieve competition for substrates from contaminating proteins) did not yield any further change. Therefore, the functionality of PfIMPDH could not be established owing to the presence of contaminating *E. coli* molecules or due to the tight association with the chaperone proteins. PfIMPDH/PfIMPDH$^{\Delta CBS}$ in H1174$^{\Delta guaC}$ strain of *E. coli* (co-transformed with plasmids expressing T7 RNA polymerase and pKJE7) examined for its ability to catalyze GMP reductase reaction through genetic complementation assay was found unsuccessful (discussed in Chapter 2). Thereafter, these *E. coli* lysates were analyzed for protein solubility through Western detection. However, no protein was found in soluble fraction and therefore could not examine the ability of PfIMPDH to catalyze NADPH dependent reductive deamination of GMP.

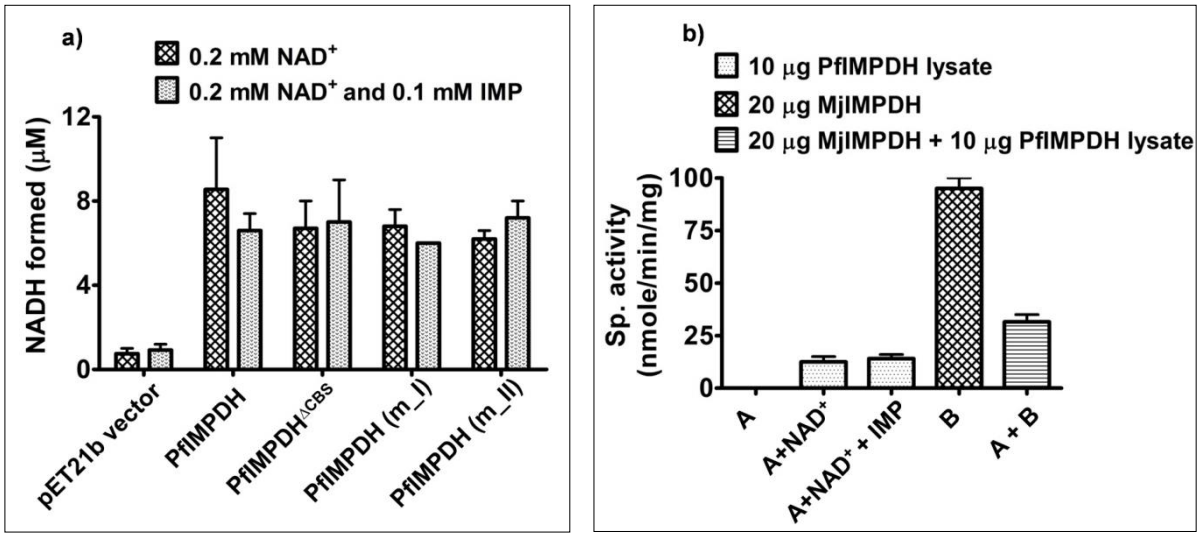

Figure 10. Activity measurements. *Activity measurements were recorded at 37 °C by an increase in absorbance at 340 nm with the formation of NADH as a function of time (ε= 6.22 $mM^{-1}.cm^{-1}$). Standard assay mixture contained 50 mM Tris HCl, pH 8.0, 100 mM KCl, 3 mM EDTA, 1 mM DTT, 0.1 mM IMP and 0.2 mM NAD^+ in 250 μl final volume. The data were replotted using GraphPad Prism, version 5 (GraphPad Software Inc., San Diego, CA).* ***a) Lysates of Δ$guaB^K$(DE3) strain*** *of E. coli obtained from induction of cells containing pET21b neat vector, pET21b_PfIMPDH$(His)_6$, pET21b_PfIMPDH$^{\Delta CBS}(His)_6$, pET21b_PfIMPDH$(His)_6$(m_I) and pET21b_PfIMPDH$(His)_6$(m_II) in the presence of helper plasmids (pKJE7 and pRIL) examined for IMP dehydrogenase activity. Each lysate corresponding to 3.2 ml of culture equivalent is shown on the x-axis with the concentration of NADH formed on the y-axis. Black bars represent NAD^+ to NADH conversion independent of IMP and grey shaded bars represent NADH formation in the presence of IMP. Background NAD^+ to NADH conversion was observed in the absence of IMP with no significant increase upon addition of IMP.* ***b) Activity measurements of IMPDH from M. jannaschii*** *in the absence and presence of lysates obtained from Δ$guaB^K$(DE3) expressing PfIMPDH. Activity corresponding to the lysate is shown on the x-axis with specific activity (nmol min^{-1} mg^{-1}) on the y-axis. A on the x-axis corresponds to activity measurement of 10 μg of PfIMPDH$(His)_6$ lysate in the absence of substrates. A+NAD^+, in the presence of 0.2 mM NAD^+; A+NAD^++IMP, in the presence of both the substrates; B represents enzyme activity measured with 20 μg of MjIMPDH; A+B indicates the drop in activity of MjIMPDH with the addition of 10 μg of PfIMPDH lysate. Experiments were performed at least twice in duplicate and the error bars represent the standard deviation of data.*

3.5.5 Codon harmonization

Eugene, an online gene optimization tool was used to re-design PfIMPDH gene for maximal expression in *E. coli* without changing the amino acid sequence. Codon adaptation index (CAI) value of native PfIMPDH gene was found to be 0.64 for expression in *E. coli* while codon harmonized gene sequence yielded a value of 0.87 (Table 7). CAI value >0.8 indicates a high probability of the recombinant protein expressing in the heterologous system, *E. coli* in this case. Manual curation of the negative CIS elements was done, checked for inclusion of any restriction site or STOP codons during the process of re-design. Lastly, the harmonized gene sequence was represented graphically on a graphical codon usage analysis tool, GCUA (Fuhrmann M *et al.*, 2004) (Fig. 11).

Codon harmonization refers to synonymous codon replacement without changing the amino acid residue. One of the reasons attributed to low expression or formation of insoluble aggregates is the differences in synonymous codon usage between expression and natural hosts. Slowing down or a halt of the ribosomal progression may occur upon encounter with such a discrepancy in codon usage. The aim of codon harmonization is to achieve the translational rates of the protein of interest in the heterologous expression system similar to its origin. The challenges associated with the discrepancy in codon usage patterns of *P. falciparum* when expressed in *E. coli* has been identified owing to the bias introduced by the high (80 %) AT content (Weber JL, 1987). A significant increase in the yield of the soluble protein was reported for five different proteins from the malarial parasite through codon harmonization (Angov E *et al*., 2008) while codon optimization which simply changes all the native codons to maximal usage in *E. coli* was found to yield only insoluble protein (Pan W *et al*., 1999 and Singh S *et al*., 2003).

Table 7. Genescript analysis of PfIMPDH native and Eugene codon harmonized gene sequences (Gaspar P *et al.*, 2012). CAI refers to codon adaptability index.

Gene	CAI	GC %	Negative CIS elements
PfIMPDH	0.64	30.04	3
Eugene harmonized	0.86	46.41	2
Manual curation	0.87	47.03	2

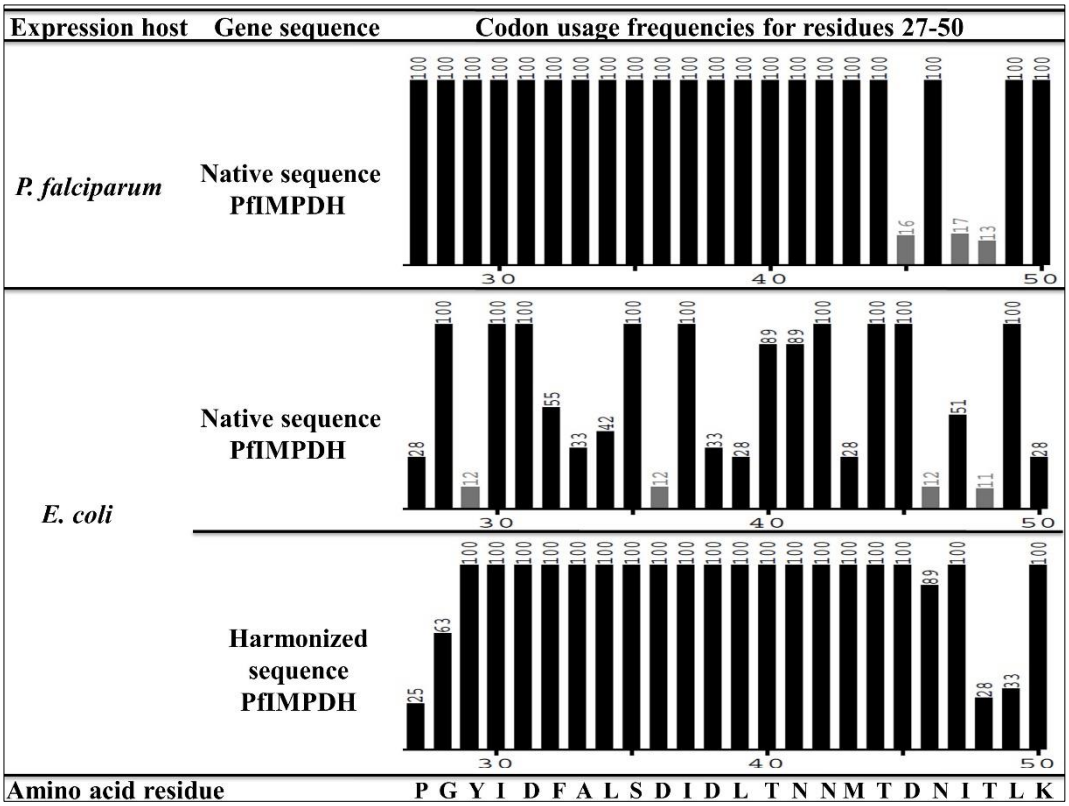

Figure 11. Codon harmonization of PfIMPDH gene sequence for optimal expression in E. coli. *Codon usage frequencies of PfIMPDH gene in P. falciparum vs. expression in E. coli highlights the dissimilarities. Codon harmonization brings back the profile of these frequencies similar to that of the native host rather than simply modifying all the less represented codons to high frequency as in the case of optimization. Harmonization was performed using the tool Eugene (Gaspar P et al., 2012). Codon region of amino acids from 27 to 50 has been depicted graphically on graphical codon usage analysis tool, GCUA (Fuhrmann M et al., 2004) with residues indicated on the bottom vs. codon usage frequencies on top of the bar graph.*

3.5.5.1 Sub-cloning of codon harmonized PfIMPDH gene for expression in *E. coli*

Codon harmonized PfIMPDH gene sequence was custom synthesized at Biomatik Corporation, Canada. Synthesized gene was supplied as a clone in pUC57 vector with multiple restriction sites upstream and downstream of the gene. Expression of codon harmonized PfIMPDH gene was simultaneously tested in both *in vivo* (*E. coli*) and *in vitro* (cell-free protein synthesis) systems. Using suitable restriction enzymes, insert was sub-cloned into pNEB or pST expression vectors yielding untagged (pNEB_hPfIMPDH), C-terminal $(His)_6$-tag (pNEB_hPfIMPDH$(His)_6$ and pNEB_hPfIMPDH$^{\Delta CBS}(His)_6$) or C-

terminal Strep-tag II (pST_hPfIMPDH(StrII)) constructs which were expressed in *ΔguaB*^{K}(DE3) strain of *E. coli* in the presence or absence of pKJE7 helper plasmid. Expression levels of untagged hPfIMPDH from pNEB_hPfIMPDH vector was observed to be low in comparison to that of pNEB_hPfIMPDH(His)$_6$ and pST_hPfIMPDH(StrII) constructs expressing C-terminal (His)$_6$-tag or Strep-tag II, respectively (Fig. 12). Codon harmonization of PfIMPDH gene for expression in *E. coli* did not yield the expressed protein in soluble form under any tested condition (Fig. 12). Failure of codon harmonization in producing a soluble form of protein may probably indicate the existence of translation-independent mRNA toxicity in bacterial gene expression which is a recent addition to the repertoire of solubility determinants of a recombinant protein (Mittal P *et al.*, 2018).

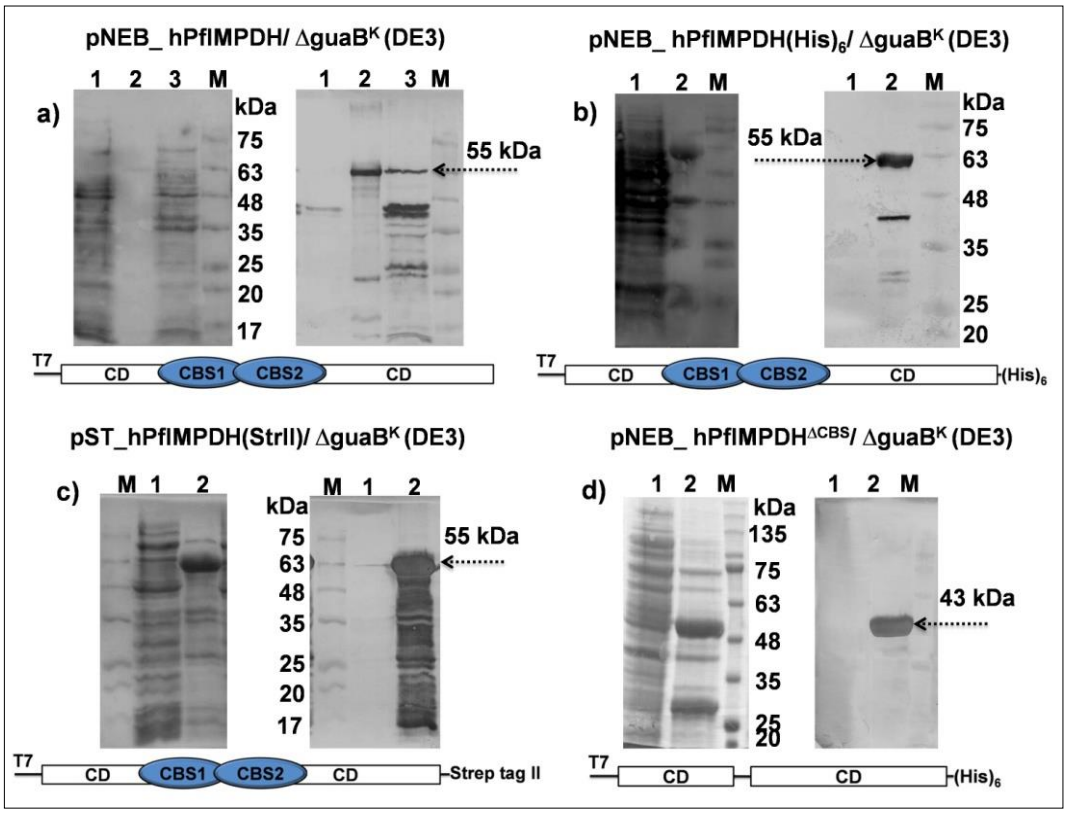

Figure 12. Expression and solubility check of codon harmonized PfIMPDH full-length and core catalytic domain in ΔguaB^{K}(DE3) strain of E. coli. *In each image, left and right panels correspond to Coomassie-stained SDS-PAGE and Western blot, respectively. hPfIMPDH and hPfIMPDH$^{\Delta CBS}$* ***that*** *correspond to molecular weight of 55 kDa and 43 kDa, respectively are indicated by black arrows. M is the pre-stained protein molecular weight marker (Abcam, USA).* ***a) Expression of hPfIMPDH.*** *Lanes 1 and 3 correspond to soluble and insoluble fractions of codon harmonized PfIMPDH, respectively; lane 2, a protein used as positive control for antibody detection.* ***b)***

Expression of hPfIMPDH(His)$_6$. *Lanes 1 and 2 have soluble and insoluble fractions of codon harmonized PfIMPDH with a C-terminal (His)$_6$ tag, respectively.* ***c) Expression of hPfIMPDH(StrII).*** *Lanes 1 and 2 have soluble and insoluble fractions of codon harmonized PfIMPDH with a C-terminal Strep-tag II, respectively.* ***d) Expression of hPfIMPDH$^{\Delta CBS}$(His)$_6$.*** *Lanes 1 and 2 represent soluble and insoluble fractions of codon harmonized PfIMPDH$^{\Delta CBS}$ with a C-terminal (His)$_6$ tag, respectively. a) and c) Western blots were probed using anti-PfIMPDH antibody raised in mouse. b) and d) Western blots were probed using mouse anti-(His)$_6$ antibody (Sigma Aldrich, USA). Secondary anti-mouse antibody conjugated to HRP was purchased from Sigma Aldrich, USA.* AEC *(3-amino-9-ethylcarbazole) was used as a substrate for HRP yielding a colored precipitate on the membrane. Schematic of each construct is represented below the respective expression profiles where CD refers to the catalytic domain.*

3.5.6 Cell-free protein synthesis

3.5.6.1 Wheat germ system

The most widely used heterologous expression system, *E. coli* was chosen to serve the purpose of producing recombinant protein. A broad spectrum of strategies including the use of different expression strains of *E. coli*, supplemented with or without helper plasmids (pRIL, pLysS and/or pKJE7), various commercially available solubility enhancing tags and a multitude of expression conditions (varied induction time, temperature and inducer concentrations) were employed (Table 1, Table 5 and Table 8). Despite extensive efforts in achieving expression of the soluble protein, the protein largely remained in inclusion bodies or purification could not be achieved. This stands as a huge impediment for proceeding onto further characterization of *P. falciparum* IMPDH, a highly promising drug target.

It was decided at this point to try *in vitro* translation system. The first *in vitro* translation system used was wheat germ extract procured from Promega Corporation, USA. This system was provided with bacterial transcription machinery which includes T7 RNA polymerase that binds to the T7 promoter for transcription. Wheat germ extract in the kit provided the translation components. The reaction was set up with native PfIMPDH gene using pET21b_PfIMPDH(His)$_6$ and pET21b_PfIMPDH$^{\Delta CBS}$(His)$_6$ as a template followed by detection on Western blot using anti-(His)$_6$ antibody. Examination of the Western blot showed that PfIMPDH was not synthesized (Fig. 13) although the synthesis of luciferase, positive control supplied with the kit had worked efficiently as detected by a luminometer.

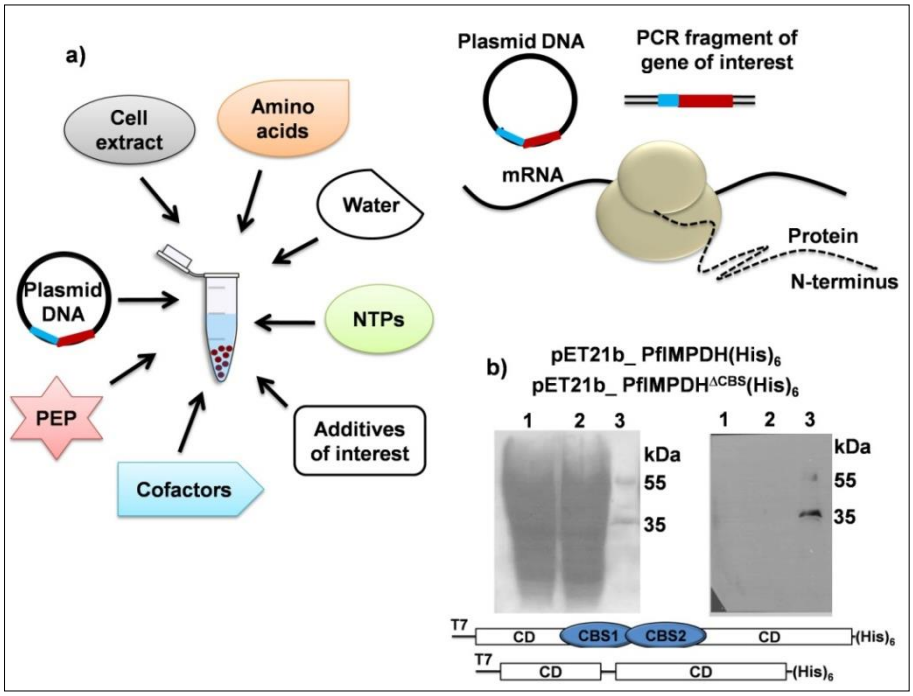

Figure 13. Cell-free synthesis of PfIMPDH and PfIMPDH$^{\Delta CBS}$ proteins using wheat germ extract. ***a) The depiction of components*** *that in general constitute a cell-free reaction where plasmid or PCR amplicon acts as a template. Addition of DNA template initiates the cell-free transcription coupled translation reaction.* ***b) Left panel*** *– In vitro T7 transcription coupled translation (eukaryotic machinery) reaction mixture was resolved on SDS-PAGE and electrotransferred to PVDF membrane. Blot was stained with Ponceau S dye to visualize the transfer of proteins. Lane 1 and 2 correspond to the reaction sample for the synthesis of PfIMPDH and PfIMPDH$^{\Delta CBS}$ using the plasmid templates pET21b_PfIMPDH(His)$_6$ and pET21b_PfIMPDH$^{\Delta CBS}$(His)$_6$, respectively. C-terminal (His)$_6$-tagged proteins of 35 kDa and 55 kDa were used as positive control for Western detection.* ***Right panel****- Western blot was probed with anti-(His)$_6$ antibody and developed using ECL chemiluminescence kit (Thermo Scientific, USA). Only a signal from the control was observed with the in-vitro reaction being unsuccessful. Schematic of each construct is represented below the respective expression profiles where CD refers to the catalytic domain.*

3.5.6.2 NEB PURExpress system

In vitro protein synthesis was also performed using *E. coli* S30 extract from PURExpress, New England Biolabs, USA. Apart from the ribosomes, tRNAs, creatine kinase, myokinase, nucleoside-diphosphate kinase, and pyrophosphatase, all other components of the transcription and translational machinery provided in the kit are purified (His)$_6$-tagged recombinant proteins (Shimizu Y *et al*., 2001). Therefore, to enable purification of PfIMPDH codon harmonized gene was subcloned with no tag into the plasmid

provided with the kit (pNEB). This will enable removal of the kit components by Ni-NTA chromatography as untagged PfIMPDH enzyme will not bind to the matrix. After incubation at 37 °C for 2 h, the sample was centrifuged at 10000g for 10 min and the supernatant was examined on SDS-PAGE. A distinct band of 55 kDa representing PfIMPDH was seen in comparison with no DNA control reaction on Coomassie-stained SDS-PAGE (Fig. 14). For the first time, we observed soluble protein synthesized in a cell-free reaction which was confirmed by Western blot using *in-house* generated anti-PfIMPDH antibody (Fig. 14).

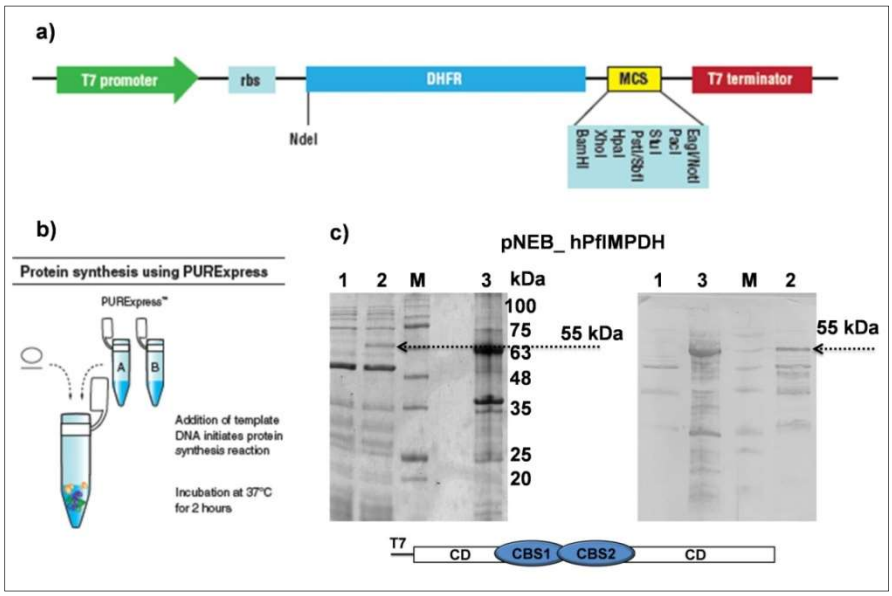

Figure 14. Detection of PfIMPDH protein synthesized from E. coli S30 system. a) All key features of the expression vector *from PURExpress (New England Biolabs, England) used in the cell-free reaction with E. coli S30 extract are indicated. Codon harmonized PfIMPDH gene has been subcloned into this commercially supplied vector (pNEB).* ***b) The reaction*** *is set up by mixing components of tube A and B in recommended ratios and addition of DNA template initiates the T7 transcription coupled translation (prokaryotic) reaction. The reaction is set for 2 h at 37 °C.* ***c) left panel -*** *2.0 µl of the in-vitro transcription coupled translation reaction with pNEB_ hPfIMPDH as template was resolved on 12 % SDS-PAGE and Coomassie stained. Lane 1 is no template control and includes only the reaction components from the NEB kit; lane 2 is the cell-free reaction with pNEB_ hPfIMPDH as a template; lane 3, a protein used as positive control for Western detection and M, pre-stained protein molecular weight marker (Abcam, USA).* ***Right panel-*** *Western blot probed with an anti-PfIMPDH antibody generated in-house and developed using AEC as a substrate for HRP conjugated to the secondary antibody. PfIMPDH, synthesized (55 kDa) in the cell-free reaction is highlighted with a black arrow. Use of polyclonal antibody generated using PfIMPDH(His)$_6$ might have resulted in non-specific bands on the Western blot (reaction components of the in vitro translation are as well (His)$_6$-tagged). Schematic of each construct is represented below the respective expression profiles where CD refers to catalytic domain.*

3.5.6.3 Scaling up of the cell-free protein synthesis

We attempted to measure the enzyme activity of *in vitro* translated PfIMPDH. However, the assay with the S30 reaction mix did not report back on IMP-specific conversion of NAD^+ to NADH. This could be due to the presence of nucleotides, salts, ribosomes, and other *E. coli* proteins in the cell free protein synthesis reaction. As PfIMPDH activity could not be monitored in the presence of S30 reaction mix, we attempted to separate the synthesized protein from other reaction components using ultracentrifugation. The molecular weight of PfIMPDH monomer is 55 kDa. Based on the oliogomeric state of other studied IMPDHs (Hedstrom L, 2009; Labesse G *et al.,* 2013; Buey RM *et al.,* 2015; Anthony SA *et al.,* 2017 and Buey RM *et al.,* 2017), the parasite enzyme could exist as either a tetramer of 220 kDa or octamer of 440 kDa in solution. Bacterial ribosomal complex present in the cell-free reaction mixture corresponds to about 2000-2500 kDa. The aim of the experiment was to separate this huge complex in the first step using 1000 kDa molecular weight cut-off centrifugal filter units (Sartorius, Germany) followed by capture of $(His)_6$-tagged PURE components from the flow through on to Ni-NTA affinity matrix. However, the flow through from ultrafiltration lacked the synthesized PfIMPDH protein. Intriguingly, it was found to be retained in the retentate along with the ribosomal machinery (Fig. 15). This indicates that the *in vitro* synthesized PfIMPDH is larger than either a tetramer or octamer and must be existing in large multimeric forms. The retentate with PfIMPDH did not show enzyme activity. This could be due to the presence of the components of the S30 reaction mix.

Alternate tagging strategy using Strep-tag II was performed to achieve separation of *in vitro* synthesized protein from the $(His)_6$-tagged PURE components and ribosomal complex. A 12.5 µl reaction was set up using pST_hPfIMPDH(StrII) as DNA template. After 2.5 h incubation at 37 °C sample was divided into two equal fractions. One was directly resolved on SDS-PAGE while other was centrifuged at 10000g for 10 min at 4 °C and only the supernatant was analyzed. As detected from Coomassie and confirmed by Western blot, PfIMPDH with C-terminal Strep-tag II synthesized in *in vitro* reaction has precipitated during the course of the reaction and hence no further experiments were carried out using this construct (Fig. 15).

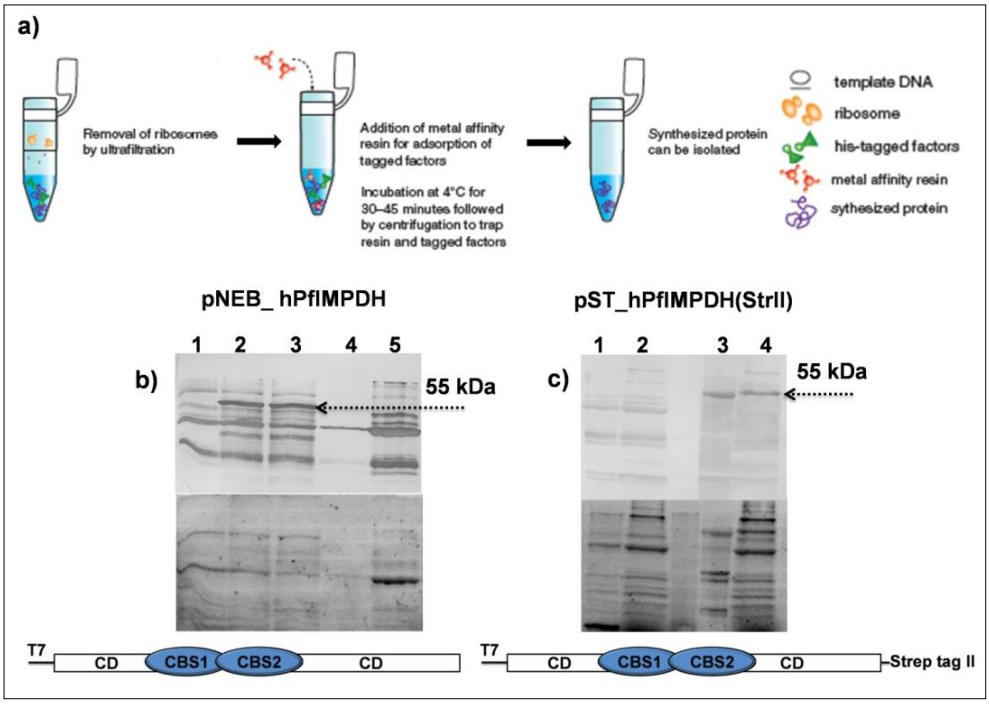

Figure 15. An attempt at the purification of PfIMPDH protein synthesized using E. coli S-30 extract from NEB with pNEB_hPfIMPDH as a template. a) Schematic *followed for purification of PfIMPDH expressed from pNEB_hPfIMPDH involves ultra-filtration using 1000 kDa cutoff centrifugal filter units (Sartorius, Germany) followed by collection of ultrafiltrate and passing it through Ni-NTA affinity matrix for the capture of $(His)_6$-tagged reaction components.* ***Top panels of b) and c)*** *highlight Western detection of proteins synthesized in the in-vitro transcription coupled translation reaction using protein-specific antibodies and with pNEB_hPfIMPDH and pST_hPfIMPDH(StrII) as DNA templates, respectively while* ***bottom panels*** *represent chloroform stained (Kazmin D et al., 2002) and UV visualized protein profiles on SDS-PAGE. PfIMPDH synthesized in the cell-free reaction is highlighted with a black arrow (55 kDa).* ***b) An attempt at the purification*** *of PfIMPDH protein synthesized using E. coli S-30 extract from NEB kit. Lane 1, 2.0 µl of no template control; lane 2, 2.0 µl of the in-vitro reaction with pNEB_hPfIMPDH as a template; lane 3, ultrafiltration retentate; lane 4, Ni-NTA flow through; lane 5, Ni-NTA retentate.* ***c) Cell-free protein synthesis using*** *pST_hPfIMPDH(StrII)* ***as a template.*** *Lane 1, 2.0 µl of no template control; lane 2, 6.25 µl of supernatant from cell-free reaction with pST_hPfIMPDH(StrII)* ***as a template*** *after centrifugation; lane M, pre-stained protein molecular weight marker (Abcam, USA); lane 3- protein used as positive control for Western detection; lane 4, 6.25 µl of cell-free reaction with pST_hPfIMPDH(StrII)* ***as a template*** *resolved without centrifugation. Use of polyclonal antibody generated using $(His)_6$-tagged PfIMPDH might have resulted in non-specific bands on the Western blot (reaction components of the in vitro translation are as well $(His)_6$-tagged). Schematic of each construct is represented below the respective expression profiles where CD refers to the catalytic domain.*

Table 8. Various expression constructs of codon harmonized PfIMPDH.

Expression Vector	Expression construct	Expression host	Observations
pET21b C-terminal $(His)_6$-tag	pET21b_hPfIMPDH$(His)_6$	Δ*guaB*^{K}(DE3)	hyperexpression, insoluble
pET21b C-terminal $(His)_6$-tag	pET21b_hPfIMPDH$^{\Delta CBS}(His)_6$	Δ*guaB*^{K}(DE3)	hyperexpression, insoluble
pET22b N-terminal pelB sequence and C-terminal $(His)_6$-tag	pET22b_(PelB)hPfIMPDH$(His)_6$	Δ*guaB*^{K}(DE3)	moderate level of expression, insoluble
NEB PURE kit template, no tag	pNEB_hPfIMPDH	Δ*guaB*^{K}(DE3)	low level of expression, completely insoluble with degradation
NEB PURE Kit template C- terminal $(His)_6$-tag	pNEB_hPfIMPDH$(His)_6$	Δ*guaB*^{K}(DE3)	hyperexpression, insoluble
NEB PURE kit template Catalytic core C-terminal $(His)_6$-tag	pNEB_hPfIMPDH$^{\Delta CBS}(His)_6$	Δ*guaB*^{K}(DE3)	hyperexpression, insoluble
NEB PURE kit template CBS domain C-terminal $(His)_6$-tag	pNEB_hPfCBS$(His)_6$	Δ*guaB*^{K}(DE3)	hyperexpression, and soluble
pST50Trc4-STRDHFR N-terminal Strep-tag II	pST_(StrII)hPfIMPDH	Δ*guaB*^{K}(DE3)	extremely low level of expression, insoluble
pST50Trc4-DHFRSTR C-terminal Strep-tag II	pST_hPfIMPDH(StrII)	Δ*guaB*^{K}(DE3)	hyperexpression, insoluble
pTrc99a_PfIMPDH^h C-term $(His)_6$ tag	pTrc_hPfIMPDH$(His)_6$	H1174$^{\Delta guaC}$	extremely low level of expression, insoluble
pTrc99a_PfIMPDH$^{h\Delta CBS}$ C-term $(His)_6$ tag	pTrc_hPfIMPDH$^{\Delta CBS}(His)_6$	H1174$^{\Delta guaC}$	hyperexpression, insoluble

3.5.7 Sequence analysis

Multiple sequence alignment of *P. falciparum* IMPDH with other well-characterized IMPDH/GMPR family of proteins using Clustal Omega helped in identification of conserved structural motifs that include catalytic cysteine loop, phosphate binding loop, finger loop, mobile flap loop, and the C-terminal loop. The alignment also facilitated the demarcation of CBS and catalytic core domains in *P. falciparum* IMPDH (Fig. 16 and Fig. 17).

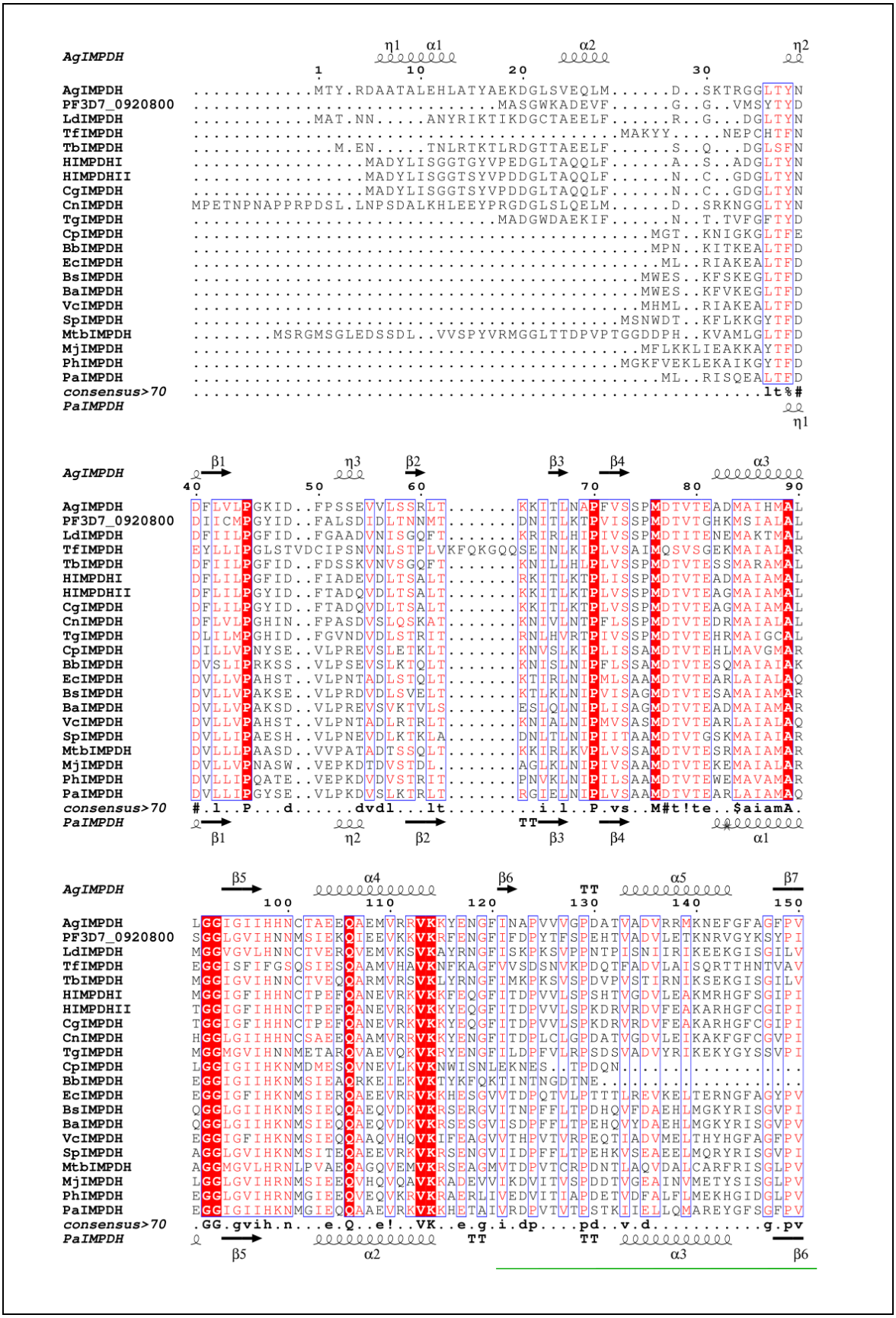
AgIMPDH
AgIMPDH
PF3D7_0920800
LdIMPDH
TfIMPDH
TbIMPDH
HIMPDHI
HIMPDHII
CgIMPDH
CnIMPDH
TgIMPDH
CpIMPDH
BbIMPDH
EcIMPDH
BsIMPDH
BaIMPDH
VcIMPDH
SpIMPDH
MtbIMPDH
MjIMPDH
PhIMPDH
PaIMPDH
consensus>70
PaIMPDH
AgIMPDH
AgIMPDH
AgIMPDH
PaIMPDH
consensus>70
PaIMPDH

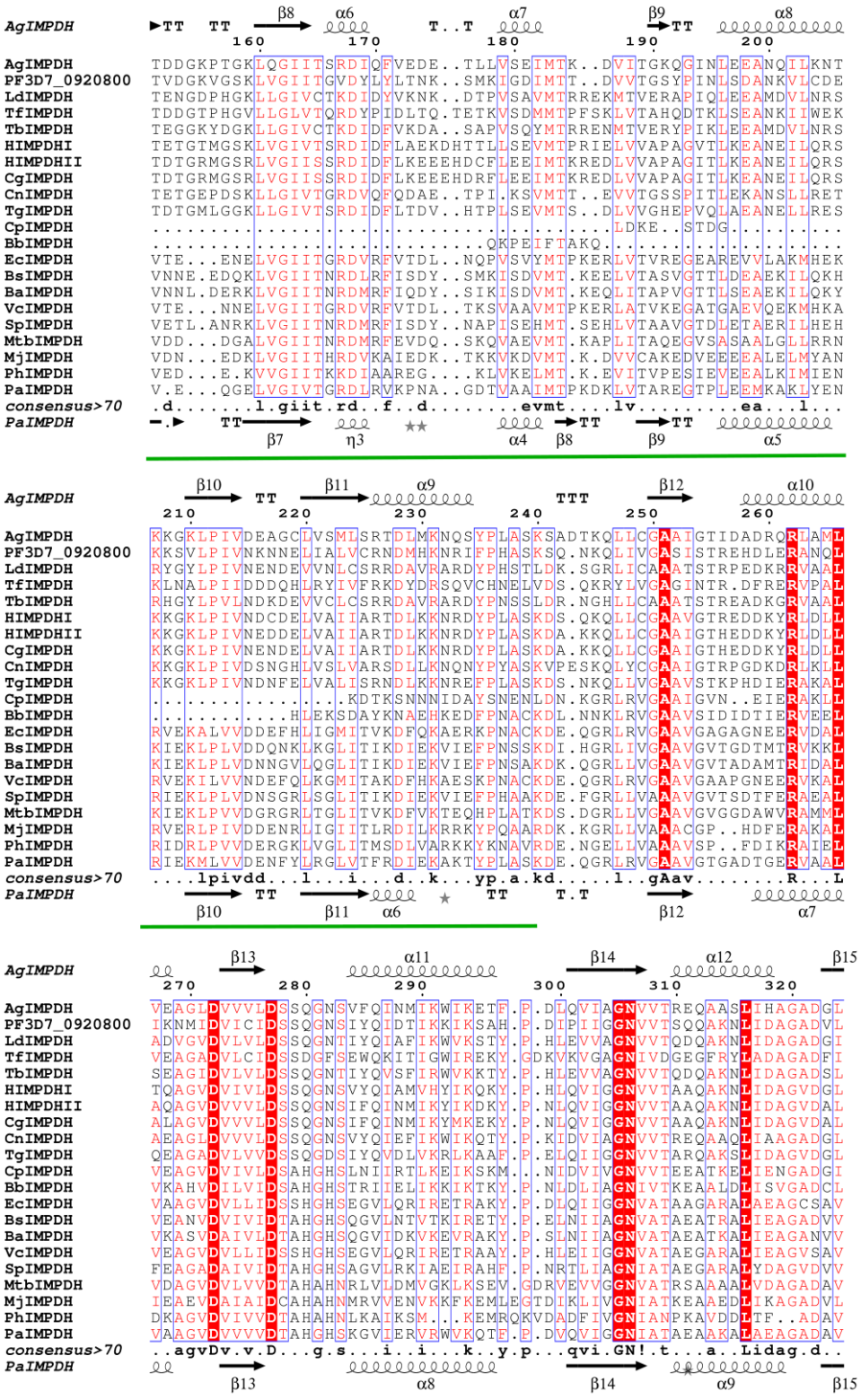
AgIMPDH
PF3D7_0920800
LdIMPDH
TfIMPDH
TbIMPDH
HIMPDHI
HIMPDHII
CgIMPDH
CnIMPDH
TgIMPDH
CpIMPDH
BbIMPDH
EcIMPDH
BsIMPDH
BaIMPDH
VcIMPDH
SpIMPDH
MtbIMPDH
MjIMPDH
PhIMPDH
PaIMPDH
consensus>70
PaIMPDH

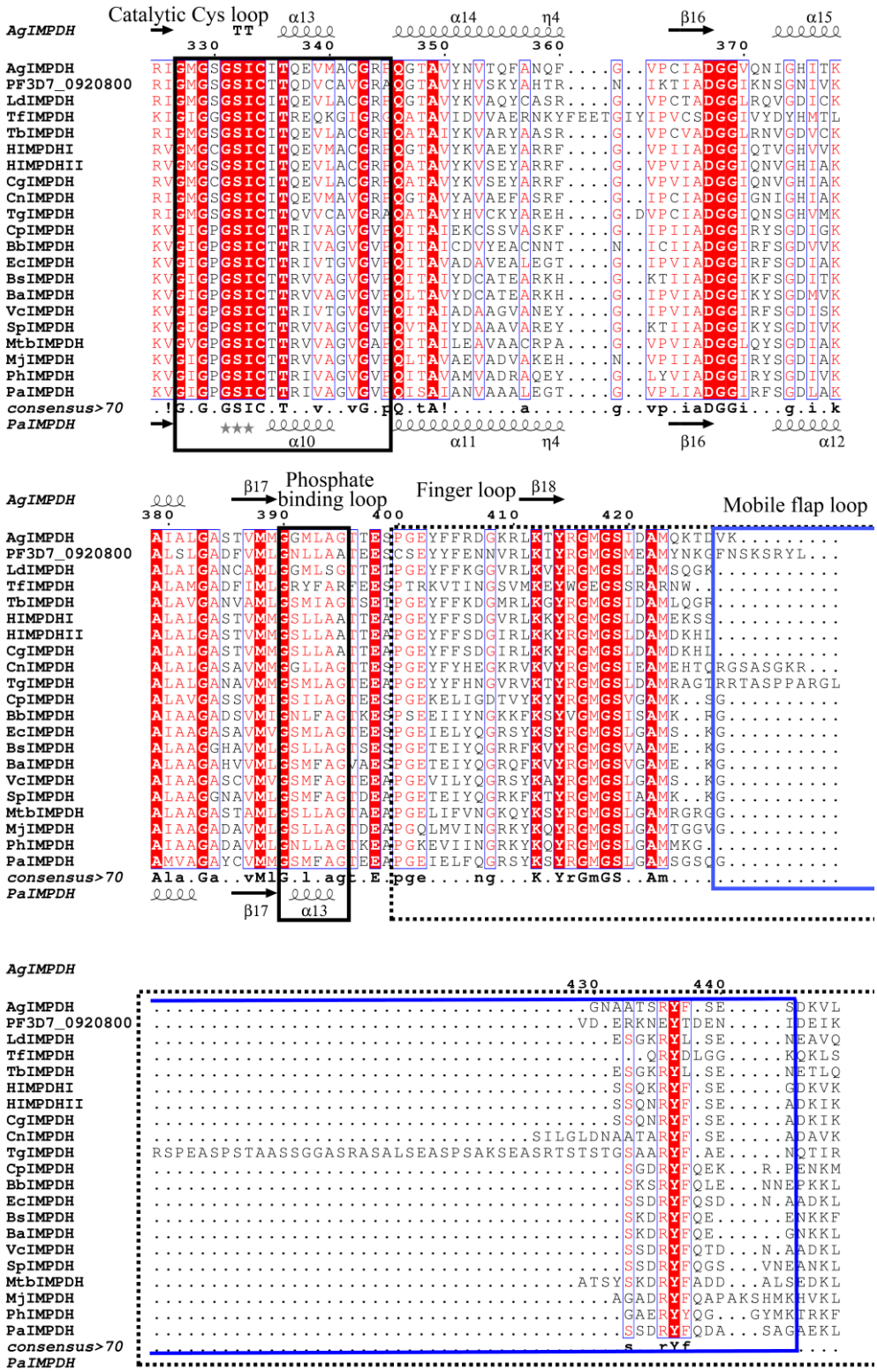
Catalytic Cys loop
Phosphate binding loop
Finger loop
Mobile flap loop
AgIMPDH
PF3D7_0920800
LdIMPDH
TfIMPDH
TbIMPDH
HIMPDHI
HIMPDHII
CgIMPDH
CnIMPDH
TgIMPDH
CpIMPDH
BbIMPDH
EcIMPDH
BsIMPDH
BaIMPDH
VcIMPDH
SpIMPDH
MtbIMPDH
MjIMPDH
PhIMPDH
PaIMPDH
consensus>70
PaIMPDH

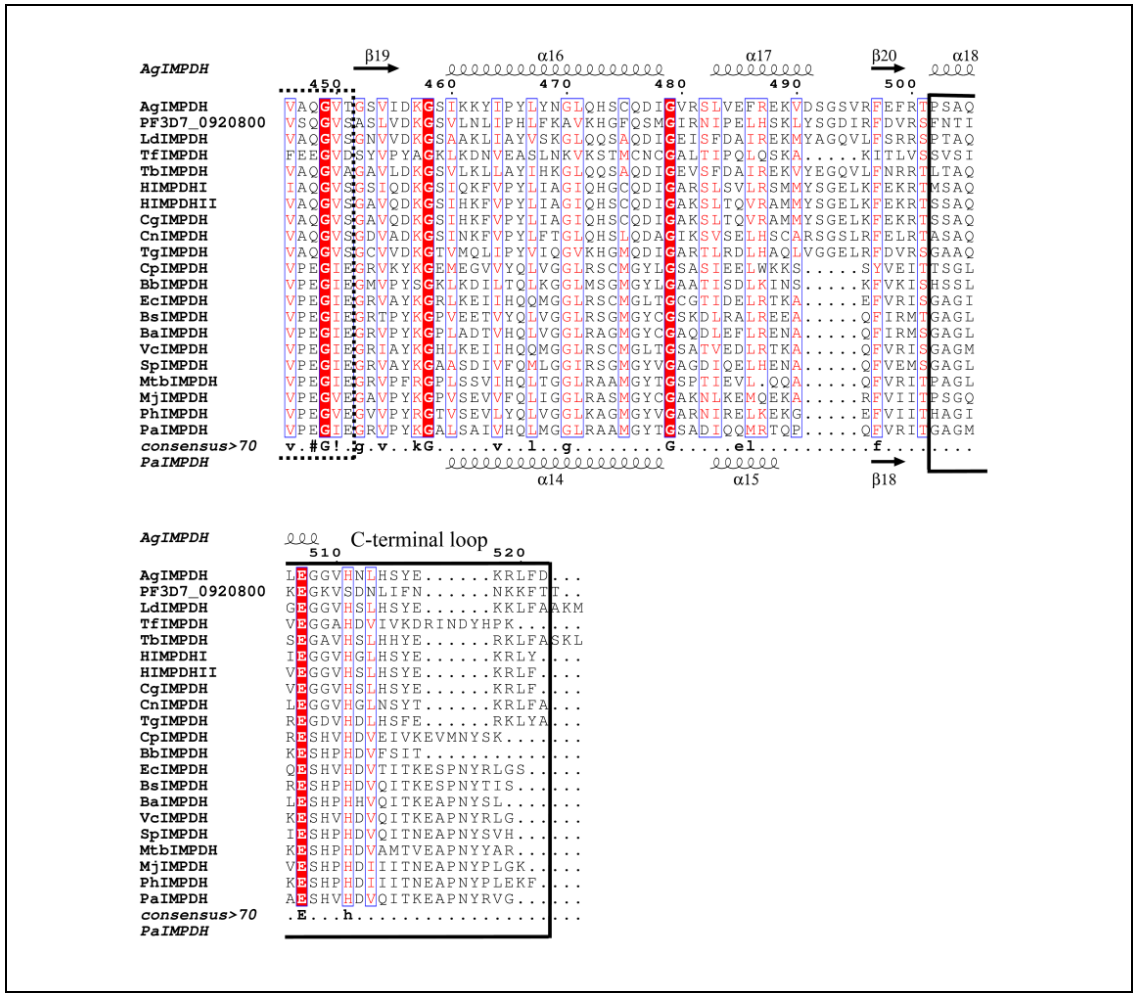

Figure 16. Multiple sequence alignment of IMP dehydrogenases from various organisms. *The sequence of PF3D7_0920800 annotated as inosine 5'-monophosphate dehydrogenase in PlasmoDB (PfIMPDH) is compared across various characterized IMPDHs that include Ashbya gossypium (Ag), Leishmania donovani (Ld), Tritrichomonas foetus (Tf), Trypanosome brucei (Tb), Human type I (HI), Human type II (HII), Cricetulus griseus (Cg), Cryptococcus neoformans (Cn), Toxoplasma gondii (Tg), Cryptosporidium parvum (Cp), Borrelia burgdorferi (Bb), Escherichia coli (Ec), Bacillus subtilis (Bs), Bacillus anthracis (Ba), Vibrio cholerae (Vc), Streptococcus pyogenes (Sp), Mycobacterium tuberculosis (Mtb), Methanocaldococcus jannaschii (Mj), Pyrococcus horikoshii (Ph) and Pseudomonas aeruginosa (Pa). All sequences were aligned with Clustal Omega (Sievers F et al., 2011; Sievers F and Higgins DG, 2018) and rendered using ESPRIPT (Robert X and Gouet P, 2014). A consensus of >70 was found across sequences analyzed. The secondary structure of IMPDH from a eukaryote, A. gossypium (PDB 5TC3) and a prokaryote, P. aeruginosa (PDB 4DQW) are shown at the top and bottom of the sequence alignment, respectively. α-helices and β-strands are rendered as large squiggles and arrows, respectively. TT and TTT correspond to beta and alpha turns, respectively. The red shaded regions indicate identical residues while residues represented in red, highlight similarity among the sequences compared. CBS domain is underlined with a green line. The segments involved in the catalysis are enclosed in black and blue boxes which include catalytic cysteine loop, phosphate binding loop, finger loop, mobile flap loop, and the C-terminal loop.*

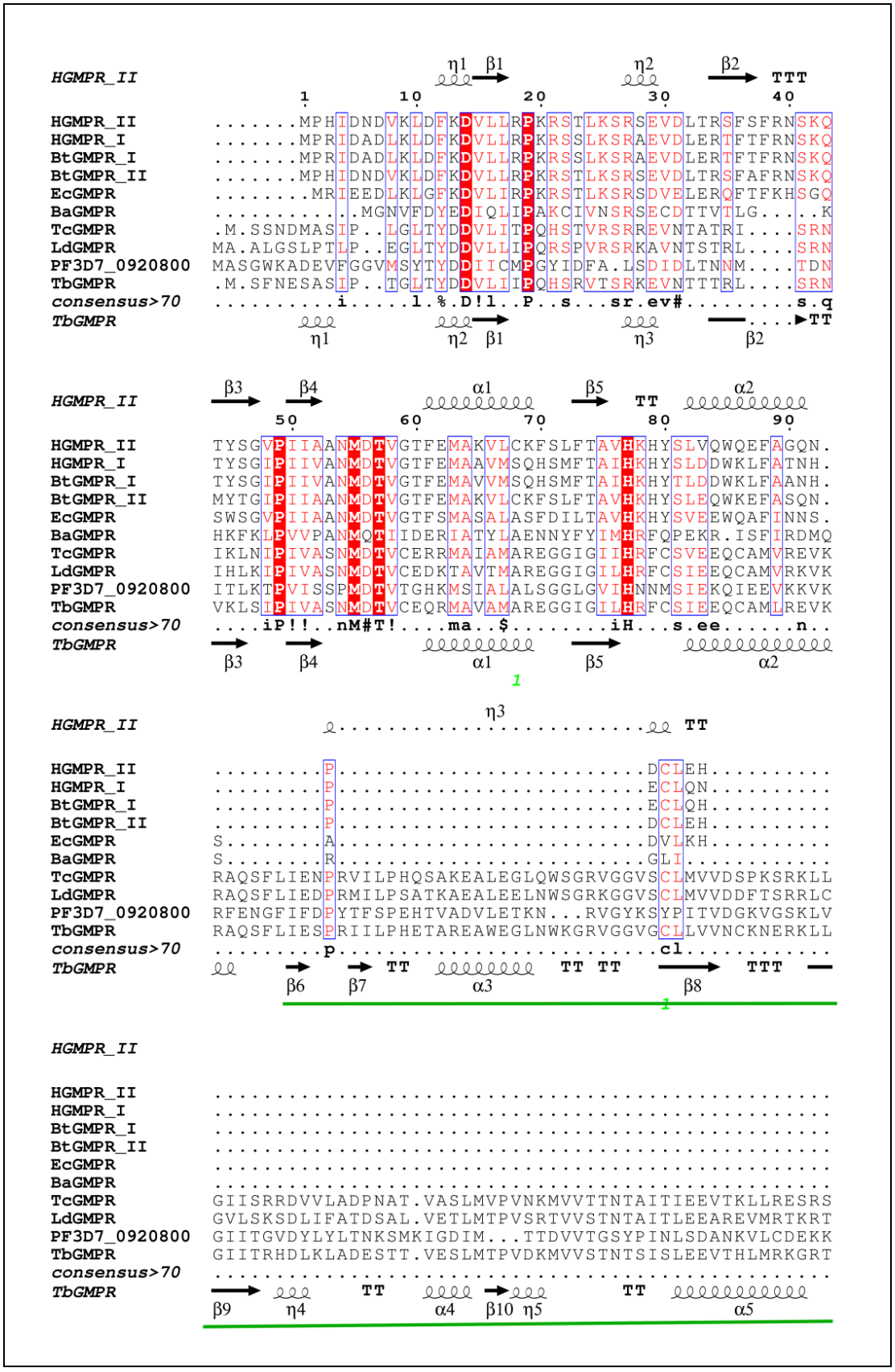
HGMPR_II
HGMPR_I
BtGMPR_I
BtGMPR_II
EcGMPR
BaGMPR
TcGMPR
LdGMPR
PF3D7_0920800
TbGMPR
consensus>70
TbGMPR

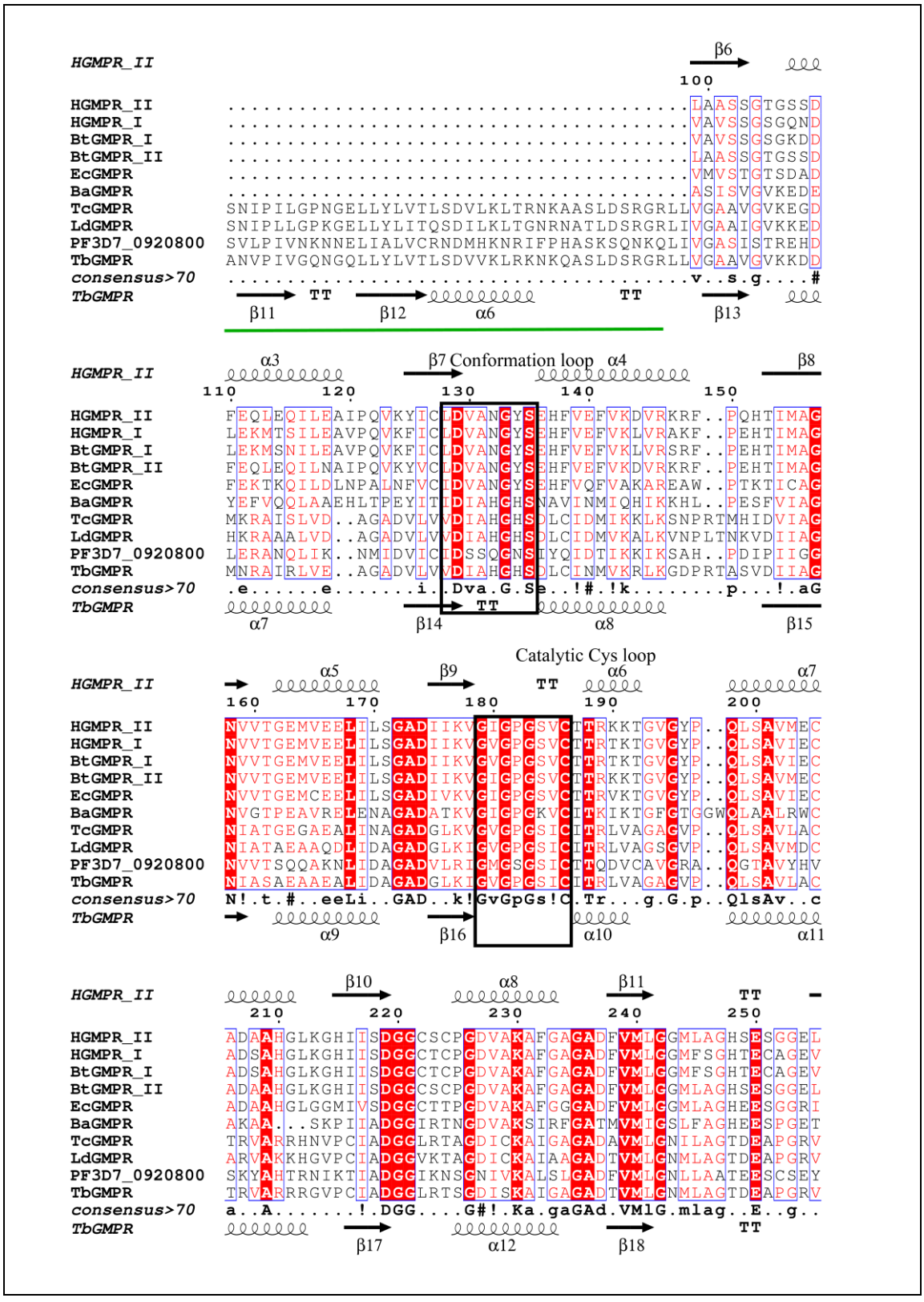
HGMPR_II
HGMPR_I
BtGMPR_I
BtGMPR_II
EcGMPR
BaGMPR
TcGMPR
LdGMPR
PF3D7_0920800
TbGMPR
consensus>70
TbGMPR
β6
β11
β12
α6
β13
α3
β7 Conformation loop
α4
β8
α7
β14
α8
β15
Catalytic Cys loop
α5
β9
α6
α7
α9
β16
α10
α11
β10
α8
β11
β17
α12
β18

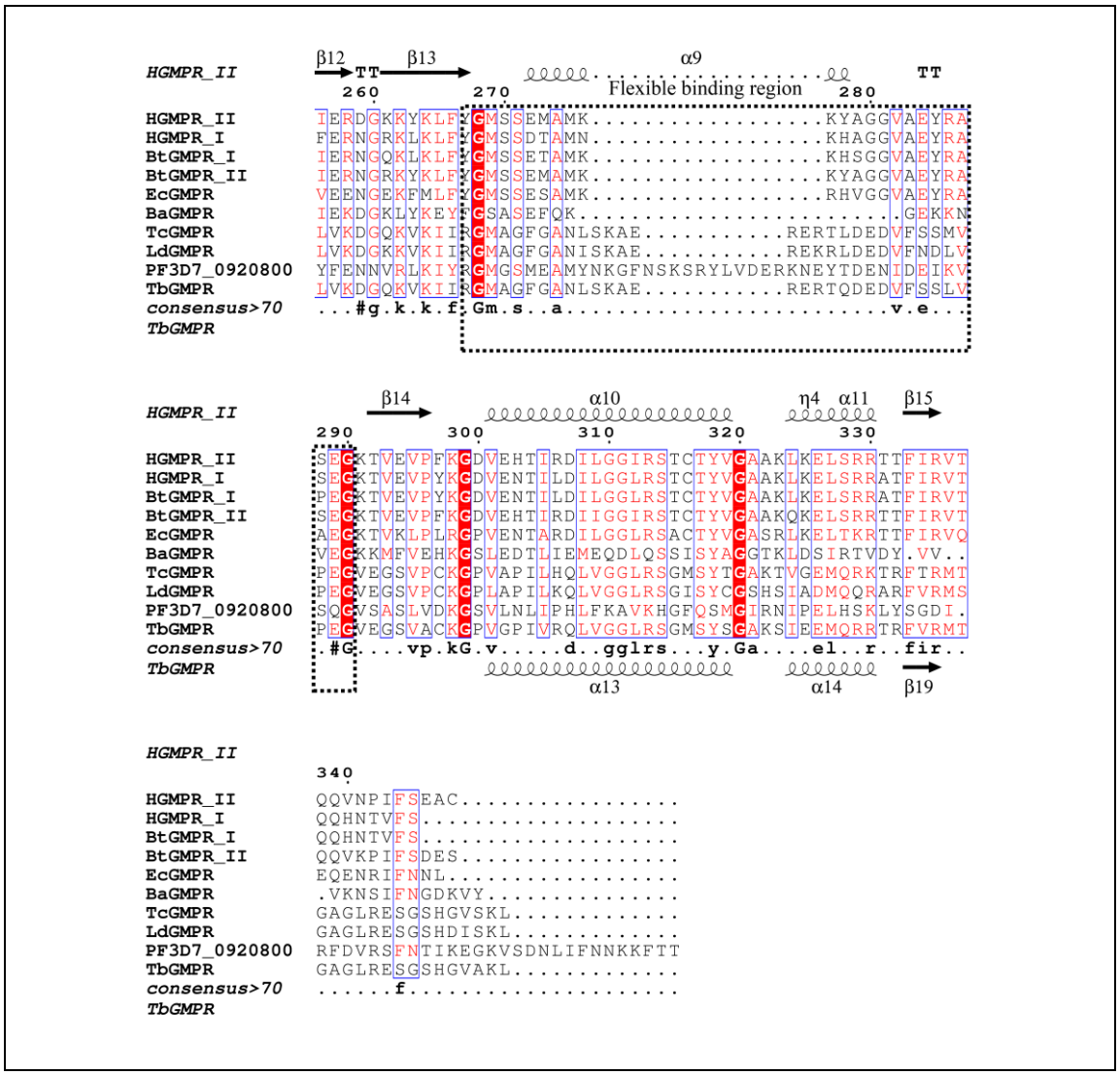

Figure 17. Multiple sequence alignment of GMP reductases from various sources. *The sequence of PfIMPDH is compared across various biochemically characterized guanosine 5'-monophosphate reductases that include Human type I (H_I), Human type II (H_II), Bos taurus type I (Bt_I), Bos taurus type II (Bt_II), Escherichia coli (Ec), Bacillus anthracis (Ba), Trypanosoma congolense (Tc), Leishmania donovani (Ld), and Trypanosome brucei (Tb). All the sequences were aligned with Clustal Omega (Sievers F et al., 2011; Sievers F and Higgins DG, 2018) and rendered using ESPRIPT (Robert X and Gouet P, 2014). A consensus of >70 was found across sequences analyzed. The secondary structure of GMPR from Human type II (PDB 2C6Q) and T. brucei (PDB 5X8O) are shown at the top and bottom of the sequence alignment, respectively. α-helices and β-strands are rendered as large squiggles and arrows, respectively. TT and TTT correspond to beta and alpha turns, respectively. The red shaded regions indicate identical residues while residues in red highlight*

similarity among the sequences compared. CBS domain is underlined by a green line. Catalytic cysteine loop, conformational loop, and the flexible binding region are highlighted in black boxes.

3.5.8 Analysis of amino acid composition across IMPDH/GMPR sequences

Percentage occurrence of each amino acid in a given IMPDH sequence was calculated. An average of this calculated percentage across various *Plasmodium* species has been compared with that from other biochemically characterised IMPDH and GMPR sequences (Fig. 18). Six (L, W, T, C, M, and K) of the twenty amino acids in the plasmodial group do not significantly differ from their respective averages in the other group that constitutes soluble IMPDHs and GMPRs, while percentage of occurrence for the rest of the fourteeen was found to vary significantly. The implication of such a bias in amino acid composition of PfIMPDH and the associated consequences are yet to be understood (Fig. 18).

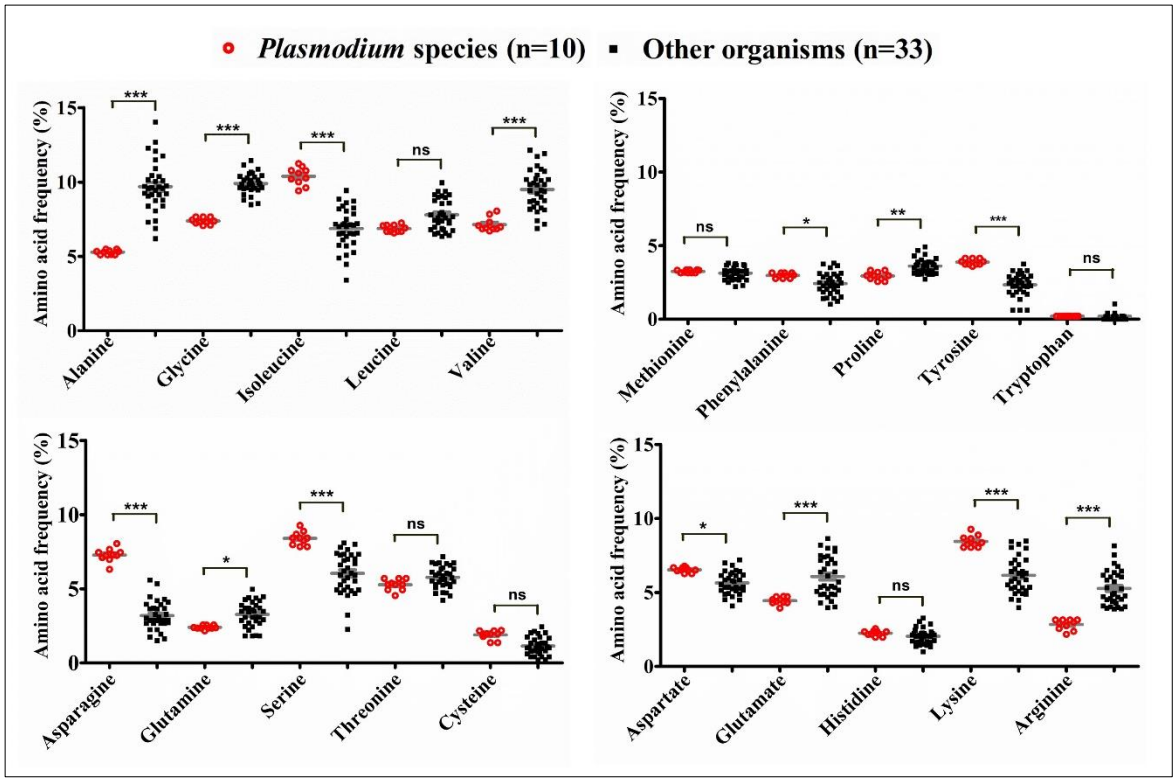

Figure 18. Scatter plot for average amino acid composition (%) of IMPDH from Plasmodial species compared across various other biochemically characterised IMPDH and GMPR sequences. *One-way analysis of variance (ANOVA, ***p<0.001, **p<0.01, and *p<0.05) followed by Bonferroni's multiple comparison test performed to calculate the statistically significant differences*

in amino acid composition between the means of two groups (red spheres and black squares) is indicated. ns refers to not significant. Shown on the x-axis is the amino acid residue within a group vs. its average percentage of occurrence on the y-axis. Shown in red spheres is group1 (n=10) that includes IMPDH from P. falciparum 3D7, P. berghei ANKA, P. vivax P01, P. chabaudi chabaudi, P. yoelli 17X, P. ovale GH01, P. knowlesi strain H, P. malariae UG01, P. cynomolgi strain B and P. reichenowi CDC while the group2 (n=33) in black squares correspond to IMPDHs from human (type 1 and type 2), L. donovani, T. brucei, T. congolense, B. gibsoni, T. gondii, T. foetus, E. coli, S. pyogenes, A. gossypium, P. aeruginosa, M. tuberculosis, B. subtilis, B. anthracis, V. cholerae, P. horikoshii, M. jannaschii, C. perfringens, E. tenella, B. thailandensis, L. pneumophila, N. meningitidis, K. pneumonia, S. aureus, S. cerevisiae, C. jejuni, L. monocytogenes, M. thermoresistible, B. subtilis, and C. neoformans and GMPRs that contain CBS domain from L. donovani, T. brucei and T. congolense (expressed in E. coli in soluble form). Horizontal bars in grey represent mean and s.e.m of the data. Protein calculator v3.4 tool was used for the analysis (http://protcalc.sourceforge.net/).

3.5.9 β-aggregation propensity

TANGO is a statistical mechanics algorithm to predict the beta-aggregation nucleating regions in unfolded polypeptide chains. It was developed based on simple physicochemical principles of secondary structure formation and the assumption that the core regions of an aggregate are fully buried. This algorithm was shown to predict accurately the regions experimentally reported to be involved in the aggregation process that includes β-peptide from Alzheimer's along with 20 other proteins (Linding R *et al*., 2004; Fernandez-Escamilla AM *et al*., 2004). They observe a higher propensity for beta-aggregation among cytoplasmic, and globular proteins than membrane-bound or intrinsically disordered proteins.

Each residue in a peptide is given a percentage occupancy in the β-aggregation conformation and a peptide is considered to be potential β-aggregation nucleation site when a segment of at least five consecutive residues, each accounting to more than 5 % of β-aggregated conformation is predicted. PfIMPDH$^{\Delta CBS}$ protein sequence was used as input as we obtained PfCBS domain in soluble form when expressed in *E. coli* (presented in Chapter 4). Two segments of length 14 and 19 amino acids each having a significantly high β-aggregation score of 40 – 50 % was observed (Fig. 19). MjIMPDH has been found to be highly soluble and share a sequence identity of 35 % with PfIMPDH (discussed in Chapter 5). Such potential nucleation sites were not observed in MjIMPDH. Upon swapping the sequence of these two regions identified in *P. falciparum* enzyme with that from *M.*

jannaschii IMPDH yielded significantly lowered score (40 % and 50 % have dropped down to 3 % and 14 %, respectively) (Fig. 19). This could serve as a possible future direction to generate mutants with improved solubility.

a)

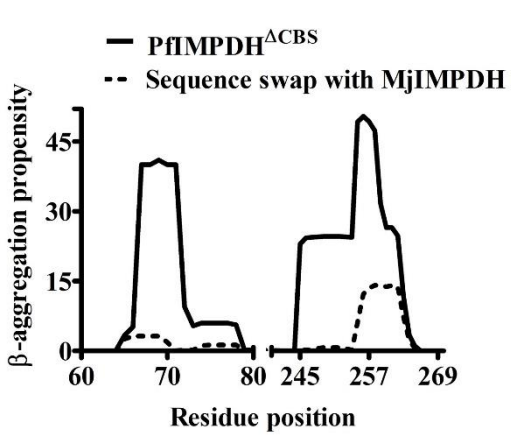

b)

Native sequence and score in parenthesis	Segment length	Sequence swap with MjIMPDH and score in parenthesis
67-78, MSIALALSGGLGVI (3-40)	14	MAIALARLGGLGVI (0-3)
245- 263, IVKALSLGADFVMLGNLLA (3-50)	19	IAKAIAAGADAVMLGSLLA (3-14)

Figure 19. The beta-aggregation propensity of PfIMPDH$^{\Delta CBS}$. *The analysis was performed using a computer algorithm for prediction of aggregating regions in unfolded polypeptide chains on TANGO web server (http://tango.crg.es) (Linding R et al., 2004; Fernandez-Escamilla AM et al., 2004).* ***a)*** *Amino acid position is on the x-axis with the corresponding beta-aggregation propensity on the y-axis. Two segments with significantly high score have been identified in PfIMPDH$^{\Delta CBS}$ indicated in continuous black line which upon shuffling with that of a known soluble protein, MjIMPDH resulted in the loss of aggregation-prone regions indicated in dotted black line.* ***b)*** *Tabulation of the aggregation-prone sequence, swap with MjIMPDH residues and the corresponding score.*

3.6 Conclusion

PfIMPDH and PfIMPDH$^{\Delta CBS}$ overexpressed in *E. coli* remained insoluble despite various efforts to maximize the yield of soluble protein. Presence of helper plasmids were found to be essential for hyperexpression of PfIMPDH/PfIMPDH$^{\Delta CBS}$ and yield low levels of soluble protein. However, separation of chaperone proteins from PfIMPDH was not successful. Enzymatic activity of PfIMPDH from bacterial lysates (obtained after protein induction and cell lysis) could not be verified due to the presence of contaminants from *E. coli*. Ability of PfIMPDH to catalyze GMP reductase reaction could not be examined as it was found to be insoluble when expressed in H1174$^{\Delta guaC}$ strain of *E. coli*. Codon harmonization of gene sequence to obtain soluble protein was also found not fruitful. *In vitro* protein production using wheat germ extract was unsuccessful while for the first time soluble and detectable level of PfIMPDH protein on Coomassie-stained SDS-PAGE was achieved with *E. coli* S-30 extract. Scaling-up and attempt to isolate the *in vitro* synthesized protein remained unsuccessful largely due to protein aggregation/multimerization or probably due to strong association with the ribosomal complex. Bias in amino acid composition, prediction of aggregation-prone regions and domain swapping could be the possible future approaches in generating mutants with improved solubility of recombinant PfIMPDH.

Chapter 4. Biophysical and biochemical examination of PfCBS

Bateman domain or cystathionine beta-synthase (CBS) domain of PfIMPDH (PfCBS) was cloned into a T7 expression vector carrying a C-terminal $(His)_6$-tag. Unlike the core catalytic domain or the full-length construct, PfCBS was obtained in soluble form and purified to homogeneity. PfCBS was found to exist as a monomer in solution as determined from analytical size-exclusion chromatography. PfCBS, as inferred from far-UV CD measurement, was found to be largely disordered similar to that of the CBS domain from human IMPDH2. Both adenylate and guanylate nucleotides were found to bind PfCBS as determined by intrinsic tyrosine fluorescence measurements.

4.1 Introduction

4.1.1 Discovery and prevalence

CBS motifs occur in a wide variety of functionally unrelated family of proteins that were first identified by Alexander Bateman in human cystathionine β-synthase along with fifteen other protein families (comprising a total of thirty-three copies) in the genome of the archaeon, *Methanocaldococcus jannaschii* (Bateman A, 1997 and Bult CJ *et al.*, 1996). They exist in tandem of two or four of approximately sixty amino acids each motif and together referred to as Bateman module or CBS domain. CBS domains carry no defined function yet are known to regulate a wide number of proteins (from all kingdoms of life) including voltage-gated channels, ABC protein transporter family, Mg^{2+}-transporters, AMP-activated protein kinase, and GMP reductase/IMP dehydrogenase protein family. Overview of the CBS domain with emphasis on IMPDH/GMPR family of proteins is discussed in this chapter.

4.1.2 Topology, structure, and conserved sequence motifs

Two α-helices and three β-strands in the order of β1-α1-β2-β3-α2 constitute a CBS motif, generally preceded by a common flexible linker (α0) (that comprises of one turn of helix succeeded by an unstructured region to confer flexibility) although some proteins are found to have unstructured β1 strand (Fig. 1). In addition to the α0, a β-strand (β0) has been recently identified as part of the common linker (Fig. 1) (Anishkin VA *et al*., 2017). Each N-

terminal helix turn (α0/α0') of the flexible linker packs into anti-parallel arrangement between its C-terminal β strand (β3/β3') and α helix (α2/α2') forming an integral part of the other CBS motif and thus results in CBS motifs forming a nested overall structure with two-fold axis of pseudo-C2 symmetry that runs parallel with the central β-sheets (Fig. 2) (Ereco-Orbea J *et al.,* 2013; Anashkin VA *et al*., 2017).

CBS domains always occur in tandem and the interaction between the β-sheets within the CBS domain constitutes a functional unit known as Bateman module, a pseudo-dimer. Each CBS motif carries two major cavities referred to as site-1 and site-2 separated by the dyad axis running parallel to the central β-sheets (Fig. 2a). Each canonical binding site of a CBS motif is divided into three structural blocks (Fig. 1b and Fig. 2a). Block I includes residues in the flexible linker preceding first strand (β1/β1') with the highest diversity observed in length and identity. Three residues of this segment are found to be essential in the determination of the specificity and adenosyl group binding. A threonine or serine (T/S) interacts through its side chain with hydroxyls of the ribose ring of nucleotide and when replaced by a hydrophobic residue, twist of the ribose ring could occur accompanied by phosphate group displacement. (T/S) is found to be often replaced by arginine or a lysine (R/K) carrying out a similar function. The second key residue is usually placed two or three residues before the beginning of the first strand (β1/β1'). The main chain of this residue (a variable) sterically hinders potential accommodation of the 2-amino group of guanine derivates by locating its carbonyl oxygen in the vicinity of the C2 atom of the adenine ring. The third residue is placed two positions after the second residue described above which favors adenosine binding by H-bonding the N6-exocyclic amino group and/or N7 amino group of adenine ring through its carbonyl oxygen. Block II comprises residues from the second strand (β2/β2') that accommodate adenine ring by providing hydrophobic residues (h-y-y-h-P where h is any hydrophobic residue, and y can be any residue). The first residue of β2(y) simultaneously impairs the potential binding of guanosine derivatives while H-bonding the 6-amino exocyclic group and the N7 amino group of adenine ring and the hydrophobic residue (h) present two positions before, packs against the adenine ring. Block III corresponds to the most conserved segment among all proteins which includes residues located on the third strand (β3/β3'). It comprises of characteristic ribose-phosphate binding

motif G-h-h-(T/S)-x-x-(D/N), where h is any hydrophobic residue, and x can be any residue. The hydrophobic residue (h) interacts with the adenine ring, threonine/serine (T/S) binds phosphate and aspartate (D) binds ribose hydroxyls through H-bond. Lack of any of these two residues (threonine/serine or aspartate) is known to impair nucleotide binding. Residue preceding aspartate affects phosphate containing nucleotides and contributes significantly to determine the overall fold of the bound nucleotide. Replacement of this residue by a negatively charged or bulky hydrophobic residue fixes the site more compatible for adenosine derivates such as AMP, ADP, ATP, NAD^+, s-adenosylmethionine (SAM), methylthioadenosine (SMT) (Baykov AA *et al.*, 2011 and Ereño-Orbea J *et al.*, 2013).

The spatial arrangement of the subdomain was first observed in the X-ray crystal structure of *S. pyogenes* IMPDH (Zhang R *et al.*, 1999). Since then, most of the PDB entries for IMPDHs report tetrameric association of the core domains that comprise the central catalytic site, while the CBS domains (each is a tandem of CBS motif 1 and CBS motif 2) from four subunits are located at the periphery of the enzyme complex (Fig. 2b) (Hedstrom L, 2009). However, a CBS deletion mutant of human IMPDH2 remains fully active *in vitro* (Sintchak MD *et al.*, 1996) with oligomerization unchanged (Nimmesgern E *et al.*, 1999). These observations indicate the intramolecular interaction among CBS modules is neither a structural determinant for protein multimerization nor essential for catalysis as they do not form a part of the catalytic center, however, regulation is found to be perturbed upon deletion or point mutations (Ignoul S and Eggermont J, 2005).

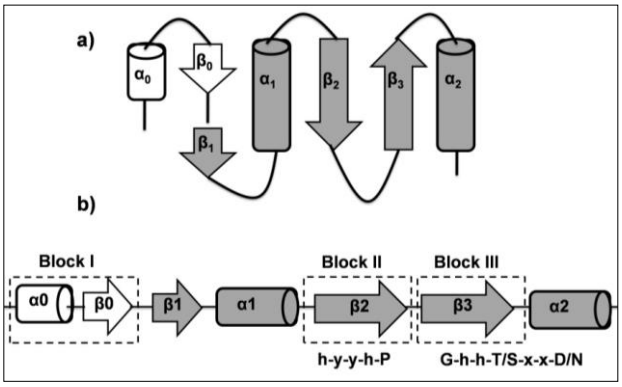

Figure 1. The topology and canonical binding sites of the CBS motif. a) *Shown in white is the common linker present across various CBS domain containing proteins (α0 and β0) and grey corresponds to a CBS motif. CBS motifs occur in tandem of two or four copies within a CBS domain.* ***b) Structural blocks of the canonical binding site*** *in a CBS motif with conserved nucleotide binding sequence. h represents a hydrophobic residue and x, y represents any residue. P, G, T, S, D, and N are the amino acids proline, glycine, threonine, serine, aspartic acid, and asparagine, respectively. The figure is regenerated using information from the articles Ereco-Orbea J et al., 2013 and Anashkin VA et al., 2017.*

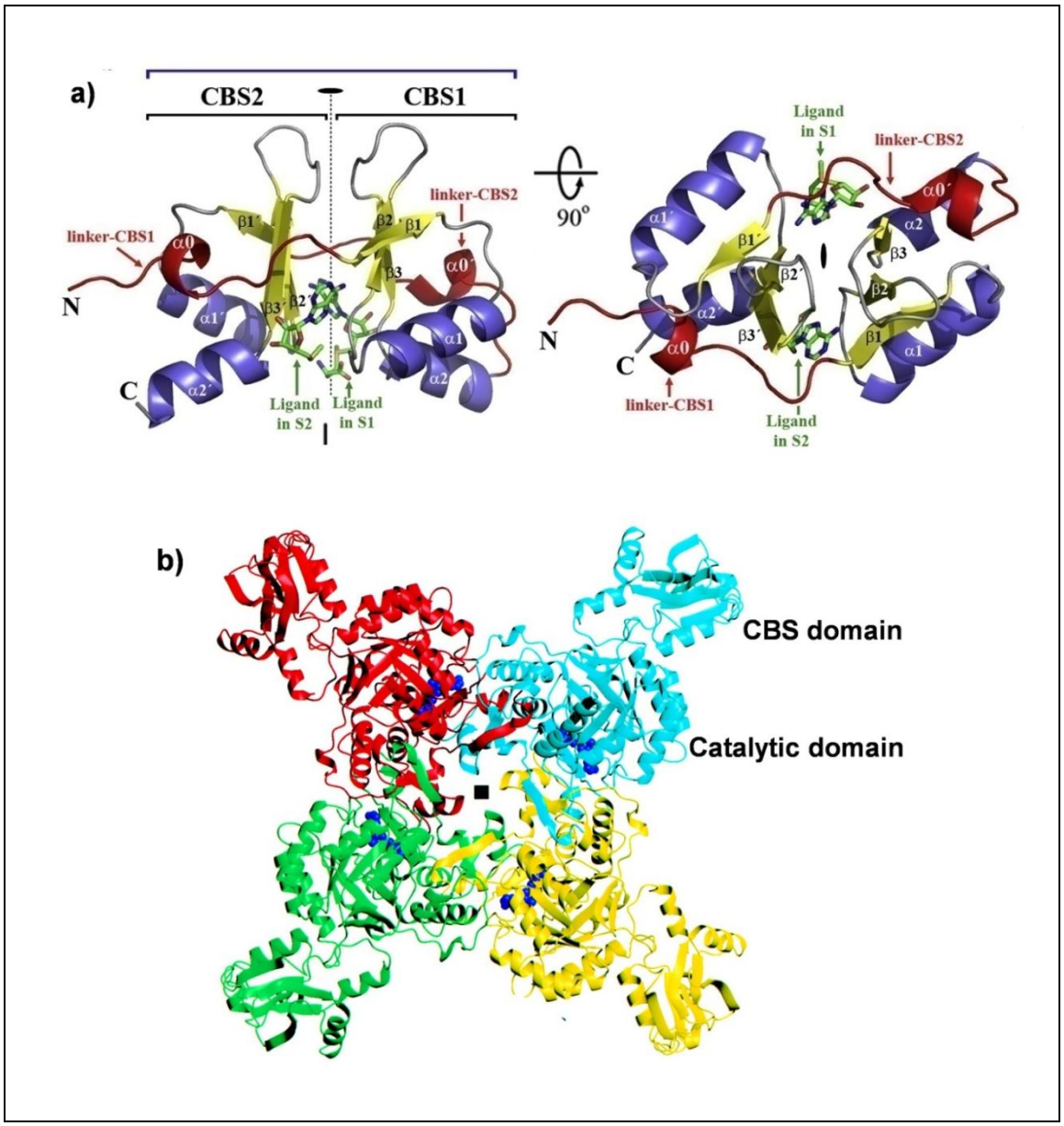

Figure 2. Domain architecture and spatial arrangement. a) CBS motifs and the structural elements. *The structure corresponds to CBS domain of protein MJ0100 from M. jannaschii (PDB*

3KPC) represented with copyright grant from Ereño-Orbea J et al., 2013 (refer to Appendix A). The two CBS motifs (CBS1 and CBS2) are related by a pseudo-2-fold symmetry within the Bateman module. The right panel is the tertiary structure up on 90° rotation vertically. Linkers are indicated in red, α helices in blue and β sheets in yellow. Nucleotide accommodating pocket in each motif is indicated (S1 and S2). ***b) The tetrameric structure of S. pyogenes IMPDH (PDB 1ZFJ)*** *parallel to the 4-fold axis of symmetry is shown in ribbon diagram. Each subunit is represented in a different color with each catalytic pocket occupied with a molecule of IMP represented in a space-filling model. CBS subdomain from each of the subunit points away from the catalytic core. The image was rendered using NGL viewer (Rose AS et al., 2018).*

4.1.3 Ligand binding, regulation, and disease perspective

The initial screen of ligands that were found to bind the CBS domains of various proteins largely includes adenine moieties modulating the enzyme activities (AMP, ADP, ATP, S-adenosylmethionine, NAD^+, diadenosine polyphosphates). The ability of CBS modules to bind single and double-stranded nucleic acids and their association with polyribosomes have also been reported (McLean JE *et al.,* 2004; Mortimer SE *et al.,* 2008 and Aguado-Llera D *et al.,* 2010). Adding to the repertoire of ligands, recent studies have found GMP, GDP, and GTP to bind to eukaryotic IMPDHs (*Ashbya gossypium* and human) and inhibit the enzyme activity (Buey RM *et al.,* 2015). Further, another study demonstrated that both adenylate and guanylate nucleotides bind CBS domains of *L. donovani* IMPDH and *L. major* GMPR and potentially modulate enzymatic activity (Smith S *et al.,* 2016). Earlier studies have shown that deletion of the CBS subdomain of IMPDH leads to the disruption of coordinated regulation of the adenine and guanine nucleotide pools in *E. coli* (Pimkin M and Markham GD, 2008, Pimkin M *et al.,* 2009). Intriguingly, ATP binding and allosteric activation of human IMPDH2 was abolished by a mutation (R224P) in the second CBS motif which corresponds to retinitis pigmentosa causing mutation in IMPDH1 (Scott JW *et al*., 2004 and Bowne SJ *et al.,* 2002). Role of CBS domain has been indicated in the regulation of translation and transcription (Cornuel JF *et al.,* 2002; McLean JE *et al.,* 2004; Mortimer SE and Hedstrom L, 2005; Bowne SJ *et al.,* 2006; Mortimer SE *et al.,* 2008; Park JH and Ahn SH, 2010). However, molecular and the mechanistic basis of regulation by CBS domain is yet to be understood.

Ligands binding to CBS domain also include metal cofactors like Mg^{2+} and Zn^{2+} ions (Hattori M *et al.,* 2007 and Sharp M *et al.,* 2008) and huge structural rearrangement of CBS

domains has been well documented in case of Mg^{2+} transporters (MgtE). In the Mg^{2+} free form, CBS domains remain apart from each other by a 40° rotation compared to that of the bound form providing a gating mechanism for ion conductance (Hattori M *et al.,* 2007 and Hattori M *et al.,* 2009). Conformational flexibility is also displayed by nucleotide binding in the CBS domain of *Clostridium perfringens* pyrophosphatase (CBS_PPase) and Mj0100 (a protein of unknown function from *M. jannaschii*) (Tuominen H *et al.,* 2010 and Lucas M *et al.,* 2010).

Such ligand-induced conformational studies on IMPDH/GMPR family of proteins remained unclear for a long time largely due to the disordered nature of CBS domains. It has been observed that removal of CBS domain facilitates crystallization (Hedstrom L, 2009). Till date, about 91 X-ray crystal structures of IMPDH are found deposited in PDB, of which, 65 correspond to CBS deletion constructs. However, the CBS domain is found to be completely mapped in only 8 of the total 26 full-length IMPDHs. The report suggesting an octameric association of IMPDH from *P. aeroginosa,* observed dimer of tetramers being stabilized by interactions between the Bateman modules in the MgATP-bound structure (PDB 4DQW). Their analysis of macromolecular assembly using PISA (Krissinel E and Henrick K, 2007) revealed similar octameric association to be present in all the PDB deposited IMPDH structures except for human IMPDH1. Cryo-EM experiments of human IMPDH1 revealed the presence of two types of complementary octamers with 69 % having concave structures (have CBS pointing outward) and 31 % with convex assembly with CBS subdomains involved in tetramer interface. In the presence of MgATP, these complementary octamers pile up into individual fibers. The aggregation of these fibers in the autosomal dominant mutant, D226N of human IMPDH1, is proposed as an indication for the onset of the autosomal dominant retinitis pigmentosa (adRP10) (Labesse G *et al.,* 2013). However, polymerized filaments and non-assembled octamers of human IMPDH2 were found to have comparable catalytic activity, substrate affinity, and GTP sensitivity (Anthony SA *et al.,* 2017). In contrast, Cryo-EM and X-ray crystal structure analysis of *A. gossypium* IMPDH found that ligands (ATP, GDP, and GTP) bound to the regulatory Bateman domain induces different enzyme conformations with significantly distinct catalytic activities. GDP and GTP were found to inactivate ATP-induced AgIMPDH octamers (Buey RM *et al.,* 2015;

Buey RM *et al.,* 2017). Since IMPDH forms the rate-limiting step of GTP biosynthesis and IMP being a precursor for ATP formation, regulation of IMPDH becomes crucial for maintenance of balance among purine nucleotides (Weber G *et al.,* 1992).

Several hereditary diseases have been linked with mutations in the CBS domains such as retinitis pigmentosa (RP) and Leber congenital amaurosis (LCA) (mutations in human IMPDH1) (Kennan A *et al.,* 2002; Bowne SJ *et al.,* 2006), homocystinuria (CBS) (Shan X *et al.,* 2001), familial hypertrophic cardiomyopathy with Wolff-Parkinson-White syndrome (mutations in AMP-activated protein kinase (AMPK)) (Blair E *et al.,* 2001; Gollob MH *et al.,* 2001 and Gollob MH *et al.,* 2001), congenital myotonia (mutations in chloride channel, ClC-1), Dent's disease (mutations in chloride channel, ClC-5) (Lloyd SE *et al.,* 1997), osteopetrosis (mutations in chloride channel, ClC-7) (Cleiren E *et al.,* 2001; Kornak U *et al.,* 2001), and Bartter syndrome (mutations in chloride channel, ClC-Kb) (Konrad M *et al.,* 2001).

4.2 Experimental Procedure

4.2.1 Chemicals and reagents

Phusion DNA polymerase was purchased from Thermo-Scientific, USA. Restriction enzymes and T4 DNA ligase were from NEB and were used according to the manufacturer's instructions. Primers were custom synthesized at Sigma-Aldrich, India. All chemical reagents were of high quality and obtained from Sigma-Aldrich, USA or Merck, USA. Media components were from HiMedia laboratories, India. PfCBS has been cloned into a T7 expression vector supplied in the NEB PURE kit. In-house generated IMPDH deletion strain of *E. coli* (Δ*guaB*^{K}(DE3)) was used for protein expression.

4.2.2 Cloning, expression, and purification

CBS subdomain of *P. falciparum* IMPDH was PCR amplified using the following set of primers.

Fp_5'GTA***CATATG***TTTATCTTTGATCCGTATACC3'
Rp_5'GTA***CTGCAG***TCAGTGGTGGTGGTGGTGGTG***CTCGAG***AATGCGGTTTTTATG CATATC 3'**.**

The DNA fragment was cloned into a modified T7 expression vector (PURExpress kit, NEB, USA) between restriction sites *NdeI* and *PstI* resulting in a C-terminal $(His)_6$-tag and the clone was confirmed error-free by DNA sequencing. The protein was expressed in BL21(DE3) strain of *E. coli* deficient of IMPDH, Δ*guaB*^{k} (DE3). Cells were grown at 37 ˚C to an A_{600nm} of 0.6 prior to induction with 0.1 mM IPTG for 14 h at 25 ˚C. The cells were harvested by centrifugation at 6000g for 10 min at 4 ˚C and resuspended in lysis buffer containing 100 mM potassium phosphate, pH 8.0, 10 % glycerol, 100 mM KCl, 2 mM DTT, and 0.1 mM PMSF and lysed using a French press. After removal of the cellular debris, the supernatant was applied to Ni-NTA affinity matrix (Thermo-scientific, USA) and incubated for 2 h at 4 ˚C. Unbound sample was collected and the matrix was washed with 20 column volumes of lysis buffer followed by elution of protein with 250 mM imidazole, pH 8.0. Fractions were collected, pooled according to purity after examination on SDS-PAGE and concentrated using 10 kDa molecular weight cutoff centrifugal filter units (Merck Millipore, USA). The sample was then subjected to size-exclusion chromatography on Superdex 200 column of dimension 1.6 cm x 60 cm (GE healthcare, USA). Fractions were analyzed for purity by 10 % SDS-PAGE (Laemmli UK, 1970), pooled, concentrated and quantified by the method of Bradford (Bradford MM, 1976). The identity of the recombinant protein was confirmed through Western blot using anti-PfIMPDH antibodies generated in-house.

4.2.3 Analytical size-exclusion chromatography

Analytical size-exclusion chromatography was performed on a Superdex 300 column (1 cm × 30 cm) attached to an AKTA basic HPLC system. The column was equilibrated with 50 mM Tris HCl pH 7.4 and 100 mM KCl and calibrated with the standards apoferritin (443 kDa), β-amylase (200 kDa), alcohol dehydrogenase (150 kDa), bovine serum albumin (66 kDa), carbonic anhydrase (29 kDa) and cytochrome c (12.4 kDa). PfCBS at 50 µM and 100 µM concentrations in a volume of 100 µl each were injected separately into the column and eluted at a flow rate of 0.5 ml min^{-1} with detection at 220 nm.

4.2.4 Circular dichroism spectroscopy

Circular dichroism (CD) spectra of PfCBS were recorded on a J-810 spectropolarimeter (Jasco Corporation, Tokyo, Japan) using a 1 mm path length quartz cuvette. Far-UV CD spectra were recorded between 260 to 195 nm with a bandwidth of 2 nm and at a scan speed of 50 nm min^{-1} using 30 μM of PfCBS in 5 mM potassium phosphate, pH 8.0 at 25 °C. Each spectrum was an average of three scans with data pitch of 0.5 nm and appropriate blank spectra were subtracted. The resulting data were converted from millidegree $[\theta]_{obs}$ to molar ellipticity $[\theta]_M$ using equation 4.1.

$$[\theta]_M = [\theta]_{obs} * \text{Molecular weight}/10cl \text{ ---------- Equation 4.1}$$

where $[\theta]_{obs}$ is the ellipticity in millidegrees after correction for buffer components, c is protein concentration (in mg/ml) and l is the optical path length of the cell (in cm).

4.2.5 Fluorescence spectroscopy

Intrinsic tyrosine fluorescence measurements were recorded on Hitachi F-2500 spectrofluorimeter (Hitachi high-technologies corporation, Tokyo, Japan). Spectra were recorded in 20 mM Tris HCl, pH 8.0 at 25 °C. 10 μM protein samples in the presence or absence of ligands were excited at 278 nm and emission was monitored from 280 nm to 500 nm at a scan speed of 1500 nm min^{-1}. Excitation and emission bandwidths were set to 2.5 nm and 5 nm, respectively. Baseline corrections were done by subtraction of the buffer spectrum. Fluorescence quenching was used to determine the dissociation constants of PfCBS complexed to various ligands. Varying concentrations of the ligands were titrated with the protein solution. Samples were incubated at room temperature for 2 min before the spectra were recorded and subtracted from appropriate buffer blanks. Inner filter effect from ligands was corrected using equation 4.2.

$$F_{corr} = F_{obs} \text{ antilog } [(A_{ex}+A_{em})/2] \quad \text{---------- Equation 4.2}$$

where, F_{corr} and F_{obs} are the corrected and measured fluorescence intensities, respectively. A_{ex} and A_{em} are the absorbance of the ligands at excitation and emission wavelengths, respectively. Binding constants were determined by plotting the corrected change in

fluorescence intensity at a λ_{max} of 304 nm versus the concentration of ligand. The data were fit to one site binding equation (Equation 4.3)

$$\Delta F = (\Delta F_{max} X)/ (K_d + X) \quad \text{----------} \quad \text{Equation 4.3}$$

where, ΔF is the observed change in fluorescence intensity, ΔF_{max} is the maximum change in fluorescence in the presence of a ligand, X is a concentration of ligand and K_d is the dissociation constant for PfCBS complexed with the ligand.

4.3 Results and discussion

4.3.1 Sequence analysis

Gene sequence of PfIMPDH retrieved from the PlasmoDB database has been compared with various IMPDH/GMPR family of proteins. Insertion of a CBS domain (CBS motif 1 and motif 2) within the core catalytic $(\beta/\alpha)_8$ barrel has been identified through multiple sequence alignment (Fig. 3 and Fig. 5). A detailed description of sequence identity and similarity of this gene in comparison with other IMPDH/GMPR family of proteins is provided in the previous chapters. Sequence conservation and the archetypal nucleotide binding motifs of CBS domain from PfIMPDH have been identified through multiple sequence alignment using Clustal Omega (Sievers F *et al.*, 2011; Sievers F and Higgins DG, 2018) and rendered using ESPIRPT 3.0 (Robert X and Gouet P *et al*., 2014) (Fig. 3). Presence of CBS domains and mycophenolic acid (MPA) binding site were believed to be the major differentiating factors of IMPDH from a GMPR (Hedstrom L, 2012). However, identification of *L. donovani* GMPR (Smith S *et al.,* 2016) followed by characterization of *T. brucei* and *T. congolense* GMPR carrying CBS domains and also inhibited by MPA (Bessho T *et al.,* 2016; Sarwono AEY *et al.,* 2017) strongly suggest the possibility of misannotation due to the presence of identical catalytic site residues, substantial sequence similarity and structural features. Hence, a comparative sequence alignment of PfCBS with characterized GMPRs carrying CBS subdomain was also examined (Fig. 4).

A very few examples are available on ligand binding of CBS domain among the various IMPDH/GMPR proteins such as *P. aeroginosa*, *A. gossypium*, *human*, *L. donovani*, *T. brucei* and *T. congolense* (Labesse G *et al*., 2013, Buey RM *et al*., 2015; Smith S *et al*., 2016; Bessho T *et al*., 2016; Sarwono AEY *et al*., 2017). A thorough understanding of ligand

binding and allostery through both kinetic and structural analysis has been reported for IMPDH from *P. aeroginosa* (PaIMPDH) and *A. gossypium* (AgIMPDH) (Labesse G *et al*., 2013; Buey RM *et al*., 2015; Buey RM *et al*., 2017). PaIMPDH in the uncomplexed-state, is reported to display an octameric organisation of subunits. Nevertheless, binding of Mn^{2+}-ATP was found to activate PaIMPDH and further stabilize the dimer of tetramer through the CBS domains. In contrast, guanylate nucleotides, specifically GDP/GTP were found to bind the CBS domain of AgIMPDH and were able to induce octamerization and allosterically inhibit the enzyme activity. An elaborate description of ligand binding and allostery is included in Chapter 5. However, ligand binding pockets within CBS domains observed in PaIMPDH and AgIMPDH and the key residues interacting with Mn^{2+}-ATP and GDP are found to be largely conserved in PfCBS (Fig. 3 and Table 1). Also, contact analysis of GTP binding residues (within 4 Å) in GMPR from *T. brucei* (PDB 5X8O) was performed using the PyMOL molecular graphics system, version 1.7.4 Schrodinger, LLC. The residues from canonical binding sites of CBS domain were found to make key contacts with GTP similar to that observed in Mn^{2+}-ATP bound PaIMPDH structure (Fig. 4 and Table 2).

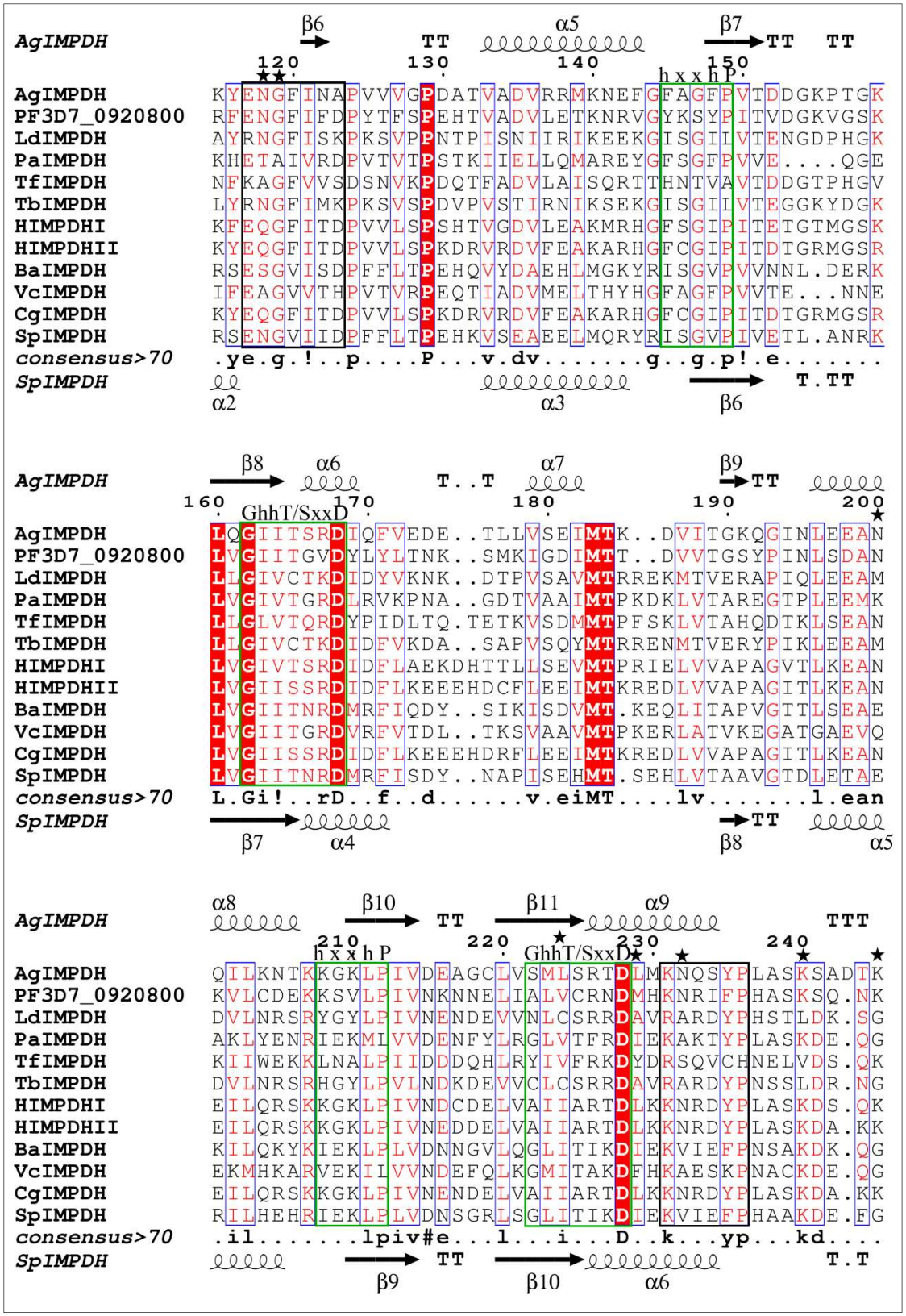
AgIMPDH
PF3D7_0920800
LdIMPDH
PaIMPDH
TfIMPDH
TbIMPDH
HIMPDHI
HIMPDHII
BaIMPDH
VcIMPDH
CgIMPDH
SpIMPDH
consensus>70
SpIMPDH
β6
α5
β7
α2
α3
β6
β8
α6
α7
β9
β7
α4
β8
α5
α8
β10
β11
α9
β9
β10
α6
GhhT/SxxD
h x x h P

Figure 3. Multiple sequence alignment of PfCBS with the subdomain from other IMPDHs *which include Ag-Ashbya gossypium, Ld-Leishmania donovani, Pa-Pseudomonas aeruginosa, Tf-Tritrichomonas foetus, Tb-Trypanosoma brucei, HI- Human type 1, HII-Human type 2, Ba-Bacillus anthracis, Vc-vibrio cholera, Cg- Cricetulus griseus, Sp-streptococcus pyogenes. Secondary structural elements of AgIMPDH (PDB 5TC3) and SpIMPDH (PDB 1ZFJ) from PDB are included on the top and bottom of the sequence alignment, respectively. The sequences were aligned using Clustal Omega (Sievers F et al., 2011; Sievers F and Higgins DG, 2018) and rendered using ESPRIPT v3 (Robert X and Gouet P et al., 2014). Canonical nucleotide binding sites h-x-x-h-P and G-h-h-T/S-x-x-D in both the motifs are enclosed in green boxes while common linkers are in black boxes. α-helices and β-strands are rendered as large squiggles and arrows, respectively. TT and TTT correspond to beta and alpha turns, respectively. Indicated in black asterisk are the non-canonical binding sites for GDP identified in AgIMPDH (PDB ID 5TC3). Shaded in red are identical residues while indicated in red with a grey box are similar.*

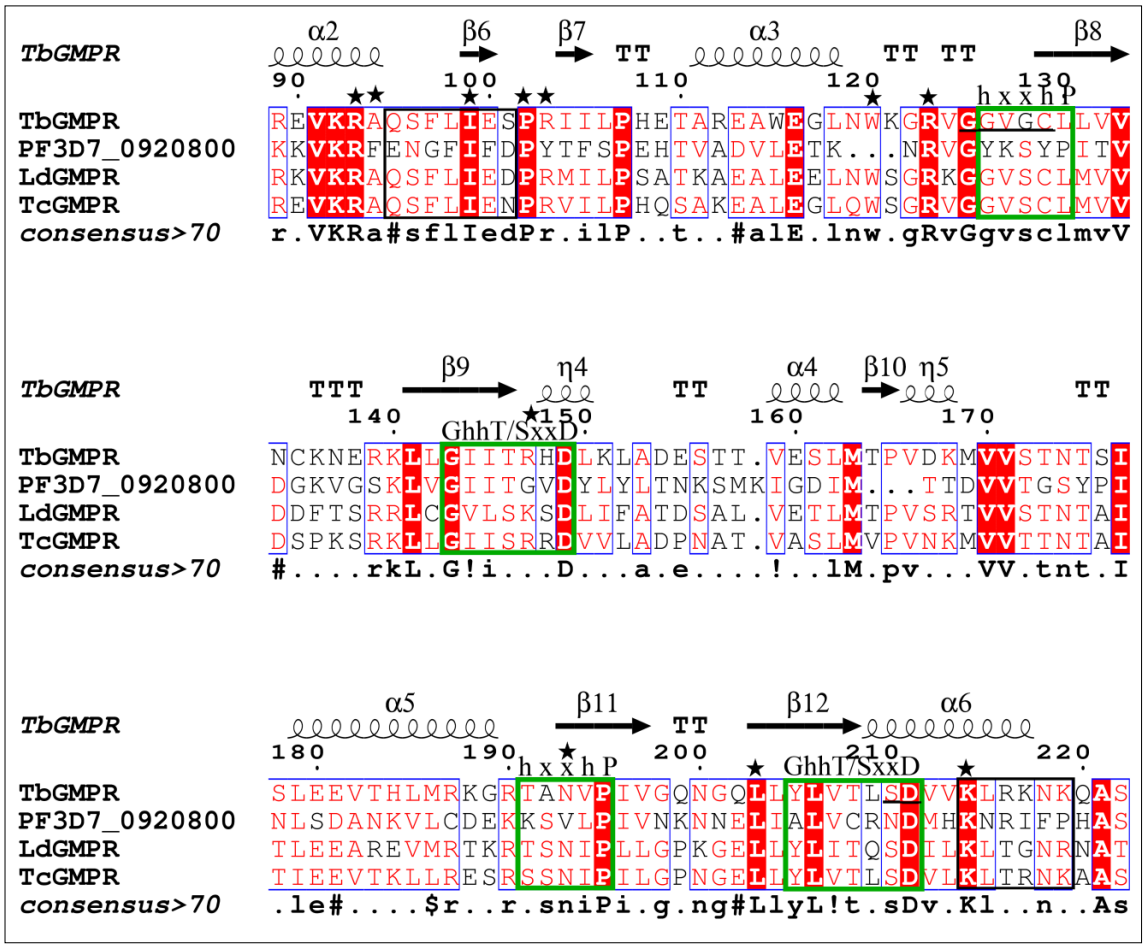

Figure 4. Multiple sequence alignment of PfCBS with the subdomain from other GMPRs *that include Tb-Trypanosoma brucei, Ld-Leishmania donovani, and Tc-Trypanosoma congolense. Secondary structural elements of TbGMPR (PDB 5X8O) from PDB are included on the top of the sequence alignment. The sequences were aligned with Clustal Omega (Sievers F et al., 2011; Sievers F and Higgins DG, 2018) and rendered using ESPRIPT v3 (Robert X and Gouet P et al., 2014). Canonical nucleotide binding sites h-x-x-h-P and G-h-h-T/S-x-x-D in both the motifs are in green boxes while common linkers are in black boxes. α-helices and β-strands are rendered as large squiggles and arrows, respectively. TT and TTT correspond to beta and alpha turns, respectively. Residues that contact (within 4 Å) GTP in the TbGMPR structure (PDB 5X8O) are indicated in black asterisk and underlined. Shaded in red are identical residues while indicated in red with a grey box are similar.*

Table 1. Key residues in PaIMPDH that contact Mn^{2+}ATP (PDB 4DQW). Three structural blocks from each CBS motif comprising of the nucleotide binding residues of PaCBS and corresponding residues in PfCBS are indicated in black and blue colors, respectively along with their specific role in the interactome.

Motif 1/Motif 2	PaCBS/PfCBS	Interactions
Block 1 (linker)	★ 94 VRDPV 98 102 IFDPY 106	★ H-bonds with the adenine ring
Block 2 (h-x-x-h-P)	● ★ 118 FSGFP 122 126 YKSYP 130	● Packs nucelobase
Block 3 (G-h-h-T/S-x-x-D)	● ■▲ 131 GIVTGRD 137 143 GIITGVD 149	▲ H-bonds with the ribose moieties
Block 1' (linker)	★ 157 KLV 159 167 DVV 169	■ Ionic interactions with the phosphate group
Block 2' (h-x-x-h-P)	■ ●▼★ 179 IEKML183 189 KSVLP 193	▼ Coordinates Mn^{2+} ions
Block 3' (G-h-h-T/S-x-x-D)	● ■▲ 193 GLVTFRD 199 203 ALVCRND 209	

Table 2. Key residues in AgIMPDH that contact GDP (PDB 5TC3). Three molecules of GDP were found in each motif. Two of these sites correspond to canonical binding sites described earlier while the third GDP binds elsewhere. Three structural blocks comprising of the nucleotide binding residues of AgCBS and corresponding residues in PfCBS are indicated in black and blue colors, respectively. Underlined residues in bold correspond to the specificity determining positions (SDP). Indicated in a blue triangle, black square and pink circle represent the residues involved in binding of GDP1, GDP2, and GDP3, respectively. GDP3 binds to non-canonical binding cleft formed by α6-α7 helices and α2-α3 loop. Residues K240 and K245 beyond motif 2 also bind GDP3.

Motif 1/Motif 2	AgCBS/PfCBS	Interactions
Block 1 (linker)	115 KYENGFINAPV 125 96 RFENGFIFDPY 106	▲ Residues interacting with GDP 1 ■ Residues interacting with GDP 2 GDP3 binds to the cleft formed by the α6 -α7 helices and the α2–α3 loop. ● Other residues include K240 and K245.
Block 2 (h-x-x-h-P)	145 FAGFP 149 126 YKSYP 130	
Block 3 (G-h-h-T/S-x-x-D)	162 GIITSRD 168 143 GIITGVD 149	
Block 1' (linker)	183 MTKDVITG190_195NLEEAN 200 164 MTTDVVTG171_176NLSDAN 181	
Block 2' (h-x-x-h-P)	204 KNTK**KG**KLP 212 185 CDEKKSVLP 193	
Block 3' (G-h-h-T/S-x-x-D)	222 SMLS**RT**DLMKN 232 203 ALVCRNDMHKN 213	

4.3.2 Cloning, expression, and purification

The codon harmonized gene segment for PfCBS subdomain was cloned into modified T7 expression vector obtained with NEB PURExpress kit between *NdeI* and *PstI* restriction sites resulting in C-terminal $(His)_6$-tag. DNA sequencing of the insert confirmed the clone error-free and identical to the entry in PlasmoDB.

IMPDH deletion strain of *E. coli*, Δ*guaB*^{K}(DE3) transformed with the PfCBS expression plasmid and induced with 0.1 mM IPTG at 25 °C resulted in hyperexpression of

PfCBS with most of the protein in the soluble fraction (Fig. 5). The cell lysate applied to Ni-NTA matrix and eluted with 0.25 M imidazole has yielded significantly pure protein. As a final clean up procedure, Ni-NTA eluates were pooled, concentrated and applied on to the preparative grade size-exclusion chromatography (Superdex S-200, GE Healthcare, USA) which resulted in a highly homogenous sample of PfCBS. The purity as judged by SDS-PAGE was found to be 95-98 % and the identity of the protein was confirmed by Western blot using anti-PfIMPDH antibodies raised in mouse (Fig. 5). The yield of soluble PfCBS protein was about 15-20 mg/L of bacterial culture. Unlike the full-length PfIMPDH or the core catalytic domain, PfCBS was found to be highly soluble. Recombinant PfCBS protein was found to be stable in solution up to a concentration of 35 µM (~ 5 mg/ml) while any further increase in concentration led to immediate precipitation. PROSO II analysis described in Chapter 3 has predicted that the solubility of CBS domain with a C-terminal $(His)_6$-tag is significantly higher (0.645, soluble) than an untagged construct (0.364, insoluble). These observations indicate that the insolubility feature of recombinant PfIMPDH is plausibly due to its core catalytic domain.

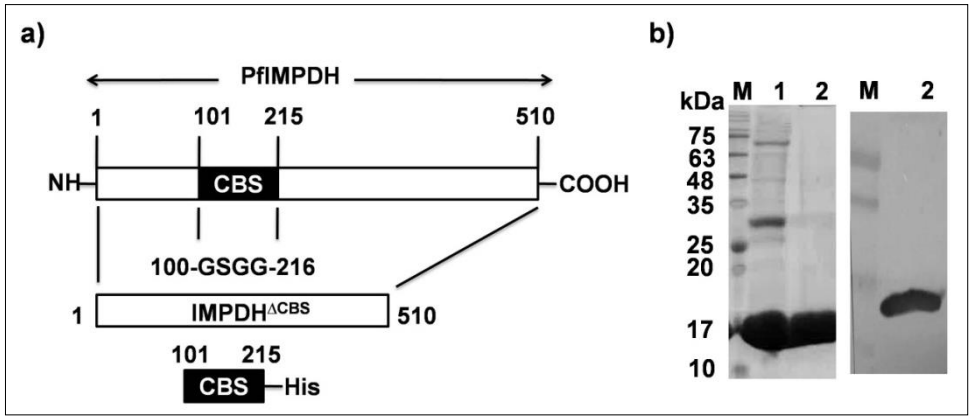

Figure 5. Schematic representation of PfIMPDH protein constructs and purification of PfCBS. a) *Constructs examined in the current thesis are the full length (1-510 residues), the core catalytic domain (1-100-GSGG-216-510 residues) and CBS subdomain (101-215 residues). Codon harmonized PfCBS gene with a C-terminal $(His)_6$-tag cloned into T7 expression vector obtained from PURExpress kit, NEB was used for protein expression in $\Delta guaB^K$(DE3) strain of E. coli.* ***b) Western detection.*** *Lane 1, Ni-NTA eluate; Lane 2, eluate from size-exclusion column; M, Pre-stained protein molecular weight marker, Abcam, USA. Protein was detected by Coomassie Blue staining (left panel) and confirmed by Western blotting using anti-PfIMPDH antibodies raised in mouse (right panel).*

4.3.3 The subunit association of PfCBS

The subunit assembly of the purified recombinant PfCBS was examined by analytical size-exclusion chromatography on a pre-calibrated Superdex 300 column. The experimentally determined molecular mass of PfCBS by extrapolating elution volume from the standard plot indicated PfCBS to exist as a monomer in solution (Fig. 6). The elution profile remained stable under varying protein concentrations (Fig. 6) and with the inclusion of 1M KCl. Till date, the only other reports available on CBS domains examined in isolation are from human and *L. donovani*. Molecular mass of CBS subdomain from human IMPDH2 as determined from analytical size-exclusion chromatography was found to be 24 kDa, between the expected molecular weight of a monomer (16.7 kDa) and a dimer (32 kDa) of the protein while subunit assembly of LdCBS (of IMPDH and GMPR) was not reported (Nimmesgern E *et al.,* 1999 and Smith S *et al.,* 2016).

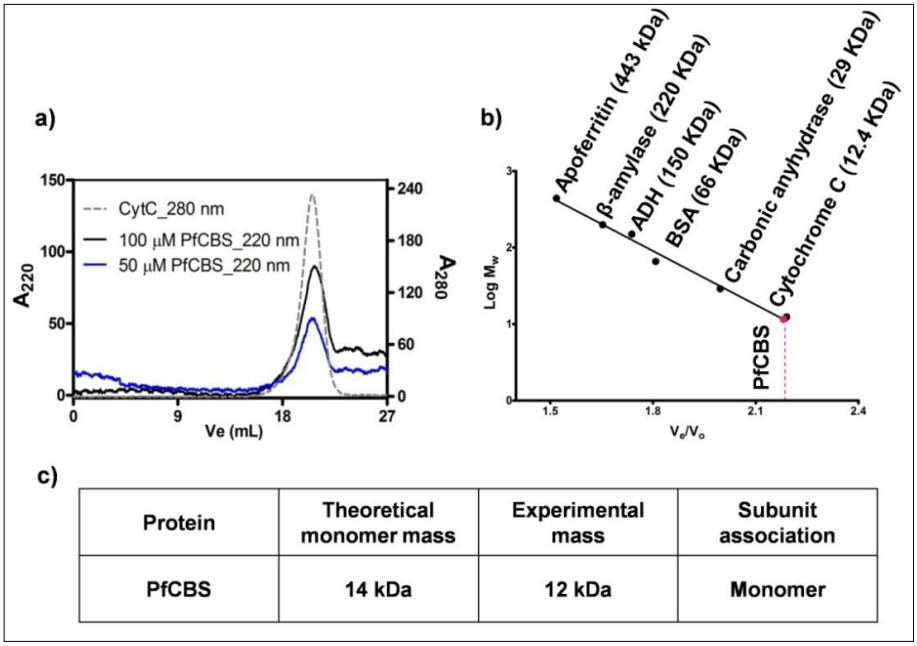

Protein	Theoretical monomer mass	Experimental mass	Subunit association
PfCBS	14 kDa	12 kDa	Monomer

Figure 6. Oligomeric state of PfCBS. a) Elution profile of PfCBS from analytical size-exclusion chromatography. *Elution profiles indicated in blue and black lines correspond to PfCBS at 50 µM and 100 µM, respectively. Grey dashed line corresponds to cytochrome C (12. 4 kDa) used as a standard.* ***b) The standard plot of retention volume*** *(elution volume, Ve/void volume, Vo) versus log molecular weight (M_w). Standards used were apoferritin (443 kDa), β-amylase (200 kDa), alcohol dehydrogenase (ADH, 150 kDa), bovine serum albumin (BSA, 66 kDa), carbonic anhydrase (29 kDa)*

and cytochrome C (12.4 kDa). Size exclusion chromatography was carried out using a superdex 300 column (1 cm x 30 cm). Buffer conditions are as described in the Methods section. V_e/V_0 and log Mol Wt. corresponding to PfCBS are indicated in pink dotted line and pink sphere on standard plot, respectively. ***c) Tabulation of molecular mass.*** *Experimentally observed elution volume corresponds to a molecular mass of 12 kDa similar to that of theoretical monomer mass (14 kDa) indicating the existence of PfCBS as a monomer in solution.*

4.3.4 Circular dichroism

Secondary structural features of purified recombinant PfCBS were examined by CD spectroscopy. The far UV-CD spectral pattern measured from 260 nm-195 nm was found to be largely disordered similar to that of human IMPDH2 with one (negative) signature at 203 nm and another spectral signature at 215 nm (Nimmesgern E *et al.*,1999) (Fig.7). The composition of secondary structural elements was calculated using deconvolution algorithm available at the web server www.bestsel.elte.hu. (Micsonai A *et al.,* 2015 and Micsonai A *et al.,* 2018). The α-helical, β-sheet and other random structures of PfCBS were found to be largely similar as in CBS domain of human IMPDH2 with the only exception of β-turns being half the number in hIMPDH2 (Fig. 7). This supports the fact that despite the sequence variation the overall fold of CBS domain across various proteins of unrelated function remains identical (Ereño-Orbea J *et al.,* 2013). Near UV-CD spectrum of PfCBS could not be measured due to the poor aromaticity (no tryptophan, 3 tyrosine, and 6 phenylalanine) and lack of solubility/stability beyond a concentration of 35 µM (~5 mg ml^{-1}).

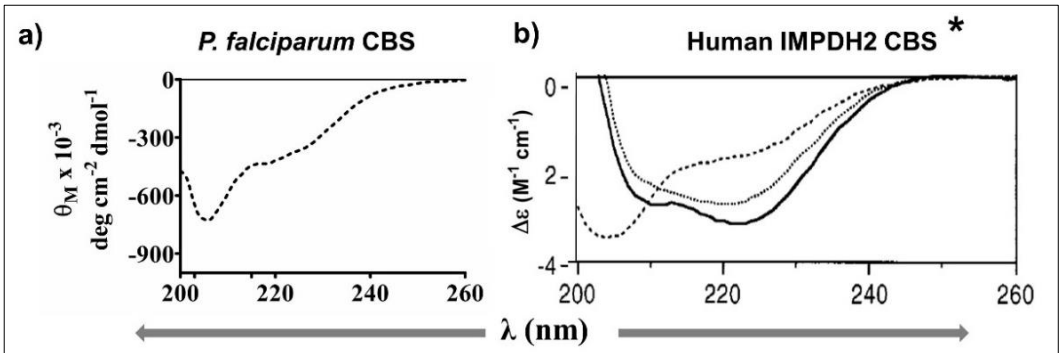

c)

CBS	α-Helix %	β-sheet %		β-Turns %	Other %
		Anti-parallel	Parallel		
Human*	15	11	4	36	33
P. falciparum	**18.4**	**21**	**0**	**16.4**	**44.3**

Figure 7. Far-UV circular dichroism spectrum of PfCBS. a) CD spectrum *of 30 μM PfCBS in 5 mM potassium phosphate, pH 8.0. Cuvettes of 0.1 cm path length were used. The x-axis indicates the wavelength (nm) vs molar ellipticity of PfCBS on the y-axis.* ***b) Comparison with CBS subdomain of human IMPDH2.*** *The x-axis indicates the wavelength (nm) vs difference in molar extinction coefficient Δε (M^{-1} cm^{-1}) on the y-axis. The secondary structure of PfCBS was found to be similar to that of human IMPDH2 CBS (taken from Nimmesgern E et al., 1999) with one (negative) signature at 203 nm and another spectral signature at 215 nm. The solid black line, grey line, and the dotted line indicates the spectra of the full length, core domain and CBS subdomain of human IMPDH2, respectively.* ***c) The composition of secondary structural elements in the CBS domain.*** *Percentage of each secondary structural element of PfCBS was calculated using the deconvolution tool available online (Micsonai A et al., 2015 and Micsonai A et al., 2018) and compared with that of CBS domain from hIMPDH2 (Nimmesgern E et al., 1999).*

4.3.5 Fluorescence spectroscopy

The aromatic amino acid composition of PfCBS includes six tyrosines and three phenylalanines with tryptophan being absent. Intrinsic tyrosine fluorescence measurements were performed in the presence or absence of various purine nucleotides to determine the binding affinity. Upon excitation at 278 nm, the wavelength of maximum fluorescence intensity (λ_{max}) was found to be 304 nm which remained unchanged across apo and complexed forms of the enzyme. However, the addition of purine nucleotides resulted in quenching of fluorescence at emission maximum (λ_{max}) indicative of binding. The difference in fluorescence intensity *vs.* ligand concentration has been plotted and the binding constants (K_d) were determined through non-linear regression of data, fit to one site binding equation (Equation 4.3).

Presence of free phosphate ions has been reported to quench tyrosine fluorescence (Alev-Behmoaras T *et al.,* 1979). Control fluorescence measurements of PfCBS performed with dipotassium hydrogen phosphate (HPO_4^{2-}) displayed no change in the intensity of intrinsic tyrosine fluorescence up to 400 µM (Fig. 8). Addition of substrates (NAD^+, IMP) and products (XMP, and NADH) of IMP dehydrogenase reaction caused no change in fluorescence (Fig. 8). However, both adenylate and guanylate nucleotides (except GMP) quenched fluorescence in a concentration-dependent manner indicative of binding to PfCBS with a strong affinity (Fig. 9 and Table. 3). NAD^+ has been reported to bind CBS domains of various proteins (Baykov AA *et al.,* 2011), however, no significant binding event was observed with CBS domain of PfIMPDH. Similar nucleotide binding experiments for LdCBS have been reported by Smith S *et al.,* 2016 using intrinsic tyrosine fluorescence as the probe. No binding was observed for IMP while ATP, GMP, and GTP were found to bind LdCBS (both IMPDH and GMPR) with ~2-3 fold lower affinity than PfCBS (Table. 3).

In conclusion, *Plasmodium falciparum* has retained evolutionarily conserved CBS domain as part of PfIMPDH gene. PfCBS domain identified through sequence alignment and homology search was found to carry the characteristic protein fold similar to that of human CBS (IMPDH2). Presence of archetypal binding motifs and the ability to bind both the purine nucleotides indicate the probable role of PfCBS as an internal sensor for modulation of purine nucleotide metabolism in the malarial parasite.

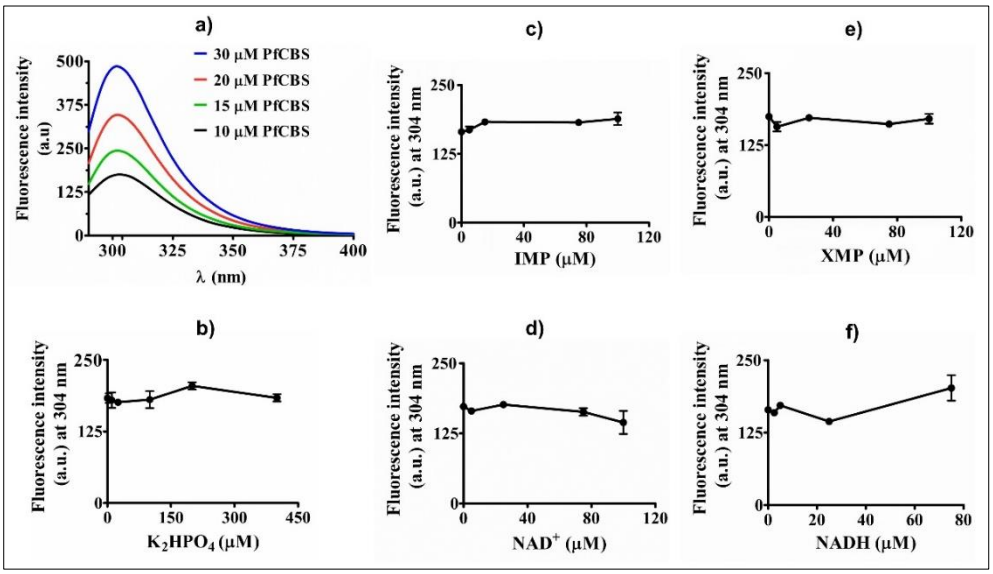

Figure 8. Binding of substrates and products of IMPDH to PfCBS. *Intrinsic tyrosine fluorescence of PfCBS was measured with excitation at 278 nm and emission spectra recorded from 280 nm to 500 nm. Ligand binding was monitored as a change in the intensity of the intrinsic fluorescence at an emission maximum of 304 nm. The spectra were corrected for buffer components and inner filter effect by the ligands. 10 µM or 15 µM of PfCBS was used for each measurement.* ***a) Intrinsic tyrosine fluorescence emission profile of PfCBS at varied protein concentrations. b) Effect of phosphate on tyrosine fluorescence.*** *Presence of phosphate ions up to 400 µM did not interfere in the tyrosine fluorescence measurements.* ***Panel c, d, e, and f correspond to fluorescence measurements made in the presence of substrates and products of IMP dehydrogenase.*** *No significant change in fluorescence intensity was observed in the presence of IMP, NAD^+, XMP, and NADH indicating the absence of ligand binding to the protein. Binding experiments were performed in two technical replicates containing two biological replicates each. Representative plots from one technical replicate are shown. Each data point represents the mean fluorescence intensity. Error bars represent the standard deviation of the data (n=2).*

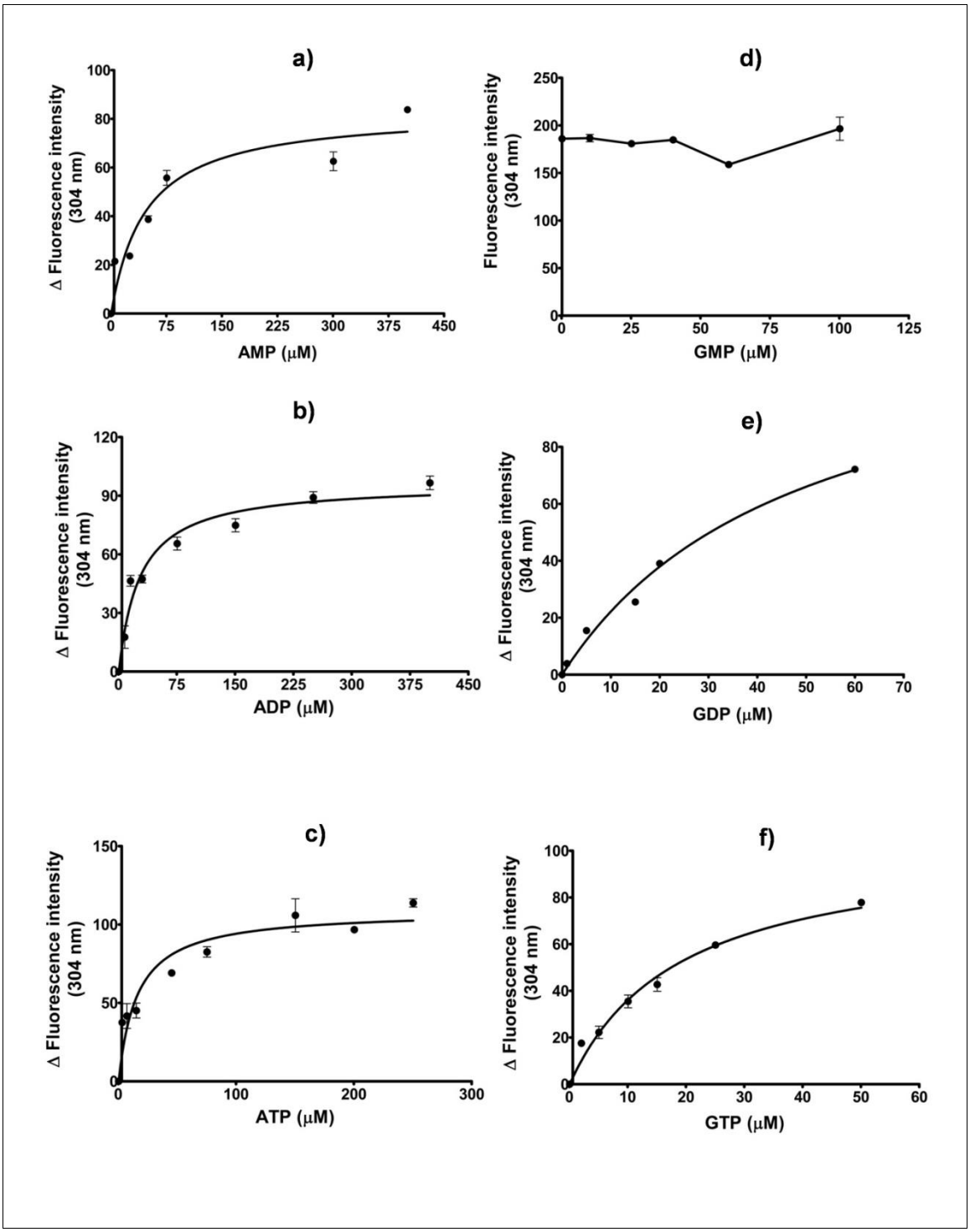
a)
Δ Fluorescence intensity (304 nm)
AMP (μM)
d)
Fluorescence intensity (304 nm)
GMP (μM)
b)
Δ Fluorescence intensity (304 nm)
ADP (μM)
e)
Δ Fluorescence intensity (304 nm)
GDP (μM)
c)
Δ Fluorescence intensity (304 nm)
ATP (μM)
f)
Δ Fluorescence intensity (304 nm)
GTP (μM)

Figure 9. Ligand binding studies on PfCBS. *15 µM PfCBS in the presence of varying concentrations of adenine (a, b, c) and guanine (d, e and f) nucleotides was excited at 278 nm and emission spectra were recorded from 280 nm to 500 nm. Ligand binding was monitored as changes in the intrinsic tyrosine fluorescence at an emission maximum of 304 nm. The resultant spectra were corrected for buffer components and inner filter effect by the ligands. No binding event was observed in the presence of GMP while binding of GDP, GTP, AMP, ADP, and ATP resulted in fluorescence quenching. The difference in the fluorescence intensity upon addition of the ligands was plotted on the y-axis vs. concentration of ligand on the x-axis. Data were analyzed through non-linear regression, fit to one site binding equation using Graph Pad version 5, K_d values were determined and are tabulated in Table 3. Binding experiments were performed in two technical replicates containing two biological replicates each. Representative plots from one technical replicate are shown. Each data point represents the mean fluorescence intensity. Error bars represent the standard deviation of the data (n=2).*

**Table 3. Nucleotide binding affinity of PfCBS in comparison with that of CBS subdomains from *Leishmania donovani* IMPDH and GMPR. ***data is taken from Smith S *et al*., 2016. PfCBS displayed a much higher affinity for the purine nucleotides as compared to that of LdCBS. The standard deviation of the data is provided (n=2).

<table>
<tr><th rowspan="2">Ligand</th><th colspan="3">K_d (µM)</th></tr>
<tr><th>PfCBS</th><th>LdCBS* (IMPDH)</th><th>LdCBS* (GMPR)</th></tr>
<tr><td>AMP</td><td>46 ± 14</td><td rowspan="2">Not determined</td><td rowspan="3">Not determined</td></tr>
<tr><td>ADP</td><td>27 ± 5</td></tr>
<tr><td>ATP</td><td>16 ± 4</td><td>148 ± 19</td></tr>
<tr><td>GMP</td><td>No binding</td><td>92 ± 6</td><td>333 ± 27</td></tr>
<tr><td>GDP</td><td>49 ± 9</td><td>Not determined</td><td>Not determined</td></tr>
<tr><td>GTP</td><td>19 ± 4</td><td>89 ± 11</td><td>188 ± 19</td></tr>
<tr><td>NAD$^+$</td><td rowspan="4">No binding</td><td rowspan="4">No binding</td><td rowspan="4">Not determined</td></tr>
<tr><td>NADH</td></tr>
<tr><td>IMP</td></tr>
<tr><td>XMP</td></tr>
</table>

4.4 Conclusion

CBS domain of the *P. falciparum* protein PfIMPDH has been identified through multiple sequence alignment with various IMPDH/GMPR family of proteins and characteristic nucleotide binding motifs have been mapped. PfCBS was found to be highly soluble unlike the core catalytic domain and has been purified to homogeneity. Recombinant PfCBS was found to be a monomer in solution. The secondary structure composition obtained through the far-UV CD spectrum was comparable to that of CBS domain from human IMPDH2. PfCBS protein was found to bind both adenine and guanine nucleotides except GMP as evidenced by changes in intrinsic tyrosine fluorescence measurements upon ligand binding while neither substrates nor products affected the fluorescence intensity.

Chapter 5. Biochemical and kinetic characterization of inosine 5'-monophosphate dehydrogenase from *Methanocaldococcus jannaschii*

This part of the work is focussed on understanding the functioning of inosine 5'-monophosphate dehydrogenase (IMPDH) from Methanocaldococcus jannaschii (Mj), a hyperthermophilic archaeon. Gene sequence encoding full-length MjIMPDH and the core catalytic domain MjIMPDH$^{\Delta CBS}$ were cloned into E. coli expression system carrying a C-terminal (His)$_6$-tag. Both the enzymes were found to be highly soluble and purified to homogeneity. Deletion of CBS subdomain does not affect the enzyme activity. Both the constructs displayed optimal activity with a very weak dependence on monovalent cations, unlike various other characterized IMPDHs. MjIMPDH and MjIMPDH$^{\Delta CBS}$ exhibited similar kinetic features with maximal activity displayed at pH 8.0/70 °C and no drop in activity was observed up to 95 °C. Examination of subunit assembly in solution revealed the existence of MjIMPDH as octamers and higher order oligomers while the CBS deletion construct was found to be a tetramer which remained stable under all tested conditions. Saturation kinetics and product inhibition studies were performed to determine the kinetic parameters. This chapter also summarizes the effect of various purine nucleotides and the role of CBS domain in regulation of NAD$^+$-dependent IMP specific dehydrogenase activity.

5.1 Purine biosynthesis in *M. jannaschii*

Purine biosynthesis in *M. jannaschii* can occur through the *de novo* route (Bult CJ et al., 1996; Selkov E *et al*., 1997; Ownby K *et al*., 2005; Brown AM *et al*., 2011) or by salvage of adenine and guanine (Armenta-Medina D *et al*., 2014; Miller DV *et al*., 2016). Formation of 5-phospho-α-D-ribosyl-1-pyrophosphate (PRPP) from α-D-ribose-5-phosphate (R5P) and ATP is the first committed step in purine *de novo* synthesis followed by a series of enzymatic conversions to yield inosine 5'-monophosphate (IMP).

M. jannaschii lacks the enzyme adenine phosphoribosyltransferase (APRT), thus direct condensation of adenine with PRPP to produce adenosine 5'-monophosphate (AMP) is not possible. The alternate route includes conversion of adenine to adenosine by a purine nucleoside phosphorylase; then subsequent phosphorylation to AMP by an adenosine kinase

(AK). However, the purine nucleoside phosphorylase, annotated as a methylthioinosine phosphorylase, in *M. jannaschii* utilizes inosine to form hypoxanthine but not adenosine as a substrate (Miller DV *et al.,* 2016) and no adenosine kinase homolog has been identified in the *M. jannaschii* genome (Armenta-Medina D *et al.,* 2014). These findings suggest that adenine is not directly salvaged in *M. jannaschii* but proceeds through deamination of adenine to hypoxanthine by adenine deaminase (Ade) followed by condensation with PRPP by hypoxanthine (guanine) phosphoribosyltransferase (MjHGPRT) to form IMP. MjHGPRT is found to exhibit equal specificity for hypoxanthine and guanine while no detectable activity was observed with adenine as a substrate. Also, no inosine kinase (IK) homolog in the *M. jannaschii* genome has been identified for the direct formation of IMP from inosine (Miller DV *et al*., 2016). Source of adenine remains unknown, yet predicted sources include exogenous adenine taken up by the cells and thermal decomposition of DNA under extreme temperature or pressure conditions (Boonyaratanakornkit BB *et al.,* 2007). Therefore, IMP obtained from either *de novo* or salvage route becomes the central metabolite of AMP and GMP biosynthesis. On one arm adenylosuccinate synthetase (ADSS) catalyzes the formation of succinyl AMP from IMP followed by the action of adenylosuccinate lyase (ASL) to form AMP, while on the other arm inosine 5'-monophosphate dehydrogenase (IMPDH) catalyzes the conversion of IMP to xanthosine 5'-monophosphate (XMP) followed by catalysis of XMP to GMP by the enzyme GMP synthetase (Fig. 1). MjADSS and MjGMPS have been well characterized earlier from our laboratory (Mehrotra S and Balaram H, 2007 and Ali R *et al*., 2012; Ali R *et al*., 2013). MjASL activity has been confirmed while detailed characterization is not available (White RH, 2011).

Inosine 5'-monophosphate dehydrogenase (IMPDH, EC 1.1.1.205) catalyzes the oxidation of IMP to XMP with the concordant reduction of nicotinamide adenine dinucleotide (NAD^+) to NADH. The reaction is a branch point between the adenine and guanine nucleotide biosynthesis, and a rate-limiting step of GMP biosynthesis (Fig. 1). IMPDH is crucial for DNA and RNA synthesis, signal transduction, and other processes involved in cell proliferation (Allison AC *et al*., 2000). A detailed description of IMPDH family of proteins is provided in Chapter 1. Biochemical investigations on *M. jannaschii* IMPDH are presented in the current chapter.

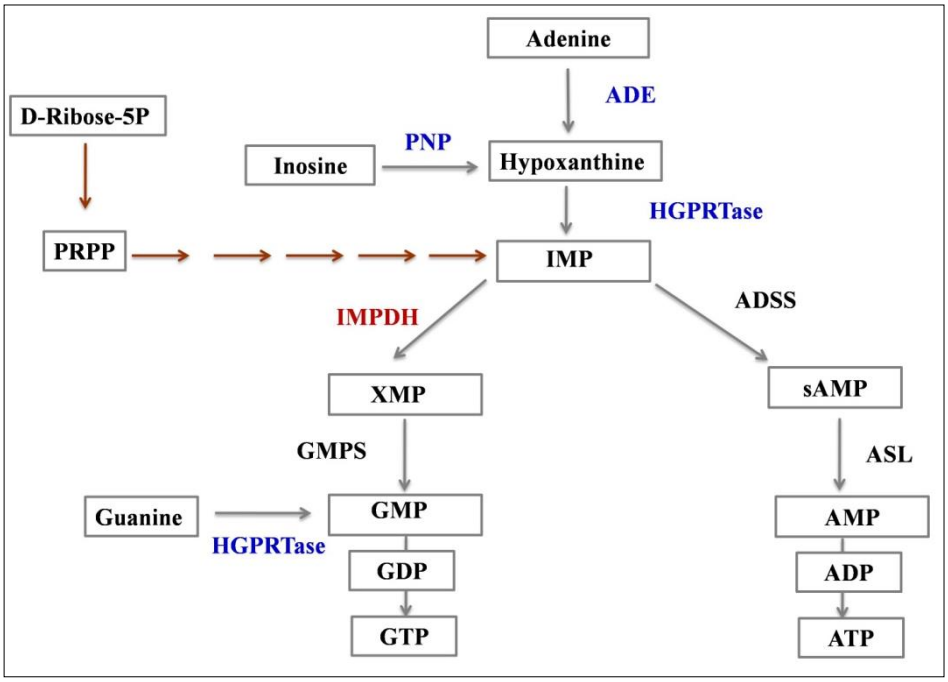

Figure 1. Purine nucleotide biosynthesis in Methanocaldococcus jannaschii. *Adenine is salvaged to form hypoxanthine by the action of adenine deaminase (ADE). Hypoxanthine is also formed from inosine by purine nucleoside phosphorylase (PNP). Hypoxanthine is further acted upon by phosphoribosyltransferase (HGPRTase) to yield inosine 5'-monophosphate (IMP). The conversion of D-ribose-5-phosphate to PRPP includes the first step in the de novo path and subsequent steps are indicated in brown arrows to yield IMP. IMP which is also obtained through de novo path forms the central metabolite to yield adenosine 5'-monophosphate (AMP) and guanosine 5'-monophosphate (GMP). IMP dehydrogenase (IMPDH) and GMP synthetase (GMPS) on one arm yield GMP while on the other by the sequential action of adenylosuccinate synthase (ADSS) and adenylosuccinate lyase (ASL) forms AMP. HGPRTase could directly phosphoribosylate guanine to GMP. Indicated in blue are the enzymes involved in the salvage of purines. The enzyme under study, IMPDH is highlighted in red while all other enzymes are indicated in black.*

5.2 Experimental procedure

5.2.1 Chemicals and reagents

Restriction enzymes, Taq DNA polymerase, and T4 DNA ligase were from NEB and were used according to the manufacturer's instructions. Phusion DNA polymerase was purchased from Thermo-Scientific, India. Primers were custom synthesized at Sigma-Aldrich, India. All chemical reagents were of high quality and obtained from Sigma-Aldrich, USA or Merck, USA. Media components were from HiMedia laboratories, India. IMP, NAD^+ and other biochemicals were of the highest quality available from Sigma-Aldrich, USA.

5.2.2 Cloning, expression and purification

MjIMPDH gene (MJ1616) was PCR amplified from *M. jannaschii* genomic DNA using gene-specific primers (Table 1). The gene was cloned into pET21b+ expression vector (Novagen, USA) between restriction sites *NdeI* and *XhoI* resulting in a C-terminal $(His)_6$-tag fusion and the clone was confirmed error-free by DNA sequencing. Core catalytic domain was amplified using full-length MjIMPDH as a template. Using oligonucleotide primers, T7 promoter, and p2, N-terminus was amplified (PCR 1). C-terminus was amplified with T7 terminator and p1 (PCR 2) (Table 1). N- and C-termini were fused by overlap PCR (PCR 3) using T7 primers (promoter, terminator) (Table 1). The clone for catalytic domain carrying C-terminal $(His)_6$-tag was confirmed error-free by DNA sequencing.

Table 1. Oligonucleotide primers used for amplification of MjIMPDH and MjIMPDH$^{\Delta CBS}$

S. No.	Forward primer and sequence	Reverse primer and sequence
1	5'GTC***CATATG***TTTTTAAAAAAACTAATTGAGGCAAAGAAG3'	5'GTA***CTCGAG***TTTACCCAGTGGATAATTCGGAGC3'
2	**T7 promoter** 5'TAATACGACTCACTATAGGG3'	**p2** 5'CTACCTTTTTTATCCCTTGCAGCTTGAGGATAACCGCCGGATCCAATAACTACTTCATCAGCTTTTTTAACTGCCTG3'
3	**p1** 5'CAGGCAGTTAAAAAAGCTGATGAAGTAGTTATTGGATCCGGCGGTTATCCTCAAGCTGCAAGGGATAAAAAAGGTAG3'	**T7 terminator** 5'GCTAGTTATTGCTCAGCGG3'
4	**T7 promoter** 5'TAATACGACTCACTATAGGG3'	**T7 terminator** 5'GCTAGTTATTGCTCAGCGG3'

The MjIMPDH$(His)_6$ protein was expressed in BL21(DE3) strain of *E. coli* lacking the endogenous enzyme, Δ*guaB*^{K}(DE3) (generation of the strain and its validation is described in Chapter 2). Cells were grown at 37 ˚C to an A_{600nm} of 0.6 prior to induction with 0.05 mM IPTG for 12 h at 16 ˚C. The cells were harvested by centrifugation at 6000g for 10 min at 4 ˚C and re-suspended in lysis buffer containing 50 mM Tris HCl, pH 7.0, 10 % glycerol, 2 mM DTT, 0.1 mM PMSF and lysed using a French press. After removal of the cellular debris by centrifugation, the supernatant was subjected to thermal precipitation at 70 ˚C for 30 min. The lysate was then centrifuged at 28000g to remove the precipitated *E. coli* proteins, followed by 0.01 % PEI treatment to remove nucleic acids. This solution containing MjIMPDH$(His)_6$ was purified by anion-exchange chromatography on a Q-sepharose column

using a gradient of lysis buffer containing 1 M KCl. Fractions were collected, examined by SDS-PAGE, pooled according to purity and precipitated with ammonium sulfate at 90 % saturation. The precipitate was dissolved in lysis buffer and purified by size-exclusion chromatography on Superdex 200 column of dimension 1.6 cm x 60 cm (GE healthcare, USA). Fractions were analyzed for purity by SDS-PAGE (Laemmli UK, 1970), pooled, concentrated and quantified by the method of Bradford (Bradford MM, 1976). The identity of the recombinant protein was assessed by Western blotting using anti-$(His)_6$ antibody (Sigma-Aldrich, USA). Expression and purification procedures of $MjIMPDH^{\Delta CBS}$ remained identical to that of MjIMPDH with a minor change that included 50 mM Tris HCl, pH 8.4 for anion exchange and 50 mM Tris HCl, pH 8.0 for size-exclusion chromatography and final storage.

5.2.3 Circular dichroism

Circular dichroism (CD) spectra of MjIMPDH and $MjIMPDH^{\Delta CBS}$ were recorded on a J-810 spectropolarimeter (Jasco Corporation, Tokyo, Japan) using a 1 mm path length quartz cuvette. Far-UV CD spectra were recorded between 260 to 195 nm with a bandwidth of 2 nm and a scan speed of 200 nm min^{-1} using 5 μM of each protein in 10 mM Tris HCl, pH 8.0 at room temperature. Each spectrum was an average of three scans with data pitch of 0.5 nm and appropriate blank spectra were subtracted. The resulting data were converted from millidegree $[\theta]_{obs}$ to molar ellipticity $[\theta]_M$ using equation 5.2.

$[\theta]_M = [\theta]_{obs} * \text{Molecular weight}/10cl$ ---------- Equation 5.2

where $[\theta]_{obs}$ is the ellipticity in millidegrees after correction for buffer components, c is protein concentration (in mg/ml) and l is the optical path length of the cell (in cm).

5.2.4 Fluorescence spectroscopy

Fluorescence measurements were recorded on Hitachi F-2500 spectrofluorimeter (Hitachi high-technologies corporation, Japan). Spectra were recorded in 50 mM Tris-HCl, pH 8.0, 100 mM KCl and 1 mM DTT at room temperature. 5 μM protein samples were excited at 295 nm and emission was monitored from 298 nm to 500 nm at a scan speed of

1500 nm min^{-1}. Both excitation and emission bandwidths were set to 5 nm. Baseline corrections were done by subtraction of the buffer spectrum.

5.2.5 Analytical size-exclusion chromatography

Analytical size-exclusion chromatography was performed on a Superdex 300 column (1 cm × 30 cm) attached to an AKTA basic HPLC system. The column was equilibrated with 50 mM Tris HCl, pH 7.4 and 100 mM KCl and calibrated with the standards apoferritin (443 kDa), β-amylase (200 kDa), alcohol dehydrogenase (150 kDa), bovine serum albumin (66 kDa), carbonic anhydrase (29 kDa) and cytochrome c (12.4 kDa). Various fractions of MjIMPDH and $MjIMPDH^{\Delta CBS}$ from the preparative grade size-exclusion chromatography, at multiple concentrations in a volume of 100 µl each were injected separately into the column and eluted at a flow rate of 0.5 ml min^{-1} with detection at 220 nm.

5.2.6 Dehydrogenase assay

The standard assay conditions included 50 mM TAPS, pH 8.0, 100 mM KCl, 3 mM EDTA, 1 mM DTT, 0.1 mM IMP, 0.2 mM NAD^+ and 1 µg of either MjIMPDH or $MjIMPDH^{\Delta CBS}$ in 250 µl volume unless otherwise mentioned. The reaction mix was pre-incubated at 70 ˚C for 5 min before initiation with IMP. All the assays were carried out at 70 ˚C on a Hitachi-U 2010 spectrophotometer fitted with a water circulated cell holder. The enzymatic activity was measured by the increase in absorbance at 340 nm with the formation of NADH as a function of time (ε= 6.22 mM^{-1} cm^{-1}). With acetylpyridine adenine dinucleotide ($APAD^+$) as the substrate, production of APADH (reduced form) was monitored at 363 nm (ε= 9.1 mM^{-1} cm^{-1}).

For the determination of kinetic constants, IMP was varied between 1 µM to 500 µM and NAD^+ between 3 µM to 5000 µM, while their fixed saturation concentrations were 0.1 mM and 0.2 mM, respectively. The data were fitted to either Michaelis-Menten equation (equation 5.3) or substrate inhibition (equation 5.4) and analyzed by nonlinear regression using GraphPad Prism, version 5 (GraphPad Software Inc., USA). The effect of monovalent (Na^+, K^+, Li^+, Rb^+, Cs^+, NH_4^+) and divalent metal ions (Mg^{2+}, Ca^{2+}) were examined using 100 mM concentration of each with no EDTA included in the reaction mixture. The effect of products and various purine nucleobases, nucleosides, and nucleotides on dehydrogenase

activity was monitored keeping concentrations of IMP, NAD^+ and KCl fixed at 5 μM, 20 μM and 100 mM, respectively. All assays were performed twice in duplicates and the standard deviation of the data is represented.

$v = V_{max}[S] / K_m + [S]$ Michaelis-Menten Equation 5.3

$v = V_{max}[S] / K_m + [S] (1+[S]/K_i)$ Substrate inhibition Equation 5.4

where v and V_{max} are the initial and maximum velocity, respectively. S is the variable substrate concentration, K_m is the Michaelis constant for the variable substrate, and K_i is the inhibition constant.

5.2.7 pH dependence

The effect of pH on the activity of MjIMPDH and $MjIMPDH^{\Delta CBS}$ was examined at fixed substrate concentrations of 100 mM KCl, 0.2 mM NAD^+ and 0.1 mM IMP. 50 mM mixed buffer containing MES (pH 5.5-6.7), HEPES (pH 6.8-8.2), CAPS (pH 9.7-11.1) and Glycine-NaOH (pH 8.8-10.6) was used for activity measurements with pH adjusted at 70 °C. Spline fit of the data was achieved using GraphPad Prism, version 5 (GraphPad Software Inc., USA).

5.2.8 Temperature dependence

The effect of temperature on the activity of MjIMPDH and $MjIMPDH^{\Delta CBS}$ was monitored at fixed substrate concentrations of 100 mM KCl, 0.2 mM NAD^+ and 0.1 mM IMP. 50 mM TAPS, pH 8.0 prepared at various temperatures ranging from 25 °C to 95 °C was used for activity measurements. Spline fit of the data was achieved using GraphPad Prism, version 5 (GraphPad Software Inc., USA).

5.3 Results and discussion

5.3.1 Sequence analysis

Genome analysis of *M. jannaschii* reveals that at the molecular level archaea more closely resemble eukaryotes (Bult CJ *et al.*, 1996). The archaeal genome is about 70 % AT-rich while that of the protozoan parasite *P. falciparum* is about 80 % (Bult CJ *et al.*, 1996; Gardner MJ *et al.*, 2002). IMP dehydrogenase from the hyperthermophilic archaea *M. jannaschii* is similar in polypeptide length (496 amino acids) to that of eukaryotic

counterparts including human (Isoform I and II), *Tritrichomonas foetus* and *P. falciparum* which have 514, 503 and 510 amino acid residues, respectively. An alignment of MjIMPDH with the *P. falciparum* enzyme clearly shows a consensus of >70, with 47 % similarity and 35 % identity (Fig. 2). MjIMPDH has been compared with various other characterized IMPDHs and was found to share an average of 50 % sequence identity and 63 % similarity with prokaryotic IMPDHs (*Mycobacterium tuberculosis*, *Bacillus anthracis*, *Borrelia burgdorferi*, *Escherichia coli*, *Bacillus subtilis* and *Pseudomonas aeruginosa*) and an average of 35 % identity and 50 % similarity with the eukaryotic counterparts (*Ashbya gossypium, Leishmania donovani, Human I, II, Cryptosporidium parvum, Tritrichomonas foetus and Plasmodium falciparum*) while *Pyrococcus horikoshii*, an archaeon shares 63 % identity and 75 % similarity. *C. parvum* and *B. burgdorferi* are the two known examples with no CBS domain in IMPDH. However, IMPDH from the eukaryotic protozoan parasite, *C. parvum* shares 50 % identity with MjIMPDH. Five structural features involved in the determination of ligand binding and catalysis which include catalytic cysteine loop, phosphate binding loop, finger loop, C-terminal loop, and mobile flap loop are identified in MjIMPDH through multiple sequence alignment (Fig. 3). The catalytic loop, mobile flap, and C-terminal loop all display varying degrees of flexibility and disorder in various X-ray crystal structures of IMPDH deposited in protein databank (PDB) (described in Chapter 1). The key catalytic residues cysteine, threonine, arginine, and tyrosine and the residues that interact with IMP are highly conserved and largely invariant. The residues that interact with the adenine ring of NAD^+, however, vary to a large extent and are frequently difficult to identify in sequence alignments (Hedstrom L, 2009). Comparison of conservation of critical residues identified in *T. foetus* IMPDH through X-ray crystallographic studies and kinetic analysis with that of proteins annotated as IMPDH from *M. jannaschii* and *P. falciparum* are tabulated (Table 2)

Table 2. Tabulation of key residues involved in ligand binding and catalysis.

MjIMPDH	PfIMPDH	TfIMPDH[a]	Interaction[a]
C306, T308, R405, Y406	C314, T316, R413, Y414	C319, T321, R418, Y419	Key catalytic residues
D339	D347	D358	H-bonds to the ribose hydroxyls of IMP
S304, Y386	S312, Y394	S317, Y405	H-bonds to the phosphate of IMP via their hydroxyl groups.
G341, G362	G349, G370	G360, G381	interact with the phosphate of IMP via main chain NH
G390	G398	G409	forms an H-bond to the purine ring via its NH
S363	N378	R382	interacts with the phosphate of IMP
M389, E423	M397, Q435	E408, E431	main chain atoms H- bond with the purine ring
D247	D257	D261	The carboxyl group H-bonds with the ribose hydroxyls of the nicotinamide portion of NAD^+.
G299, G301	G307, G309	G312, G314	The only other conserved interaction includes H-bonds with the carboxamide of NAD^+.
R309	Q317	R322	The carboxamide can also make an alternative H-bond with the side chain but Q and G are also found at this position.
C248, A249	S258, S259	S262, S263	The OH group interacts with the phosphates of NAD^+. Neither of these residues is conserved. Position 262 usually contains a T or C that preserves this interaction. Position 263 is often an A.
E423	Q435	E431	Variability plays a role in catalysis and drug selectivity.

[a] Hedstrom L, 2009.

M. jannaschii lives under conditions of high temperature and pressure whereas *P. falciparum* does not experience temperatures greater than 41˚C during its life cycle. The cellular machinery of the two organisms is adapted to function at their optimal growth temperature. However, enzymes which are biological catalysts are sensitive to the environmental conditions. Structural similarity of the active site and conservation of the catalytic residues exist between mesophilic and thermophilic counterparts. The increased conformational rigidity serves to stabilize thermophilic proteins at extreme temperatures (Fields PA, 2001). Studies on the archaeal enzyme are aimed at understanding kinetic and regulatory features of the thermophilic IMPDH.

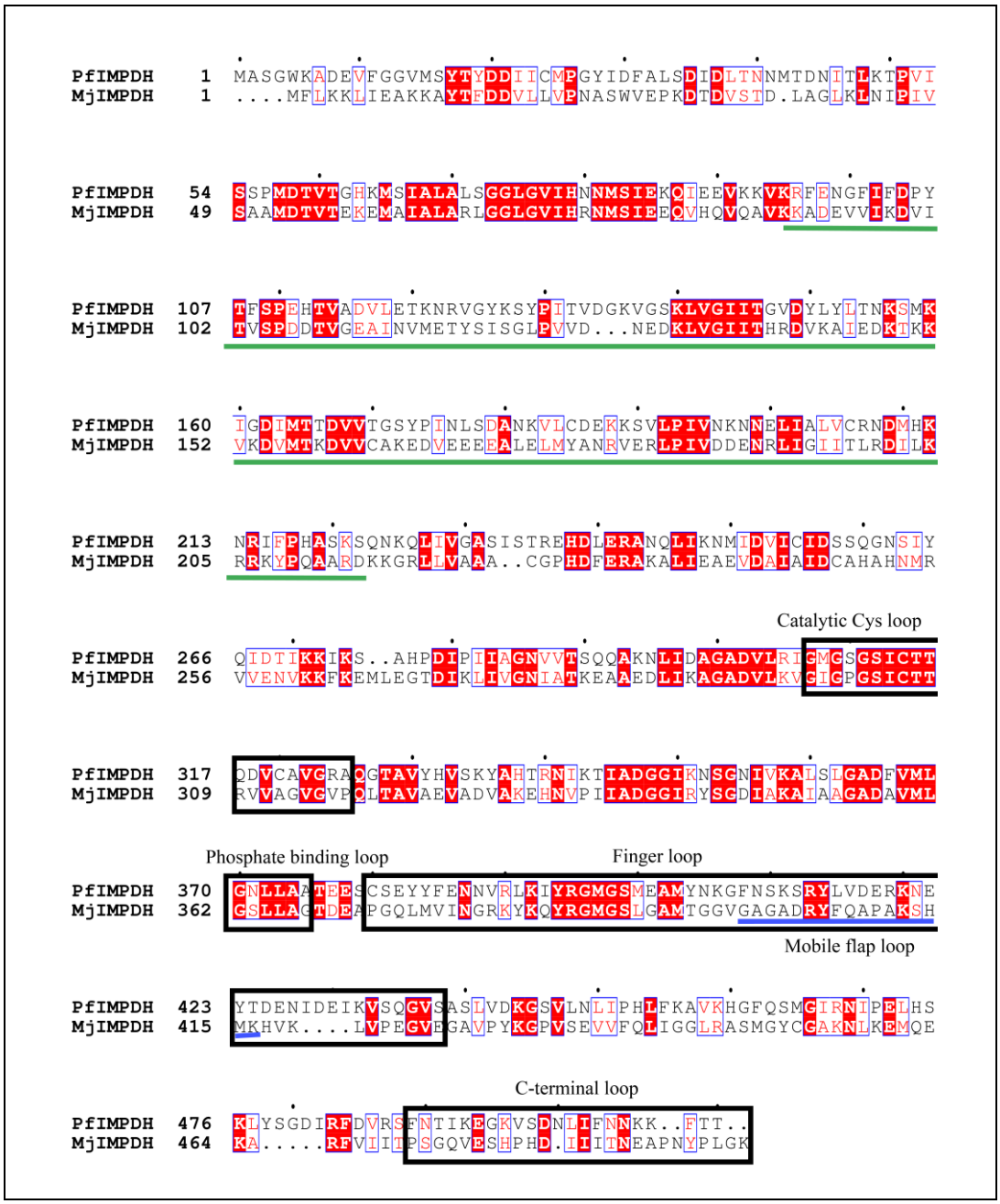

Figure 2. Sequence alignment of the annotated IMP dehydrogenase from the mesophilic protozoan parasite P. falciparum and the thermophilic archaeon M. jannaschii. *The sequences were aligned using Clustal Omega (Sievers F et al., 2011; Sievers F and Higgins DG, 2018) and rendered using ESPRIPT v3 (Robert X and Gouet P, 2014). The red shaded regions indicate the identical residues while residues represented in red highlight similarity among the sequences compared. CBS domain is demarcated in the green line. The segments involved in the catalysis are in black boxes which include catalytic cysteine loop, phosphate binding loop, finger loop, and the C-terminal loop. Residues that constitute mobile flap are underlined in blue.*

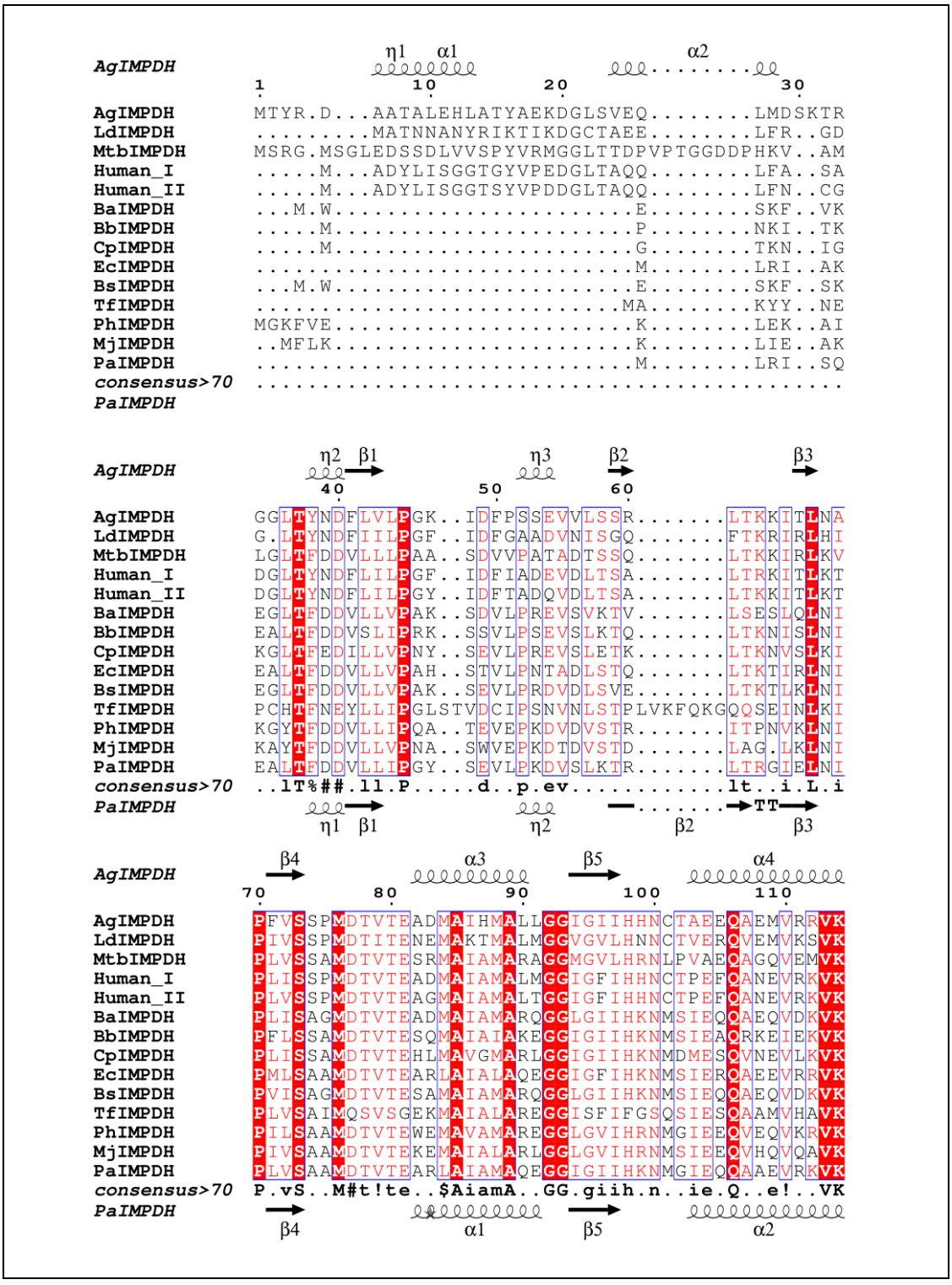
AgIMPDH
η1 α1 α2
1 10 20 30
AgIMPDH MTYR.D...AATALEHLATYAEKDGLSVEQ.....LMDSKTR
LdIMPDH .....MATNNANYRIKTIKDGCTAEE.....LFR..GD
MtbIMPDH MSRG.MSGLEDSSDLVVSPYVRMGGLTTDPVPTGGDDPHKV..AM
Human_I .....M...ADYLISGGTGYVPEDGLTAQQ.....LFA..SA
Human_II .....M...ADYLISGGTSYVPDDGLTAQQ.....LFN..CG
BaIMPDH ...M.W.....E.....SKF..VK
BbIMPDH .....M.....P.....NKI..TK
CpIMPDH .....M.....G.....TKN..IG
EcIMPDH .....M.....LRI..AK
BsIMPDH ...M.W.....E.....SKF..SK
TfIMPDH .....MA.....KYY..NE
PhIMPDH MGKFVE.....K.....LEK..AI
MjIMPDH ..MFLK.....K.....LIE..AK
PaIMPDH .....M.....LRI..SQ
consensus>70 .....
PaIMPDH
AgIMPDH
η2 β1 η3 β2 β3
40 50 60
AgIMPDH GGLTYNDFLVLPGK..IDFPSSEVVLSSR.....LTKKITLNA
LdIMPDH G.LTYNDFIILPGF..IDFGAADVNISGQ.....FTKRIRLHI
MtbIMPDH LGLTFDDVLLLPAA..SDVVPATADTSSQ.....LTKKIRLKV
Human_I DGLTYNDFLILPGF..IDFIADEVDLTSA.....LTRKITLKT
Human_II DGLTYNDFLILPGY..IDFTADQVDLTSA.....LTKKITLKT
BaIMPDH EGLTFDDVLLVPAK..SDVLPREVSVKTV.....LSESLQLNI
BbIMPDH EALTFDDVSLIPRK..SSVLPSEVSLKTQ.....LTKNISLNI
CpIMPDH KGLTFEDILLVPNY..SEVLPREVSLETK.....LTKNVSLKI
EcIMPDH EALTFDDVLLVPAH..STVLPNTADLSTQ.....LTKTIRLNI
BsIMPDH EGLTFDDVLLVPAK..SEVLPRDVDLSVE.....LTKTLKLNI
TfIMPDH PCHTFNEYLLIPGLSTVDCIPSNVNLSTPLVKFQKGQQSEINLKI
PhIMPDH KGYTFDDVLLIPQA..TEVEPKDVDVSTR.....ITPNVKLNI
MjIMPDH KAYTFDDVLLVPNA..SWVEPKDTDVSTD.....LAG.LKLNI
PaIMPDH EALTFDDVLLIPGY..SEVLPKDVSLKTR.....LTRGIELNI
consensus>70 ..lT%##.ll.P.....d..p.ev.....lt..i.L.i
PaIMPDH
η1 β1 η2 β2 β3
AgIMPDH
β4 α3 β5 α4
70 80 90 100 110
AgIMPDH PFVSSPMDTVTEADMAIHMALLGGIGIIHHNCTAEEQAEMVRRVK
LdIMPDH PIVSSPMDTITENEMAKTMALMGGVGVLHNNCTVERQVEMVKSVK
MtbIMPDH PLVSSAMDTVTESRMAIAMARAGGMGVLHRNLPVAEQAGQVEMVK
Human_I PLISSPMDTVTEADMAIAMALMGGIGFIHHNCTPEFQANEVRKVK
Human_II PLVSSPMDTVTEAGMAIAMALTGGIGFIHHNCTPEFQANEVRKVK
BaIMPDH PLISAGMDTVTEADMAIAMARQGGLGIIHKNMSIEQQAEQVDKVK
BbIMPDH PFLSSAMDTVTESQMAIAIAKEGGIGIIHKNMSIEAQRKEIEKVK
CpIMPDH PLISSAMDTVTEHLMAVGMARLGGIGIIHKNMDMESQVNEVLKVK
EcIMPDH PMLSAAMDTVTEARLAIALAQEGGIGFIHKNMSIERQAEEVRRVK
BsIMPDH PVISAGMDTVTESAMAIAMARQGGLGIIHKNMSIEQQAEQVDKVK
TfIMPDH PLVSAIMQSVSGEKMAIALAREGGISFIFGSQSIESQAAMVHAVK
PhIMPDH PILSAAMDTVTEWEMAVAMAREGGLGVIHRNMGIEEQVEQVKRVK
MjIMPDH PIVSAAMDTVTEKEMAIALARLGGLGVIHRNMSIEEQVHQVQAVK
PaIMPDH PLVSAAMDTVTEARLAIAMAQEGGIGIIHKNMGIEQQAAEVRKVK
consensus>70 P.vS..M#t!te..$AiamA..GG.giih.n..ie.Q..e!..VK
PaIMPDH
β4 α1 β5 α2

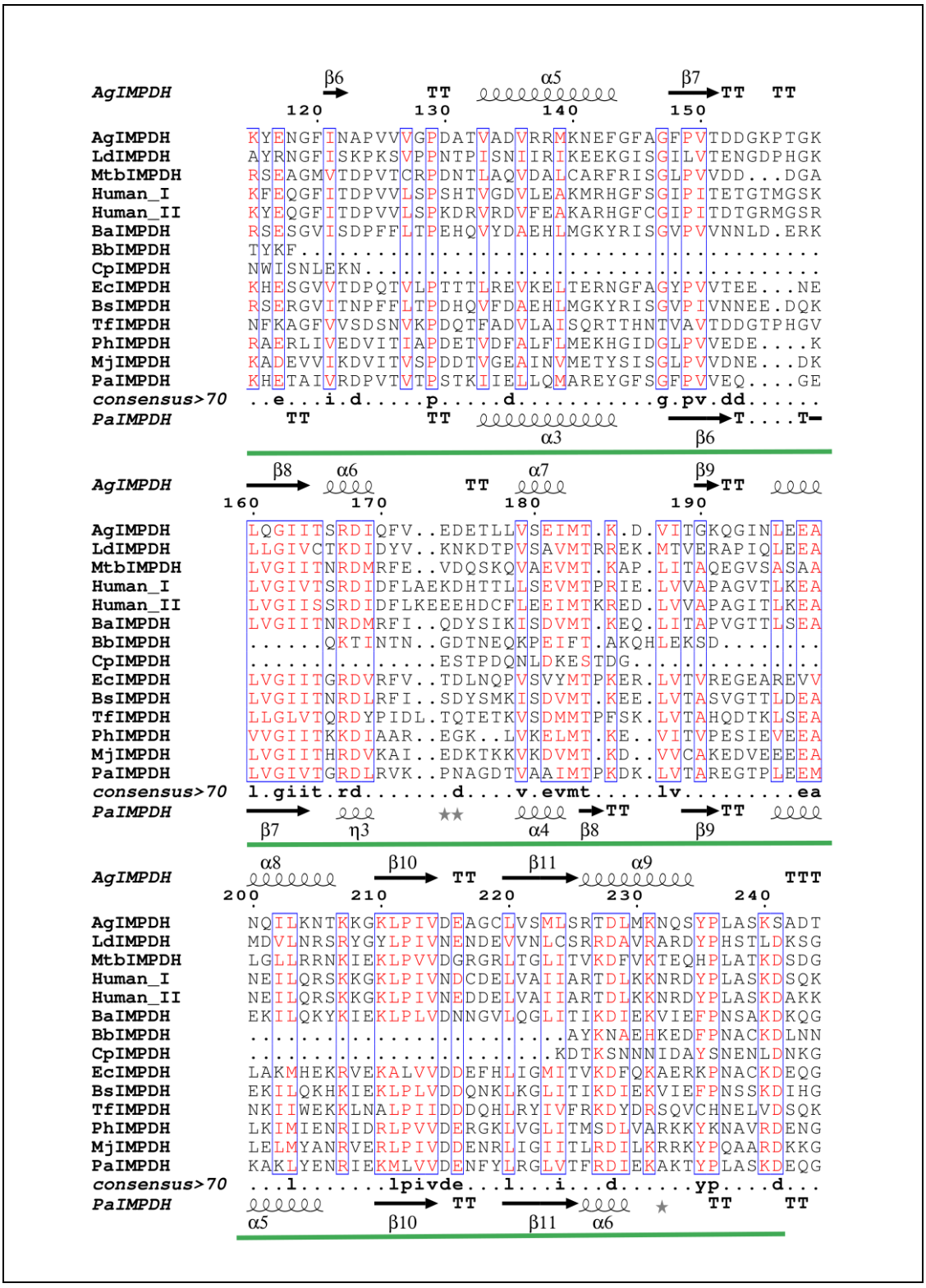
AgIMPDH
β6 TT α5 β7 TT TT
120 130 140 150
AgIMPDH KYENGFINAPVVVGPDATVADVRRMKNEFGFAGFPVTDDGKPTGK
LdIMPDH AYRNGFISKPKSVPPNTPISNIIRIKEEKGISGILVTENGDPHGK
MtbIMPDH RSEAGMVTDPVTCRPDNTLAQVDALCARFRISGLPVVDD...DGA
Human_I KFEQGFITDPVVLSPSHTVGDVLEAKMRHGFSGIPITETGTMGSK
Human_II KYEQGFITDPVVLSPKDRVRDVFEAKARHGFCGIPITDTGRMGSR
BaIMPDH RSESGVISDPFFLTPEHQVYDAEHLMGKYRISGVPVVNNLD.ERK
BbIMPDH TYKF..........
CpIMPDH NWISNLEKN..........
EcIMPDH KHESGVVTDPQTVLPTTTLREVKELTERNGFAGYPVVTEE...NE
BsIMPDH RSERGVITNPFFLTPDHQVFDAEHLMGKYRISGVPIVNNEE.DQK
TfIMPDH NFKAGFVVSDSNVKPDQTFADVLAISQRTTHNTVAVTDDGTPHGV
PhIMPDH RAERLIVEDVITIAPDETVDFALFLMEKHGIDGLPVVEDE....K
MjIMPDH KADEVVIKDVITVSPDDTVGEAINVMETYSISGLPVVDNE...DK
PaIMPDH KHETAIVRDPVTVTPSTKIIELLQMAREYGFSGFPVVEQ....GE
consensus>70 ..e...i.d.....p.....d...........g.pv.dd......
PaIMPDH TT TT α3 T....T
β6
β8 α6 α7 β9 TT
160 170 180 190
AgIMPDH LQGIITSRDIQFV..EDETLLVSEIMT.K.D.VITGKQGINLEEA
LdIMPDH LLGIVCTKDIDYV..KNKDTPVSAVMTRREK.MTVERAPIQLEEA
MtbIMPDH LVGIITNRDMRFE..VDQSKQVAEVMT.KAP.LITAQEGVSASAA
Human_I LVGIVTSRDIDFLAEKDHTTLLSEVMTPRIE.LVVAPAGVTLKEA
Human_II LVGIISSRDIDFLKEEEHDCFLEEIMTKRED.LVVAPAGITLKEA
BaIMPDH LVGIITNRDMRFI..QDYSIKISDVMT.KEQ.LITAPVGTTLSEA
BbIMPDH ......QKTINTN..GDTNEQKPEIFT.AKQHLEKSD.......
CpIMPDH ..........ESTPDQNLDKESTDG.....
EcIMPDH LVGIITGRDVRFV..TDLNQPVSVYMTPKER.LVTVREGEAREVV
BsIMPDH LVGIITNRDLRFI..SDYSMKISDVMT.KEE.LVTASVGTTLDEA
TfIMPDH LLGLVTQRDYPIDL.TQTETKVSDMMTPFSK.LVTAHQDTKLSEA
PhIMPDH VVGIITKKDIAAR..EGK..LVKELMT.KE..VITVPESIEVEEA
MjIMPDH LVGIITHRDVKAI..EDKTKKVKDVMT.KD..VVCAKEDVEEEEA
PaIMPDH LVGIVTGRDLRVK..PNAGDTVAAIMTPKDK.LVTAREGTPLEEM
consensus>70 l.giit.rd.....d....v.evmt.....lv.....ea
PaIMPDH TT TT
β7 η3 α4 β8 β9
α8 β10 TT β11 α9 TTT
200 210 220 230 240
AgIMPDH NQILKNTKKGKLPIVDEAGCLVSMLSRTDLMKNQSYPLASKSADT
LdIMPDH MDVLNRSRYGYLPIVNENDEVVNLCSRRDAVRARDYPHSTLDKSG
MtbIMPDH LGLLRRNKIEKLPVVDGRGRLTGLITVKDFVKTEQHPLATKDSDG
Human_I NEILQRSKKGKLPIVNDCDELVAIIARTDLKKNRDYPLASKDSQK
Human_II NEILQRSKKGKLPIVNEDDELVAIIARTDLKKNRDYPLASKDAKK
BaIMPDH EKILQKYKIEKLPLVDNNGVLQGLITIKDIEKVIEFPNSAKDKQG
BbIMPDH ..........AYKNAEHKEDFPNACKDLNN
CpIMPDH ..........KDTKSNNNIDAYSNENLDNKG
EcIMPDH LAKMHEKRVEKALVVDDEFHLIGMITVKDFQKAERKPNACKDEQG
BsIMPDH EKILQKHKIEKLPLVDDQNKLKGLITIKDIEKVIEFPNSSKDIHG
TfIMPDH NKIIWEKKLNALPIIDDDQHLRYIVFRKDYDRSQVCHNELVDSQK
PhIMPDH LKIMIENRIDRLPVVDERGKLVGLITMSDLVARKKYKNAVRDENG
MjIMPDH LELMYANRVERLPIVDDENRLIGIITLRDILKRRKYPQAARDKKG
PaIMPDH KAKLYENRIEKMLVVDENFYLRGLVTFRDIEKAKTYPLASKDEQG
consensus>70 ...l.....lpivde...l...i...d.....yp....d...
PaIMPDH TT TT TT
α5 β10 β11 α6

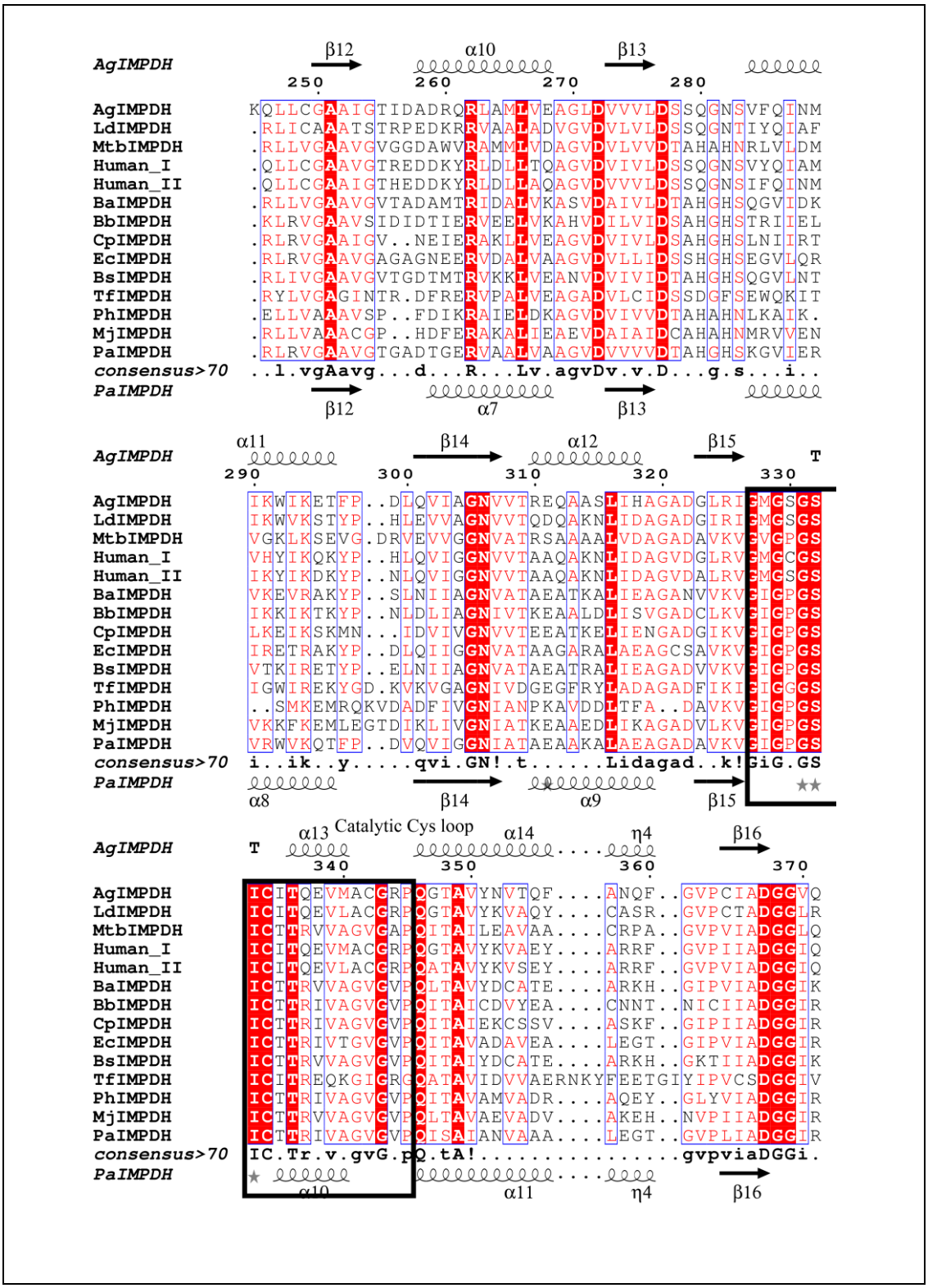
AgIMPDH
β12 α10 β13
250 260 270 280
AgIMPDH KQLLCGAAIGTIDADRQRLAMLVEAGLDVVVLDSSQGNSVFQINM
LdIMPDH .RLICAAATSTRPEDKRRVAALADVGVDVLVLDSSQGNTIYQIAF
MtbIMPDH .RLLVGAAVGVGGDAWVRAMMLVDAGVDVLVVDTAHAHNRLVLDM
Human_I .QLLCGAAVGTREDDKYRLDLLTQAGVDVIVLDSSQGNSVYQIAM
Human_II .QLLCGAAIGTHEDDKYRLDLLAQAGVDVVVLDSSQGNSIFQINM
BaIMPDH .RLLVGAAVGVTADAMTRIDALVKASVDAIVLDTAHGHSQGVIDK
BbIMPDH .KLRVGAAVSIDIDTIERVEELVKAHVDILVIDSAHGHSTRIIEL
CpIMPDH .RLRVGAAIGV..NEIERAKLLVEAGVDVIVLDSAHGHSLNIIRT
EcIMPDH .RLRVGAAVGAGAGNEERVDALVAAGVDVLLIDSSHGHSEGVLQR
BsIMPDH .RLIVGAAVGVTGDTMTRVKKLVEANVDVIVIDTAHGHSQGVLNT
TfIMPDH .RYLVGAGINTR.DFRERVPALVEAGADVLCIDSSDGFSEWQKIT
PhIMPDH .ELLVAAAVSP..FDIKRAIELDKAGVDVIVVDTAHAHNLKAIK.
MjIMPDH .RLLVAAACGP..HDFERAKALIEAEVDAIAIDCAHAHNMRVVEN
PaIMPDH .RLRVGAAVGTGADTGERVAALVAAGVDVVVVDTAHGHSKGVIER
consensus>70 ..l.vgAavg...d...R...Lv.agvDv.v.D...g.s...i..
PaIMPDH
β12 α7 β13
α11 β14 α12 β15 T
290 300 310 320 330
AgIMPDH IKWIKETFP..DLQVIAGNVVTREQAASLIHAGADGLRIGMGSGS
LdIMPDH IKWVKSTYP..HLEVVAGNVVTQDQAKNLIDAGADGIRIGMGSGS
MtbIMPDH VGKLKSEVG.DRVEVVGGNVATRSAAAALVDAGADAVKVGVGPGS
Human_I VHYIKQKYP..HLQVIGGNVVTAAQAKNLIDAGVDGLRVGMGCGS
Human_II IKYIKDKYP..NLQVIGGNVVTAAQAKNLIDAGVDALRVGMGSGS
BaIMPDH VKEVRAKYP..SLNIIAGNVATAEATKALIEAGANVVKVGIGPGS
BbIMPDH IKKIKTKYP..NLDLIAGNIVTKEAALDLISVGADCLKVGIGPGS
CpIMPDH LKEIKSKMN...IDVIVGNVVTEEATKELIENGADGIKVGIGPGS
EcIMPDH IRETRAKYP..DLQIIGGNVATAAGARALAEAGCSAVKVGIGPGS
BsIMPDH VTKIRETYP..ELNIIAGNVATAEATRALIEAGADVVKVGIGPGS
TfIMPDH IGWIREKYGD.KVKVGAGNIVDGEGFRYLADAGADFIKIGIGGGS
PhIMPDH ..SMKEMRQKVDADFIVGNIANPKAVDDLTFA..DAVKVGIGPGS
MjIMPDH VKKFKEMLEGTDIKLIVGNIATKEAAEDLIKAGADVLKVGIGPGS
PaIMPDH VRWVKQTFP..DVQVIGGNIATAEAAKALAEAGADAVKVGIGPGS
consensus>70 i..ik..y.....qvi.GN!.t.....Lidagad..k!GiG.GS
PaIMPDH
α8 β14 α9 β15
α13 Catalytic Cys loop α14 η4 β16
AgIMPDH T
340 350 360 370
AgIMPDH ICITQEVMACGRPQGTAVYNVTQF....ANQF..GVPCIADGGVQ
LdIMPDH ICITQEVLACGRPQGTAVYKVAQY....CASR..GVPCTADGGLR
MtbIMPDH ICTTRVVAGVGAPQITAILEAVAA....CRPA..GVPVIADGGLQ
Human_I ICITQEVMACGRPQGTAVYKVAEY....ARRF..GVPIIADGGIQ
Human_II ICITQEVLACGRPQATAVYKVSEY....ARRF..GVPVIADGGIQ
BaIMPDH ICTTRVVAGVGVPQLTAVYDCATE....ARKH..GIPVIADGGIK
BbIMPDH ICTTRIVAGVGVPQITAICDVYEA....CNNT..NICIIADGGIR
CpIMPDH ICTTRIVAGVGVPQITAIEKCSSV....ASKF..GIPIIADGGIR
EcIMPDH ICTTRIVTGVGVPQITAVADAVEA....LEGT..GIPVIADGGIR
BsIMPDH ICTTRVVAGVGVPQITAIYDCATE....ARKH..GKTIIADGGIK
TfIMPDH ICITREQKGIGRGQATAVIDVVAERNKYFEETGIYIPVCSDGGIV
PhIMPDH ICTTRIVAGVGVPQITAVAMVADR....AQEY..GLYVIADGGIR
MjIMPDH ICTTRVVAGVGVPQLTAVAEVADV....AKEH..NVPIIADGGIR
PaIMPDH ICTTRIVAGVGVPQISAIANVAAA....LEGT..GVPLIADGGIR
consensus>70 IC.Tr.v.gvG.pQ.tA!.....gvpviaDGGi.
PaIMPDH
α10 α11 η4 β16

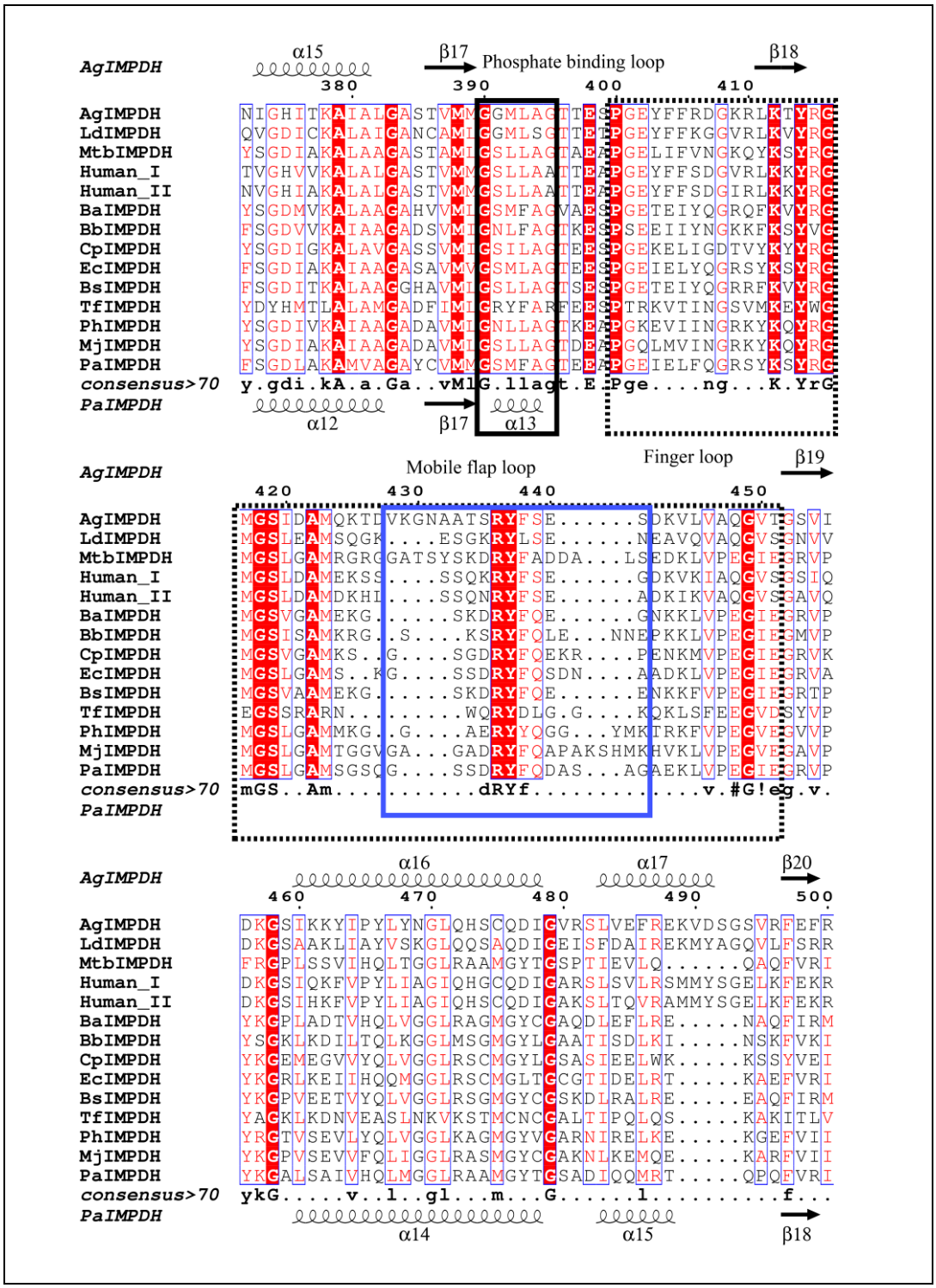
α15
β17
Phosphate binding loop
β18
380
390
400
410
AgIMPDH
LdIMPDH
MtbIMPDH
Human_I
Human_II
BaIMPDH
BbIMPDH
CpIMPDH
EcIMPDH
BsIMPDH
TfIMPDH
PhIMPDH
MjIMPDH
PaIMPDH
consensus>70
PaIMPDH
α12
β17
α13
AgIMPDH
Mobile flap loop
Finger loop
β19
420
430
440
450
AgIMPDH
LdIMPDH
MtbIMPDH
Human_I
Human_II
BaIMPDH
BbIMPDH
CpIMPDH
EcIMPDH
BsIMPDH
TfIMPDH
PhIMPDH
MjIMPDH
PaIMPDH
consensus>70
PaIMPDH
AgIMPDH
α16
α17
β20
460
470
480
490
500
AgIMPDH
LdIMPDH
MtbIMPDH
Human_I
Human_II
BaIMPDH
BbIMPDH
CpIMPDH
EcIMPDH
BsIMPDH
TfIMPDH
PhIMPDH
MjIMPDH
PaIMPDH
consensus>70
PaIMPDH
α14
α15
β18

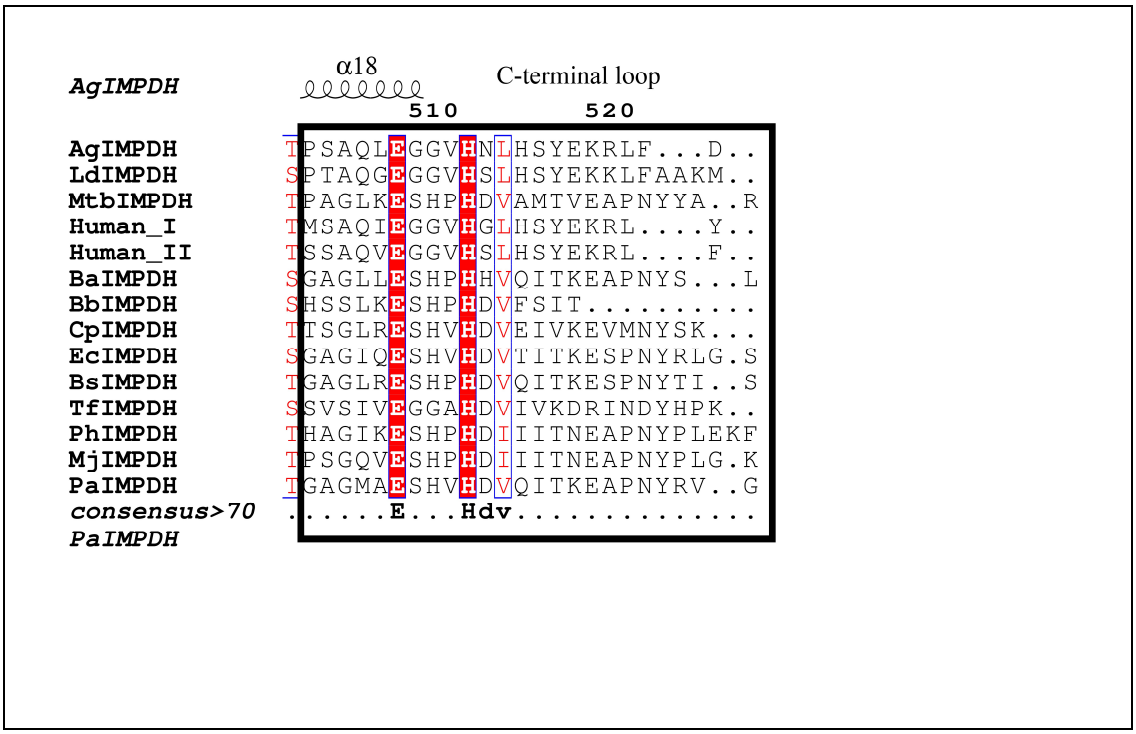

Figure 3. Multiple sequence alignment of IMP dehydrogenases from various sources. *The sequences of IMPDHs from various sources that include Ag-Ashbya gossypium, Ld-Leishmania donovani, Mtb-Mycobacterium tuberculosis, Human IMPDH isoforms (I and II), Ba-Bacillus anthracis, Bb-Borrelia burgdorferi, Cp-Cryptosporidium parvum, Ec-Escherichia coli, Bs-Bacillus subtilis, Tf-Tritrichomonas foetus, Ph-Pyrococcus horikoshii, Mj-Methanocaldococcus jannaschii, and Pa-Pseudomonas aeruginosa were aligned with Clustal Omega (Sievers F et al., 2011; Sievers F and Higgins DG, 2018) and rendered using ESPRIPT (Robert X and Gouet P, 2014). The consensus of >70 was found across sequences analyzed. The secondary structure of IMPDH from a eukaryote, A. gossypium (PDB 5TC3) and a prokaryote, P. aeruginosa (PDB 4DQW) are shown at the top and bottom of the sequence alignment, respectively. α-helices and β-strands are rendered as large squiggles and arrows, respectively. TT and TTT correspond to beta and alpha turns, respectively. The red shaded regions indicate identical residues while residues printed in red, highlight similarity among the sequences compared. CBS domain is underlined by a green line. The segments involved in the catalysis are indicated in black boxes which include the catalytic cysteine loop, phosphate binding loop, finger loop, and the C-terminal loop. Residues that constitute mobile flap are highlighted in a blue box.*

5.3.2 Cloning, expression, and purification of MjIMPDH and MjIMPDH$^{\Delta CBS}$

The gene coding for MjIMPDH was cloned into pET 21b+ expression vector between *NdeI* and *XhoI* restriction sites resulting in a C-terminal $(His)_6$-tag. Overlap PCR to amplify the core catalytic domain introduced a linker sequence "GSGG" joining the two parts of the TIM $(\beta/\alpha)_8$ barrel (Fig. 4). DNA sequencing of both the constructs confirmed the clones error-free and the full-length sequence was identical to the entry in NCBI gene database.

Rosetta(DE3)pLysS strain of *E. coli* was used as expression host in the initial protein expression experiments and the protein was found to be highly soluble, unlike PfIMPDH, despite the high sequence similarity and completely conserved catalytic core segments (Fig. 2). Attempt to purify protein on Ni-NTA affinity chromatography, however, lead to very poor yields with most of the soluble protein in the unbound fraction. Proteins belonging to the IMPDH/GMPR family are reported to exist as tetramers or octamers along with the presence of higher order multimers (Hedstrom L, 2009) (described in Chapter 1). The large size of protein could plausibly be burying hexa-histidine tag that makes it inaccessible for binding to the Ni-NTA affinity matrix. However, purification procedures including anion exchange chromatography and size-exclusion chromatography yielded pure homogenous preparation of protein as judged by Coomassie-stained SDS-PAGE. Enzymatic activity, however, showed enormous variation across different batches of purified protein possibly due to co-purification of *E. coli* IMPDH. Construction of deletion strain of BL21(DE3) lacking IMPDH, Δ*guaB*^{K}(DE3) (discussed in Chapter 2) helped immensely in the reproducibility of purity and thereby activity. Further, MjIMPDH$^{\Delta CBS}$ was not subjected to Ni-NTA chromatography but similar purification procedures that were found efficient in the purification of the full-length enzyme were employed.

Due to the presence of rare codons in *M. jannaschii* IMPDH gene, deletion strain was always co-transformed with pLysS plasmid from Rosetta(DE3) coding for tRNA synthetases for rare codons. Induction with 0.05 mM IPTG at 16 °C for 12 h resulted in hyperexpression of both MjIMPDH and MjIMPDH$^{\Delta CBS}$ proteins with most of it in the soluble fraction (Fig. 4). MjIMPDH applied to anion exchange on Q-sepharose matrix was consistently found to elute between a gradient of 250 mM to 350 mM KCl (Fig. 4). However, on the preparative

grade size-exclusion chromatography, about 50 % -70 % of the total protein across various batches was found to be in a higher order oligomeric state with the elution volume corresponding to void volume of the Superdex S200 column (Fig. 4). The purity of the protein after anion exchange chromatography followed by size-exclusion chromatography was found to be 95-98 % as judged by Coomassie-stained SDS-PAGE (Laemmli UK, 1970) (Fig. 4). The yield of MjIMPDH protein was about 35-40 mg L^{-1} of culture (~28 mg of aggregate and ~12 mg of octameric species). A similar methodology was employed in obtaining $MjIMPDH^{\Delta CBS}$ protein with a yield of 40-50 mg L^{-1}. However, higher order oligomers were not observed upon CBS deletion on the preparative grade size-exclusion chromatography.

Interestingly, the recombinant *M. jannaschii* proteins, in the absence or presence β-mercaptoethanol and without prior heating, were found to migrate at molecular weights corresponding to higher order oligomers when resolved on SDS-PAGE (Fig. 4). However, they were found to migrate at their respective expected monomer mass (54 kDa and 43 kDa, respectively) upon heat treatment (Fig. 4). This could probably indicate the existence of multimers *in vivo*. In support of the oligomeric association *in vivo,* indirect evidence through mass spectrometry of cross-linked cell lysates in *P. aeruginosa* (Navare AT *et al*., 2015) was observed. Wherein bridging of K157 from one monomer to other (K'157) with the linker length of 35 Å indicative of an octamer was found which otherwise would have been 100 Å in case of a tetramer. Also, octameric species of *A. gossypium* IMPDH have been identified through cross-linked HA-tagged protein constructs, resolved on SDS-PAGE and confirmed by Western blot (Buey RM *et al*., 2015). The identity of the recombinant *M. jannaschii* proteins was confirmed by Western blot using anti-$(His)_6$ antibodies (Sigma-Aldrich, USA) (Fig. 4). Far-UV CD spectra of MjIMPDH and $MjIMPDH^{\Delta CBS}$ were found to be similar and indicated ordered secondary structure (Fig. 5). Emission maximum of intrinsic Tryptophan fluorescence across the two proteins was also found to be similar (Fig. 5). The far-UV CD and intrinsic fluorescence measurements indicate that removal of CBS domain does not perturb the $(\beta/\alpha)_8$ barrel of core catalytic domain (Fig. 5).

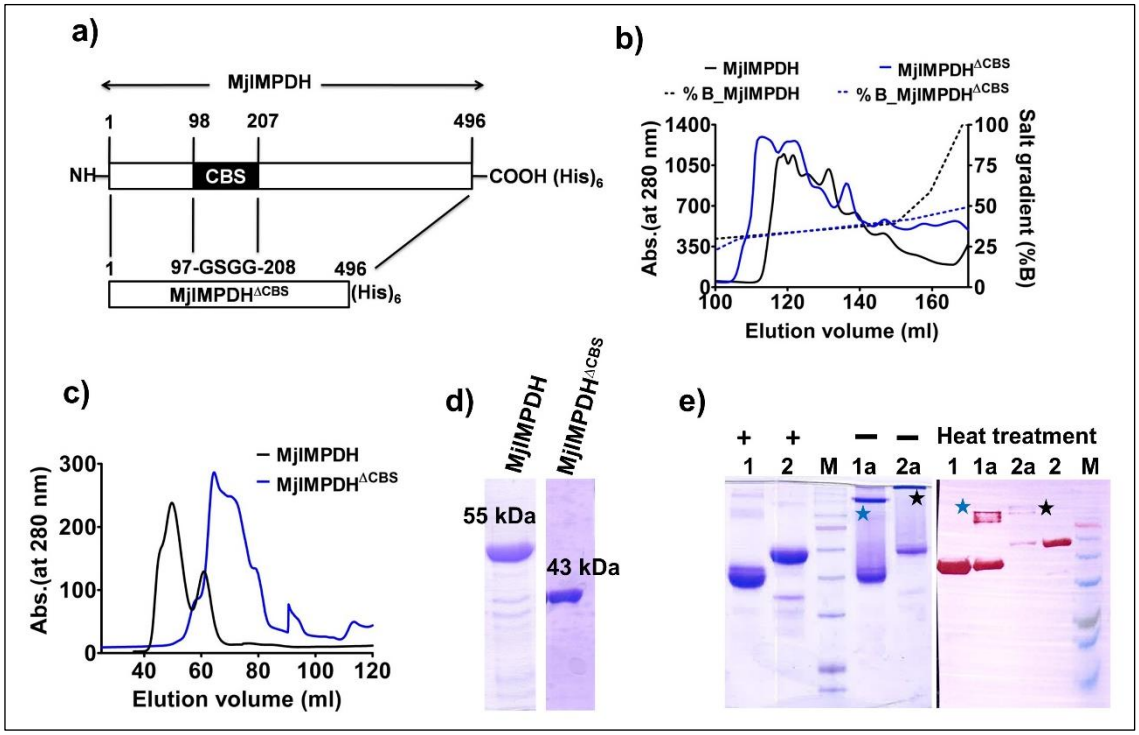

Figure 4. Expression and purification of MjIMPDH and MjIMPDH$^{\Delta CBS}$. a) Schematic representation of MjIMPDH protein constructs. *Constructs examined in this thesis are full length (1-496 residues) and core catalytic domain (1-97-GSGG-208-496 residues). Both the proteins carry a C-terminal (His)$_6$ -tag.* ***b) Anion-exchange chromatogram on Q-sepharose HP (GE healthcare, USA).*** *The cell lysate was subjected to thermal precipitation followed by PEI treatment for nucleic acid removal. Thereafter, anion-exchange chromatography was performed and bound proteins were eluted using a gradient of the lysis buffer containing 1 M KCl. The salt gradient is represented on the right y-axis while elution volume and UV absorbance (280 nm) on the x-axis and the left y-axis, respectively.* ***c) Elution profile on preparative grade size-exclusion chromatography. d) Purified fractions of MjIMPDH (55 kDa) and MjIMPDH$^{\Delta CBS}$ (43 kDa) examined by SDS-PAGE. e) The SDS-PAGE analysis of the purified protein with and without boiling****. 140 mM β-me was used as the reducing agent and protein samples were resolved on 12 % SDS-PAGE with and without boiling. Left panel represents Coomassie stained SDS-PAGE while the right panel indicates the identity of the proteins confirmed by Western blot using anti-(His)$_6$ antibodies. Lane 1, 1a- MjIMPDH$^{\Delta CBS}$ with and without boiling, respectively; lane 2, 2a MjIMPDH with and without boiling, respectively. M is the pre-stained protein molecular weight marker (Abcam, USA). MjIMPDH and MjIMPDH$^{\Delta CBS}$ resolved to respective monomer mass of 55 kDa and 43 kDa, respectively upon heat treatment. A fraction of the full length and CBS deletion proteins found to exist as higher-order oligomers when not subjected to heat are indicated in black and blue asterisks, respectively.*

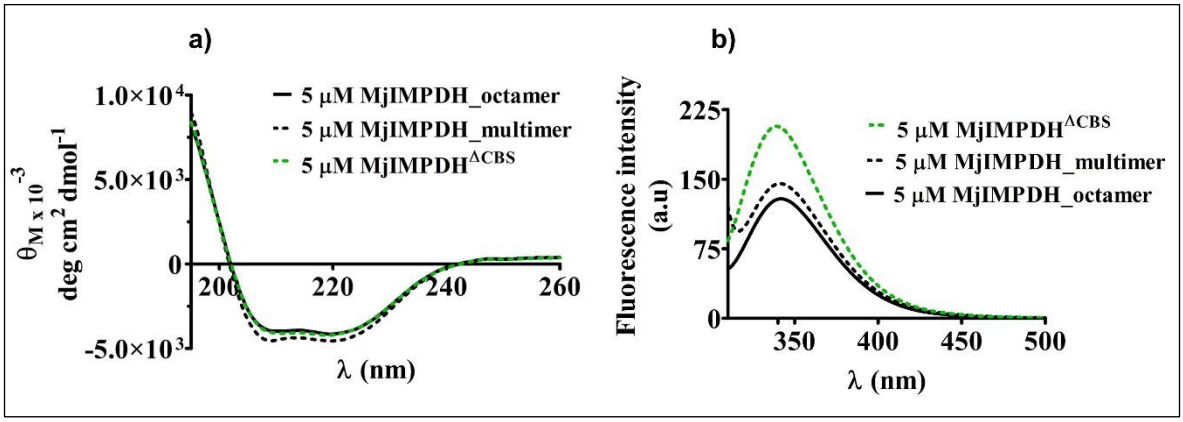

Figure 5. a) Far-UV CD spectra and b) intrinsic tryptophan fluorescence spectra of MjIMPDH and MjIMPDH$^{\Delta CBS}$, respectively. *Solid black, dotted black and dotted green lines indicate spectra of MjIMPDH (5 µM of octameric species), MjIMPDH (5 µM of multimeric species), and 5 µM of MjIMPDH$^{\Delta CBS}$, respectively. All the spectra were acquired in 5 mM Tris HCl, pH 8.0 and were subtracted from that of the buffer blank. CD measurements were recorded from 260 nm to 195 nm using the cuvettes of 0.1 cm path length. Molar ellipticity (θ_M) is on the y-axis with corresponding wavelength (λ) on the x-axis.* ***b) Intrinsic tryptophan fluorescence.*** *Excitation was at 295 nm and fluorescence emission spectra were recorded from 298 nm to 500 nm with a scan speed of 1500 nm min^{-1}. The excitation and emission slit widths were kept at 5 nm. Fluorescence intensity in the arbitrary units (a.u.) is on the y-axis and the corresponding wavelength (λ) on the x-axis.*

5.3.3 The quaternary structure of MjIMPDH/MjIMPDH$^{\Delta CBS}$

Elution of full-length MjIMPDH was found to be spread out with two distinct peaks on a preparative grade size-exclusion chromatography commencing almost at the void volume of the column while removal of CBS domain resulted in a single but broad peak (Fig. 4). The subunit assembly of both the recombinant proteins was examined by analytical size-exclusion chromatography on a pre-calibrated Superdex 300 column. The calculated molecular mass of MjIMPDH and MjIMPDH$^{\Delta CBS}$ is 54382 Da and 42194 Da, respectively. Individual fractions of MjIMPDH obtained from preparative grade size-exclusion column when examined on analytical size-exclusion column yielded protein species with molecular weights of 1400 kDa, 1081 kDa, and 430 kDa as determined from molecular weight protein standards (Fig. 6). This confirms the presence of various higher order assemblies of MjIMPDH with the least molecular weight corresponding to an octameric species. Presence of higher order oligomers has been considered as aggregates and ignored until recent reports on *Pseudomonas aeruginosa* IMPDH (Labesse G *et al*., 2013) which reanalyzed and identified such association in all the IMPDHs characterized to date. They have also observed

the formation of fibers upon association of two complementary octamers (concave and convex, described in Chapter 1) found in Human IMPDH1. However, the elution volume of MjIMPDH$^{\Delta CBS}$ confirmed the presence of only one species that corresponded to a tetramer (Fig. 6). The elution profile for all examined fractions remains unchanged under all tested conditions (presence of 1 M KCl or 50 µM of NAD^+ or 50 µM IMP).

Through solution studies (analytical size-exclusion chromatography; analytical ultracentrifugation, AUC; small angle X-ray studies, SAXS; electron microscopy, EM, and Cryo-EM) *P. aeruginosa* IMPDH was found to be octamer in solution and activated by MgATP while CBS deletion yielded a tetramer insensitive to MgATP (Labesse G *et al*., 2013). *A. gossypium* IMPDH apo- and GMP bound forms were shown to be tetramer in solution and the presence of GDP and GTP induced dimerization of tetramers. Removal of CBS domain from AgIMPDH, however, yielded only tetramers in any tested condition (Buey RM *et al*., 2015). Another study has categorized bacterial IMPDHs into class I which are cooperative enzymes for IMP, activated by MgATP, and octameric while, class II enzymes follow Michaelis-Menten kinetics for both substrates and are tetramers in their apo- state or in the presence of IMP, and get shifted to octamers in the presence of NAD^+ or MgATP (Alexandre T *et al.*, 2015). The octameric association observed in three-dimensional structures include *V. cholera* IMPDH$^{\Delta CBS}$ (PDB 4QNE), *P. aeruginosa* IMPDH (PDB 4DQW), PaIMPDH$^{\Delta CBS}$ (PDB 5AHL and 5AHM), and *A. gossypium* (PDB 4Z87, 5MCP and 5TC3). The significance of such assemblies in the cellular context is not understood yet and may play a role in metabolic regulation through protein associations or perform moonlighting functions which are yet to be discovered.

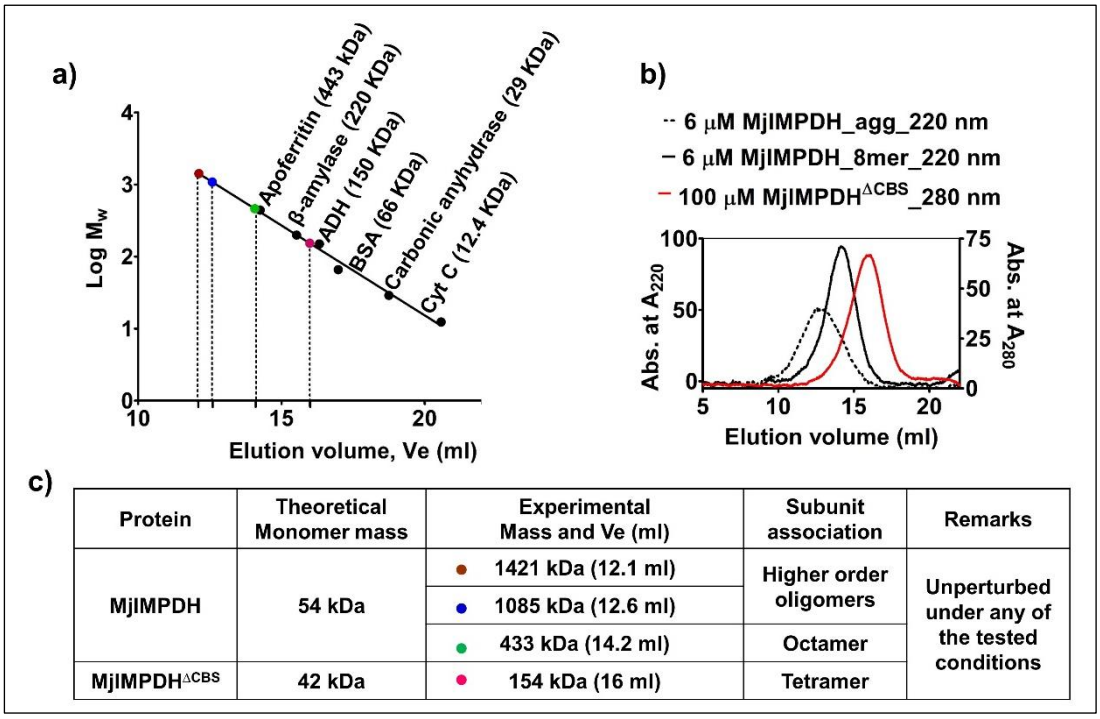

Protein	Theoretical Monomer mass	Experimental Mass and Ve (ml)	Subunit association	Remarks
MjIMPDH	54 kDa	1421 kDa (12.1 ml)	Higher order oligomers	Unperturbed under any of the tested conditions
		1085 kDa (12.6 ml)		
		433 kDa (14.2 ml)	Octamer	
MjIMPDH$^{\Delta CBS}$	42 kDa	154 kDa (16 ml)	Tetramer	

Figure 6. Subunit association of MjIMPDH and MjIMPDH$^{\Delta CBS}$. a) The standard plot of elution volume, Ve on the x-axis versus log molecular weight on the y-axis. *Standards used were apoferritin (443 kDa), β-amylase (200 kDa), alcohol dehydrogenase (150 kDa), bovine serum albumin (66 kDa), carbonic anhydrase (29 kDa) and cytochrome oxidase (12.4 kDa) and are represented in black spheres. Brown and blue spheres correspond to higher order oligomers (fractions correspond to elution volumes of 43 ml and 50 ml, respectively collected from preparative grade size-exclusion chromatography column, refer to Fig. 4c) of MjIMPDH (1421 kDa and 1085 kDa) while green and pink spheres represent the octameric form (fraction corresponds to elution volume of 60 ml on preparative grade size-exclusion chromatography column, refer to Fig. 4c) of MjIMPDH (433 kDa) and tetrameric form of MjIMPDH$^{\Delta CBS}$ (154 kDa), respectively.* ***b) Analytical size-exclusion chromatography (SEC) profile on Superdex 300 column (1 cm x 30 cm).*** *6 μM of MjIMPDH fraction collected from the preparative grade size-exclusion column at elution volumes of 50 ml and 60 ml and 100 μM of MjIMPDH$^{\Delta CBS}$ were examined by analytical SEC. The dotted black line and solid black line correspond to elution profiles of a higher order multimer (1085 kDa) and octameric form (433 kDa) of MjIMPDH, respectively. MjIMPDH$^{\Delta CBS}$ exists as a tetramer in solution (154 kDa) represented in red. Buffer containing 50 mM Tris HCl, pH 7.4 and 100 mM KCl was used to equilibrate the column and elute protein samples.* ***c) Tabulation*** *of experimental, theoretical mass values and respective oligomeric forms of both the constructs. Presence of 1 M KCl or ligands (50 μM IMP or 50 μM NAD^+) did not alter the respective subunit assemblies. Also, the elution profile of each protein remains unperturbed upon any change in concentration (data not shown).*

5.3.4 Dehydrogenase activity

The NAD^+ dependent dehydrogenase activity of MjIMPDH/MjIMPDH$^{\Delta CBS}$ was monitored at 340 nm as the formation of NADH from NAD^+ with an absorption coefficient of 6.22 mM^{-1} cm^{-1}. The higher order oligomers observed for the full-length protein when tested for the activity were found to display 80-90 % activity of the octameric species. Hence, for all the activity measurements only the octameric fraction was used. Optimum pH for the enzyme assay was determined by estimating the specific activity under different pH conditions, with pH calibrated at 70 °C. Both MjIMPDH and MjIMPDH$^{\Delta CBS}$ exhibited similar catalytic properties with maximum dehydrogenase activity at pH 8.5 (Fig. 7). Majority of the IMP dehydrogenases examined till date display a pH optimum of 8.0 (Hedstrom L, 2009), with few bacterial enzymes at pH 9.0 (Alexandre T *et al.,* 2015). Steady-state saturation kinetics was performed for MjIMPDH at pH 8.0, pH 8.5 and pH 9.0. Catalytic efficiency (k_{cat}/ K_m) of the full-length enzyme was found to vary (with pH) with NAD^+ or $APAD^+$ as a substrate while no significant change was observed with IMP as the variable substrate. k_{cat}/ K_m value of 2.4 μM^{-1} min^{-1} at pH 9.0 has increased to 5.4 μM^{-1} min^{-1} at pH 8.0 with NAD^+ as the variable substrate while the efficiency increased from 0.86 μM^{-1} min^{-1} at pH 9.0 to 3 μM^{-1} min^{-1} at pH 8.0 in the presence of $APAD^+$. Therefore, all subsequent assays were performed at pH 8.0.

Intriguingly, dehydrogenase activity of *M. jannaschii* enzymes was observed even in the absence of a metal ion cofactor although all reported IMPDHs displayed activation of at least 100 fold in the presence of K^+ ions (Hedstrom L, 2009). No significant activation or inhibition of enzyme activity was observed in the presence of any tested cation (Na^+, Li^+, Rb^+, Cs^+, $Mg^{+,}$ and Ca^+) and inclusion of a monovalent cation (K^+) in the enzyme assays resulted in only a marginal increase in the dehydrogenase activity (Fig. 7). Being a thermophilic enzyme, no drop in activity was observed up to 95 °C (Fig. 7). All IMPDHs characterized till date are found to be activated ~100-fold by K^+ ions and similar monovalent cations. The specificity of K^+ ion activation varies considerably among IMPDHs from different sources. Ions with a similar size which include K^+, $NH_4^{+,}$ and Rb^+ are always found to activate, while smaller ions such as Li^+, Na^+ activate some IMPDHs, inhibit some, and

have no effect on others. Human IMPDH2 was found to be activated by K^+, NH_4^+, Na^+, Tl^+, and Rb^+ ions but Li^+ ion had no effect (Xiang B *et al*., 1996). Both *E. coli* and *B. burgdorferi* IMPDHs are known to be activated by K^+, NH_4^+, and Cs^+ ions but inhibited by Na^+ and Li^+ ions (Zhou X *et al*., 1997). Na^+ ion was reported to have no effect on *C. parvum* IMPDH (Riera TV *et al*., 2012). However, it has been shown that IMPDH from *T. foetus*, *B. subtilis,* and Sarcoma 180 cells retained only a basal level of activity in the absence of K^+ ion (Verham R *et al*., 1987; Anderson J and Sartorelli A, 1968; Wu T and Scrimgeour K, 1973). Stability of the tetramer is not affected by the monovalent cation though it was observed to prevent the formation of higher order aggregates (Zhou X *et al*., 1997; Heyde E and Morrison J, 1976; Xiang B *et al*., 1996). The Cys loop of a monomer and the C-terminal segment from an adjacent monomer form monovalent cation binding site. These residues are not conserved and therefore, predicted to account for the differences in monovalent cation specificity and other catalytic properties among enzymes from different sources (Hedstrom L, 2012)

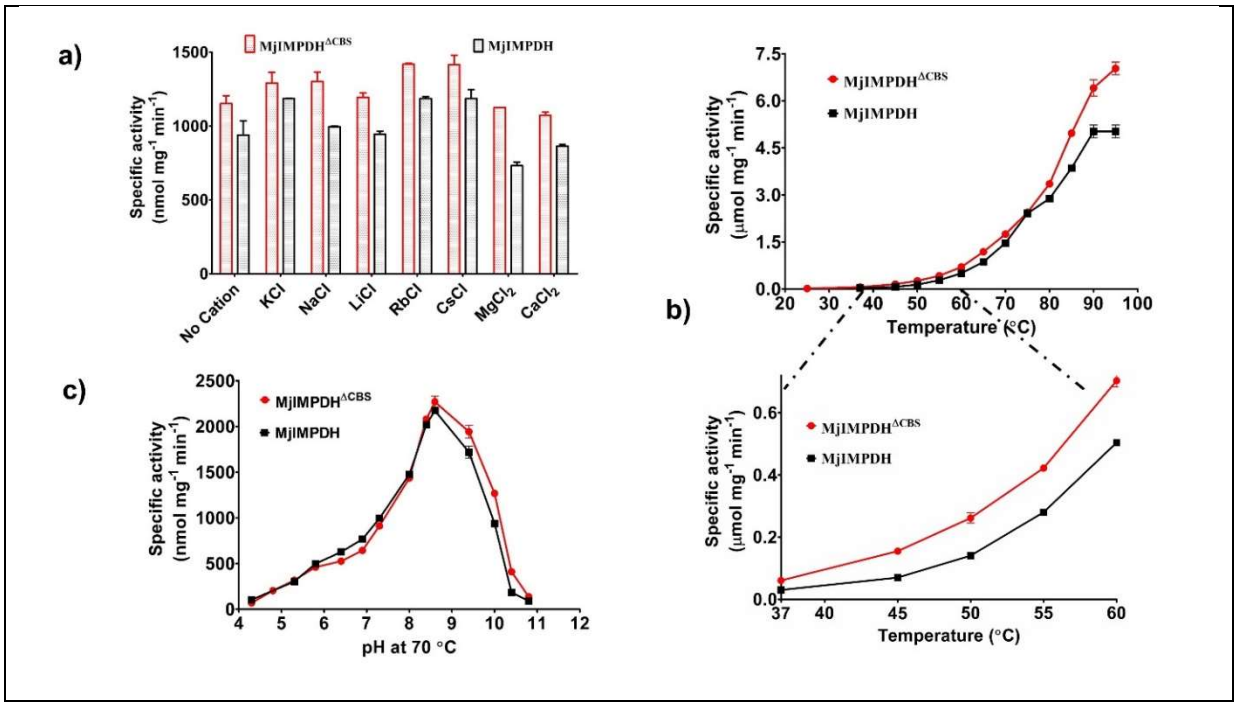

Figure 7. Metal ion requirement, temperature and pH dependence of MjIMPDH and MjIMPDH$^{\Delta CBS}$. ***a) Effect of monovalent and divalent cations (100 mM) on the enzyme activity****. No significant activation or inhibition was exhibited by any of the examined cations (Na^+, K^+, Rb^+, Cs^+, Li^+, Mg^{2+} and Ca^{2+}) under standard assay conditions.* ***b) Temperature dependence.*** *No drop in activity was observed up to 95 °C, a characteristic feature of a hyperthermophilic enzyme. A zoomed in image of the plot at lower temperatures from 37 °C to 60 °C is presented at the bottom.* ***c) pH dependence examined at 70 °C****. 50 mM mixed buffer containing MES (pH 5.5-6.7), HEPES (pH 6.8-8.2), CAPS (pH 9.7-11.1) and Glycine-NaOH (pH 8.8-10.6) with pH adjusted at 70 °C was used to assay the dehydrogenase activity. Optimum pH for maximal enzyme activity was found to be 8.5. Standard assay conditions are as mentioned in the materials and methods section. All the experiments were performed in two technical replicates containing two biological replicates each. Representative plots from one technical replicate are shown. Each data point represents the mean specific activity value. Error bars represent the standard deviation of the data (n=2).*

5.3.5 Saturation kinetics

The kinetic parameters of MjIMPDH and MjIMPDH$^{\Delta CBS}$ determined in the presence or absence of a monovalent cation (K^+ ion) from the saturation kinetics for each substrate are found to be similar and are summarized in Table 3. MjIMPDH exhibits Michaelis-Menten kinetics for IMP as a substrate which displayed the highest affinity for the enzyme as evident from the low

K_m values (4.6 ± 0.3 μM) (Fig. 8, Table 3) while NAD^+, exhibited substrate inhibition (K_m 13.5 ± 0.7 μM and K_i 1678 ± 52 μM) (Fig. 8, Table 3).

Majority of the characterized IMPDHs follow Michaelis-Menten kinetics for the substrate IMP while, NAD^+ is known to exhibit substrate inhibition. However, no substrate inhibition was observed for IMPDHs from *L. donovani*, *P. aeruginosa, L. pneumophila*, *N. meningitidis, B. thailandensis, B. anthracis, K. pneumonia, and S. aureus* (Dobie F *et al*., 2007; Labesse G *et al*, 2013; Alexandre T *et al*., 2015). Sigmoidal behavior with respect to IMP was observed in class I bacterial enzymes which include *L. pneumophila*, *N. meningitidis* and *P. aeroginosa* (Alexandre T *et al*., 2015; Labesse G *et al*, 2013). NAD^+ at high concentration traps E-XMP* intermediate causing inhibition, which further leads to the ordered release of products (NADH followed by XMP) (Hedstrom L, 2009). Acetylpyridine adenine dinucleotide ($APAD^+$) was found to be an alternate substrate of the *M. jannaschii* enzyme with less pronounced substrate inhibition and lowered affinity as compared to NAD^+ (Fig. 8, Table 3). However, catalytic efficiency remains similar across both NAD^+ and $APAD^+$ indicating that hydride transfer is not rate-limiting as reported in the literature (Hedstrom L, 1999).

Absence of K^+ ions in the assay mixture resulted in only a minor drop in activity with NAD^+ or IMP as variable substrate. All IMPDHs reported till date require a monovalent cation to exhibit optimal/maximal enzyme activity. There exists no example in the literature of an IMPDH with kinetic parameters determined in the absence of a monovalent cation. We on the other hand, could determine these parameters for MjIMPDH without K^+ ions in the assay mix. Further, addition of K^+ ions in the enzyme reaction, resulted in 1.3 to 1.5 and 1.5 to 2-fold increase in the V_{max} and K_m values, respectively for the natural substrate (Fig. 8, Table 3). Nevertheless, this is only a minor change in the overall catalytic activity of MjIMPDH unlike all other reported IMPDHs till date, that exhibit a 100-150-fold increase in enzyme activity in the presence of K^+ ions. It is reported that only ~5 % and <1 % of the maximal activity was observed in the absence of a monovalent cation for *E. coli* and Human type II IMPDHs, respectively (Pimkin M and Markham GD, 2009). In the absence of K^+ ions, the k_{cat} value for IMPDH from *T. foetus* was found to be lowered by about 100fold and 8-fold increase in K_m value for NAD^+ while the K_m values for IMP remained similar. Further, substrate inhibition by NAD^+ was not observed in the absence of K^+ ions (Gan L *et al*., 2002). A comparison of the kinetic parameters from various characterized IMPDHs is presented in Table 4.

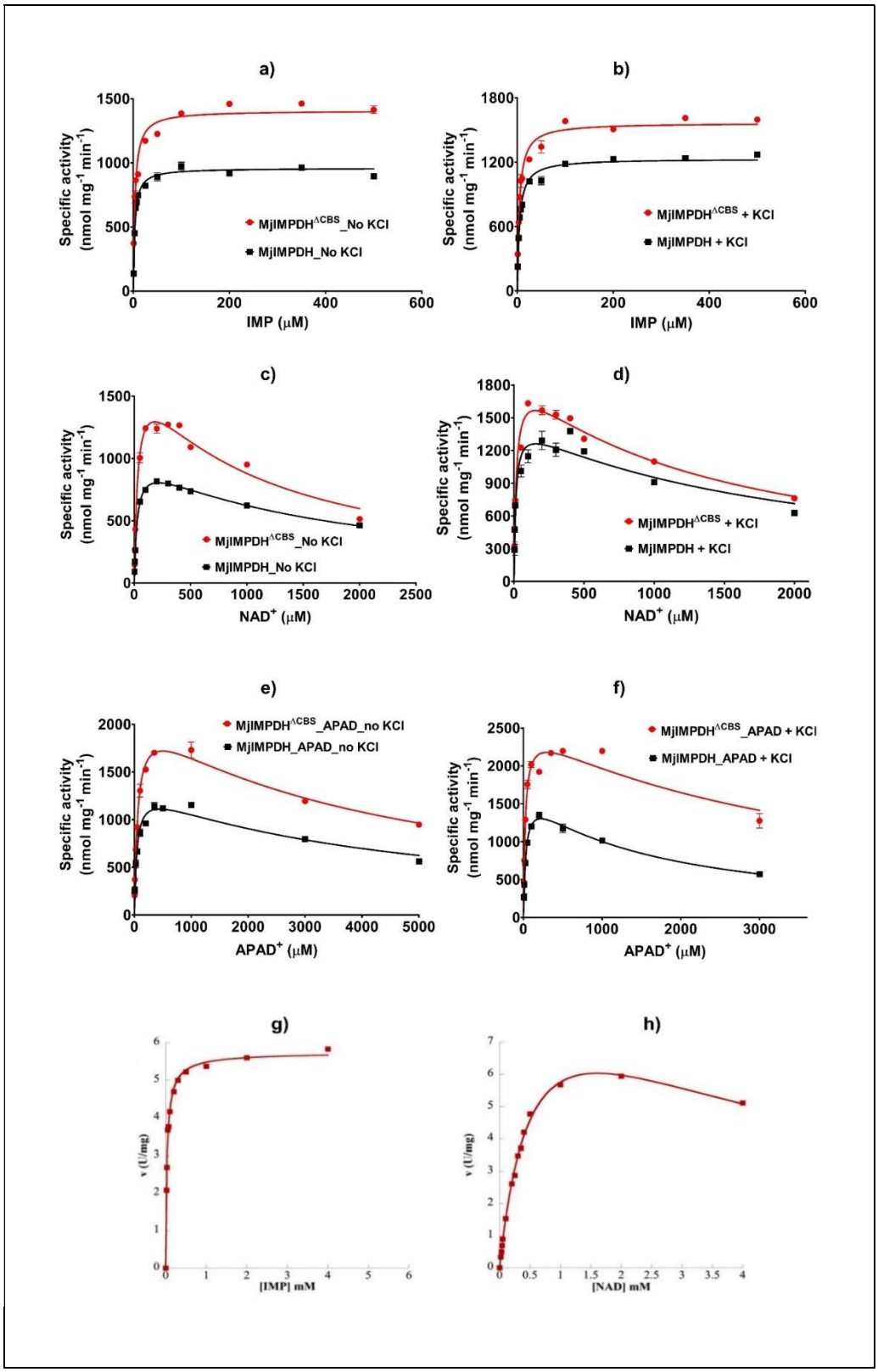
a)
Specific activity (nmol mg-1 min-1)
MjIMPDHΔCBS_No KCl
MjIMPDH_No KCl
IMP (μM)
b)
MjIMPDHΔCBS + KCl
MjIMPDH + KCl
IMP (μM)
c)
MjIMPDHΔCBS_No KCl
MjIMPDH_No KCl
NAD+ (μM)
d)
MjIMPDHΔCBS + KCl
MjIMPDH + KCl
NAD+ (μM)
e)
MjIMPDHΔCBS_APAD_no KCl
MjIMPDH_APAD_no KCl
APAD+ (μM)
f)
MjIMPDHΔCBS_APAD + KCl
MjIMPDH_APAD + KCl
APAD+ (μM)
g)
v (U/mg)
[IMP] mM
h)
v (U/mg)
[NAD] mM

Figure 8. Steady-state kinetics of MjIMPDH and MjIMPDH$^{\Delta CBS}$. *Shown here are the substrate saturation plots with concentrations of variable substrates on the x-axis and the corresponding specific activity (nmol mg^{-1} min^{-1}) on the y-axis in the absence or presence of KCl.* ***a)*** *and* ***b) Michaelis-Menten plots with varying concentrations of IMP. c)*** *and* ***d) Substrate inhibition by NAD$^+$. e)*** *and* ***f) APAD$^+$ as an alternate substrate. g) and h) Substrate titration plots for P. aeruginosa IMPDH as reported by Labesse G et al., 2013*** *(copyright permission © 2013 Elsevier Ltd. Published by Elsevier Inc.) Inhibition effect was much less pronounced with APAD$^+$ as a substrate, a common observation among various IMPDHs. Reaction mixture contained 50 mM TAPS pH 8.0 at 70 °C, 100 mM KCl, 3 mM EDTA, 1 mM DTT and 1 µg of enzyme in a total volume of 0.25 ml. Fixed saturating concentrations of IMP, NAD$^+$, and KCl used were 0.1 mM, 0.2 mM, and 100 mM, respectively. Data were fit to the equation for rectangular hyperbola (Michaelis-Menten model or substrate inhibition) using GraphPad Prism, version 5. Steady-state kinetic parameters determined from substrate saturation plots are tabulated in Table 3a and 3b. All the experiments were performed in two technical replicates containing two biological replicates each. Representative plots from one technical replicate are shown. Each data point represents the mean specific activity value. Error bars represent the standard deviation of the data (n=2).*

Table 3. Steady-state kinetic parameters of MjIMPDH (a) and the core catalytic domain, MjIMPDH$^{\Delta CBS}$ (b). All assays were performed as described in materials and methods section. The standard deviation of the data is provided (n=2). n.a refers to not applicable.

a) MjIMPDH	**IMP**		**NAD$^+$**		**APAD$^+$**	
KCl	--	+	--	+	--	+
V_{max} (nmol mg^{-1} min^{-1})	958 ± 6	1232 ± 16	1030 ± 18	1495 ± 42	1333 ± 21	1787 ± 146
K_m (µM)	3.0 ± 0.3	4.6 ± 0.3	28.2 ± 1.1	13.5 ± 0.7	44 ± 4	36 ± 7
K_i (µM)	n.a		1523 ± 93	1678 ± 52	4448 ± 158	1441 ± 283
k_{cat} (min^{-1})	52 ± 0.4	67.0 ± 0.9	56.0 ± 0.9	81.2 ± 2.3	72.4 ± 1.1	97 ± 8
k_{cat}/K_m (µM^{-1} min^{-1})	17.5 ± 1.8	14.6 ± 0.7	2.0 ± 0.1	6.0 ± 0.1	1.7 ± 0.2	2.7 ± 0.3

b) MjIMPDH$^{\Delta CBS}$	**IMP**		**NAD$^+$**		**APAD$^+$**	
KCl	--	+	--	+	--	+
V_{max} (nmol mg^{-1} min^{-1})	1408 ± 6	1546 ± 14	1749 ± 29	1948 ± 19	2217 ± 11	2518 ± 40
K_m (µM)	3.4 ± 0.3	4.3 ± 0.3	33 ± 2	18.0 ± 2.1	65 ± 2	24.0 ± 0.7
K_i (µM)	n.a		1046 ± 21	1258 ± 43	3851 ± 36	3938 ± 745
k_{cat} (min^{-1})	59.4 ± 0.3	66.0 ± 0.6	74.0 ± 1.1	82.0 ± 0.8	94.0 ± 0.6	106.0 ± 1.7
k_{cat}/K_m (µM^{-1} min^{-1})	17.4 ± 1.6	15.5 ± 0.7	2.3 ± 0.1	4.7 ± 0.5	1.5 ± 0.1	4.6 ± 0.1

Table 4. Comparison of kinetic parameters from other studied IMPHs.

Organism	K_m ^{IMP} (μM)	K_m $^{NAD+}$ (μM)	K_i $^{NAD+}$ (μM)	k_{cat}^{IMP} (s^{-1})
Human I	18 ± 2.2	46 ± 2.8	n.d	1.5 ± 0.1
Human II	9.3 ± 1.0	32 ± 3.4	590 ± 20[a]	1.3 ± 0.0
B. burdorferi	29 ± 8	1100 ± 160	2300 ± 390	2.6 ± 0.3[b]
C. parvum	20 ± 3	110 ± 20	2900 ± 700	1.3 ± 0.2
E. coli	61	2000	2800	13
P. aeruginosa	1760 ± 109	139 ± 14	n.a	2.13 ± 0.07[c]
L. donovani	33 ± 2	390 ± 30	n.a	0.7 ± 0.1
M. tuberculosis	120 ± 2	1900 ± 500	6300 ± 1900	2.2 ± 0.02
A. gossypium	90.2 ± 5.6	279.8 ± 24.7	3600 ± 500	2.46 ± 0.04
A. gossypium $^{\Delta CBS}$	118 ± 13.1	386.6 ± 38.7	4500 ± 1200	3.06 ± 0.06
T. foetus	1.7 ± 0.4	150 ± 30	6800 ± 1800	1.9 ± 0.2
T. brucei	30 ±1·2	1300 ± 300	3000 ± 800	0·28
L. pneumophila	297 ± 30	998 ± 96	n.a	1.79 ± 0.07
N. meningitidis	315 ± 18	269 ± 22	n.a	1.41 ± 0.03
B. thailandensis	52 ± 4	355 ± 27	n.a	2.56 ± 0.04
B. anthracis	120 ± 15	2209 ± 232	n.a	5.04 ± 0.27
K. pneumoniae	58 ± 14	1175 ± 103	n.a	11.6 ± 0.9
S. aureus	196 ± 8	2350 ± 215	n.a	10.1 ± 0.12
M. jannaschii	4.6 ± 0.3	13.5 ± 0.7	1678 ± 52	1.1 ± 0.01

n.a refers to not applicable (no substrate inhibition). n.d refers to not determined. Kinetic parameters of IMPDH from various organisms include Carr SF et al., 1993 (human); [a] Value is taken from Wang W and Hedstrom L, 1997; Zhou X et al., 1997 (B. burgdorferi); [b] K_{cat} with NAD^+ as a variable. Umejiego NN et al., 2004 (C. parvum); Kerr KM and Hedstrom L, 1997 (E. coli); Labesse G et al., 2013 (P. aeruginosa); [c] refers to V_{max} value; Dobie F et al., 2007 (L. donovani); Rostirolla DC et al., 2014 (M. tuberculosis); Buey RM et al., 2015 (A. gossypium); Digits JA and Hedstrom L, 1999 (T. foetus); Bessho T et al., 2013 (T. brucei); Alexandre T et al., 2015 (L. pneumophila, N. meningitidis, B. thailandensis, B. anthracis, K. pneumoniae, S. aureus) this study (M. jannaschii).

5.3.6 Product inhibition

Inhibition kinetics was analyzed by non-linear analysis of the global fit of the data using equations for the competitive, noncompetitive or uncompetitive mode of inhibition.

$v = V_{max}[S] / \{K_m (1+I/K_i) + [S]\}$ competitive inhibition Equation 5.5

$v = V_{max}[S] / \{Km (1+I/K_i) + [S] (1+I/K_i)\}$ noncompetitive inhibition Equation 5.6

$v = V_{max}[S] / \{K_m + [S] (1+I/K_i)\}$ uncompetitive inhibition Equation 5.7

In a bi-bi reaction, the nature of product inhibition (competitive, noncompetitive and uncompetitive) depends on the kinetic mechanism exhibited by the enzyme. It is known that IMPDH does not adopt a ping-pong mechanism and could follow either ordered or random substrate binding. In addition, the kinetic mechanism could be either rapid equilibrium or steady state. Product inhibition studies of MjIMPDH carried out with XMP and NADH had shown XMP as a competitive inhibitor of IMP binding and noncompetitive of NAD^+ binding. NADH was found to be a noncompetitive inhibitor of both IMP and NAD^+ binding. XMP was found to be a more potent inhibitor (K_i 4.9 ± 0.04 μM) than NADH (K_i 58 ± 2 μM) (Fig. 9, Table 5) (refer to Appendix E for secondary plots).

XMP is unequivocally reported to be a competitive inhibitor of IMP binding across various IMPDHs (Hedstrom L, 2009). A study on human IMPDH has shown NADH as an uncompetitive inhibitor of IMP and mixed type inhibitor of NAD^+ (Carr SF *et al*., 1993), while other studies on human, *T. foetus*, *C. parvum* and *M. tuberculosis* IMPDHs indicate NADH to be a noncompetitive inhibitor of both the substrates (IMP and NAD^+) (Xiang B *et al*., 1995; Digits JA and Hedstrom L, 1999; Guillen SYV *et al*., 2004; Umejiego NN *et al*., 2004; Rostirolla DC *et al*., 2014). This noncompetitive behavior (with respect to both the substrates) arises from NADH binding to E-IMP and E-XMP* complexes (Hedstrom L, 2009). A competitive inhibitor that competes for NAD^+ binding has not been reported till date.

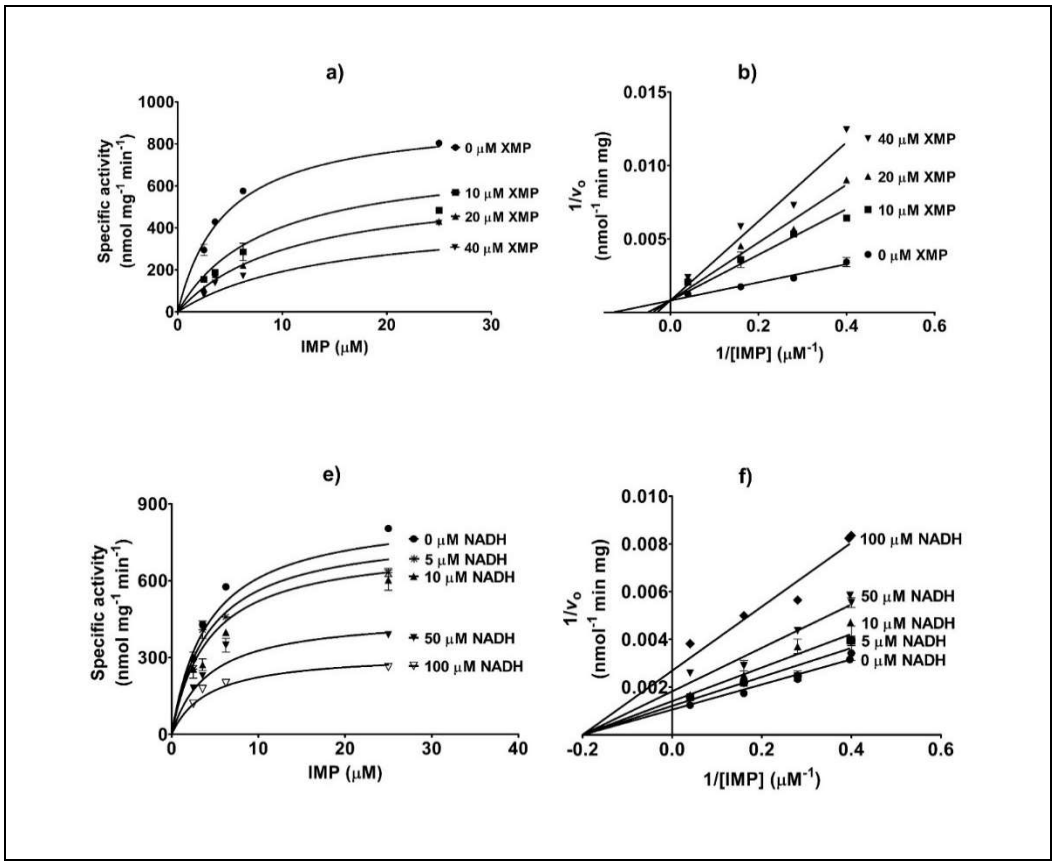

Figure 9. Product inhibition kinetics of MjIMPDH. *Global fit of the data and corresponding double reciprocal Line-weaver Burk plots are represented with XMP and NADH as inhibitors with respect to substrates (IMP). At each fixed concentration of inhibitor, one substrate was varied while the other was kept at a sub-saturating concentration (at K_m value). Fixed sub-saturating concentrations of NAD^+ and IMP were 20 μM and 5 μM, respectively. Assay conditions are as described in the materials and methods section.* ***a)*** *and* ***b) Inhibition plot for XMP*** *versus IMP as the variable substrate (competitive inhibition).* ***e)*** *and* ***f) Inhibition plot for NADH*** *with respect to IMP (noncompetitive inhibition). All the experiments were performed in two technical replicates containing two biological replicates each. Representative plots from one technical replicate are shown. Each data point represents the mean specific activity value. Error bars represent the standard deviation of the data (n=2).*

Table 5. Product inhibition constants of MjIMPDH determined from the global fit of the data and from the secondary plots of slope and intercept versus inhibitor concentration [I]. (refer to Appendix E for secondary plots). Reaction mix contained 100 mM KCl. Varied concentrations of IMP and NAD^+ were (2.5 µM, 3.57 µM, 6.25 µM and 25 µM) and (10 µM, 14.3 µM, 25 µM, and 100 µM), respectively. The standard deviation of the data is presented (n=2).

Inhibitor	Type of inhibition	K_i from global fit (µM)	K_i from the secondary plot of slope vs [I] (µM)	K_i from the secondary plot of intercept vs [I] (µM)
XMP_IMP	Competitive	4.9 ± 0.04	7.2 ± 0.8	-
NADH_IMP	Noncompetitive	58 ± 2	78 ± 8.5	73 ± 8

5.3.7 Modulation of enzyme activity - the role of CBS domain

Various purines including nucleobases (adenine, guanine, xanthine, inosine, and hypoxanthine), nucleosides (adenosine and guanosine), nucleotides (AMP, ADP, ATP, GMP, GDP, and GTP) and known inhibitors like mycophenolic acid (MPA) were tested as effectors of MjIMPDH activity (refer to Appendix E). In an initial screen, among all tested compounds

(at 0.5 mM) only nucleotides (except ATP) and MPA were found to significantly inhibit both the full length and the core catalytic domain. No activators of the *M. jannaschii* enzyme were found. Initial velocity measurements of MjIMPDH in the presence of added inhibitors were analyzed through non-linear regression by a global fit of the data using the equation for competitive (equation 5.5), non-competitive (equation 5.6) and uncompetitive inhibition (equation 5.7). Linear regression of the data was performed to verify the pattern of inhibition determined from the global fits. Secondary replots of intercept and slope from the double reciprocal plots are provided in the Appendix E at the end of the thesis. Inhibition constants were calculated from the global fit of the data and from secondary plots of slope and intercepts (Fig. 10, Fig. 11, and Table 6)

AMP was found to be noncompetitive inhibitor of IMP binding while ADP was noncompetitive with respect to IMP. AMP was found to be a more potent inhibitor than ADP while ATP was found to be a non-effector (Fig. 10, Table 6). Guanine nucleotides were found to be more potent inhibitors than adenine nucleotides. Among guanine nucleotides, the order of inhibition observed was GMP followed by GDP and GTP, all of which were found to be noncompetitive in nature against IMP (Fig. 11, Table 6). Inhibition by nucleotides is found to be highly effective only in the presence of CBS domain (Fig. 10, Fig. 11, Fig. 12 and Table 6). No nucleotide was found to bind to the active site, while removal of CBS resulted in AMP competing for the IMP binding site albeit with a weaker affinity (increase in K_i value by 10-fold). However, upon of deletion of CBS domain, GMP continued to be a noncompetitive inhibitor of IMP binding but with affinity lowered by 100-140 fold (Table 6). This study highlights the feedback inhibition of MjIMPDH through the regulatory CBS domain by both the purine nucleotides (adenine and guanine) indicating a key role for this domain in the control of metabolic flux balance. A similar observation is reported for GDP and GTP inhibition of AgIMPDH$^{\Delta CBS}$ which also displayed noncompetitive inhibition (Buey RM *et al*., 2015). A pictorial representation of the inhibition kinetics observed in MjIMPDH is shown in Figure 13.

There is no extensive literature available on modulation of IMPDH activity by various purine nucleotides. Until recently, only ATP and GMP were mainly tested as the effectors of IMPDH activity. GMP was found to inhibit IMPDHs from *B. burgdorferi* (Zhou X *et al*., 1997), *C. parvum* (Umejiego NN *et al*., 2004) and *E. coli* (Kerr KM and Hedstrom L, 1997). Both GMP

and GTP were reported to inhibit *L. donovani* enzyme while no effect of ATP was observed (Dobie F *et al*., 2007). *M. tuberculosis* IMPDH was also found to be inhibited by GMP (Rostirolla DC *et al*., 2014) but no effect of AMP, ATP, and GTP was observed. The two recent studies on *P. aeruginosa* and *A. gossypium* IMPDH discuss features of allostery and associated subunit organization (Labesse G *et al*., 2013; Buey RM *et al*., 2015; Buey RM *et al*., 2017). PaIMPDH was observed to be present as octameric in solution and allosterically activated by MgATP (Labesse G *et al*., 2013). Also, modulation of the catalytic activity by Mg^{2+}-ATP has been reported for Class I enzymes that includes IMPDHs from *Pseudomonas aeruginosa*, *Legionella pneumophila subsp.* and *Pneumophila*, *Neisseria meningitidis* (Alexandre T *et al*., 2015). Study on AgIMPDH highlighted that adenine moieties had no effect on enzyme activity while guanine moieties (GDP and GTP) inhibited eukaryotic IMPDHs (*A. gossypium*, Human type I and type II) but not prokaryotic enzymes (*E. coli* and *B. subtilis*). However, GMP was found to be a weak competitive inhibitor of both prokaryotic and eukaryotic IMPDHs. The study also indicates the glutamate residue within "RIEK" motif is strictly conserved in prokaryotic IMPDHs and coordinates Mg^{2+} to the γ-ATP to enhance catalytic activity. "RIEK" motif is found replaced by "KKGK" motif in eukaryotes with glycine interacting specifically with α-phosphate of GDP and similar to GTP inhibits catalysis independent of Mg^{2+}. However, MjIMPDH has an "RVER" motif in place of "RIEK" and despite the presence of the glutamate, the enzyme was found insensitive to Mg^{2+}-ATP up to 5 mM concentration. However, potent inhibition was observed by guanine moieties despite the lack of glycine (independent of Mg^{2+}). MjIMPDH shares high sequence identity (50%) with prokaryotic IMPDHs, but displays features like guanine inhibition which are reported to be present only in eukaryotic IMPDHs. This study highlights the feedback inhibition of MjIMPDH through the regulatory CBS subdomain by both the purine nucleotides (adenine and guanine) indicating a key role in the control of the metabolic flux balance (Fig. 14).

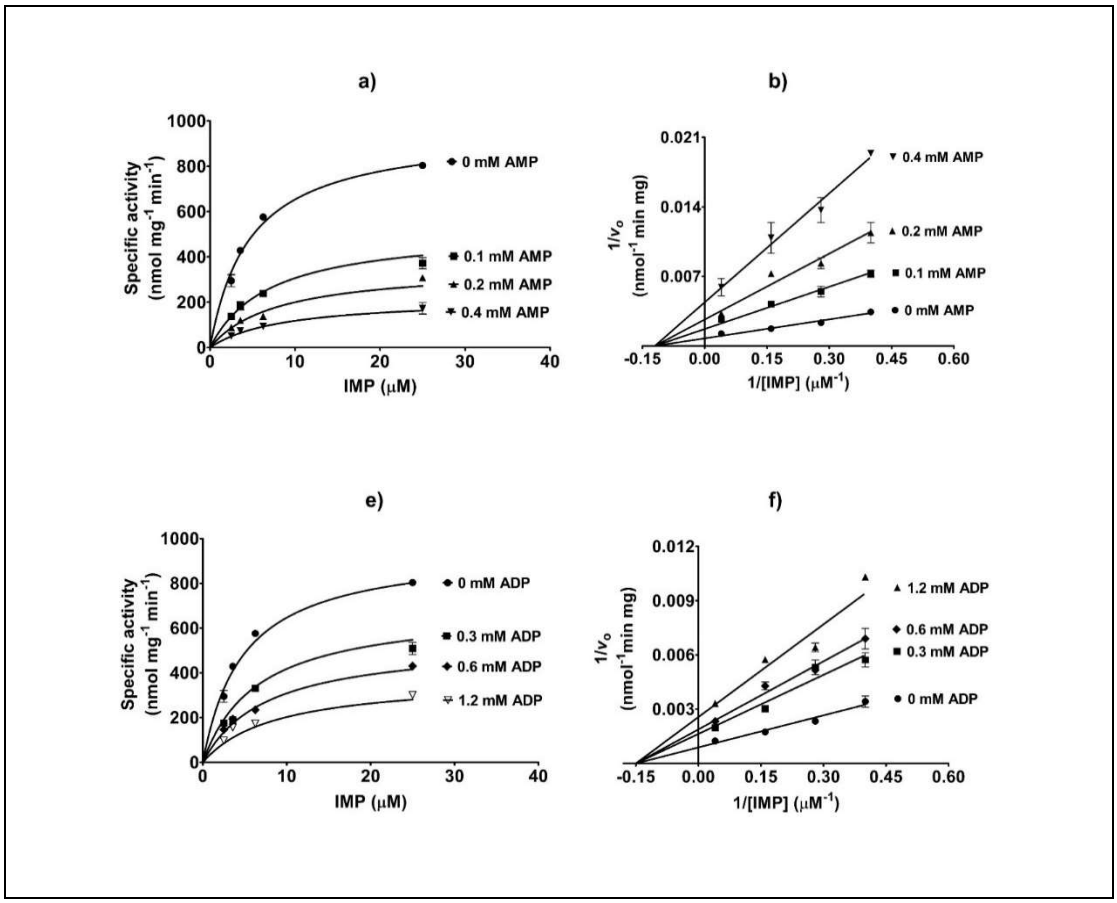
a)
Specific activity (nmol mg-1 min-1)
IMP (μM)
0 mM AMP
0.1 mM AMP
0.2 mM AMP
0.4 mM AMP
b)
1/vo (nmol-1 min mg)
1/[IMP] (μM-1)
0.4 mM AMP
0.2 mM AMP
0.1 mM AMP
0 mM AMP
e)
Specific activity (nmol mg-1 min-1)
IMP (μM)
0 mM ADP
0.3 mM ADP
0.6 mM ADP
1.2 mM ADP
f)
1/vo (nmol-1 min mg)
1/[IMP] (μM-1)
1.2 mM ADP
0.6 mM ADP
0.3 mM ADP
0 mM ADP

Figure 10. Effect of adenine nucleotides on dehydrogenase activity of MjIMPDH. *Global fit of the data and corresponding double reciprocal Line-weaver Burk plots are shown. At each fixed concentration of inhibitor, one substrate was varied while the other was kept at the concentration required for half-maximal activity (at K_m value). Sub-saturating concentrations of NAD^+ and IMP used were 20 µM and 5 µM, respectively. A detailed description of assay conditions is provided in the materials and methods section.* ***a), and b)*** *Plots indicating AMP as a non-competitive inhibitor against IMP.* ***e), and f)*** *Plots representing ADP as non-competitive against IMP. No modulation of dehydrogenase activity by Mg^{2+}-ATP was observed up to 5 mM. All the experiments were performed in two technical replicates containing two biological replicates each. Representative plots from one technical replicate are shown. Each data point represents the mean specific activity value. Error bars represent the standard deviation of the data (n=2).*

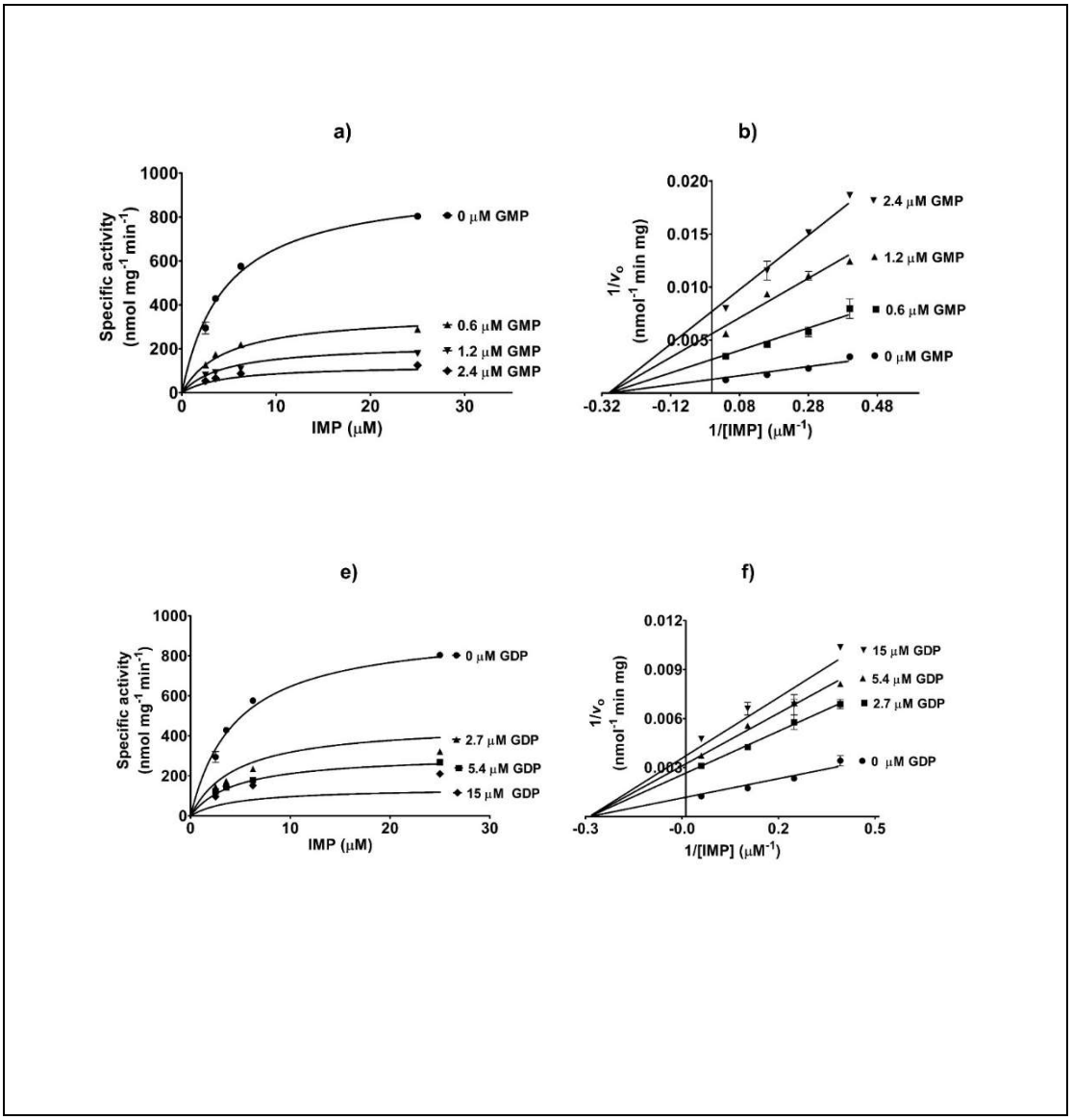

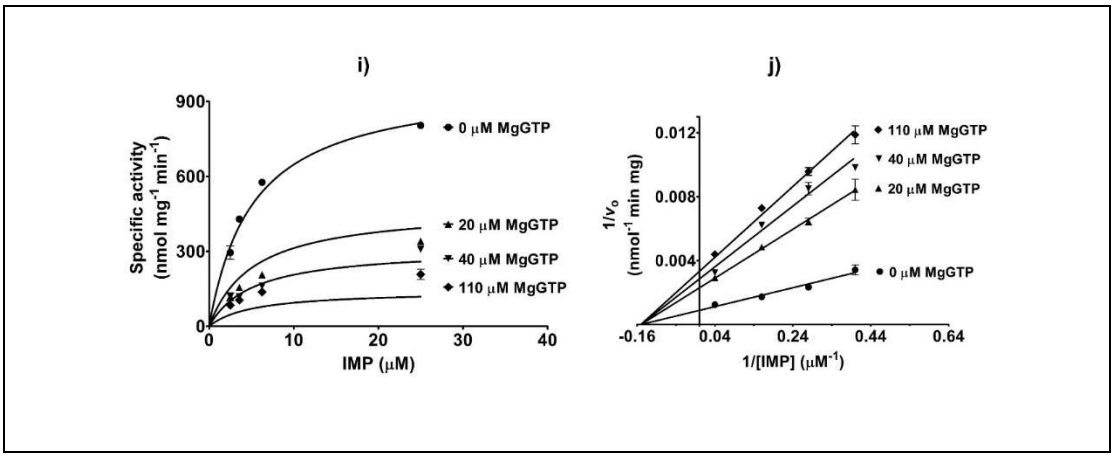

Figure 11. Effect of guanine nucleotides on dehydrogenase activity of MjIMPDH. *Global fit of the data and corresponding double reciprocal Line-weaver Burk plots are shown. At each fixed concentration of inhibitor, one substrate was varied while the other was kept at the concentration required for half-maximal activity (K_m). Sub-saturating concentrations of NAD^+ and IMP were 20 μM and 5 μM, respectively. A detailed description of assay conditions is provided in the materials and methods section.* ***a), and b)*** *Plots indicating GMP as a non-competitive inhibitor against IMP.* ***e), and f)*** *Plots showing GDP as noncompetitive against IMP binding.* ***i), and j)*** *Data showing Mg^{2+}-GTP as a non-competitive inhibitor against IMP binding. All the experiments were performed in two technical replicates containing two biological replicates each. Representative plots from one technical replicate are shown. Each data point represents the mean specific activity value. Error bars represent the standard deviation of the data (n=2).*

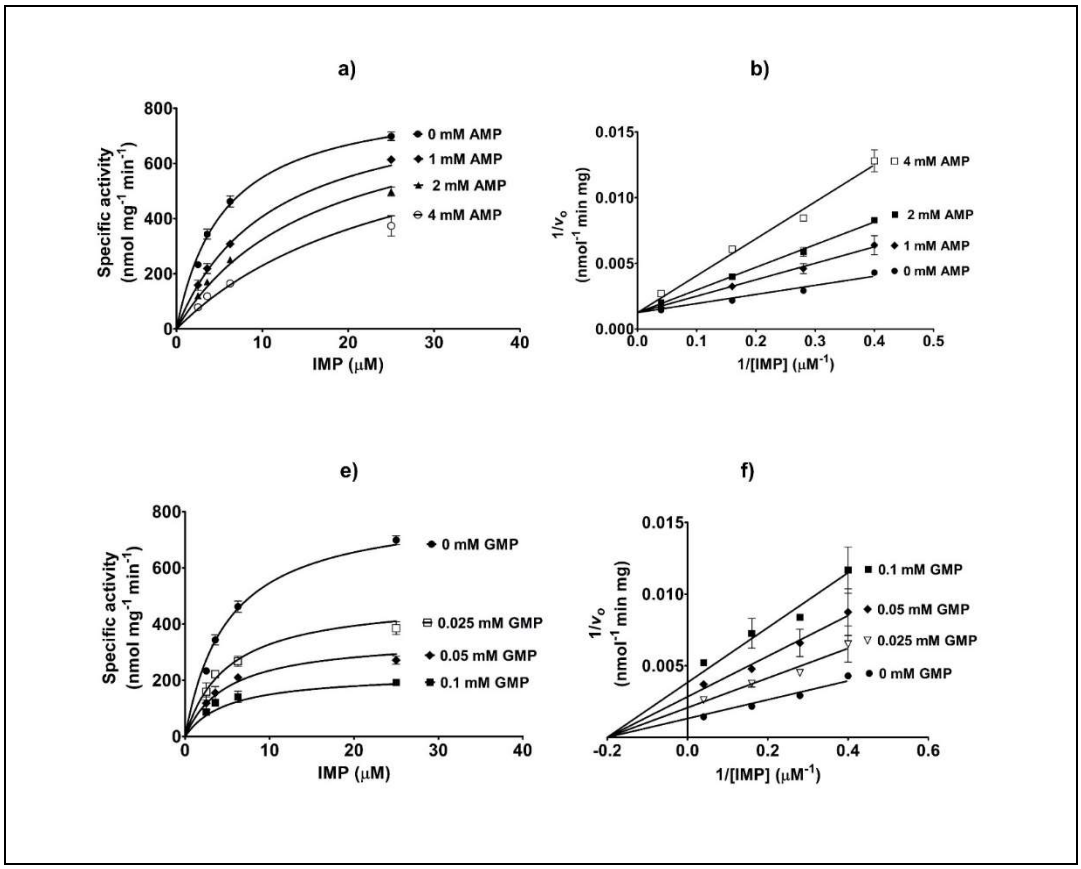

Figure 12. Modulation of IMP dehydrogenase activity by AMP and GMP- the effect of deletion of CBS domain. *Global fit of the data and corresponding double reciprocal Line-weaver Burk plots are shown. At each fixed concentration of inhibitor, one substrate was varied while the other was kept at the concentration required for half-maximal activity (K_m). Sub-saturating concentrations of NAD^+ and IMP were 20 μM and 5 μM, respectively. A detailed description of assay conditions is mentioned in the materials and methods section.* ***a), and b)*** *Plots indicating AMP as a competitive inhibitor of IMP which in the presence of CBS was found to be non-competitive.* ***e), and f)*** *Plots representing GMP as non-competitive against IMP binding which in the presence of CBS was found to be noncompetitive. All the experiments were performed in two technical replicates containing two biological replicates each. Representative plots from one technical replicate are shown. Each data point represents the mean specific activity value. Error bars represent the standard deviation of the data (n=2).*

(This page is left blank intentionally)

Table 6. Modulation of *M. jannaschii* IMP dehydrogenase activity by purine nucleotides as determined from the global fit of the data and from the secondary plots of slope and intercepts versus inhibitor concentration [I]. (refer to Appendix E for secondary plots). Varied concentrations of IMP and NAD^+ were (2.5 µM, 3.57 µM, 6.25 µM and 25 µM) and (10 µM, 14.3 µM, 25 µM, and 100 µM), respectively. The standard deviation of the data is presented (n=2).

MjIMPDH **Inhibitor_variable substrate**	**Type of inhibition**	**K_i from global fit (µM)**	**K_i from the secondary plot of slope vs [I] (µM)**	**K_i from the secondary plot of intercept vs [I] (µM)**
AMP_IMP	Noncompetitive	89 ± 1.4	88 ± 22	82 ± 13
ADP_IMP		565 ± 32	605 ± 54	579 ± 91
ATP	**----------No effect----------**			
GMP_IMP	Noncompetitive	0.37 ± 0.02	0.31 ± 0.06	0.32 ± 0.06
GDP_IMP		2.6 ± 0.4	3.5 ± 0.4	5 ± 2.4
GTP_IMP		18.7 ± 0.14	24.5 ± 0.7	25 ± 1.4
$MjIMPDH^{\Delta CBS}$				
AMP_IMP	Competitive	1027 ±0148	1725 ± 318	-
GMP_IMP	Noncompetitive	42 ± 7	42 ± 15	43 ± 17

Only the most potent inhibitor of MjIMPDH among adenine and guanine nucleotides was tested for its effect on $MjIMPDH^{\Delta CBS}$.

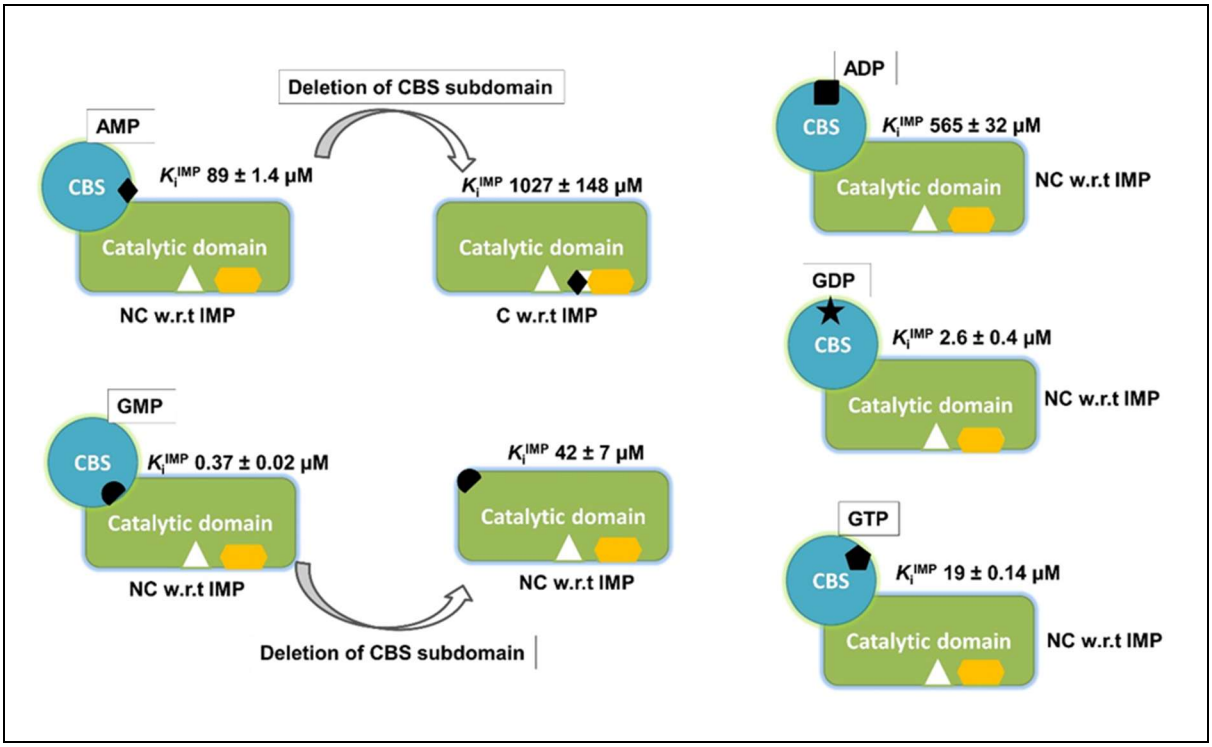

Figure 13. Binding of purine nucleotides and inhibition of MjIMPDH and MjIMPDH$^{\Delta CBS}$ - a schematic representation. *The catalytic domain is shown as a green rectangle while CBS domain as a blue circle. NAD^+ and IMP binding sites are shown vacant in white and when occupied in orange. Mode of inhibition and corresponding inhibition constant are indicated. Black shaded triangle, hemisphere, square, asterisk, and hexagon represent ligands AMP, ADP, GMP, GDP, and GTP, respectively.*

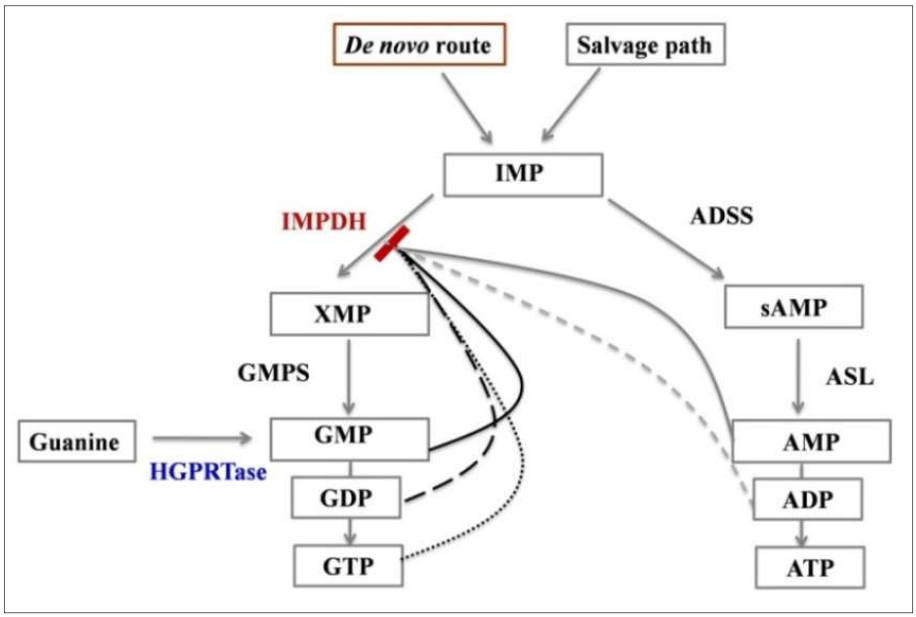

Figure 14. Feedback regulation of MjIMPDH by purine nucleotides. *In the current study, guanine nucleotides were found to be more potent inhibitors of IMPDH activity than adenine nucleotides. Nucleobases (guanine, adenine, xanthine, and hypoxanthine) and nucleosides (guanosine, adenosine, and inosine) at 0.5 mM were found to have no significant effect on MjIMPDH activity (refer to Appendix E). Order of inhibition potency was GMP (solid black line) >GDP (discontinuous black line) >GTP (dotted grey line) >AMP (solid grey line) >ADP (discontinuous grey line). Inhibition by AMP and GMP was relieved to an extent of 50 and 140-fold, respectively upon deletion of the CBS domain.*

5.3.8 Functional complementation assay

MjIMPDH was examined for its ability to the rescue growth of *impdh* deletion strain of *E. coli*, Δ*guaB*^{K}(DE3). Intriguingly, heterologous expression of MjIMPDH that yielded high levels of soluble protein could not complement the growth deficiency of the purine auxotroph on M9 minimal medium agar plates grown at 42 °C. However, IMPDH from *T. foetus* used as a positive control was found to support the growth deficiency (discussed in Chapter 2). The turn over number (k_{cat}) for MjIMPDH measured at 37 °C, 45 °C and 70 °C was found to be 0.027 s^{-1}, 0.064 s^{-1} and 1.0 s^{-1}, respectively. A 15-fold drop in enzyme activity was observed at 45 °C as compared to the activity measurements performed at 70 °C. The turnover number (k_{cat}) for *T. foetus* IMPDH (used as positive control in the growth rescue experiments) at 25 °C is reported to be 2.0 s^{-1}, while MjIMPDH at 70 °C was found to be 1.0 s^{-1}. Although extremely high levels of expression of recombinant MjIMPDH was observed, drop in catalytic rates at lower temperatures and modulation of the enzyme activity by purine nucleotides (independently or in combination) could have led to the no growth phenotype of *impdh*$^{-}$ deletion strain of *E coli* on M9 minimal medium.

Also, bacterial cells are known to synthesize the alarmone, guanosine tetraphosphate (ppGpp) in response to nutritional stress. ppGpp is known to directly/indirectly target and inhibit the activity of RNA polymerase, GMP Kinase, HGPRT, and IMPDH in *E. coli*, *Bacillus subtilis*, *Streptococcus griesus* and *Thermus thermophilus* (Lecoq K *et al*., 2000; Kasai K *et al*., 2006; Brittner AN *et al*., 2014; Liu K *et al*., 2015). Further, in the current study, we found adenine nucleotides as potent inhibitors of MjIMPDH with inhibition constants varying between 100 μM to 400 μM. Therefore, probable differential inhibition of MjIMPDH as compared to *T. foetus* enzyme within the bacterial cells by either ppGpp or adenine nucleotides could have plausibly resulted in no rescue of the deletion strain.

5.4 Conclusion

In conclusion, recombinant MjIMPDH protein was found highly soluble and octameric in association. Presence of higher order oligomers in large proportion was observed similar to other characterized IMPDHs although its cellular significance remains unknown. Deletion of CBS domain led to the formation of a tetramer with no compromise in enzyme activity. *M. jannaschii* enzyme was found to obey Michaelis-Menten kinetics for IMP while NAD^+ displayed substrate inhibition similar to other known IMPDHs. This study stands as the first example of an IMPDH which is feebly dependent on a monovalent cation (K^+) for its activity. It is found to be sensitive to both the purine nucleotides (except ATP), with more potent inhibition exhibited by guanine nucleotides. Deletion of CBS domain relieves inhibition by the purines significantly thereby acting as a sensor to maintain balance in the nucleotide metabolism. MjIMPDH shares high sequence identity with prokaryotic IMPDHs but displays features like guanine nucleotide inhibition which is reported to be present only in eukaryotic IMPDHs. Further investigations on to the three-dimensional structure in apo- and complexed- forms would unveil the mechanism of enzyme modulation in detail.

Perspectives of the current study

Current thesis work is focused on understanding the working mechanism of IMP dehydrogenase, a key enzyme in purine nucleotide metabolism and a potent drug target. IMPDHs from two different organisms namely mesophilic protozoan parasite *Plasmodium falciparum* and hyper-thermophilic archaeon *Methanocaldococcus jannaschii* were chosen as experimental models. Enzyme in its purest form stands as a prerequisite for a thorough structural and biochemical analysis. Intriguingly, we failed to purify recombinant PfIMPDH despite extensive efforts put in optimizations while recombinant MjIMPDH could be purified to its homogeneity. This study highlights in-detail the challenges posed by the parasite enzyme. Protein folding, multimerization, and sequence derived unknown complexities independently or in combination could stand as possible reasons for the failure. On the other hand, with high level of sequence conservation (including the catalytic pocket) and over all identical structural fold, MjIMPDH could still be hyperexpressed, and purified to homogeneity for further enzymatic studies. This study is the first report on the biochemical characterization of an archaeal IMPDH from *M. jannaschii* that shares high sequence identity (50%) with prokaryotic IMPDHs but displays features like guanine nucleotide inhibition that are reported to be present only in eukaryotic IMPDHs. Further investigations focused on the three-dimensional structure analysis in apo- and complexed- forms should unveil the mechanistic insights of enzyme modulation in detail."

Conclusions and future directions

We have examined the gene PF3D7_0920800 annotated as IMPDH from the mesophilic malarial parasite *Plasmodium falciparum* for its subcellular localization in the intraerythrocytic stages of the parasite and functionality using heterologous expression hosts (*E. coli* and *S. cerevisiae*). Indirect immunofluorescence microscopy has revealed the subcellular localization of IMPDH to be largely cytoplasmic with a partial nuclear signal in the parasite during intra-erythrocytic asexual stages of the life cycle. Also, similar to immature cytoophidia of human IMPDH, small distinct foci of PfIMPDH have been observed across various stages of the parasite. Experiments focussed on generating parasites (*P. falciparum* and *P. berghei*) with endogenous GFP tag, followed by microscopic examination and pull-down assays could be the possible future directions in the understanding of these structural elements of PfIMPDH. Functional identity of PfIMPDH could not be established through genetic complementation assay owing to either the lack of sufficient soluble and therefore functional enzyme (in *E. coli*) or lack of mRNA translation (in *S. cerevisiae*). Various efforts including codon harmonization of gene sequence in obtaining recombinant PfIMPDH protein in soluble form was not fruitful. For the first time, soluble and detectable level of PfIMPDH protein on Coomassie-stained SDS-PAGE was achieved with *E. coli* S-30 extract. An attempt to isolate the *in vitro* synthesized protein remained unsuccessful largely due to protein multimerization or protein aggregation or strong association with the ribosomal machinery. However, recombinant PfCBS protein was purified to homogeneity and was observed to bind both adenine and guanine nucleotides (except GMP) *in vitro* as evidenced by changes in intrinsic tyrosine fluorescence upon ligand binding. This may act as an intracellular sensor for purine nucleotides thereby maintaining homeostasis of the malarial parasite. Bias in amino acid composition as compared to other recombinantly expressed and biochemically characterized IMPDH/GMPR family of proteins and prediction of aggregation-prone regions could form the basis for generating mutants of PfIMPDH with possibly improved solubility.

MJ1616 from the hyperthermophilic archaeon, *Methanocaldococcus jannaschii* has been established as a bonafide IMPDH. Recombinant MjIMPDH protein was found to be highly soluble and octameric in association. Presence of higher order oligomers in large proportion was observed similar to other characterized IMPDHs although its cellular significance remains unknown. Deletion of CBS domain led to the formation of a tetramer with

no compromise in enzyme activity. MjIMPDH displayed very weak dependence on K^+ ions for its activity. *M. jannaschii* enzyme was found to obey Michaelis-Menten kinetics for IMP while NAD^+ displayed substrate inhibition similar to other known IMPDHs. Products of the enzyme reaction, XMP and NADH were found to inhibit MjIMPDH. The enzyme was found to be sensitive to both the purine nucleotides (except ATP), with more potent inhibition exhibited by guanine nucleotides. Inhibition by nucleotides was found to be highly effective only in the presence of CBS domain. No nucleotide was found to bind to the active site, while removal of CBS resulted in AMP competing for the IMP binding site albeit with weaker affinity. This study highlights the feedback inhibition of MjIMPDH through the regulatory CBS domain by both the purine nucleotides (adenine and guanine) indicating a key role for this domain in the control of metabolic flux balance. This study is the first report on the biochemical characterization of an archaeal IMPDH from *M. jannaschii* that shares high sequence identity (50%) with prokaryotic IMPDHs but displays features like guanine nucleotide inhibition which is reported to be present only in eukaryotic IMPDHs. Further investigations that focus on the three-dimensional structure analysis in apo- and complexed- forms would unveil the mechanism of enzyme modulation in detail.

Ongoing Studies

With the expression and purification conditions established, the structure of $MjIMPDH^{\Delta CBS}$ has been solved by X-ray crystallography by another member of the group in the laboratory. Detailed analysis of this structure is currently underway. Octameric and the higher order multimeric forms of MjIMPDH have been examined by transmission electron microscopy (TEM). Changes in the dimensions of the protein structure in the presence of guanine nucleotides observed through TEM further confirm the modulation of enzyme activity by these nucleotides. Lastly, our attempts at crystallizing the highly soluble CBS domain of PfIMPDH was not successful due to protein precipitation.

REFERENCES

1. Abraham, E. P. (1945) The effect of mycophenolic acid on the growth of Staphylococcus aureus in heart broth. *Biochem. J.* **39**, 398–408
2. Acharya, P., Pallavi, R., Chandran, S., Chakravarti, H., Middha, S., Acharya, J., Kochar, S., Kochar, D., Subudhi, A., Boopathi, A. P., Garg, S., Das, A., and Tatu, U. (2009) A glimpse into the clinical proteome of human malaria parasites Plasmodium falciparum and Plasmodium vivax. *Proteomics Clin Appl*. **3**, 1314–1325
3. Aguado-Llera, D., Oyenarte, I., Martinez-Cruz, L. A., and Neira, J. L. (2010) The CBS domain protein MJ0729 of Methanocaldococcus jannaschii binds DNA. *FEBS Lett*. **584**, 4485–4489
4. Alev-Behmoaras, T., Toulme, J. J., and C, H. (1979) QUENCHING OF TYROSINE FLUORESCENCE BY PHOSPHATE IONS: A MODEL STUDY FOR PROTEIN-NUCLEIC ACID COMPLEXES. *Photochem. Photobiol.* **30**, 533 to 539
5. Alexandre, T., Raynal, B., Rayna, B., and Munier-Lehmann, H. (2015) Two classes of bacterial IMPDHs according to their quaternary structures and catalytic properties. *PLoS One*. **10**, e0116578
6. Ali, R., Kumar, S., Balaram, H., and Sarma, S. P. (2013) Solution Nuclear Magnetic Resonance Structure of the GATase Subunit and Structural Basis of the Interaction between GATase and ATPPase Subunits in a *two-subunit-type* GMPS from *Methanocaldococcus jannaschii*. *Biochemistry*. **52**, 4308–4323
7. Ali, R., Kumar, S., Balaram, H., and Sarma, S. P. (2012) 1H, 13C, 15N assignment and secondary structure determination of glutamine amido transferase subunit of gaunosine monophosphate synthetase from Methanocaldococcus jannaschii. *Biomol. NMR Assign.* **6**, 193–196
8. Allison, A. C., and Eugui, E. M. (2000) Mycophenolate mofetil and its mechanisms of action. *Immunopharmacology*. **47**, 85–118
9. Allison, A. C., Kowalski, W. J., Muller, C. D., and Eugui, E. M. (1993) Mechanisms of action of mycophenolic acid. *Ann. N. Y. Acad. Sci.* **696**, 63–87
10. Almagro Armenteros, J. J., Sonderby, C. K., Sonderby, S. K., Nielsen, H., and Winther, O. (2017) DeepLoc: prediction of protein subcellular localization using deep learning. *Bioinformatics*. **33**, 3387–3395
11. Anantharaman, V., Aravind, L., and Koonin, E. V (2003) Emergence of diverse biochemical activities in evolutionarily conserved structural scaffolds of proteins. *Curr. Opin. Chem. Biol.* **7**, 12–20
12. Andrews, S. C., and Guest, J. R. (1988) Nucleotide sequence of the gene encoding the GMP reductase of Escherichia coli K12. *Biochem J.* **255**, 35–43
13. Angov, E., Hillier, C. J., Kincaid, R. L., and Lyon, J. A. (2008) Heterologous Protein Expression Is Enhanced by Harmonizing the Codon Usage Frequencies of the Target Gene with those of the Expression Host. *PLoS One*. **3**, e2189
14. Anthony, S. A., Burrell, A. L., Johnson, M. C., Duong-Ly, K. C., Kuo, Y.-M., Simonet, J. C., Michener, P., Andrews, A., Kollman, J. M., and Peterson, J. R. (2017) Reconstituted

IMPDH polymers accommodate both catalytically active and inactive conformations. *Mol. Biol. Cell*. 10.1091/mbc.E17-04-0263

15. Arad, M., Benson, D. W., Perez-Atayde, A. R., McKenna, W. J., Sparks, E. A., Kanter, R. J., McGarry, K., Seidman, J. G., and Seidman, C. E. (2002) Constitutively active AMP kinase mutations cause glycogen storage disease mimicking hypertrophic cardiomyopathy. *J. Clin. Invest.* **109**, 357–362

16. Armenta-Medina, D., Segovia, L., and Perez-Rueda, E. (2014) Comparative genomics of nucleotide metabolism: a tour to the past of the three cellular domains of life. *BMC Genomics*. **15**, 800

17. Aughey, G. N., Grice, S. J., Shen, Q.-J., Xu, Y., Chang, C.-C., Azzam, G., Wang, P.-Y., Freeman-Mills, L., Pai, L.-M., Sung, L.-Y., Yan, J., and Liu, J.-L. (2014) Nucleotide synthesis is regulated by cytoophidium formation during neurodevelopment and adaptive metabolism. *Biol. Open*. **3**, 1045–1056

18. Aurrecoechea, C., Brestelli, J., Brunk, B. P., Dommer, J., Fischer, S., Gajria, B., Gao, X., Gingle, A., Grant, G., Harb, O. S., Heiges, M., Innamorato, F., Iodice, J., Kissinger, J. C., Kraemer, E., Li, W., Miller, J. A., Nayak, V., Pennington, C., Pinney, D. F., Roos, D. S., Ross, C., Stoeckert, C. J., Treatman, C., and Wang, H. (2009) PlasmoDB: a functional genomic database for malaria parasites. *Nucleic Acids Res.* **37**, D539-43

19. Bacher, A., Eberhardt, S., Fischer, M., Kis, K., and Richter, G. (2000) B IOSYNTHESIS OF V ITAMIN B $_2$ (RIBOFLAVIN). *Annu. Rev. Nutr.* **20**, 153–167

20. Bacus, S. S., Kiguchi, K., Chin, D., King, C. R., and Huberman, E. (1990) Differentiation of cultured human breast cancer cells (AU-565 and MCF-7) associated with loss of cell surface HER-2/neu antigen. *Mol carcinog*. **3**, 350–62

21. Bahl, A., Brunk, B., Crabtree, J., Fraunholz, M. J., Gajria, B., Grant, G. R., Ginsburg, H., Gupta, D., Kissinger, J. C., Labo, P., Li, L., Mailman, M. D., Milgram, A. J., Pearson, D. S., Roos, D. S., Schug, J., Stoeckert, C. J., and Whetzel, P. (2003) PlasmoDB: the Plasmodium genome resource. A database integrating experimental and computational data. *Nucleic Acids Res.* **31**, 212–215

22. Balzarini, J., Stet, L., Matsuda, A., Wiebe, L., Knauss, E., and De Clercq, E. (1998) Metabolism of EICAR (5-ethynyl-1-beta-D-ribofuranosylimidazole-4-carboxamide), a potent inhibitor of inosinate dehydrogenase. *Adv. Exp. Med. Biol.* **431**, 723–8

23. Barry, R. M., Bitbol, A.-F., Lorestani, A., Charles, E. J., Habrian, C. H., Hansen, J. M., Li, H.-J., Baldwin, E. P., Wingreen, N. S., Kollman, J. M., and Gitai, Z. (2014) Large-scale filament formation inhibits the activity of CTP synthetase. *Elife*. **3**, e03638

24. Bartfai, R., Hoeijmakers, W. A., Salcedo-Amaya, A. M., Smits, A. H., Janssen-Megens, E., Kaan, A., Treeck, M., Gilberger, T. W., Francoijs, K. J., and Stunnenberg, H. G. (2010) H2A.Z demarcates intergenic regions of the plasmodium falciparum epigenome that are dynamically marked by H3K9ac and H3K4me3. *PLoS Pathog*. **6**, e1001223

25. Barton, A. B., Bussey, H., Storms, R. K., and Kaback, D. B. (1997) Molecular Cloning of Chromosome I DNA fromSaccharomyces cerevisiae: Characterization of the 54 kb Right TerminalCDC15-FLO1-PHO11 Region. *Yeast*. **13**, 1251–1263

26. Bateman, A. (1997) The structure of a domain common to archaebacteria and the homocystinuria disease protein. *Trends Biochem. Sci.* **22**, 12–3

27. Baykov, A. A., Tuominen, H. K., and Lahti, R. (2011) The CBS Domain: A Protein Module with an Emerging Prominent Role in Regulation. *ACS Chem. Biol.* **6**, 1156–1163
28. Becker, J.-L. (1974) Métabolisme des purines dans des cellules de Drosophila melanogaster en culture in vitro : Interconversion des purines. *Biochimie*. **56**, 1249–1253
29. Bennetts, B., Rychkov, G. Y., Ng, H.-L., Morton, C. J., Stapleton, D., Parker, M. W., and Cromer, B. A. (2005) Cytoplasmic ATP-sensing Domains Regulate Gating of Skeletal Muscle ClC-1 Chloride Channels. *J. Biol. Chem.* **280**, 32452–32458
30. Benson, C. E., Brehmeyer, B. A., and Gots, J. S. (1971) Requirement of cyclic AMP for induction of GMP reductase in Escherichia coli. *Biochem Biophys Res Commun*. **43**, 1089–94
31. Berens, R. L., Marr, J. J., and Brun, R. (1980) Pyrazolopyrimidine metabolism in African trypanosomes: metabolic similarities to Trypanosoma cruzi and Leishmania spp. *Mol Biochem Parasitol*. **1**, 69–73
32. Berg, M., Van der Veken, P., Goeminne, A., Haemers, A., and Augustyns, K. (2010) Inhibitors of the Purine Salvage Pathway: A Valuable Approach for Antiprotozoal Chemotherapy? *Curr Med Chem.* **17**, 2456–81
33. Bessho, T., Okada, T., Kimura, C., Shinohara, T., Tomiyama, A., Imamura, A., Kuwamura, M., Nishimura, K., Fujimori, K., Shuto, S., Ishibashi, O., Kubata, B. K., and Inui, T. (2016) Novel Characteristics of Trypanosoma brucei Guanosine 5'-monophosphate Reductase Distinct from Host Animals. *PLoS Negl Trop Dis*. **10**, e0004339
34. Bhat, J. Y., Shastri, B. G., and Balaram, H. (2008) Kinetic and biochemical characterization of *Plasmodium falciparum* GMP synthetase. **409**, 263–273
35. Bieging, K. T., Mello, S. S., and Attardi, L. D. (2014) Unravelling mechanisms of p53-mediated tumour suppression. *Nat. Rev. Cancer*. **14**, 359–370
36. Bittner, A. N., Kriel, A., and Wang, J. D. (2014) Lowering GTP Level Increases Survival of Amino Acid Starvation but Slows Growth Rate for Bacillus subtilis Cells Lacking (p)ppGpp. *J. Bacteriol.* **196**, 2067–2076
37. Blair, E., Redwood, C., Ashrafian, H., Oliveira, M., Broxholme, J., Kerr, B., Salmon, A., Ostman-Smith, I., and Watkins, H. (2001) Mutations in the gamma(2) subunit of AMP-activated protein kinase cause familial hypertrophic cardiomyopathy: evidence for the central role of energy compromise in disease pathogenesis. *Hum. Mol. Genet.* **10**, 1215–20
38. BOLTE, S., and CORDELIÈRES, F. P. (2006) A guided tour into subcellular colocalization analysis in light microscopy. *J. Microsc.* **224**, 213–232
39. Boonyaratanakornkit, B. B., Miao, L. Y., and Clark, D. S. (2007) Transcriptional responses of the deep-sea hyperthermophile Methanocaldococcus jannaschii under shifting extremes of temperature and pressure. *Extremophiles*. **11**, 495–503
40. Bowne, S. J., Sullivan, L. S., Mortimer, S. E., Hedstrom, L., Zhu, J., Spellicy, C. J., Gire, A. I., Hughbanks-Wheaton, D., Birch, D. G., Lewis, R. A., Heckenlively, J. R., and Daiger, S. P. (2006) Spectrum and Frequency of Mutations in IMPDH1 Associated with Autosomal Dominant Retinitis Pigmentosa and Leber Congenital Amaurosis. *Investig. Opthalmology Vis. Sci.* **47**, 34

41. Bowne, S. J., Sullivan, L. S., Blanton, S. H., Cepko, C. L., Blackshaw, S., Birch, D. G., Hughbanks-Wheaton, D., Heckenlively, J. R., and Daiger, S. P. (2002) Mutations in the inosine monophosphate dehydrogenase 1 gene (IMPDH1) cause the RP10 form of autosomal dominant retinitis pigmentosa. *Hum. Mol. Genet.* **11**, 559–68

42. Bozdech, Z., and Ginsburg, H. (2004) Antioxidant defense in Plasmodium falciparum--data mining of the transcriptome. *Malar J.* **3**, 23

43. Bozdech, Z., and Ginsburg, H. (2005) Data mining of the transcriptome of Plasmodium falciparum: the pentose phosphate pathway and ancillary processes. *Malar J.* **4**, 17

44. Bozdech, Z., Llinas, M., Pulliam, B. L., Wong, E. D., Zhu, J., and DeRisi, J. L. (2003) The transcriptome of the intraerythrocytic developmental cycle of Plasmodium falciparum. *PLoS Biol*. **1**, E5

45. Bradford, M. M. (1976) A rapid and sensitive method for the quantitation of microgram quantities of protein utilizing the principle of protein-dye binding. *Anal. Biochem.* **72**, 248–54

46. Braun-Sand, S. B., and Peetz, M. (2010) Inosine monophosphate dehydrogenase as a target for antiviral, anticancer, antimicrobial and immunosuppressive therapeutics. *Futur. Med Chem*. **2**, 81–92

47. Brown, A. M., Hoopes, S. L., White, R. H., and Sarisky, C. A. (2011) Purine biosynthesis in archaea: variations on a theme. *Biol. Direct*. **6**, 63

48. Brox, L. W., and Hampton, A. (1968) Inosine 5'-phosphate dehydrogenase. Kinetic mechanism and evidence for selective reaction of the 6-chloro analog of inosine 5'-phosphate with a cysteine residue at the inosine 5'-phosphate site. *Biochemistry*. **7**, 2589–96

49. Brox, L. W., and Hampton, A. (1968) Inactivation of guanosine 5'-phosphate reductase by 6-chloro-, 6-mercapto-, and 2-amino-6-mercapto-9-β-D-ribofuranosylpurine 5'-phosphates. *Biochemistry*. **7**, 398–406

50. Buey, R. M., Fernández-Justel, D., Marcos-Alcalde, Í., Winter, G., Gómez-Puertas, P., de Pereda, J. M., and Luis Revuelta, J. (2017) A nucleotide-controlled conformational switch modulates the activity of eukaryotic IMP dehydrogenases. *Sci. Rep.* **7**, 2648

51. Buey, R. M., Ledesma-Amaro, R., Velázquez-Campoy, A., Balsera, M., Chagoyen, M., de Pereda, J. M., and Revuelta, J. L. (2015) Guanine nucleotide binding to the Bateman domain mediates the allosteric inhibition of eukaryotic IMP dehydrogenases. *Nat. Commun.* **6**, 8923

52. Bult, C. J., White, O., Olsen, G. J., Zhou, L., Fleischmann, R. D., Sutton, G. G., Blake, J. A., FitzGerald, L. M., Clayton, R. A., Gocayne, J. D., Kerlavage, A. R., Dougherty, B. A., Tomb, J. F., Adams, M. D., Reich, C. I., Overbeek, R., Kirkness, E. F., Weinstock, K. G., Merrick, J. M., Glodek, A., Scott, J. L., Geoghagen, N. S., and Venter, J. C. (1996) Complete genome sequence of the methanogenic archaeon, Methanococcus jannaschii. *Science*. **273**, 1058–73

53. Bulusu, V., Srinivasan, B., Bopanna, M. P., and Balaram, H. (2009) Elucidation of the substrate specificity, kinetic and catalytic mechanism of adenylosuccinate lyase from Plasmodium falciparum. *Biochim. Biophys. Acta*. **1794**, 642–54

54. Bunnik, E. M., Chung, D. W., Hamilton, M., Ponts, N., Saraf, A., Prudhomme, J., Florens, L., and Le Roch, K. G. (2013) Polysome profiling reveals translational control of gene expression in the human malaria parasite Plasmodium falciparum. *Genome Biol*. **14**, R128

55. Burgess, R. R., and Jendrisak, J. J. (1975) A procedure for the rapid, large-scall purification of Escherichia coli DNA-dependent RNA polymerase involving Polymin P precipitation and DNA-cellulose chromatography. *Biochemistry*. **14**, 4634–8

56. Bushell, E., Gomes, A. R., Sanderson, T., Anar, B., Girling, G., Herd, C., Metcalf, T., Modrzynska, K., Schwach, F., Martin, R. E., Mather, M. W., McFadden, G. I., Parts, L., Rutledge, G. G., Vaidya, A. B., Wengelnik, K., Rayner, J. C., and Billker, O. (2017) Functional Profiling of a Plasmodium Genome Reveals an Abundance of Essential Genes. *Cell*. **170**, 260–272.e8

57. Calise, S. J., Abboud, G., Kasahara, H., Morel, L., and Chan, E. K. L. (2018) Immune Response-Dependent Assembly of IMP Dehydrogenase Filaments. *Front. Immunol.* **9**, 2789

58. Calise, S. J., Keppeke, G. D., Andrade, L. E. C., and Chan, E. K. L. (2015) Anti-rods/rings: a human model of drug-induced autoantibody generation. *Front. Immunol.* **6**, 41

59. Calise, S. J., Carcamo, W. C., Krueger, C., Yin, J. D., Purich, D. L., and Chan, E. K. L. (2014) Glutamine deprivation initiates reversible assembly of mammalian rods and rings. *Cell. Mol. Life Sci.* **71**, 2963–2973

60. Carcamo, W. C., Calise, S. J., von Mühlen, C. A., Satoh, M., and Chan, E. K. L. (2014) Molecular Cell Biology and Immunobiology of Mammalian Rod/Ring Structures. in *International review of cell and molecular biology*, pp. 35–74, **308**, 35–74

61. Carcamo, W. C., Satoh, M., Kasahara, H., Terada, N., Hamazaki, T., Chan, J. Y. F., Yao, B., Tamayo, S., Covini, G., von Mühlen, C. A., and Chan, E. K. L. (2011) Induction of Cytoplasmic Rods and Rings Structures by Inhibition of the CTP and GTP Synthetic Pathway in Mammalian Cells. *PLoS One*. **6**, e29690

62. Carlton, J. M., Hirt, R. P., Silva, J. C., Delcher, A. L., Schatz, M., Zhao, Q., Wortman, J. R., Bidwell, S. L., Alsmark, U. C. M., Besteiro, S., Sicheritz-Ponten, T., Noel, C. J., Dacks, J. B., Foster, P. G., Simillion, C., Van de Peer, Y., Miranda-Saavedra, D., Barton, G. J., Westrop, G. D., Muller, S., Dessi, D., Fiori, P. L., Ren, Q., Paulsen, I., Zhang, H., Bastida-Corcuera, F. D., Simoes-Barbosa, A., Brown, M. T., Hayes, R. D., Mukherjee, M., Okumura, C. Y., Schneider, R., Smith, A. J., Vanacova, S., Villalvazo, M., Haas, B. J., Pertea, M., Feldblyum, T. V., Utterback, T. R., Shu, C.-L., Osoegawa, K., de Jong, P. J., Hrdy, I., Horvathova, L., Zubacova, Z., Dolezal, P., Malik, S.-B., Logsdon, J. M., Henze, K., Gupta, A., Wang, C. C., Dunne, R. L., Upcroft, J. A., Upcroft, P., White, O., Salzberg, S. L., Tang, P., Chiu, C.-H., Lee, Y.-S., Embley, T. M., Coombs, G. H., Mottram, J. C., Tachezy, J., Fraser-Liggett, C. M., and Johnson, P. J. (2007) Draft Genome Sequence of the Sexually Transmitted Pathogen Trichomonas vaginalis. *Science (80-.).* **315**, 207–212

63. Caro, F., Ahyong, V., Betegon, M., and DeRisi, J. L. (2014) Genome-wide regulatory dynamics of translation in the Plasmodium falciparum asexual blood stages. *Elife*. 10.7554/eLife.04106

64. Carr, S. F., Papp, E., Wu, J. C., and Natsumeda, Y. (1993) Characterization of human type I and type II IMP dehydrogenases. *J. Biol. Chem.* **268**, 27286–90
65. Cassera, M. B., Hazleton, K. Z., Merino, E. F., Obaldia, N., Ho, M.-C., Murkin, A. S., DePinto, R., Gutierrez, J. A., Almo, S. C., Evans, G. B., Babu, Y. S., and Schramm, V. L. (2011) Plasmodium falciparum Parasites Are Killed by a Transition State Analogue of Purine Nucleoside Phosphorylase in a Primate Animal Model. *PLoS One*. **6**, e26916
66. Cassera, M. B., Hazleton, K. Z., Riegelhaupt, P. M., Merino, E. F., Luo, M., Akabas, M. H., and Schramm, V. L. (2008) Erythrocytic Adenosine Monophosphate as an Alternative Purine Source in *Plasmodium falciparum*. *J Biol Chem*. **283**, 32889–32899
67. Catanzariti, A.-M., Soboleva, T. A., Jans, D. A., Board, P. G., and Baker, R. T. (2004) An efficient system for high-level expression and easy purification of authentic recombinant proteins. *Protein Sci*. **13**, 1331–1339
68. Chang, C.-C., Lin, W.-C., Pai, L.-M., Lee, H.-S., Wu, S.-C., Ding, S.-T., Liu, J.-L., and Sung, L.-Y. (2015) Cytoophidium assembly reflects upregulation of IMPDH activity. *J. Cell Sci.* **128**, 3550–3555
69. Chen, K., Zhang, J., Tastan, Ö. Y., Deussen, Z. A., Siswick, M. Y.-Y., and Liu, J.-L. (2011) Glutamine analogs promote cytoophidium assembly in human and Drosophila cells. *J. Genet. Genomics*. **38**, 391–402
70. Chen, L., Petrelli, R., Olesiak, M., Wilson, D. J., Labello, N. P., and Pankiewicz, K. W. (2008) Bis(sulfonamide) isosters of mycophenolic adenine dinucleotide analogues: Inhibition of inosine monophosphate dehydrogenase. *Bioorg Med Chem*. **16**, 7462–7469
71. Chen, L., Wilson, D., Jayaram, H. N., and Pankiewicz, K. W. (2007) Dual Inhibitors of Inosine Monophosphate Dehydrogenase and Histone Deacetylases for Cancer Treatment. *J Med Chem*. **50**, 6685–6691
72. Cheung, P. C., Salt, I. P., Davies, S. P., Hardie, D. G., and Carling, D. (2000) Characterization of AMP-activated protein kinase gamma-subunit isoforms and their role in AMP binding. *Biochem. J.* **346 Pt 3**, 659–69
73. Chong, C. R., Qian, D. Z., Pan, F., Wei, Y., Pili, R., Sullivan, D. J., Liu, J. O., Sullivan, D. J., and Liu, J. O. (2006) Identification of Type 1 Inosine Monophosphate Dehydrogenase as an Antiangiogenic Drug Target. **49**, 2677–2680
74. Chu, E., and Allegra, C. J. (1996) The role of thymidylate synthase in cellular regulation. *Adv. Enzyme Regul.* **36**, 143–63
75. Cleiren, E., Bénichou, O., Van Hul, E., Gram, J., Bollerslev, J., Singer, F. R., Beaverson, K., Aledo, A., Whyte, M. P., Yoneyama, T., deVernejoul, M.-C., and Van Hul, W. (2001) Albers-Schonberg disease (autosomal dominant osteopetrosis, type II) results from mutations in the ClCN7 chloride channel gene. *Hum. Mol. Genet.* **10**, 2861–2867
76. Climent, J., Morandeira, F., Castellote, J., Xiol, J., Niubó, J., Calatayud, L., Mestre, M., and Bas, J. (2016) Clinical correlates of the "rods and rings" antinuclear antibody pattern. *Autoimmunity*. **49**, 102–108
77. Cobbold, S. A., Santos, J. M., Ochoa, A., Perlman, D. H., and Llinas, M. (2016) Proteome-wide analysis reveals widespread lysine acetylation of major protein complexes in the malaria parasite. *Sci Rep*. **6**, 19722

78. Cole, S. T., Brosch, R., Parkhill, J., Garnier, T., Churcher, C., Harris, D., Gordon, S. V., Eiglmeier, K., Gas, S., Barry, C. E., Tekaia, F., Badcock, K., Basham, D., Brown, D., Chillingworth, T., Connor, R., Davies, R., Devlin, K., Feltwell, T., Gentles, S., Hamlin, N., Holroyd, S., Hornsby, T., Jagels, K., Krogh, A., McLean, J., Moule, S., Murphy, L., Oliver, K., Osborne, J., Quail, M. A., Rajandream, M.-A., Rogers, J., Rutter, S., Seeger, K., Skelton, J., Squares, R., Squares, S., Sulston, J. E., Taylor, K., Whitehead, S., and Barrell, B. G. (1998) Deciphering the biology of Mycobacterium tuberculosis from the complete genome sequence. *Nature*. **393**, 537–544

79. Collart, F. R., Chubb, C. B., Mirkin, B. L., and Huberman, E. (1992) Increased inosine-5'-phosphate dehydrogenase gene expression in solid tumor tissues and tumor cell lines. *Cancer Res.* **52**, 5826–8

80. Collart, F. R., and Huberman, E. (1990) Expression of IMP dehydrogenase in differentiating HL-60 cells. *Blood*. **75**, 570–6

81. Collart, F. R., and Huberman, E. (1988) Cloning and sequence analysis of the human and Chinese hamster inosine-5'-monophosphate dehydrogenase cDNAs. *J. Biol. Chem.* **263**, 15769–72

82. Collins, M. O., Wright, J. C., Jones, M., Rayner, J. C., and Choudhary, J. S. (2014) Confident and sensitive phosphoproteomics using combinations of collision induced dissociation and electron transfer dissociation. *J Proteomics*. **103**, 1–14

83. Collins, S. R., Kemmeren, P., Zhao, X.-C., Greenblatt, J. F., Spencer, F., Holstege, F. C. P., Weissman, J. S., and Krogan, N. J. (2007) Toward a Comprehensive Atlas of the Physical Interactome of *Saccharomyces cerevisiae*. *Mol. Cell. Proteomics*. **6**, 439–450

84. Cooney, D. A., Jayaram, H. N., Gebeyehu, G., Betts, C. R., Kelley, J. A., Marquez, V. E., and Johns, D. G. (1982) The conversion of 2-beta-D-ribofuranosylthiazole-4-carboxamide to an analogue of NAD with potent IMP dehydrogenase-inhibitory properties. *Biochem. Pharmacol.* **31**, 2133–6

85. Cornuel, J. F., Moraillon, A., and Guéron, M. (2002) Participation of yeast inosine 5'-monophosphate dehydrogenase in an in vitro complex with a fragment of the C-rich telomeric strand. *Biochimie*. **84**, 279–89

86. Cossins, E. A., and Chen, L. (1997) Folates and one-carbon metabolism in plants and fungi. *Phytochemistry*. **45**, 437–52

87. Crompton, P. D., Kayala, M. A., Traore, B., Kayentao, K., Ongoiba, A., Weiss, G. E., Molina, D. M., Burk, C. R., Waisberg, M., Jasinskas, A., Tan, X., Doumbo, S., Doumtabe, D., Kone, Y., Narum, D. L., Liang, X., Doumbo, O. K., Miller, L. H., Doolan, D. L., Baldi, P., Felgner, P. L., and Pierce, S. K. (2010) A prospective analysis of the Ab response to Plasmodium falciparum before and after a malaria season by protein microarray. *Proc Natl Acad Sci U S A.* **107**, 6958–6963

88. Crotty, S., Cameron, C. E., and Andino, R. (2001) RNA virus error catastrophe: Direct molecular test by using ribavirin. *Proc. Natl. Acad. Sci.* **98**, 6895–6900

89. Daniel, T., and Carling, D. (2002) Functional Analysis of Mutations in the γ_2 Subunit of AMP-activated Protein Kinase Associated with Cardiac Hypertrophy and Wolff-Parkinson-White Syndrome. *J. Biol. Chem.* **277**, 51017–51024

90. Date, S. V, and Stoeckert C. J., J. (2006) Computational modeling of the Plasmodium falciparum interactome reveals protein function on a genome-wide scale. *Genome Res*. **16**, 542–549
91. Datsenko, K. A., and Wanner, B. L. (2000) One-step inactivation of chromosomal genes in Escherichia coli K-12 using PCR products. *Proc Natl Acad Sci U S A*. **97**, 6640–6645
92. De Haan, P. G., Hoekstra, W. P., Verhoef, C., and Felix, H. S. Recombination in Escherichia coli. 3. Mapping by the gradient of transmission. *Mutat Res*. **8**, 505–12
93. Deitsch, K. W., Driskill, C. L., and Wellems, T. E. (2001) Transformation of malaria parasites by the spontaneous uptake and expression of DNA from human erythrocytes. 10.1093/nar/29.3.850
94. Deng, Y., Wang, Z., Ying, K., Gu, S., Ji, C., Huang, Y., Gu, X., Wang, Y., Xu, Y., Li, Y., Xie, Y., and Mao, Y. (2002) NADPH-dependent GMP reductase isoenzyme of human (GMPR2). Expression, purification, and kinetic properties. *Int J Biochem Cell Biol*. **34**, 1035–50
95. Digits, J. A., and Hedstrom, L. (1999) Kinetic mechanism of Tritrichomonas foetus inosine 5 ’-monophosphate dehydrogenase. *Biochemistry*. **38**, 2295–2306
96. Digits, J. A., and Hedstrom*, L. (2000) Drug Selectivity Is Determined by Coupling Across the NAD+ Site of IMP Dehydrogenase†. *Biochemistry*. **39**, 1771–1777
97. Dobie, F., Berg, A., Boitz, J. M., and Jardim, A. (2007) Kinetic characterization of inosine monophosphate dehydrogenase of Leishmania donovani. *Mol Biochem Parasitol*. **152**, 11–21
98. Duong-Ly, K. C., Kuo, Y.-M., Johnson, M. C., Cote, J. M., Kollman, J. M., Soboloff, J., Rall, G. F., Andrews, A. J., and Peterson, J. R. (2018) T cell activation triggers reversible inosine-5′-monophosphate dehydrogenase assembly. *J. Cell Sci.* **131**, jcs223289
99. El-Manzalawy, Y., Munoz, E. E., Lindner, S. E., and Honavar, V. (2016) PlasmoSEP: Predicting surface-exposed proteins on the malaria parasite using semisupervised self-training and expert-annotated data. *Proteomics*. **16**, 2967–2976
100. Ereno-Orbea, J., Oyenarte, I., and Martinez-Cruz, L. A. (2013) CBS domains: Ligand binding sites and conformational variability. *Arch Biochem Biophys*. **540**, 70–81
101. Eriksson, B., Helgstrand, E., Johansson, N. G., Larsson, A., Misiorny, A., Norén, J. O., Philipson, L., Stenberg, K., Stening, G., Stridh, S., and Oberg, B. (1977) Inhibition of influenza virus ribonucleic acid polymerase by ribavirin triphosphate. *Antimicrob. Agents Chemother.* **11**, 946–51
102. Estévez, R., Pusch, M., Ferrer-Costa, C., Orozco, M., and Jentsch, T. J. (2004) Functional and structural conservation of CBS domains from CLC chloride channels. *J. Physiol.* **557**, 363–378
103. Faesen, A. C., Dirac, A. M. G., Shanmugham, A., Ovaa, H., Perrakis, A., and Sixma, T. K. (2011) Mechanism of USP7/HAUSP Activation by Its C-Terminal Ubiquitin-like Domain and Allosteric Regulation by GMP-Synthetase. *Mol. Cell*. **44**, 147–159
104. Fernandez-Escamilla, A.-M., Rousseau, F., Schymkowitz, J., and Serrano, L. (2004) Prediction of sequence-dependent and mutational effects on the aggregation of peptides and proteins. *Nat Biotechnol*. **22**, 1302–1306

105. Fields, P. A. (2001) Review: Protein function at thermal extremes: balancing stability and flexibility. *Comp Biochem Physiol A Mol Integr Physiol*. **129**, 417–431
106. Finkelstein, J. D. (1998) The metabolism of homocysteine: pathways and regulation. *Eur. J. Pediatr.* **157 Suppl 2**, S40-4
107. Fleischmann, R. D., Adams, M. D., White, O., Clayton, R. A., Kirkness, E. F., Kerlavage, A. R., Bult, C. J., Tomb, J. F., Dougherty, B. A., and Merrick, J. M. (1995) Whole-genome random sequencing and assembly of Haemophilus influenzae Rd. *Sci.* . **269**, 496–512
108. Florens, L., Liu, X., Wang, Y., Yang, S., Schwartz, O., Peglar, M., Carucci, D. J., Yates J. R., 3rd, and Wu, Y. (2004) Proteomics approach reveals novel proteins on the surface of malaria-infected erythrocytes. *Mol Biochem Parasitol*. **135**, 1–11
109. Florens, L., Washburn, M. P., Raine, J. D., Anthony, R. M., Grainger, M., Haynes, J. D., Moch, J. K., Muster, N., Sacci, J. B., Tabb, D. L., Witney, A. A., Wolters, D., Wu, Y., Gardner, M. J., Holder, A. A., Sinden, R. E., Yates, J. R., and Carucci, D. J. (2002) A proteomic view of the Plasmodium falciparum life cycle. *Nature*. **419**, 520–526
110. Floryk, D., and Huberman, E. (2006) Mycophenolic acid-induced replication arrest, differentiation markers and cell death of androgen-independent prostate cancer cells DU145. *Cancer Lett*. **231**, 20–29
111. Floryk, D., Tollaksen, S. L., Giometti, C. S., and Huberman, E. (2004) Differentiation of Human Prostate Cancer PC-3 Cells Induced by Inhibitors of Inosine 5′-Monophosphate Dehydrogenase. *Cancer Res*. **64**, 9049–9056
112. Franklin, T. J., Jacobs, V., Jones, G., Plé, P., and Bruneau, P. (1996) Glucuronidation associated with intrinsic resistance to mycophenolic acid in human colorectal carcinoma cells. *Cancer Res*. **56**, 984–7
113. Frappier, L., and Verrijzer, C. P. (2011) Gene expression control by protein deubiquitinases. *Curr. Opin. Genet. Dev.* **21**, 207–213
114. Fraser, C. M., Gocayne, J. D., White, O., Adams, M. D., Clayton, R. A., Fleischmann, R. D., Bult, C. J., Kerlavage, A. R., Sutton, G., Kelley, J. M., Fritchman, R. D., Weidman, J. F., Small, K. V, Sandusky, M., Fuhrmann, J., Nguyen, D., Utterback, T. R., Saudek, D. M., Phillips, C. A., Merrick, J. M., Tomb, J. F., Dougherty, B. A., Bott, K. F., Hu, P. C., Lucier, T. S., Peterson, S. N., Smith, H. O., Hutchison, C. A., and Venter, J. C. (1995) The minimal gene complement of Mycoplasma genitalium. *Sci.* . **270**, 397–403
115. Fridland, A., Connelly, M. C., and Robbins, T. J. (1986) Tiazofurin metabolism in human lymphoblastoid cells: evidence for phosphorylation by adenosine kinase and 5'-nucleotidase. *Cancer Res.* **46**, 532–7
116. Fuhrmann, M., Hausherr, A., Ferbitz, L., Schödl, T., Heitzer, M., and Hegemann, P. (2004) Monitoring dynamic expression of nuclear genes in Chlamydomonas reinhardtii by using a synthetic luciferase reporter gene. *Plant Mol Biol*. **55**, 869–881
117. Gan, L., Petsko, G. A., and Hedstrom, L. (2002) Crystal structure of a ternary complex of Tritrichomonas foetus inosine 5'-monophosphate dehydrogenase: NAD+ orients the active site loop for catalysis. *Biochemistry*. **41**, 13309–17
118. Gan, L., Seyedsayamdost, M. R., Shuto, S., Matsuda, A., Petsko, G. A., and Hedstrom, L. (2003) The Immunosuppressive Agent Mizoribine Monophosphate Forms a Transition

State Analogue Complex with Inosine Monophosphate Dehydrogenase †. *Biochemistry*. **42**, 857–863

119. Garber, B. B., Jochimsen, B. U., and Gots, J. S. (1980) Glutamine and related analogs regulate guanosine monophosphate reductase in Salmonella typhimurium. *J Bacteriol*. **143**, 105–11

120. .Gardner, M. J., Hall, N., Fung, E., White, O., Berriman, M., Hyman, R. W., Carlton, J. M., Pain, A., Nelson, K. E., Bowman, S., Paulsen, I. T., James, K., Eisen, J. A., Rutherford, K., Salzberg, S. L., Craig, A., Kyes, S., Chan, M.-S., Nene, V., Shallom, S. J., Suh, B., Peterson, J., Angiuoli, S., Pertea, M., Allen, J., Selengut, J., Haft, D., Mather, M. W., Vaidya, A. B., Martin, D. M. A., Fairlamb, A. H., Fraunholz, M. J., Roos, D. S., Ralph, S. A., McFadden, G. I., Cummings, L. M., Subramanian, G. M., Mungall, C., Venter, J. C., Carucci, D. J., Hoffman, S. L., Newbold, C., Davis, R. W., Fraser, C. M., and Barrell, B. (2002) Genome sequence of the human malaria parasite Plasmodium falciparum. *Nature*. **419**, 498–511

121. Gaspar, P., Oliveira, J. L., Frommlet, J., Santos, M. A. S., and Moura, G. (2012) EuGene: maximizing synthetic gene design for heterologous expression. *Bioinformatics*. **28**, 2683–2684

122. Gharehbaghi, K., Sreenath, A., Hao, Z., Paull, K. D., Szekeres, T., Cooney, D. A., Krohn, K., and Jayaram, H. N. (1994) Comparison of biochemical parameters of benzamide riboside, a new inhibitor of IMP dehydrogenase, with tiazofurin and selenazofurin. *Biochem. Pharmacol.* **48**, 1413–9

123. Gilbert, H. J., and Drabble, W. T. (1980) Active-site modification of native and mutant forms of inosine 5'-monophosphate dehydrogenase from Escherichia coli K12. *Biochem. J.* **191**, 533–41

124. Gish, R. G. (2006) Treating HCV with ribavirin analogues and ribavirin-like molecules. *J. Antimicrob. Chemother.* **57**, 8–13

125. Gollob, M. H., Seger, J. J., Gollob, T. N., Tapscott, T., Gonzales, O., Bachinski, L., and Roberts, R. (2001) Novel PRKAG2 mutation responsible for the genetic syndrome of ventricular preexcitation and conduction system disease with childhood onset and absence of cardiac hypertrophy. *Circulation*. **104**, 3030–3

126. Gollob, M. H., Green, M. S., Tang, A. S.-L., Gollob, T., Karibe, A., Hassan, A.-S., Ahmad, F., Lozado, R., Shah, G., Fananapazir, L., Bachinski, L. L., Tapscott, T., Gonzales, O., Begley, D., Mohiddin, S., and Roberts, R. (2001) Identification of a Gene Responsible for Familial Wolff–Parkinson–White Syndrome. *N. Engl. J. Med.* **344**, 1823–1831

127. Gorla, S. K., Kavitha, M., Zhang, M., Liu, X., Sharling, L., Gollapalli, D. R., Striepen, B., Hedstrom, L., and Cuny, G. D. (2012) Selective and Potent Urea Inhibitors of Cryptosporidium parvum Inosine 5′-Monophosphate Dehydrogenase. *J. Med. Chem.* **55**, 7759–7771

128. Gou, K.-M., Chang, C.-C., Shen, Q.-J., Sung, L.-Y., and Liu, J.-L. (2014) CTP synthase forms cytoophidia in the cytoplasm and nucleus. *Exp. Cell Res.* **323**, 242–253

129. Gross, S. S., and Levi, R. (1992) Tetrahydrobiopterin synthesis. An absolute requirement for cytokine-induced nitric oxide generation by vascular smooth muscle. *J. Biol. Chem.* **267**, 25722–9

130. Guddat, L. W., Vos, S., Martin, J. L., Keough, D. T., and de Jersey, J. (2002) Crystal structures of free, IMP-, and GMP-bound Escherichia coli hypoxanthine phosphoribosyltransferase. *Protein Sci*. **11**, 1626–1638

131. Guillén Schlippe, Y. V., and Hedstrom, L. (2005) Guanidine Derivatives Rescue the Arg418Ala Mutation of *Tritrichomonas foetus* IMP Dehydrogenase †. *Biochemistry*. **44**, 16695–16700

132. Guillén Schlippe, Y. V., Riera, T. V., Seyedsayamdost, M. R., and Hedstrom, L. (2004) Substitution of the Conserved Arg-Tyr Dyad Selectively Disrupts the Hydrolysis Phase of the IMP Dehydrogenase Reaction †. *Biochemistry*. **43**, 4511–4521

133. Hall, N., Pain, A., Berriman, M., Churcher, C., Harris, B., Harris, D., Mungall, K., Bowman, S., Atkin, R., Baker, S., Barron, A., Brooks, K., Buckee, C. O., Burrows, C., Cherevach, I., Chillingworth, C., Chillingworth, T., Christodoulou, Z., Clark, L., Clark, R., Corton, C., Cronin, A., Davies, R., Davis, P., Dear, P., Dearden, F., Doggett, J., Feltwell, T., Goble, A., Goodhead, I., Gwilliam, R., Hamlin, N., Hance, Z., Harper, D., Hauser, H., Hornsby, T., Holroyd, S., Horrocks, P., Humphray, S., Jagels, K., James, K. D., Johnson, D., Kerhornou, A., Knights, A., Konfortov, B., Kyes, S., Larke, N., Lawson, D., Lennard, N., Line, A., Maddison, M., McLean, J., Mooney, P., Moule, S., Murphy, L., Oliver, K., Ormond, D., Price, C., Quail, M. A., Rabbinowitsch, E., Rajandream, M.-A., Rutter, S., Rutherford, K. M., Sanders, M., Simmonds, M., Seeger, K., Sharp, S., Smith, R., Squares, R., Squares, S., Stevens, K., Taylor, K., Tivey, A., Unwin, L., Whitehead, S., Woodward, J., Sulston, J. E., Craig, A., Newbold, C., and Barrell, B. G. (2002) Sequence of Plasmodium falciparum chromosomes 1, 3–9 and 13. *Nature*. **419**, 527–531

134. . Hamilton, S. R., Stapleton, D., O'Donnell, J. B., Kung, J. T., Dalal, S. R., Kemp, B. E., and Witters, L. A. (2001) An activating mutation in the gamma1 subunit of the AMP-activated protein kinase. *FEBS Lett.* **500**, 163–8

135. HAMPTON, A. (1963) REACTIONS OF RIBONUCLEOTIDE DERIVATIVES OF PURINE ANALOGUES AT THE CATALYTIC SITE OF INOSINE 5'-PHOSPHATE DEHYDROGENASE. *J. Biol. Chem.* **238**, 3068–74

136. Hansen, A. K., and Moran, N. A. (2011) Aphid genome expression reveals host-symbiont cooperation in the production of amino acids. *Proc Natl Acad Sci U S A*. **108**, 2849–2854

137. Hansen, B. G., Genee, H. J., Kaas, C. S., Nielsen, J. B., Regueira, T. B., Mortensen, U. H., Frisvad, J. C., and Patil, K. R. (2011) A new class of IMP dehydrogenase with a role in self-resistance of mycophenolic acid producing fungi. *BMC Microbiol*. **11**, 202

138. Han-Zhong Zhang, †, Kotesvar Rao, †, Stephen F. Carr, ‡, Eva Papp, ‡, Kenneth Straub, ‡, John C. Wu, ‡, § and, and Josef Fried*, † (1997) Rationally Designed Inhibitors of Inosine Monophosphate Dehydrogenase∇. *J. Med. Chem.* **40**, 4–8

139. Hardie, D. G., and Hawley, S. A. (2001) AMP-activated protein kinase: the energy charge hypothesis revisited. *BioEssays*. **23**, 1112–1119

140. Hattori, M., Iwase, N., Furuya, N., Tanaka, Y., Tsukazaki, T., Ishitani, R., Maguire, M. E., Ito, K., Maturana, A., and Nureki, O. (2009) Mg(2+)-dependent gating of bacterial MgtE channel underlies Mg(2+) homeostasis. *Embo j*. **28**, 3602–3612

141. Hattori, M., Tanaka, Y., Fukai, S., Ishitani, R., and Nureki, O. (2007) Crystal structure of the MgtE Mg2+ transporter. *Nature*. **448**, 1072–1075

142. Hedstrom L. (1999) IMP Dehydrogenase: Mechanism of Action and Inhibiton. *Curr. Med. Chem.* **6**, 545–560

143. Hedstrom, L., Cheung, K. S., and Wang, C. C. (1990) A novel mechanism of mycophenolic acid resistance in the protozoan parasite Tritrichomonas foetus. *Biochem. Pharmacol.* **39**, 151–60

144. Hedstrom, L., Liechti, G., Goldberg, J. B., and Gollapalli, D. R. (2011) The antibiotic potential of prokaryotic IMP dehydrogenase inhibitors. *Curr. Med. Chem.* **18**, 1909–18

145. Hedstrom, L. (2012) The dynamic determinants of reaction specificity in the IMPDH/GMPR family of (β/α)(8) barrel enzymes. *Crit. Rev. Biochem. Mol. Biol.* **47**, 250–63

146. Hedstrom, L. (2009) IMP Dehydrogenase: Structure, Mechanism, and Inhibition. *Chem. Rev.* **109**, 2903–2928

147. Henikoff, S., and Smith, J. M. (1989) The human mRNA that provides the N-terminus of chimeric G6PD encodes GMP reductase. *Cell*. **58**, 1021–2

148. Heyde, E., Nagabhushanam, A., Vonarx, M., and Morrison, J. F. (1976) Studies on inosine monophosphate dehydrogenase. Steady state kinetics. *Biochim. Biophys. Acta*. **429**, 645–60

149. Ho, Y., Gruhler, A., Heilbut, A., Bader, G. D., Moore, L., Adams, S.-L., Millar, A., Taylor, P., Bennett, K., Boutilier, K., Yang, L., Wolting, C., Donaldson, I., Schandorff, S., Shewnarane, J., Vo, M., Taggart, J., Goudreault, M., Muskat, B., Alfarano, C., Dewar, D., Lin, Z., Michalickova, K., Willems, A. R., Sassi, H., Nielsen, P. A., Rasmussen, K. J., Andersen, J. R., Johansen, L. E., Hansen, L. H., Jespersen, H., Podtelejnikov, A., Nielsen, E., Crawford, J., Poulsen, V., Sørensen, B. D., Matthiesen, J., Hendrickson, R. C., Gleeson, F., Pawson, T., Moran, M. F., Durocher, D., Mann, M., Hogue, C. W. V., Figeys, D., and Tyers, M. (2002) Systematic identification of protein complexes in Saccharomyces cerevisiae by mass spectrometry. *Nature*. **415**, 180–183

150. Hsiao, L. L., Howard, R. J., Aikawa, M., and Taraschi, T. F. (1991) Modification of host cell membrane lipid composition by the intra-erythrocytic human malaria parasite Plasmodium falciparum. *Biochem J*. **274 (Pt 1**, 121–132

151. Hupe, D. J., Azzolina, B. A., and Behrens, N. D. (1986) IMP dehydrogenase from the intracellular parasitic protozoan Eimeria tenella and its inhibition by mycophenolic acid. *J. Biol. Chem.* **261**, 8363–9

152. Huthmacher, C., Hoppe, A., Bulik, S., and Holzhutter, H. G. (2010) Antimalarial drug targets in Plasmodium falciparum predicted by stage-specific metabolic network analysis. *BMC Syst Biol*. **4**, 120

153. Hyle, J. W., Shaw, R. J., and Reines, D. (2003) Functional distinctions between IMP dehydrogenase genes in providing mycophenolate resistance and guanine prototrophy to yeast. *J. Biol. Chem.* **278**, 28470–8

154. Ignoul, S., and Eggermont, J. (2005) CBS domains: structure, function, and pathology in human proteins. *Am. J. Physiol. Physiol.* **289**, C1369–C1378

155. Ingerson-Mahar, M., Briegel, A., Werner, J. N., Jensen, G. J., and Gitai, Z. (2010) The metabolic enzyme CTP synthase forms cytoskeletal filaments. *Nat. Cell Biol.* **12**, 739–746

156. Ingley, E., and Hemmings, B. A. (2000) PKB/Akt interacts with inosine-5' monophosphate dehydrogenase through its pleckstrin homology domain. *FEBS Lett.* **478**, 253–9

157. Ishikawa, H. (1999) Mizoribine and mycophenolate mofetil. *Curr. Med. Chem.* **6**, 575–97

158. Iwanaga, S., Kato, T., Kaneko, I., and Yuda, M. (2012) Centromere plasmid: a new genetic tool for the study of Plasmodium falciparum. *PLoS One*. **7**, e33326

159. Iwanaga, S., Khan, S. M., Kaneko, I., Christodoulou, Z., Newbold, C., Yuda, M., Janse, C. J., and Waters, A. P. (2010) Functional Identification of the Plasmodium Centromere and Generation of a Plasmodium Artificial Chromosome. *Cell Host Microbe*. **7**, 245–255

160. Jackson, R. C., Weber, G., and Morris, H. P. (1975) IMP dehydrogenase, an enzyme linked with proliferation and malignancy. *Nature*. **256**, 331–3

161. Jämsen, J., Tuominen, H., Salminen, A., Belogurov, G. A., Magretova, N. N., Baykov, A. A., and Lahti, R. (2007) A CBS domain-containing pyrophosphatase of *Moorella thermoacetica* is regulated by adenine nucleotides. *Biochem. J.* **408**, 327–333

162. Janosík, M., Kery, V., Gaustadnes, M., Maclean, K. N., and Kraus, J. P. (2001) Regulation of human cystathionine beta-synthase by S-adenosyl-L-methionine: evidence for two catalytically active conformations involving an autoinhibitory domain in the C-terminal region. *Biochemistry*. **40**, 10625–33

163. Jayaram, H. N., Gharehbaghi, K., Jayaram, N. H., Rieser, J., Krohn, K., and Paull, K. D. (1992) Cytotoxicity of a new IMP dehydrogenase inhibitor, benzamide riboside, to human myelogenous leukemia K562 cells. *Biochem. Biophys. Res. Commun.* **186**, 1600–6

164. Jayaram, H., Yalowitz, J., Arguello, F., and Greene,Jr, J. (2002) Toxicity and Efficacy of Benzamide Riboside in Cancer Chemotherapy Models. *Curr. Med. Chem.* **9**, 787–792

165. Jentsch, T. J., Stein, V., Weinreich, F., and Zdebik, A. A. (2002) Molecular Structure and Physiological Function of Chloride Channels. *Physiol. Rev.* **82**, 503–568

166. Ji, Y., Gu, J., Makhov, A. M., Griffith, J. D., and Mitchell, B. S. (2006) Regulation of the Interaction of Inosine Monophosphate Dehydrogenase with Mycophenolic Acid by GTP. *J. Biol. Chem.* **281**, 206–212

167. Ji, Y., Gu, J., Makhov, A. M., Griffith, J. D., and Mitchell, B. S. (2006) Regulation of the Interaction of Inosine Monophosphate Dehydrogenase with Mycophenolic Acid by GTP. *J. Biol. Chem.* **281**, 206–212

168. Jiang, H., Patel, J. J., Yi, M., Mu, J., Ding, J., Stephens, R., Cooper, R. A., Ferdig, M. T., and Su, X. Z. (2008) Genome-wide compensatory changes accompany drug- selected mutations in the Plasmodium falciparum crt gene. *PLoS One*. **3**, e2484

169. Jones, M. L., Collins, M. O., Goulding, D., Choudhary, J. S., and Rayner, J. C. (2012) Analysis of protein palmitoylation reveals a pervasive role in Plasmodium development and pathogenesis. *Cell Host Microbe*. **12**, 246–258

170. Josephine, H. R., Ravichandran, K. R., and Hedstrom, L. (2010) The Cys319 Loop Modulates the Transition between Dehydrogenase and Hydrolase Conformations in Inosine 5′-Monophosphate Dehydrogenase. *Biochemistry*. **49**, 10674–10681

171. Kapust, R. B., and Waugh, D. S. (1999) *Escherichia coli* maltose-binding protein is uncommonly effective at promoting the solubility of polypeptides to which it is fused. *Protein Sci*. **8**, 1668–1674

172. Kasai, K., Nishizawa, T., Takahashi, K., Hosaka, T., Aoki, H., and Ochi, K. (2006) Physiological Analysis of the Stringent Response Elicited in an Extreme Thermophilic Bacterium, Thermus thermophilus. *J. Bacteriol.* **188**, 7111–7122

173. Kehr, S., Jortzik, E., Delahunty, C., Yates J. R., 3rd, Rahlfs, S., and Becker, K. (2011) Protein S-glutathionylation in malaria parasites. *Antioxid Redox Signal*. **15**, 2855–2865

174. Kennan, A., Aherne, A., Palfi, A., Humphries, M., McKee, A., Stitt, A., Simpson, D. A. C., Demtroder, K., Orntoft, T., Ayuso, C., Kenna, P. F., Farrar, G. J., and Humphries, P. (2002) Identification of an IMPDH1 mutation in autosomal dominant retinitis pigmentosa (RP10) revealed following comparative microarray analysis of transcripts derived from retinas of wild-type and Rho-/- mice. *Hum. Mol. Genet.* **11**, 547–558

175. Keppeke, G. D., Calise, S. J., Chan, E. K. L., and Andrade, L. E. C. (2015) Assembly of IMPDH2-Based, CTPS-Based, and Mixed Rod/Ring Structures Is Dependent on Cell Type and Conditions of Induction. *J. Genet. Genomics*. **42**, 287–299

176. Keppeke, G. D., Chang, C. C., Peng, M., Chen, L.-Y., Lin, W.-C., Pai, L.-M., Andrade, L. E. C., Sung, L.-Y., and Liu, J.-L. (2018) IMP/GTP balance modulates cytoophidium assembly and IMPDH activity. *Cell Div.* **13**, 5

177. Keppeke, G. D., Nunes, E., Ferraz, M. L. G., Silva, E. A. B., Granato, C., Chan, E. K. L., and Andrade, L. E. C. (2012) Longitudinal study of a human drug-induced model of autoantibody to cytoplasmic rods/rings following HCV therapy with ribavirin and interferon-α. *PLoS One*. **7**, e45392

178. Kerr, K. M., and Hedstrom, L. (1997) The Roles of Conserved Carboxylate Residues in IMP Dehydrogenase and Identification of a Transition State Analog †. *Biochemistry*. **36**, 13365–13373

179. Kessler, A. I., and Gots, J. S. (1985) Regulation of guaC expression in Escherichia coli. *J Bacteriol*. **164**, 1288–93

180. Kiguchi, K., Collart, F. R., Henning-Chubb, C., and Huberman, E. (1990) Induction of cell differentiation in melanoma cells by inhibitors of IMP dehydrogenase: altered patterns of IMP dehydrogenase expression and activity. *Cell Growth Differ*. **1**, 259–70

181. Kiguchi, K., Collart, F. R., Henning-Chubb, C., and Huberman, E. (1990) Cell differentiation and altered IMP dehydrogenase expression induced in human T-lymphoblastoid leukemia cells by mycophenolic acid and tiazofurin. *Exp Cell Res*. **187**, 47–53

182. Kim, H. S., Mittenthal, J. E., and Caetano-Anollés, G. (2006) MANET: tracing evolution of protein architecture in metabolic networks. *BMC Bioinformatics*. **7**, 351

183. Kluijtmans, L. A., Boers, G. H., Stevens, E. M., Renier, W. O., Kraus, J. P., Trijbels, F. J., van den Heuvel, L. P., and Blom, H. J. (1996) Defective cystathionine beta-synthase

regulation by S-adenosylmethionine in a partially pyridoxine responsive homocystinuria patient. *J. Clin. Invest.* **98**, 285–9

184. Köhler, G. A., White, T. C., and Agabian, N. (1997) Overexpression of a cloned IMP dehydrogenase gene of Candida albicans confers resistance to the specific inhibitor mycophenolic acid. *J. Bacteriol.* **179**, 2331–8

185. Kohler, G. A., Gong, X., Bentink, S., Theiss, S., Pagani, G. M., Agabian, N., and Hedstrom, L. (2005) The Functional Basis of Mycophenolic Acid Resistance in Candida albicans IMP Dehydrogenase. *J. Biol. Chem.* **280**, 11295–11302

186. Konno, Y., Natsumeda, Y., Nagai, M., Yamaji, Y., Ohno, S., Suzuki, K., and Weber, G. (1991) Expression of human IMP dehydrogenase types I and II in Escherichia coli and distribution in human normal lymphocytes and leukemic cell lines. *J. Biol. Chem.* **266**, 506–9

187. Konrad, M., Vollmer, M., Lemmink, H. H., van den Heuvel, L. P., Jeck, N., Vargas-Poussou, R., Lakings, A., Ruf, R., Deschenes, G., Antignac, C., Guay-Woodford, L., Knoers, N. V, Seyberth, H. W., Feldmann, D., and Hildebrandt, F. (2000) Mutations in the chloride channel gene CLCNKB as a cause of classic Bartter syndrome. *J Am Soc Nephrol*. **11**, 1449–1459

188. Kornak, U., Kasper, D., Bösl, M. R., Kaiser, E., Schweizer, M., Schulz, A., Friedrich, W., Delling, G., and Jentsch, T. J. (2001) Loss of the ClC-7 chloride channel leads to osteopetrosis in mice and man. *Cell*. **104**, 205–15

189. Kozhevnikova, E. N., van der Knaap, J. A., Pindyurin, A. V., Ozgur, Z., van Ijcken, W. F. J., Moshkin, Y. M., and Verrijzer, C. P. (2012) Metabolic Enzyme IMPDH Is Also a Transcription Factor Regulated by Cellular State. *Mol. Cell*. **47**, 133–139

190. Krissinel, E., and Henrick, K. (2007) Inference of Macromolecular Assemblies from Crystalline State. *J Mol Biol* . **372**, 774–797

191. Krogan, N. J., Peng, W.-T., Cagney, G., Robinson, M. D., Haw, R., Zhong, G., Guo, X., Zhang, X., Canadien, V., Richards, D. P., Beattie, B. K., Lalev, A., Zhang, W., Davierwala, A. P., Mnaimneh, S., Starostine, A., Tikuisis, A. P., Grigull, J., Datta, N., Bray, J. E., Hughes, T. R., Emili, A., and Greenblatt, J. F. (2004) High-definition macromolecular composition of yeast RNA-processing complexes. *Mol. Cell*. **13**, 225–39

192. Krogh, A., Larsson, B., von Heijne, G., and Sonnhammer, E. L. (2001) Predicting transmembrane protein topology with a hidden Markov model: application to complete genomes. *J Mol Biol*. **305**, 567–580

193. Kuttan, R., Robins, R. K., and Saunders, P. P. (1982) Inhibition of inosinate dehydrogenase by metabolites of 2-beta-D-ribofuranosyl thiazole-4-carboxamide. *Biochem. Biophys. Res. Commun.* **107**, 862–8

194. Labesse, G., Alexandre, T., Gelin, M., Haouz, A., and Munier-Lehmann, H. (2015) Crystallographic studies of two variants of *Pseudomonas aeruginosa* IMPDH with impaired allosteric regulation. *Acta Crystallogr. Sect. D Biol. Crystallogr.* **71**, 1890–1899

195. Labesse, G., Alexandre, T., Vaupré, L., Salard-Arnaud, I., Him, J. L. K., Raynal, B., Bron, P., and Munier-Lehmann, H. (2013) MgATP Regulates Allostery and Fiber Formation in IMPDHs. *Structure*. **21**, 975–985

196. Laemmli, U. K. (1970) Cleavage of structural proteins during the assembly of the head of bacteriophage T4. *Nature*. **227**, 680–685

197. Lambros, C., and Vanderberg, J. P. (1979) Synchronization of Plasmodium falciparum erythrocytic stages in culture. *J Parasitol*. **65**, 418–420

198. Laskowski, R. A., and Swindells, M. B. (2011) LigPlot+: Multiple Ligand–Protein Interaction Diagrams for Drug Discovery. *J. Chem. Inf. Model.* **51**, 2778–2786

199. Lasonder, E., Green, J. L., Camarda, G., Talabani, H., Holder, A. A., Langsley, G., and Alano, P. (2012) The Plasmodium falciparum schizont phosphoproteome reveals extensive phosphatidylinositol and cAMP-protein kinase A signaling. *J Proteome Res*. **11**, 5323–5337

200. Lasonder, E., Green, J. L., Grainger, M., Langsley, G., and Holder, A. A. (2015) Extensive differential protein phosphorylation as intraerythrocytic Plasmodium falciparum schizonts develop into extracellular invasive merozoites. *Proteomics*. **15**, 2716–2729

201. Lasonder, E., Janse, C. J., van Gemert, G. J., Mair, G. R., Vermunt, A. M., Douradinha, B. G., van Noort, V., Huynen, M. A., Luty, A. J., Kroeze, H., Khan, S. M., Sauerwein, R. W., Waters, A. P., Mann, M., and Stunnenberg, H. G. (2008) Proteomic profiling of Plasmodium sporozoite maturation identifies new proteins essential for parasite development and infectivity. *PLoS Pathog*. **4**, e1000195

202. Lasonder, E., Rijpma, S. R., van Schaijk, B. C., Hoeijmakers, W. A., Kensche, P. R., Gresnigt, M. S., Italiaander, A., Vos, M. W., Woestenenk, R., Bousema, T., Mair, G. R., Khan, S. M., Janse, C. J., Bartfai, R., and Sauerwein, R. W. (2016) Integrated transcriptomic and proteomic analyses of P. falciparum gametocytes: molecular insight into sex-specific processes and translational repression. *Nucleic Acids Res*. **44**, 6087–6101

203. Le Roch, K. G., Zhou, Y., Blair, P. L., Grainger, M., Moch, J. K., Haynes, J. D., De La Vega, P., Holder, A. A., Batalov, S., Carucci, D. J., and Winzeler, E. A. (2003) Discovery of gene function by expression profiling of the malaria parasite life cycle. *Science (80-.).* **301**, 1503–1508

204. Lecoq, K., Konrad, M., and Daignan-Fornier, B. (2000) Yeast GMP kinase mutants constitutively express AMP biosynthesis genes by phenocopying a hypoxanthine-guanine phosphoribosyltransferase defect. *Genetics*. **156**, 953–61

205. Ledesma-Amaro, R., Buey, R. M., and Revuelta, J. L. (2015) Increased production of inosine and guanosine by means of metabolic engineering of the purine pathway in Ashbya gossypii. *Microb. Cell Fact.* **14**, 58

206. Lesiak, K., Watanabe, K. A., Majumdar, A., Powell, J., Seidman, M., Vanderveen, K., Goldstein, B. M., and Pankiewicz, K. W. (1998) Synthesis of a Methylenebis(phosphonate) Analogue of Mycophenolic Adenine Dinucleotide: A Glucuronidation-Resistant MAD Analogue of NAD. *J Med Chem*. **41**, 618–622

207. Leyssen, P., Balzarini, J., De Clercq, E., and Neyts, J. (2005) The predominant mechanism by which ribavirin exerts its antiviral activity in vitro against flaviviruses and paramyxoviruses is mediated by inhibition of IMP dehydrogenase. *J. Virol.* **79**, 1943–7

208. Li, J., Wei, Z., Zheng, M., Gu, X., Deng, Y., Qiu, R., Chen, F., Ji, C., Gong, W., Xie, Y., and Mao, Y. (2006) Crystal structure of human guanosine monophosphate reductase 2 (GMPR2) in complex with GMP. *J. Mol. Biol.* **355**, 980–8

209. Li, Y., Li, G., Görling, B., Luy, B., Du, J., and Yan, J. (2015) Integrative analysis of circadian transcriptome and metabolic network reveals the role of de novo purine synthesis in circadian control of cell cycle. *PLoS Comput. Biol.* **11**, e1004086

210. Linding, R., Schymkowitz, J., Rousseau, F., Diella, F., and Serrano, L. (2004) A Comparative Study of the Relationship Between Protein Structure and β-Aggregation in Globular and Intrinsically Disordered Proteins. *J Mol Biol*. **342**, 345–353

211. Lindner, S. E., Swearingen, K. E., Harupa, A., Vaughan, A. M., Sinnis, P., Moritz, R. L., and Kappe, S. H. (2013) Total and putative surface proteomics of malaria parasite salivary gland sporozoites. *Mol Cell Proteomics*. **12**, 1127–1143

212. Lindstrom, D. L., Squazzo, S. L., Muster, N., Burckin, T. A., Wachter, K. C., Emigh, C. A., McCleery, J. A., Yates, J. R., and Hartzog, G. A. (2003) Dual roles for Spt5 in pre-mRNA processing and transcription elongation revealed by identification of Spt5-associated proteins. *Mol. Cell. Biol.* **23**, 1368–78

213. Link, J. O., and Straub, K. (1996) Trapping of an IMP Dehydrogenase−Substrate Covalent Intermediate by Mycophenolic Acid. *J. Am. Chem. Soc.* **118**, 2091–2092

214. Liu, H., Luo, K., and Luo, D. (2018) Guanosine monophosphate reductase 1 is a potential therapeutic target for Alzheimer's disease. **8**, 2759

215. Liu, J.-L. (2016) The Cytoophidium and Its Kind: Filamentation and Compartmentation of Metabolic Enzymes. *Annu. Rev. Cell Dev. Biol.* **32**, 349–372

216. Liu, J.-L. (2010) Intracellular compartmentation of CTP synthase in Drosophila. *J. Genet. Genomics*. **37**, 281–296

217. Liu, K., Bittner, A. N., and Wang, J. D. (2015) Diversity in (p)ppGpp metabolism and effectors. *Curr. Opin. Microbiol.* **24**, 72–79

218. Liu, Y., Bohn, S. A., and Sherley, J. L. (1998) Inosine-5'-monophosphate dehydrogenase is a rate-determining factor for p53-dependent growth regulation. *Mol. Biol. Cell*. **9**, 15–28

219. Llinas, M., Bozdech, Z., Wong, E. D., Adai, A. T., and DeRisi, J. L. (2006) Comparative whole genome transcriptome analysis of three Plasmodium falciparum strains. *Nucleic Acids Res*. **34**, 1166–1173

220. Lloyd, S. E., Gunther, W., Pearce, S. H., Thomson, A., Bianchi, M. L., Bosio, M., Craig, I. W., Fisher, S. E., Scheinman, S. J., Wrong, O., Jentsch, T. J., and Thakker, R. V (1997) Characterisation of renal chloride channel, CLCN5, mutations in hypercalciuric nephrolithiasis (kidney stones) disorders. *Hum. Mol. Genet.* **6**, 1233–9

221. Lo Conte, L., Brenner, S. E., Hubbard, T. J. P., Chothia, C., and Murzin, A. G. (2002) SCOP database in 2002: refinements accommodate structural genomics. *Nucleic Acids Res.* **30**, 264–7

222. Long, H., Cameron, S., Yu, L., and Rao, Y. (2006) *De Novo* GMP Synthesis Is Required for Axon Guidance in Drosophila. *Genetics*. **172**, 1633–1642

223. Looker, D. L., Marr, J. J., and Berens, R. L. (1986) Mechanisms of action of pyrazolopyrimidines in Leishmania donovani. *J Biol Chem*. **261**, 9412–5

224. Lopez-Barragan, M. J., Lemieux, J., Quinones, M., Williamson, K. C., Molina-Cruz, A., Cui, K., Barillas-Mury, C., Zhao, K., and Su, X. Z. (2011) Directional gene expression

and antisense transcripts in sexual and asexual stages of Plasmodium falciparum. *BMC Genomics*. **12**, 587

225. Lucas, M., Encinar, J. A., Arribas, E. A., Oyenarte, I., Garcia, I. G., Kortazar, D., Fernandez, J. A., Mato, J. M., Martinez-Chantar, M. L., and Martinez-Cruz, L. A. (2010) Binding of S-methyl-5'-thioadenosine and S-adenosyl-L-methionine to protein MJ0100 triggers an open-to-closed conformational change in its CBS motif pair. *J Mol Biol*. **396**, 800–820

226. Mackenzie, J. J., and Sorensen, L. B. (1973) Guanosine 5'-phosphate reductase of human erythrocytes. *Biochim Biophys Acta*. **327**, 282–94

227. MacPherson, I. S., Kirubakaran, S., Gorla, S. K., Riera, T. V., D'Aquino, J. A., Zhang, M., Cuny, G. D., and Hedstrom, L. (2010) The Structural Basis of Cryptosporidium-Specific IMP Dehydrogenase Inhibitor Selectivity. *jacs*. **132**, 1230–1231

228. Maduke, M., Pheasant, D. J., and Miller, C. (1999) High-level expression, functional reconstitution, and quaternary structure of a prokaryotic ClC-type chloride channel. *J. Gen. Physiol.* **114**, 713–22

229. Maduke, M., Williams, C., and Miller, C. (1998) Formation of CLC-0 Chloride Channels from Separated Transmembrane and Cytoplasmic Domains. *Biochemistry*. **37**, 1315–1321

230. MAGER, J., and MAGASANIK, B. (1960) Guanosine 5'-phosphate reductase and its role in the interconversion of purine nucleotides. *J Biol Chem*. **235**, 1474–8

231. MANDERS, E. M. M., VERBEEK, F. J., and ATEN, J. A. (1993) Measurement of co-localization of objects in dual-colour confocal images. *J. Microsc.* **169**, 375–382

232. Martinelli, L. K. B., Ducati, R. G., Rosado, L. A., Breda, A., Selbach, B. P., Santos, D. S., and Basso, L. A. (2011) Recombinant Escherichia coli GMP reductase: kinetic, catalytic and chemical mechanisms, and thermodynamics of enzyme-ligand binary complex formation. *Mol Biosyst*. **7**, 1289–305

233. Matsuda, A., Minakawa, N., Sasaki, T., and Ueda, T. (1988) The design, synthesis and antileukemic activity of 5-alkynyl-1-beta-D-ribofuranosylimidazole-4-carboxamides. *Chem. Pharm. Bull. (Tokyo)*. **36**, 2730–3

234. McConkey, G. A. (2000) Plasmodium falciparum: Isolation and Characterisation of a Gene Encoding Protozoan GMP Synthase. *Exp. Parasitol.* **94**, 23–32

235. McLean, J. E., Hamaguchi, N., Belenky, P., Mortimer, S. E., Stanton, M., and Hedstrom, L. (2004) Inosine 5'-monophosphate dehydrogenase binds nucleic acids in vitro and in vivo. *Biochem. J.* **379**, 243–51

236. McPhillips, C. C., Hyle, J. W., and Reines, D. (2004) Detection of the mycophenolate-inhibited form of IMP dehydrogenase in vivo. *Proc Natl Acad Sci U S A*. **101**, 12171–12176

237. Mehlin, C., Boni, E., Buckner, F. S., Engel, L., Feist, T., Gelb, M. H., Haji, L., Kim, D., Liu, C., Mueller, N., Myler, P. J., Reddy, J. T., Sampson, J. N., Subramanian, E., Van Voorhis, W. C., Worthey, E., Zucker, F., and Hol, W. G. J. (2006) Heterologous expression of proteins from Plasmodium falciparum: Results from 1000 genes. *Mol Biochem Parasitol*. **148**, 144–160

238. Mehrotra, S., and Balaram, H. (2007) Kinetic Characterization of Adenylosuccinate Synthetase from the Thermophilic Archaea *Methanocaldococcus jannaschii* †. *Biochemistry*. **46**, 12821–12832

239. Mei, S., Ho, A. D., and Mahlknecht, U. (2004) Role of histone deacetylase inhibitors in the treatment of cancer (Review). *Int J Oncol*. **25**, 1509–19

240. Messina, E., Gazzaniga, P., Micheli, V., Barile, L., Lupi, F., Aglianò, A. M., and Giacomello, A. (2004) Low levels of mycophenolic acid induce differentiation of human neuroblastoma cell lines. *Int J Cancer*. **112**, 352–354

241. Messina, E., Micheli, V., and Giacomello, A. (2005) Guanine nucleotide depletion induces differentiation and aberrant neurite outgrowth in human dopaminergic neuroblastoma lines: a model for basal ganglia dysfunction in Lesch–Nyhan disease. *Neurosci Lett*. **375**, 97–100

242. Micsonai, A., Wien, F., Bulyaki, E., Kun, J., Moussong, E., Lee, Y. H., Goto, Y., Refregiers, M., and Kardos, J. (2018) BeStSel: a web server for accurate protein secondary structure prediction and fold recognition from the circular dichroism spectra. *Nucleic Acids Res*. **46**, W315-w322

243. Micsonai, A., Wien, F., Kernya, L., Lee, Y.-H., Goto, Y., Réfrégiers, M., and Kardos, J. (2015) Accurate secondary structure prediction and fold recognition for circular dichroism spectroscopy. *PNAS*. **112**, E3095–E3103

244. Milan, D., Jeon, J. T., Looft, C., Amarger, V., Robic, A., Thelander, M., Rogel-Gaillard, C., Paul, S., Iannuccelli, N., Rask, L., Ronne, H., Lundström, K., Reinsch, N., Gellin, J., Kalm, E., Roy, P. L., Chardon, P., and Andersson, L. (2000) A mutation in PRKAG3 associated with excess glycogen content in pig skeletal muscle. *Science*. **288**, 1248–51

245. Miles, E. W., and Kraus, J. P. (2004) Cystathionine β-Synthase: Structure, Function, Regulation, and Location of Homocystinuria-causing Mutations. *J. Biol. Chem.* **279**, 29871–29874

246. Miller, D. V, Brown, A. M., Xu, H., Bevan, D. R., and White, R. H. (2016) Purine salvage in Methanocaldococcus jannaschii: Elucidating the role of a conserved cysteine in adenine deaminase. *Proteins*. **84**, 828–840

247. Min, D., Josephine, H. R., Li, H., Lakner, C., MacPherson, I. S., Naylor, G. J. P., Swofford, D., Hedstrom, L., and Yang, W. (2008) An Enzymatic Atavist Revealed in Dual Pathways for Water Activation. *PLoS Biol.* **6**, e206

248. Mittal, P., Brindle, J., Stephen, J., Plotkin, J. B., and Kudla, G. (2018) Codon usage influences fitness through RNA toxicity. *Proc Natl Acad Sci U S A*. **115**, 8639–8644

249. Moffat, K. G., and Mackinnon, G. (1985) Cloning of the Escherichia coli K-12 guaC gene following its transposition into the RP4::Mu cointegrate. *Gene*. **40**, 141–3

250. Moller, D. E. (2001) New drug targets for type 2 diabetes and the metabolic syndrome. *Nature*. **414**, 821–827

251. Mori, H., Iida, A., Teshiba, S., and Fujio, T. (1995) Cloning of a guanosine-inosine kinase gene of Escherichia coli and characterization of the purified gene product. *J Bacteriol*. **177**, 4921–4926

252. Morrison, H. G., McArthur, A. G., Gillin, F. D., Aley, S. B., Adam, R. D., Olsen, G. J., Best, A. A., Cande, W. Z., Chen, F., Cipriano, M. J., Davids, B. J., Dawson, S. C.,

Elmendorf, H. G., Hehl, A. B., Holder, M. E., Huse, S. M., Kim, U. U., Lasek-Nesselquist, E., Manning, G., Nigam, A., Nixon, J. E. J., Palm, D., Passamaneck, N. E., Prabhu, A., Reich, C. I., Reiner, D. S., Samuelson, J., Svard, S. G., and Sogin, M. L. (2007) Genomic Minimalism in the Early Diverging Intestinal Parasite Giardia lamblia. *Science (80-.).* **317**, 1921–1926

253. Morrow, C. A., Valkov, E., Stamp, A., Chow, E. W. L., Lee, I. R., Wronski, A., Williams, S. J., Hill, J. M., Djordjevic, J. T., Kappler, U., Kobe, B., and Fraser, J. A. (2012) De novo GTP biosynthesis is critical for virulence of the fungal pathogen Cryptococcus neoformans. *PLoS Pathog.* **8**, e1002957

254. Mortimer, S. E., Xu, D., McGrew, D., Hamaguchi, N., Lim, H. C., Bowne, S. J., Daiger, S. P., and Hedstrom, L. (2008) IMP Dehydrogenase Type 1 Associates with Polyribosomes Translating Rhodopsin mRNA. *J. Biol. Chem.* **283**, 36354–36360

255. Mortimer, S. E., and Hedstrom, L. (2005) Autosomal dominant retinitis pigmentosa mutations in inosine 5 ’-monophosphate dehydrogenase type I disrupt nucleic acid binding. *Biochem. J.* **390**, 41–47

256. Muralidharan, V., Oksman, A., Iwamoto, M., Wandless, T. J., and Goldberg, D. E. (2011) Asparagine repeat function in a Plasmodium falciparum protein assessed via a regulatable fluorescent affinity tag. *Proc. Natl. Acad. Sci. U. S. A.* **108**, 4411–6

257. Murray, A. W. (1971) The Biological Significance of Purine Salvage. *Annu. Rev. Biochem.* **40**, 811–826

258. Nagai, M., Natsumeda, Y., Konno, Y., Hoffman, R., Irino, S., and Weber, G. (1991) Selective up-regulation of type II inosine 5’-monophosphate dehydrogenase messenger RNA expression in human leukemias. *Cancer Res.* **51**, 3886–90

259. Nagai, M., Natsumeda, Y., and Weber, G. (1992) Proliferation-linked regulation of type II IMP dehydrogenase gene in human normal lymphocytes and HL-60 leukemic cells. *Cancer Res.* **52**, 258–61

260. Nagano, N., Orengo, C. A., and Thornton, J. M. (2002) One fold with many functions: the evolutionary relationships between TIM barrel families based on their sequences, structures and functions. *J. Mol. Biol.* **321**, 741–65

261. Nair, V., and Kamboj, R. C. (2003) Inhibition of inosine monophosphate dehydrogenase (IMPDH) by 2-[2-(Z)-fluorovinyl]inosine 5’-monophosphate. *Bioorg. Med. Chem. Lett.* **13**, 645–7

262. Natsumeda, Y., Ohno, S., Kawasaki, H., Konno, Y., Weber, G., and Suzuki, K. (1990) Two distinct cDNAs for human IMP dehydrogenase. *J. Biol. Chem.* **265**, 5292–5

263. Navare, A. T., Chavez, J. D., Zheng, C., Weisbrod, C. R., Eng, J. K., Siehnel, R., Singh, P. K., Manoil, C., and Bruce, J. E. (2015) Probing the protein interaction network of Pseudomonas aeruginosa cells by chemical cross-linking mass spectrometry. *Structure*. **23**, 762–773

264. Nimmesgern, E., Black, J., Futer, O., Fulghum, J. R., Chambers, S. P., Brummel, C. L., Raybuck, S. A., and Sintchak, M. D. (1999) Biochemical Analysis of the Modular Enzyme Inosine 5′-Monophosphate Dehydrogenase. *Protein Expr. Purif.* **17**, 282–289

265. Noree, C., Monfort, E., Shiau, A. K., and Wilhelm, J. E. (2014) Common regulatory control of CTP synthase enzyme activity and filament formation. *Mol. Biol. Cell*. **25**, 2282–90

266. Noree, C., Sato, B. K., Broyer, R. M., and Wilhelm, J. E. (2010) Identification of novel filament-forming proteins in *Saccharomyces cerevisiae* and *Drosophila melanogaster*. *J. Cell Biol.* **190**, 541–551

267. Novembrino, C., Aghemo, A., Ferraris Fusarini, C., Maiavacca, R., Matinato, C., Lunghi, G., Torresani, E., Ronchi, M., Garlaschi, M. C., Ramondetta, M., and Colombo, M. (2014) Interferon-ribavirin therapy induces serum antibodies determining 'rods and rings' pattern in hepatitis C patients. *J. Viral Hepat.* **21**, 944–949

268. Oehring, S. C., Woodcroft, B. J., Moes, S., Wetzel, J., Dietz, O., Pulfer, A., Dekiwadia, C., Maeser, P., Flueck, C., Witmer, K., Brancucci, N. M., Niederwieser, I., Jenoe, P., Ralph, S. A., and Voss, T. S. (2012) Organellar proteomics reveals hundreds of novel nuclear proteins in the malaria parasite Plasmodium falciparum. *Genome Biol*. **13**, R108

269. Orengo, C. A., Michie, A. D., Jones, S., Jones, D. T., Swindells, M. B., and Thornton, J. M. (1997) CATH--a hierarchic classification of protein domain structures. *Structure*. **5**, 1093–108

270. Otto, T. D., Wilinski, D., Assefa, S., Keane, T. M., Sarry, L. R., Bohme, U., Lemieux, J., Barrell, B., Pain, A., Berriman, M., Newbold, C., and Llinas, M. (2010) New insights into the blood-stage transcriptome of Plasmodium falciparum using RNA-Seq. *Mol Microbiol*. **76**, 12–24

271. Ownby, K., Xu, H., and White, R. H. (2005) A Methanocaldococcus jannaschii Archaeal Signature Gene Encodes for a 5-Formaminoimidazole-4-carboxamide-1- -D-ribofuranosyl 5'-Monophosphate Synthetase: A NEW ENZYME IN PURINE BIOSYNTHESIS. *J. Biol. Chem.* **280**, 10881–10887

272. Page, T., Jacobsen, S. J., Smejkal, R. M., Scheele, J., Nyhan, W. L., Mangum, J. H., and Robins, R. K. (1985) Studies on the mechanism of cytotoxicity of 3-deazaguanosine in human cancer cells. *Cancer chemother pharmacol*. **15**, 59–62

273. Pal, S., Bera, B., and Nair, V. (2002) Inhibition of inosine monophosphate dehydrogenase (IMPDH) by the antiviral compound, 2-vinylinosine monophosphate. *Bioorg. Med. Chem.* **10**, 3615–8

274. Pan, W., Ravot, E., Tolle, R., Frank, R., Mosbach, R., Türbachova, I., and Bujard, H. (1999) Vaccine candidate MSP-1 from Plasmodium falciparum: a redesigned 4917 bp polynucleotide enables synthesis and isolation of full-length protein from Escherichia coli and mammalian cells. *Nucleic Acids Res*. **27**, 1094–103

275. Pankiewicz, K. W., Patterson, S. E., Black, P. L., Jayaram, H. N., Risal, D., Goldstein, B. M., Stuyver, L. J., and Schinazi, R. F. (2004) Cofactor mimics as selective inhibitors of NAD-dependent inosine monophosphate dehydrogenase (IMPDH)--the major therapeutic target. *Curr Med Chem*. **11**, 887–900

276. Park, J.-H., and Ahn, S. H. (2010) IMP dehydrogenase is recruited to the transcription complex through serine 2 phosphorylation of RNA polymerase II. *Biochem. Biophys. Res. Commun.* **392**, 588–592

277. Patton, G. C., Stenmark, P., Gollapalli, D. R., Sevastik, R., Kursula, P., Flodin, S., Schuler, H., Swales, C. T., Eklund, H., Himo, F., Nordlund, P., and Hedstrom, L. (2011) Cofactor mobility determines reaction outcome in the IMPDH and GMPR (β-α)8 barrel enzymes. *Nat Chem Biol*. **7**, 950–8

278. Pease, B. N., Huttlin, E. L., Jedrychowski, M. P., Talevich, E., Harmon, J., Dillman, T., Kannan, N., Doerig, C., Chakrabarti, R., Gygi, S. P., and Chakrabarti, D. (2013) Global analysis of protein expression and phosphorylation of three stages of Plasmodium falciparum intraerythrocytic development. *J Proteome Res*. **12**, 4028–4045

279. Pelle, K. G., Oh, K., Buchholz, K., Narasimhan, V., Joice, R., Milner, D. A., Brancucci, N. M., Ma, S., Voss, T. S., Ketman, K., Seydel, K. B., Taylor, T. E., Barteneva, N. S., Huttenhower, C., and Marti, M. (2015) Transcriptional profiling defines dynamics of parasite tissue sequestration during malaria infection. *Genome Med*. **7**, 19

280. Petrovska, I., Nüske, E., Munder, M. C., Kulasegaran, G., Malinovska, L., Kroschwald, S., Richter, D., Fahmy, K., Gibson, K., Verbavatz, J.-M., and Alberti, S. (2014) Filament formation by metabolic enzymes is a specific adaptation to an advanced state of cellular starvation. *Elife*. 10.7554/eLife.02409

281. Cook PF, and Cleland WW. (2007) *Enzyme Kinetics and Mechanism*, Garland Science Publishing, New York, Ch. 6, 121-204

282. Pimkin, M., and Markham, G. D. (2008) The CBS subdomain of inosine 5′-monophosphate dehydrogenase regulates purine nucleotide turnover. *Mol. Microbiol.* **68**, 342–359

283. Pimkin, M., Pimkina, J., and Markham, G. D. (2009) A Regulatory Role of the Bateman Domain of IMP Dehydrogenase in Adenylate Nucleotide Biosynthesis. *J. Biol. Chem.* **284**, 7960–7969

284. Prosise, G. L., Wu, J. Z., and Luecke, H. (2002) Crystal Structure of *Tritrichomonas foetus* Inosine Monophosphate Dehydrogenase in Complex with the Inhibitor Ribavirin Monophosphate Reveals a Catalysis-dependent Ion-binding Site. *J. Biol. Chem.* **277**, 50654–50659

285. Pusch, M. (2002) Myotonia caused by mutations in the muscle chloride channel geneCLCN1. *Hum. Mutat.* **19**, 423–434

286. R.L. Berens, E.C. Krug, J.J. Marr, in: J.J. Marr, M. M. (Eds. . (1995) *Biochemistry and Molecular Biology of Parasites*, Elsevier, 10.1016/b978-0-12-473345-9.x5000-4

287. Raman, J., Mehrotra, S., Anand, R. P., and Balaram, H. (2004) Unique kinetic mechanism of Plasmodium falciparum adenylosuccinate synthetase. *Mol. Biochem. Parasitol.* **138**, 1–8

288. Rao, V. A., Shepherd, S. M., Owen, R., and Hunter, W. N. (2013) Structure of *Pseudomonas aeruginosa* inosine 5′-monophosphate dehydrogenase. *Acta Crystallogr. Sect. F Struct. Biol. Cryst. Commun.* **69**, 243–247

289. Reddy, B. A., van der Knaap, J. A., Bot, A. G. M., Mohd-Sarip, A., Dekkers, D. H. W., Timmermans, M. A., Martens, J. W. M., Demmers, J. A. A., and Verrijzer, C. P. (2014) Nucleotide Biosynthetic Enzyme GMP Synthase Is a TRIM21-Controlled Relay of p53 Stabilization. *Mol. Cell*. **53**, 458–470

290. Rejman, D., Olesiak, M., Chen, L., Patterson, S. E., Wilson, D., Jayaram, H. N., Hedstrom, L., and Pankiewicz, K. W. (2006) Novel Methylenephosphophosphonate Analogues of Mycophenolic Adenine Dinucleotide. Inhibition of Inosine Monophosphate Dehydrogenase. *J Med Chem*. **49**, 5018–5022

291. Renart, M. F., Renart, J., Sillero, M. A., and Sillero, A. (1976) Guanosine monophosphate reductase from Artemia salina: Inhibition by xanthosine monophosphate and activation by diguanosine tetraphosphate. *Biochemistry*. **15**, 4962–6

292. Riera, T. V., Wang, W., Josephine, H. R., and Hedstrom, L. (2008) A Kinetic Alignment of Orthologous Inosine-5′-monophosphate Dehydrogenases †. *Biochemistry*. **47**, 8689–8696

293. Riera, T. V, Zheng, L., Josephine, H. R., Min, D., Yang, W., and Hedstrom, L. (2011) Allosteric activation via kinetic control: Potassium accelerates a conformational change in IMP dehydrogenase†. *Biochemistry*. **50**, 8508–8518

294. Rio, D. C., Ares M., J., Hannon, G. J., and Nilsen, T. W. (2010) Purification of RNA using TRIzol (TRI reagent). *Cold Spring Harb Protoc*. **2010**, pdb.prot5439

295. Rivadeneira, E. M., Wasserman, M., and Espinal, C. T. (1983) Separation and concentration of schizonts of Plasmodium falciparum by Percoll gradients. *J Protozool*. **30**, 367–370

296. Robert, X., and Gouet, P. (2014) Deciphering key features in protein structures with the new ENDscript server. *Nucleic Acids Res*. **42**, W320–W324

297. Roberts, R. E., Lienhard, C. I., Gaines, C. G., Smith, J. M., and Guest, J. R. (1988) Genetic and molecular characterization of the guaC-nadC-aroP region of Escherichia coli K-12. *J Bacteriol*. **170**, 463–7

298. Rose, A. S., Bradley, A. R., Valasatava, Y., Duarte, J. M., Prlić, A., and Rose, P. W. (2018) NGL viewer: web-based molecular graphics for large complexes. *Bioinformatics*. **34**, 3755–3758

299. Rosenberg, M. M., Redfield, A. G., Roberts, M. F., and Hedstrom, L. (2018) Dynamic Characteristics of Guanosine-5′-monophosphate Reductase Complexes Revealed by High-Resolution ^{31} P Field-Cycling NMR Relaxometry. *Biochemistry*. **57**, 3146–3154

300. Rostirolla, D. C., Milech de Assunção, T., Bizarro, C. V., Basso, L. A., Santos, D. S., Assunção, T. M. de, Bizarro, C. V., Basso, L. A., Santos, D. S., Milech de Assunção, T., Bizarro, C. V., Basso, L. A., and Santos, D. S. (2014) Biochemical characterization of Mycobacterium tuberculosis IMP dehydrogenase: kinetic mechanism, metal activation and evidence of a cooperative system. *RSC Adv.* **4**, 26271–26287

301. Rovira-Graells, N., Gupta, A. P., Planet, E., Crowley, V. M., Mok, S., de Pouplana, L., Preiser, P. R., Bozdech, Z., and Cortes, A. (2012) Transcriptional variation in the malaria parasite Plasmodium falciparum. *Genome Res*. **22**, 925–938

302. Saliba, K. J., Horner, H. A., and Kirk, K. (1998) Transport and Metabolism of the Essential Vitamin Pantothenic Acid in Human Erythrocytes Infected with the Malaria ParasitePlasmodium falciparum. 10.1074/jbc.273.17.10190

303. Salvatore, D., Bartha, T., and Larsen, P. R. (1998) The guanosine monophosphate reductase gene is conserved in rats and its expression increases rapidly in brown adipose tissue during cold exposure. *J Biol Chem*. **273**, 31092–6

304. San-Miguel, T., Pérez-Bermúdez, P., and Gavidia, I. (2013) Production of soluble eukaryotic recombinant proteins in E. coli is favoured in early log-phase cultures induced at low temperature. *Springerplus*. **2**, 89

305. Sarkari, F., Sanchez-Alcaraz, T., Wang, S., Holowaty, M. N., Sheng, Y., and Frappier, L. (2009) EBNA1-Mediated Recruitment of a Histone H2B Deubiquitylating Complex to the Epstein-Barr Virus Latent Origin of DNA Replication. *PLoS Pathog.* **5**, e1000624

306. Sarwono, A. E. Y., Mitsuhashi, S., Kabir, M. H. Bin, Shigetomi, K., Okada, T., Ohsaka, F., Otsuguro, S., Maenaka, K., Igarashi, M., Kato, K., and Ubukata, M. (2019) Repurposing existing drugs: identification of irreversible IMPDH inhibitors by high-throughput screening. *J Enzym. Inhib Med Chem*. **34**, 171–178

307. Sarwono, A. E. Y., Suganuma, K., Mitsuhashi, S., Okada, T., Musinguzi, S. P., Shigetomi, K., Inoue, N., and Ubukata, M. (2017) Identification and characterization of guanosine 5′-monophosphate reductase of Trypanosoma congolense as a drug target. *Parasitol. Int.* **66**, 537–544

308. Saunders, P. P., Spindler, C. D., Tan, M. T., Alvarez, E., and Robins, R. K. (1990) Tiazofurin is phosphorylated by three enzymes from Chinese hamster ovary cells. *Cancer Res.* **50**, 5269–74

309. Schiavon, C. R., Griffin, M. E., Pirozzi, M., Parashuraman, R., Zhou, W., Jinnah, H. A., Reines, D., and Kahn, R. A. (2018) Compositional complexity of rods and rings. *Mol. Biol. Cell*. **29**, 2303–2316

310. Schindelin, J., Arganda-Carreras, I., Frise, E., Kaynig, V., Longair, M., Pietzsch, T., Preibisch, S., Rueden, C., Saalfeld, S., Schmid, B., Tinevez, J.-Y., White, D. J., Hartenstein, V., Eliceiri, K., Tomancak, P., and Cardona, A. (2012) Fiji: an open-source platform for biological-image analysis. *Nat. Methods*. **9**, 676–682

311. Schmidt-Rose, T., and Jentsch, T. J. (1997) Reconstitution of functional voltage-gated chloride channels from complementary fragments of CLC-1. *J. Biol. Chem.* **272**, 20515–21

312. Selkov, E., Maltsev, N., Olsen, G. J., Overbeek, R., and Whitman, W. B. (1997) A reconstruction of the metabolism of Methanococcus jannaschii from sequence data. *Gene*. **197**, GC11-26

313. Shan, X., Dunbrack R. L., J., Christopher, S. A., and Kruger, W. D. (2001) Mutations in the regulatory domain of cystathionine beta synthase can functionally suppress patient-derived mutations in cis. *Hum Mol Genet*. **10**, 635–643

314. Sharpe, M. L., Gao, C., Kendall, S. L., Baker, E. N., and Lott, J. S. (2008) The structure and unusual protein chemistry of hypoxic response protein 1, a latency antigen and highly expressed member of the DosR regulon in Mycobacterium tuberculosis. *J Mol Biol*. **383**, 822–836

316. Shen, Q.-J., Kassim, H., Huang, Y., Li, H., Zhang, J., Li, G., Wang, P.-Y., Yan, J., Ye, F., and Liu, J.-L. (2016) Filamentation of Metabolic Enzymes in Saccharomyces cerevisiae. *J. Genet. Genomics*. **43**, 393–404

317. Sherley, J. L. (1991) Guanine nucleotide biosynthesis is regulated by the cellular p53 concentration. *J. Biol. Chem.* **266**, 24815–28

318. Shimizu, Y., Inoue, A., Tomari, Y., Suzuki, T., Yokogawa, T., Nishikawa, K., and Ueda, T. (2001) Cell-free translation reconstituted with purified components. *Nat Biotechnol*. **19**, 751–755

319. Sievers, F., Wilm, A., Dineen, D., Gibson, T. J., Karplus, K., Li, W., Lopez, R., McWilliam, H., Remmert, M., Soding, J., Thompson, J. D., and Higgins, D. G. (2011) Fast, scalable generation of high-quality protein multiple sequence alignments using Clustal Omega. *Mol Syst Biol*. **7**, 539

320. Sievers, F., and Higgins, D. G. (2018) Clustal Omega for making accurate alignments of many protein sequences. *Protein Sci*. **27**, 135–145

321. Silvestrini, F., Lasonder, E., Olivieri, A., Camarda, G., van Schaijk, B., Sanchez, M., Younis Younis, S., Sauerwein, R., and Alano, P. (2010) Protein export marks the early phase of gametocytogenesis of the human malaria parasite Plasmodium falciparum. *Mol Cell Proteomics*. **9**, 1437–1448

322. Singh, S., Kennedy, M. C., Long, C. A., Saul, A. J., Miller, L. H., and Stowers, A. W. (2003) Biochemical and immunological characterization of bacterially expressed and refolded Plasmodium falciparum 42-kilodalton C-terminal merozoite surface protein 1. *Infect Immun*. **71**, 6766–74

323. Sintchak, M. D., Fleming, M. A., Futer, O., Raybuck, S. A., Chambers, S. P., Caron, P. R., Murcko, M. A., and Wilson, K. P. (1996) Structure and mechanism of inosine monophosphate dehydrogenase in complex with the immunosuppressant mycophenolic acid. *Cell*. **85**, 921–30

324. Sintchak, M. D., and Nimmesgern, E. (2000) The structure of inosine 5'-monophosphate dehydrogenase and the design of novel inhibitors. *Immunopharmacology*. **47**, 163–84

325. Smialowski, P., Doose, G., Torkler, P., Kaufmann, S., and Frishman, D. (2012) PROSO II - a new method for protein solubility prediction. *FEBS J.* **279**, 2192–2200

326. SMITH, R. A., and KIRKPATRICK, W. (1980) Ribavirin: a broad spectrum antiviral agent. *Ribavirin a broad Spectr. Antivir. agent.* [online] https://www.cabdirect.org/cabdirect/abstract/19812701759 (Accessed February 24, 2019)

327. Smith, S., Boitz, J., Chidambaram, E. S., Chatterjee, A., Ait-Tihyaty, M., Ullman, B., and Jardim, A. (2016) The cystathionine-beta-synthase domains on the guanosine 5''-monophosphate reductase and inosine 5'-monophosphate dehydrogenase enzymes from Leishmania regulate enzymatic activity in response to guanylate and adenylate nucleotide levels. *Mol Microbiol*. **100**, 824–840

328. Snel, B., Lehmann, G., Bork, P., and Huynen, M. A. (2000) STRING: a web-server to retrieve and display the repeatedly occurring neighbourhood of a gene. *Nucleic Acids Res*. **28**, 3442–4

329. Solyakov, L., Halbert, J., Alam, M. M., Semblat, J. P., Dorin-Semblat, D., Reininger, L., Bottrill, A. R., Mistry, S., Abdi, A., Fennell, C., Holland, Z., Demarta, C., Bouza, Y., Sicard, A., Nivez, M. P., Eschenlauer, S., Lama, T., Thomas, D. C., Sharma, P., Agarwal, S., Kern, S., Pradel, G., Graciotti, M., Tobin, A. B., and Doerig, C. (2011) Global kinomic and phospho-proteomic analyses of the human malaria parasite Plasmodium falciparum. *Nat Commun*. **2**, 565

330. Spector, T., and Jones, T. E. (1982) Guanosine 5'-monophosphate reductase from Leishmania donovani. A possible chemotherapeutic target. *Biochem Pharmacol*. **31**, 3891–7

331. Spector, T., Jones, T. E., LaFon, S. W., Nelson, D. J., Berens, R. L., and Marr, J. J. (1984) Monophosphates of formycin B and allopurinol riboside. Interactions with leishmanial and mammalian succino-AMP synthetase and GMP reductase. *Biochem Pharmacol*. **33**, 1611–7

332. Spector, T., Jones, T. E., and Miller, R. L. (1979) Reaction mechanism and specificity of human GMP reductase. Substrates, inhibitors, activators, and inactivators. *J Biol Chem*. **254**, 2308–15

333. Stapleton, D., Mitchelhill, K. I., Gao, G., Widmer, J., Michell, B. J., Teh, T., House, C. M., Fernandez, C. S., Cox, T., Witters, L. A., and Kemp, B. E. (1996) Mammalian AMP-activated protein kinase subfamily. *J. Biol. Chem.* **271**, 611–4

334. Stephens, R. W., and Whittaker, V. K. (1973) Calf thymus GMP reductase: control by XMP. *Biochem Biophys Res Commun*. **53**, 975–81

335. Stevens, S. W., Ryan, D. E., Ge, H. Y., Moore, R. E., Young, M. K., Lee, T. D., and Abelson, J. (2002) Composition and functional characterization of the yeast spliceosomal penta-snRNP. *Mol. Cell*. **9**, 31–44

336. Striepen, B., Pruijssers, A. J. P., Huang, J., Li, C., Gubbels, M.-J., Umejiego, N. N., Hedstrom, L., and Kissinger, J. C. (2004) Gene transfer in the evolution of parasite nucleotide biosynthesis. *Proc. Natl. Acad. Sci.* **101**, 3154–3159

337. Strochlic, T. I., Stavrides, K. P., Thomas, S. V., Nicolas, E., O'Reilly, A. M., and Peterson, J. R. (2014) Ack kinase regulates CTP synthase filaments during Drosophila oogenesis. *EMBO Rep.* **15**, 1184–1191

338. Stubbs, J., Simpson, K. M., Triglia, T., Plouffe, D., Tonkin, C. J., Duraisingh, M. T., Maier, A. G., Winzeler, E. A., and Cowman, A. F. (2005) Molecular mechanism for switching of P. falciparum invasion pathways into human erythrocytes. *Science (80-.).* **309**, 1384–1387

339. Swearingen, K. E., Lindner, S. E., Flannery, E. L., Vaughan, A. M., Morrison, R. D., Patrapuvich, R., Koepfli, C., Muller, I., Jex, A., Moritz, R. L., Kappe, S. H. I., Sattabongkot, J., and Mikolajczak, S. A. (2017) Proteogenomic analysis of the total and surface-exposed proteomes of Plasmodium vivax salivary gland sporozoites. *PLoS Negl Trop Dis*. **11**, e0005791

340. Swearingen, K. E., Lindner, S. E., Shi, L., Shears, M. J., Harupa, A., Hopp, C. S., Vaughan, A. M., Springer, T. A., Moritz, R. L., Kappe, S. H., and Sinnis, P. (2016) Interrogating the Plasmodium Sporozoite Surface: Identification of Surface-Exposed

Proteins and Demonstration of Glycosylation on CSP and TRAP by Mass Spectrometry-Based Proteomics. *PLoS Pathog*. **12**, e1005606

341. Szklarczyk, D., Franceschini, A., Wyder, S., Forslund, K., Heller, D., Huerta-Cepas, J., Simonovic, M., Roth, A., Santos, A., Tsafou, K. P., Kuhn, M., Bork, P., Jensen, L. J., and von Mering, C. (2015) STRING v10: protein-protein interaction networks, integrated over the tree of life. *Nucleic Acids Res*. **43**, D447-52

342. Szklarczyk, D., Morris, J. H., Cook, H., Kuhn, M., Wyder, S., Simonovic, M., Santos, A., Doncheva, N. T., Roth, A., Bork, P., Jensen, L. J., and von Mering, C. (2017) The STRING database in 2017: quality-controlled protein–protein association networks, made broadly accessible. *Nucleic Acids Res*. **45**, D362–D368

343. Tamura, K., Peterson, D., Peterson, N., Stecher, G., Nei, M., and Kumar, S. (2011) MEGA5: molecular evolutionary genetics analysis using maximum likelihood, evolutionary distance, and maximum parsimony methods. *Mol Biol Evol*. **28**, 2731–9

344. Tawfik, O. K. and D. S., and Tawfik, D. S. (2010) Enzyme Promiscuity: A Mechanistic and Evolutionary Perspective. *Annu. Rev. Biochem.* **79**, 471–505

345. Thomas, E. C., Gunter, J. H., Webster, J. A., Schieber, N. L., Oorschot, V., Parton, R. G., and Whitehead, J. P. (2012) Different Characteristics and Nucleotide Binding Properties of Inosine Monophosphate Dehydrogenase (IMPDH) Isoforms. *PLoS One*. **7**, e51096

346. Thornton, C., Snowden, M. A., and Carling, D. (1998) Identification of a novel AMP-activated protein kinase beta subunit isoform that is highly expressed in skeletal muscle. *J. Biol. Chem.* **273**, 12443–50

347. Tiedeman, A. A., Smith, J. M., and Zalkin, H. (1985) Nucleotide sequence of the guaA gene encoding GMP synthetase of Escherichia coli K12. *J Biol Chem*. **260**, 8676–8679

348. Tiedeman, A. A., and Smith, J. M. (1985) Nucleotide sequence of the guaB locus encoding IMP dehydrogenaseof Escherichia coli K12. *Nucleic Acids Res*, **13**, 1303-1316

349. Tonkin, C. J., Carret, C. K., Duraisingh, M. T., Voss, T. S., Ralph, S. A., Hommel, M., Duffy, M. F., Silva, L. M., Scherf, A., Ivens, A., Speed, T. P., Beeson, J. G., and Cowman, A. F. (2009) Sir2 paralogues cooperate to regulate virulence genes and antigenic variation in Plasmodium falciparum. *PLoS Biol*. **7**, e84

350. Trager, W., and Jensen, J. B. (1976) Human malaria parasites in continuous culture. *Science (80-.).* **193**, 673–675

351. Tran, P. N., Brown, S. H. J., Mitchell, T. W., Matuschewski, K., McMillan, P. J., Kirk, K., Dixon, M. W. A., and Maier, A. G. (2014) A female gametocyte-specific ABC transporter plays a role in lipid metabolism in the malaria parasite. *Nat. Commun.* **5**, 4773

352. Treeck, M., Sanders, J. L., Elias, J. E., and Boothroyd, J. C. (2011) The phosphoproteomes of Plasmodium falciparum and Toxoplasma gondii reveal unusual adaptations within and beyond the parasites' boundaries. *Cell Host Microbe*. **10**, 410–419

353. Tuominen, H., Salminen, A., Oksanen, E., Jamsen, J., Heikkila, O., Lehtio, L., Magretova, N. N., Goldman, A., Baykov, A. A., and Lahti, R. (2010) Crystal structures of the CBS and DRTGG domains of the regulatory region of Clostridiumperfringens pyrophosphatase complexed with the inhibitor, AMP, and activator, diadenosine tetraphosphate. *J Mol Biol*. **398**, 400–413

354. Uetz, P., Giot, L., Cagney, G., Mansfield, T. A., Judson, R. S., Knight, J. R., Lockshon, D., Narayan, V., Srinivasan, M., Pochart, P., Qureshi-Emili, A., Li, Y., Godwin, B., Conover, D., Kalbfleisch, T., Vijayadamodar, G., Yang, M., Johnston, M., Fields, S., and Rothberg, J. M. (2000) A comprehensive analysis of protein–protein interactions inSaccharomyces cerevisiae. *Nature*. **403**, 623–627

355. Umejiego, N. N., Li, C., Riera, T., Hedstrom, L., and Striepen, B. (2004) Cryptosporidium parvum IMP dehydrogenase: identification of functional, structural, and dynamic properties that can be exploited for drug design. *J Biol Chem*. **279**, 40320–40327

356. Umejiego, N. N., Gollapalli, D., Sharling, L., Volftsun, A., Lu, J., Benjamin, N. N., Stroupe, A. H., Riera, T. V., Striepen, B., and Hedstrom, L. (2008) Targeting a Prokaryotic Protein in a Eukaryotic Pathogen: Identification of Lead Compounds against Cryptosporidiosis. *Chem Biol*. **15**, 70–77

357. Usha, V., Gurcha, S. S., Lovering, A. L., Lloyd, A. J., Papaemmanouil, A., Reynolds, R. C., and Besra, G. S. (2011) Identification of novel diphenyl urea inhibitors of Mt-GuaB2 active against Mycobacterium tuberculosis. *Microbiology*. **157**, 290–299

358. van der Knaap, J. A., Kumar, B. R. P., Moshkin, Y. M., Langenberg, K., Krijgsveld, J., Heck, A. J. R., Karch, F., and Verrijzer, C. P. (2005) GMP Synthetase Stimulates Histone H2B Deubiquitylation by the Epigenetic Silencer USP7. *Mol. Cell*. **17**, 695–707

359. van der Knaap, J. A., and Verrijzer, C. P. (2016) Undercover: gene control by metabolites and metabolic enzymes. *Genes Dev.* **30**, 2345–2369

360. van der Knaap, J. A., Kozhevnikova, E., Langenberg, K., Moshkin, Y. M., and Verrijzer, C. P. (2010) Biosynthetic enzyme GMP synthetase cooperates with ubiquitin-specific protease 7 in transcriptional regulation of ecdysteroid target genes. *Mol. Cell. Biol.* **30**, 736–44

361. van Ham, R. C. H. J., Kamerbeek, J., Palacios, C., Rausell, C., Abascal, F., Bastolla, U., Fernández, J. M., Jiménez, L., Postigo, M., Silva, F. J., Tamames, J., Viguera, E., Latorre, A., Valencia, A., Morán, F., and Moya, A. (2003) Reductive genome evolution in Buchnera aphidicola. *Proc Natl Acad Sci U S A*. **100**, 581–6

362. Veletzky, L., Rehman, K., Lingscheid, T., Poeppl, W., Loetsch, F., Burgmann, H., and Ramharter, M. (2014) In vitro activity of immunosuppressive drugs against Plasmodium falciparum. *Malar. J.* **13**, 476

363. Verham, R., Meek, T. D., Hedstrom, L., and Wang, C. C. (1987) Purification, characterization, and kinetic analysis of inosine 5'-monophosphate dehydrogenase of Tritrichomonas foetus. *Mol Biochem Parasitol*. **24**, 1–12

364. Vignali, M., Armour, C. D., Chen, J., Morrison, R., Castle, J. C., Biery, M. C., Bouzek, H., Moon, W., Babak, T., Fried, M., Raymond, C. K., and Duffy, P. E. (2011) NSR-seq transcriptional profiling enables identification of a gene signature of Plasmodium falciparum parasites infecting children. *J Clin Invest*. **121**, 1119–1129

365. Vos, S., de Jersey, J., and Martin, J. L. (1997) Crystal structure of Escherichia coli xanthine phosphoribosyltransferase. *Biochemistry*. **36**, 4125–4134

366. Wada, Y., Sandberg, M. A., McGee, T. L., Stillberger, M. A., Berson, E. L., and Dryja, T. P. (2005) Screen of the *IMPDH1* Gene among Patients with Dominant Retinitis

Pigmentosa and Clinical Features Associated with the Most Common Mutation, Asp226Asn. *Investig. Opthalmology Vis. Sci.* **46**, 1735

367. Wang, L., Delahunty, C., Prieto, J. H., Rahlfs, S., Jortzik, E., Yates J. R., 3rd, and Becker, K. (2014) Protein S-nitrosylation in Plasmodium falciparum. *Antioxid Redox Signal*. **20**, 2923–2935

368. Wang, W., and Hedstrom, L. (1997) Kinetic Mechanism of Human Inosine 5‘-Monophosphate Dehydrogenase Type II: Random Addition of Substrates and Ordered Release of Products †. *Biochemistry*. **36**, 8479–8483

369. Weber, G. (1983) Biochemical strategy of cancer cells and the design of chemotherapy: G. H. A. Clowes Memorial Lecture. *Cancer Res.* **43**, 3466–92

370. Weber, G., Nakamura, H., Natsumeda, Y., Szekeres, T., and Nagai, M. (1992) Regulation of GTP biosynthesis. *Adv Enzym. Regul*. **32**, 57–69

371. Weber, J. L. (1987) Analysis of sequences from the extremely A + T-rich genome of Plasmodium falciparum. *Gene*. **52**, 103–9

372. Webster, H. K., and Whaun, J. M. (1982) Antimalarial properties of bredinin. Prediction based on identification of differences in human host-parasite purine metabolism. *J. Clin. Invest.* **70**, 461–9

373. Weiland, O., Milich, D. R., S√§llberg, M., and Hultgren, C. (1998) The antiviral compound ribavirin modulates the T helper (Th) 1/Th2 subset balance in hepatitis B and C virus-specific immune responses. *J. Gen. Virol.* **79**, 2381–2391

374. White, R. H. (2011) The Conversion of a Phenol to an Aniline Occurs in the Biochemical Formation of the 1-(4-Aminophenyl)-1-deoxy- d -ribitol Moiety in Methanopterin. *Biochemistry*. **50**, 6041–6052

375. Whitehead, J. P., Simpson, F., Hill, M. M., Thomas, E. C., Connolly, L. M., Collart, F., Simpson, R. J., and James, D. E. (2004) Insulin and Oleate Promote Translocation of Inosine-5′ Monophosphate Dehydrogenase to Lipid Bodies. *Traffic*. **5**, 739–749

376. Wilkins, M. R., Gasteiger, E., Bairoch, A., Sanchez, J. C., Williams, K. L., Appel, R. D., and Hochstrasser, D. F. (1999) Protein identification and analysis tools in the ExPASy server. *Methods Mol Biol*. **112**, 531–52

377. Wilson, K., Berens, R. L., Sifri, C. D., and Ullman, B. (1994) Amplification of the inosinate dehydrogenase gene in Trypanosoma brucei gambiense due to an increase in chromosome copy number. *J. Biol. Chem.* **269**, 28979–87

378. Wilson, K., Collart, F. R., Huberman, E., Stringer, J. R., and Ullman, B. (1991) Amplification and molecular cloning of the IMP dehydrogenase gene of Leishmania donovani. *J. Biol. Chem.* **266**, 1665–71

379. Winder, W. W., and Hardie, D. G. (1999) AMP-activated protein kinase, a metabolic master switch: possible roles in Type 2 diabetes. *Am. J. Physiol. Metab.* **277**, E1–E10

380. Winzeler, E. A., Shoemaker, D. D., Astromoff, A., Liang, H., Anderson, K., Andre, B., Bangham, R., Benito, R., Boeke, J. D., Bussey, H., Chu, A. M., Connelly, C., Davis, K., Dietrich, F., Dow, S. W., El Bakkoury, M., Foury, F., Friend, S. H., Gentalen, E., Giaever, G., Hegemann, J. H., Jones, T., Laub, M., Liao, H., Liebundguth, N., Lockhart, D. J., Lucau-Danila, A., Lussier, M., M’Rabet, N., Menard, P., Mittmann, M., Pai, C., Rebischung, C., Revuelta, J. L., Riles, L., Roberts, C. J., Ross-MacDonald, P., Scherens,

B., Snyder, M., Sookhai-Mahadeo, S., Storms, R. K., Veronneau, S., Voet, M., Volckaert, G., Ward, T. R., Wysocki, R., Yen, G. S., Yu, K., Zimmermann, K., Philippsen, P., Johnston, M., and Davis, R. W. (1999) Functional characterization of the S. cerevisiae genome by gene deletion and parallel analysis. *Science (80-.).* **285**, 901–906

381. Witkowski, J. T., Robins, R. K., Sidwell, R. W., and Simon, L. N. (1972) Design, synthesis, and broad spectrum antiviral activity of 1- -D-ribofuranosyl-1,2,4-triazole-3-carboxamide and related nucleosides. *J. Med. Chem.* **15**, 1150–4

382. Wolfe, K. H., and Shields, D. C. (1997) Molecular evidence for an ancient duplication of the entire yeast genome. *Nature*. **387**, 708–713

383. Wu, T.-W., and Scrimgeour, K. G. (1973) Properties of Inosinic Acid Dehydrogenase from Bacillus subtilis. II. Kinetic Properties. *Can. J. Biochem*. **51**, 1380–1390

384. Xiang, B., Taylor, J. C., and Markham, G. D. (1996) Monovalent cation activation and kinetic mechanism of inosine 5'-monophosphate dehydrogenase. *J. Biol. Chem.* **271**, 1435–40

385. Xiang, B., and Markham, G. D. (1997) Probing the Mechanism of Inosine Monophosphate Dehydrogenase with Kinetic Isotope Effects and NMR Determination of the Hydride Transfer Stereospecificity. *Arch. Biochem. Biophys.* **348**, 378–382

386. Yeh, I., and Altman, R. B. (2006) Drug Targets for Plasmodium falciparum: a post-genomic review/survey. *Mini Rev Med Chem*. **6**, 177–202

387. Young, J. A., Fivelman, Q. L., Blair, P. L., de la Vega, P., Le Roch, K. G., Zhou, Y., Carucci, D. J., Baker, D. A., and Winzeler, E. A. (2005) The Plasmodium falciparum sexual development transcriptome: a microarray analysis using ontology-based pattern identification. *Mol Biochem Parasitol*. **143**, 67–79

388. Zahnle, K., Schaefer, L., and Fegley, B. (2010) Earth's earliest atmospheres. *Cold Spring Harb Perspect Biol*. **2**, a004895

389. Zalkin, H., and Dixon, J. E. (1992) De novo purine nucleotide biosynthesis. *Prog. Nucleic Acid Res. Mol. Biol.* **42**, 259–87

390. Zanghi, G., Vembar, S. S., Baumgarten, S., Ding, S., Guizetti, J., Bryant, J. M., Mattei, D., Jensen, A. T. R., Renia, L., Goh, Y. S., Sauerwein, R., Hermsen, C. C., Franetich, J. F., Bordessoulles, M., Silvie, O., Soulard, V., Scatton, O., Chen, P., Mecheri, S., Mazier, D., and Scherf, A. (2018) A Specific PfEMP1 Is Expressed in P. falciparum Sporozoites and Plays a Role in Hepatocyte Infection. *Cell Rep*. **22**, 2951–2963

391. Zhang, J., Zhang, W., Zou, D., Chen, G., Wan, T., Zhang, M., and Cao, X. (2003) Cloning and functional characterization of GMPR2, a novel human guanosine monophosphate reductase, which promotes the monocytic differentiation of HL-60 leukemia cells. *J. Cancer Res. Clin. Oncol*. **129**, 76–83

392. Zhang, J., Hulme, L., and Liu, J.-L. (2014) Asymmetric inheritance of cytoophidia in Schizosaccharomyces pombe. *Biol. Open*. **3**, 1092–7

393. Zhang, K., and Rathod, P. K. (2002) Divergent Regulation of Dihydrofolate Reductase Between Malaria Parasite and Human Host. *Science (80-.).* **296**, 545–547

394. Zhang, M., Wang, C., Otto, T. D., Oberstaller, J., Liao, X., Adapa, S. R., Udenze, K., Bronner, I. F., Casandra, D., Mayho, M., Brown, J., Li, S., Swanson, J., Rayner, J. C., Jiang, R. H. Y., and Adams, J. H. (2018) Uncovering the essential genes of the human

malaria parasite Plasmodium falciparum by saturation mutagenesis. *Science (80-.).* 10.1126/science.aap7847

394. Zhang, R., Evans, G., Rotella, F. J., Westbrook, E. M., Beno, D., Huberman, E., Joachimiak, A., and Collart, F. R. (1999) Characteristics and crystal structure of bacterial inosine-5'-monophosphate dehydrogenase. *Biochemistry*. **38**, 4691–4700

395. Zhou, X., Cahoon, M., Rosa, P., and Hedstrom, L. (1997) Expression, purification, and characterization of inosine 5'-monophosphate dehydrogenase from Borrelia burgdorferi. *J. Biol. Chem.* **272**, 21977–81

396. Zhou, Z., Yao, X., Li, S., Xiong, Y., Dong, X., Zhao, Y., Jiang, J., and Zhang, Q. (2015) Deubiquitination of Ci/Gli by Usp7/HAUSP Regulates Hedgehog Signaling. *Dev. Cell*. **34**, 58–72

397. Zillig, W., Zechel, K., and Halbwachs, H. J. (1970) A new method of large-scale preparation of highly purified DNA-dependent RNA-polymerase from E. coli. *Hoppe Seylers Z Physiol Chem*. **351**, 221–4

398. Accardi A (2015) Structure and gating of CLC channels and exchangers. *J Physiol.* **593,** 4129-38.

399. Alexandre T, Lupan A, Helynck O, Vichier-Guerre S, Dugué L, Gelin M, Haouz A, Labesse G, Munier-Lehmann H (2019) First-in-class allosteric inhibitors of bacterial IMPDHs. *Eur J Med Chem.* **167**, 124-132.

400. Pedley AM, Benkovic SJ (2017) A New View into the Regulation of Purine Metabolism: The Purinosome. *Trends Biochem Sci.* **42**, 141-154.

401. Zhao H, Chiaro CR, Zhang L, Smith PB, Chan CY, Pedley AM, Pugh RJ, French JB, Patterson AD, Benkovic SJ (2015) Quantitative analysis of purine nucleotides indicates that purinosomes increase de novo purine biosynthesis. *J Biol Chem.* **290**, 6705-13.

Appendix A

TAYLOR & FRANCIS LICENSE
TERMS AND CONDITIONS

Feb 22, 2019

This Agreement between Ms. Lakshmi Prasoona Thota ("You") and Taylor & Francis ("Taylor & Francis") consists of your license details and the terms and conditions provided by Taylor & Francis and Copyright Clearance Center.

The publisher has provided special terms related to this request that can be found at the end of the Publisher's Terms and Conditions.

License Number	4527040018305
License date	Feb 13, 2019
Licensed Content Publisher	Taylor & Francis
Licensed Content Publication	Critical Reviews in Biochemistry and Molecular Biology
Licensed Content Title	The dynamic determinants of reaction specificity in the IMPDH/GMPR family of (β/α)8 barrel enzymes
Licensed Content Author	Lizbeth Hedstrom
Licensed Content Date	Jun 1, 2012
Licensed Content Volume	47
Licensed Content Issue	3
Type of Use	I don't see my intended use
Requestor type	academic/educational
Format	print and electronic
Portion	Figure/table/questionnaire
Number of figures/tables/questionnaires	1
Figure identification	Figure 11
Will you be translating?	no
Author of this Taylor & Francis article	no
Order reference number	
Requestor Location	Ms. Lakshmi Prasoona Thota Molecular Biology and Genetics JNCASR Bangalore, Karnataka 560064 India Attn: Ms. Lakshmi Prasoona Thota
Billing Type	Invoice
Billing Address	Ms. Lakshmi Prasoona Thota Molecular Biology and Genetics JNCASR Bangalore, India 560064 Attn: Ms. Lakshmi Prasoona Thota

ELSEVIER LICENSE
TERMS AND CONDITIONS

Feb 22, 2019

This Agreement between Ms. Lakshmi Prasoona Thota ("You") and Elsevier ("Elsevier") consists of your license details and the terms and conditions provided by Elsevier and Copyright Clearance Center.

License Number	4526911197958
License date	Feb 13, 2019
Licensed Content Publisher	Elsevier
Licensed Content Publication	Archives of Biochemistry and Biophysics
Licensed Content Title	CBS domains: Ligand binding sites and conformational variability
Licensed Content Author	June Ereño-Orbea,Iker Oyenarte,Luis Alfonso Martínez-Cruz
Licensed Content Date	Dec 1, 2013
Licensed Content Volume	540
Licensed Content Issue	1-2
Licensed Content Pages	12
Start Page	70
End Page	81
Type of Use	reuse in a thesis/dissertation
Portion	figures/tables/illustrations
Number of figures/tables/illustrations	1
Format	both print and electronic
Are you the author of this Elsevier article?	No
Will you be translating?	No
Original figure numbers	Figure 1
Title of your thesis/dissertation	Biochemical studies on IMPDH/GMPR family of proteins
Expected completion date	Feb 2019
Estimated size (number of pages)	200
Requestor Location	Ms. Lakshmi Prasoona Thota Molecular Biology and Genetics JNCASR Bangalore, Karnataka 560064 India Attn: Ms. Lakshmi Prasoona Thota
Publisher Tax ID	GB 494 6272 12
Total	0.00 USD

ELSEVIER LICENSE
TERMS AND CONDITIONS

Feb 22, 2019

This Agreement between Ms. Lakshmi Prasoona Thota ("You") and Elsevier ("Elsevier") consists of your license details and the terms and conditions provided by Elsevier and Copyright Clearance Center.

License Number	4526920567657
License date	Feb 13, 2019
Licensed Content Publisher	Elsevier
Licensed Content Publication	Protein Expression and Purification
Licensed Content Title	Biochemical Analysis of the Modular Enzyme Inosine 5′-Monophosphate Dehydrogenase
Licensed Content Author	Elmar Nimmesgern,James Black,Olga Futer,John R. Fulghum,Stephen P. Chambers,Christopher L. Brummel,Scott A. Raybuck,Michael D. Sintchak
Licensed Content Date	Nov 1, 1999
Licensed Content Volume	17
Licensed Content Issue	2
Licensed Content Pages	8
Start Page	282
End Page	289
Type of Use	reuse in a thesis/dissertation
Intended publisher of new work	other
Portion	figures/tables/illustrations
Number of figures/tables/illustrations	1
Format	both print and electronic
Are you the author of this Elsevier article?	No
Will you be translating?	No
Original figure numbers	Figure 4
Title of your thesis/dissertation	Biochemical studies on IMPDH/GMPR family of proteins
Expected completion date	Feb 2019
Estimated size (number of pages)	200
Requestor Location	Ms. Lakshmi Prasoona Thota Molecular Biology and Genetics JNCASR Bangalore, Karnataka 560064 India Attn: Ms. Lakshmi Prasoona Thota
Publisher Tax ID	GB 494 6272 12
Total	0.00 USD
Terms and Conditions	

INTRODUCTION

1. The publisher for this copyrighted material is Elsevier. By clicking "accept" in connection with completing this licensing transaction, you agree that the following terms and conditions apply to this transaction (along with the Billing and Payment terms and conditions established by Copyright Clearance Center, Inc. ("CCC"), at the time that you opened your Rightslink account and that are available at any time at http://myaccount.copyright.com).

GENERAL TERMS

2. Elsevier hereby grants you permission to reproduce the aforementioned material subject to the terms and conditions indicated.

Appendix B

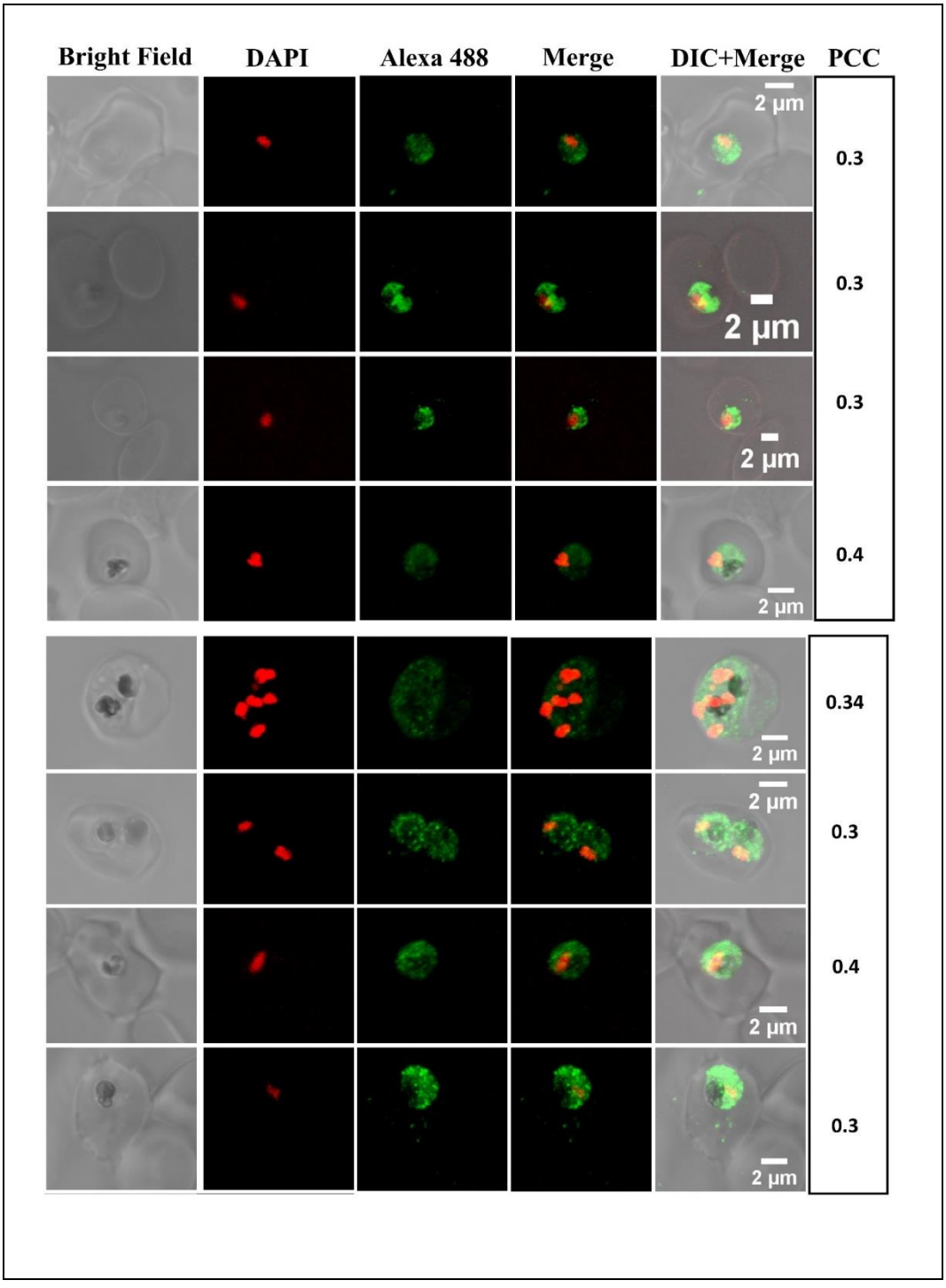
Bright Field
DAPI
Alexa 488
Merge
DIC+Merge
PCC
2 µm
0.3
0.3
0.3
0.4
0.34
0.3
0.4
0.3

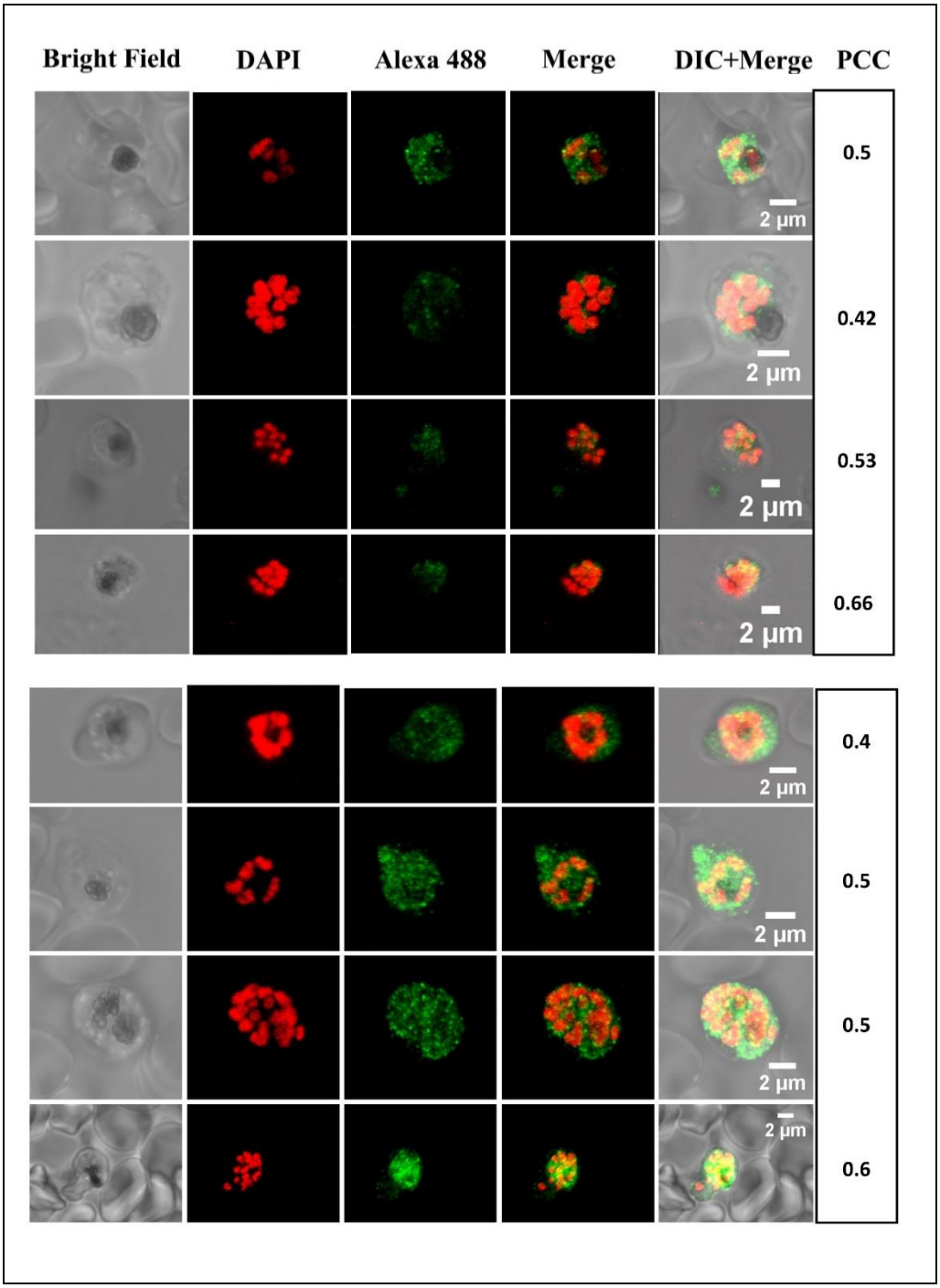
Bright Field
DAPI
Alexa 488
Merge
DIC+Merge
PCC
0.5
0.42
0.53
0.66
0.4
0.5
0.5
0.6
2 µm

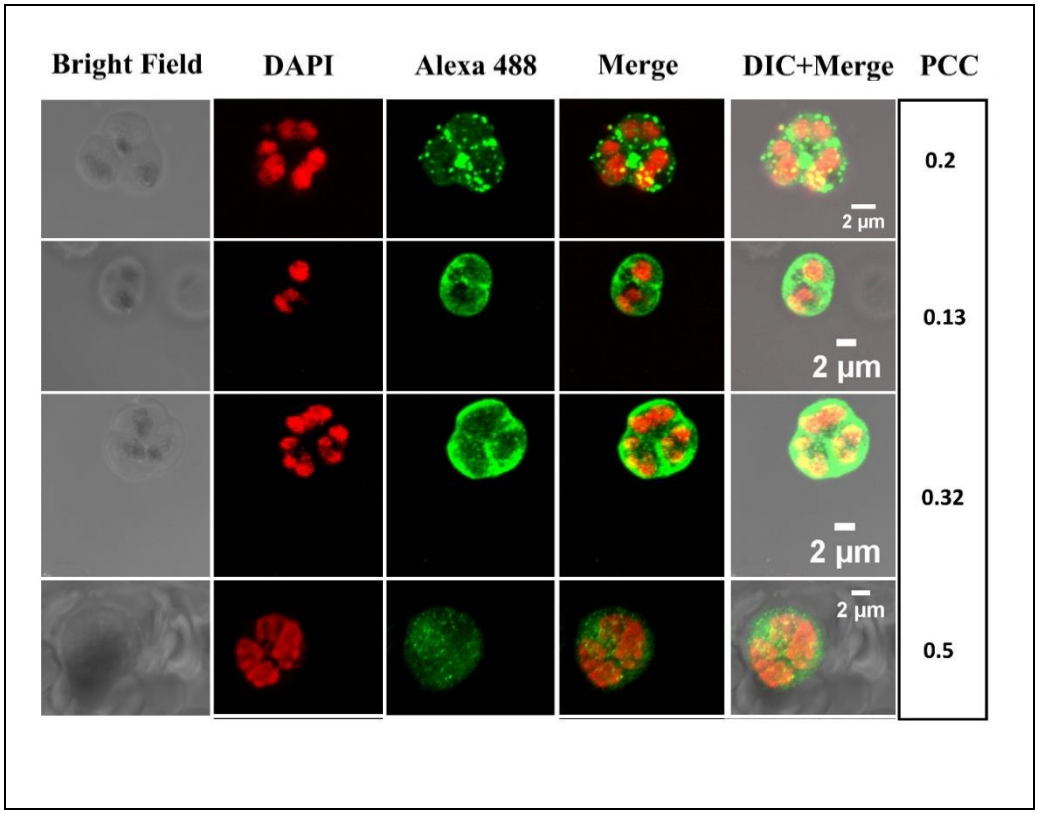

Figure B1. Subcellular localization of IMPDH in P. falciparum. *Pearsons correlation coefficient (PCC) for the nuclear overlap of PfIMPDH fluorescence signal in a single z-stack of the confocal image was determined using JACoP tool (Just Another Co-localization Plugin) (Bolte S and Cordelières FP, 2006) on Fiji image processing program (Schindelin J et al., 2012).*

Appendix C

Table C1. Various oligonucleotides used in the current study.

Primer	Sequence (5' to 3')	Expression Vector
PfIMPDH_F	TCACCATGGCTAGCGGATGGAAAGCT	pET21b+, pET28b+, pTrc99a
PfIMPDH_R	TCACTCGAGTGTAGTAAACTTTTTGTTGTTGAA	
Duet IMP_R	TCAGTCGACGCTTTGTTAGCAGCCGGATCTCAGTG	pDUET
Duet GMP_F	GGCAGATCTAGAAGGAGAGGAATATGACAAGATTTTGG	
Duet GMP_R	TCAGGTACCTCATTCGAATTCAATCGTTGCTG	
MjGAT_F	GATCCATATGATTGTTATCTTAGACAACGGAGGG	pET21b+
MjGAT_R_Fusion	GTAGGATCCGCCCTGAAAATACAGGTTTTCGCCTTCAAATTTG TAACCACAAACTTTACAAAAG	
PbIMPDH_F	GTAGGATCCATGGCAAATGGATGGGATGC	pET21b+, pET22b+,
PbIMPDH_R	GCT CTCGAG CTTTTTGGTGTTAAATATGAGATTGTCGCTG	
PfK86D_F	CATAATAATATGAGTATAGAAGATCAAATTGAAGAGGTGAAA AAG	PROSO II mutants in pET21b+
PfK86D_R	CTTTTTCACCTCTTCAATTTGATCTTCTATACTCATATTATTATG	
PfS172H_F	CTGATGTTGTTACAGGGCATTATCCCATAAATTTATCTG	
PfS172H_R	CAGATAAATTTATGGGATAATGCCCTGTAACAACATCAG	
PfS310G_F	GTTTTACGTATTGGTATGGGTGGTGGTTCAATTTGTACAACAC	
PfS310G_R	GTGTTGTACAAATTGAACCACCACCCATACCAATACGTAAAAC	
PfA325G_F	ATGTGCTGTAGGTAGAGGTCAAGGAACAGCTGTTT	
PfA325G_R	AAACAGCTGTTCCTTGACCTCTACCTACAGCACAT	
PfH218K_K221H_F	GCATAAAAATAGAATATTTCCCAAAGCGTCTCATAGTCAAAAT AAACAATTAATTG	
PfH218K_K221H_R	CAATTAATTGTTTATTTTGACTATGAGACGCTTTGGGAAATATT CTATTTTTATGC	
PfIMP_K420V_F	GATATTTAGTTGATGAAAGGGTTAATGAATATACAGATGAAA ATATTG	
PfIMP_K420V_R	CAATATTTTCATCTGTATATTCATTAACCCTTTCATCAACTAAA TATC	
$PfTIM^h$_F	GGTGAAGCGGTTTGAGAACGGCGGATCCGGCGGTTTTCCACAT GCTAGCAAAAGCCAG	Expression plasmid from NEB PURExpress
$PfTIM^h$_R	CTGGCTTTTGCTAGCATGTGGAAAACCGCCGGATCCGCCGTTC TCAAACCGCTTCACC	

Table C2. Molecular weights and isoelectric points of various proteins in the current study.

Protein	Molecular mass (kDa)	pI
PfIMPDH $(His)_6$	57	7.8
PbIMPDH $(His)_6$	57	8.0
$PfIMPDH^{\Delta CBS}$ $(His)_6$	43	6.95
PfCBS $(His)_6$	14	7.61
M_I $(His)_6$	57	7.29
M_II $(His)_6$	57	7.29
MjGAT_PfIMPDH $(His)_6$	79	7.26
$MjGAT\_PfIMPDH^{\Delta CBS}$ $(His)_6$	65	7.02
DnaK	70	4.83
DnaJ	41	7.98
grpE	22	4.68
MjIMPDH $(His)_6$	54	6.41
$MjIMPDH^{\Delta CBS}$ $(His)_6$	42	7.09

Table C3. Screening of multiple biochemical parameters aimed at improving the solubiltiy of recombinant PfIMDPH.

Buffers used	Screen for buffer conditions	Observations
Tris HCl, Phosphate (Na^+/K^+), Bicarbonate, HEPES, TAPS, CHAPS, Bis-Tris, Bicine, Tricine, and Glycine.	• pH range 5.5 to 12.0 • 50 mM to 150 mM ionic strength • 10 % to 20 % Glycerol • 0 mM KCl to 500 mM KCl (or NaCl) • 0 mM to 5 mM EDTA • 0.1 mM to 1 mM PMSF • 0.2 mM to 2 mM DTT (or TCEP) • 0 M to 6 M Guanidium HCl • 0 M to 8 M Urea • 4 °C and 25 °C	• Absence of PfIMPDH in soluble fraction. • Insufficient soluble protein to proceed for purification. • While refolding failed to yield active soluble protein or largely resulted in precipitation.

Appendix D

Transfection of *P. berghei*

Glycerol stock of *P. berghei Anka* parasites was injected into a healthy four-week-old BalBc mouse through the retro-orbital path. Parasitemia was monitored through tail snip performed at regular intervals. Giemsa stained blood smears were observed under the microscope using 100 x oil immersion objective. Blood was drawn through retro-orbital plexus using a capillary upon reaching 30-50 % parasitemia and collected into 0.5 ml of heparin (200 $U.ml^{-1}$). Further, to enrich schizonts, blood was layered on 60 % Nycodenz made in 1 x PBS and centrifuged at 400 g for 10 min. Schizonts were carefully collected and washed twice with incomplete RPMI medium. Parasite pellet was re-suspended in 90 µl of Amaxa P5 nucleofection solution, 3.5 µg of plasmid DNA in a volume of 10 µl was added and loaded into the cuvette. Nucleofection was performed using the pre-set program U-033 with Amaxa 2D nucleofector. Immediately after the pulse, 50 µl of incomplete RPMI medium was added, mixed well and injected into two fresh mice. Three days post-nucleofection, parasites were observed under a microscope and drug pressure was applied. 7 mg of pyrimethamine was dissolved in 1 ml of DMSO and further diluted in 100 ml acidified water with pH adjusted to 3.5. This drug-containing water was fed to the mice *ad libitum.* Giemsa stained smears were examined once every three days and blood was drawn once the parasitemia reached about 30 %. Glycerol stocks were made with 0.2 ml of harvested blood mixed in 0.3 ml of 30 % glycerol and stored in liquid nitrogen. For further experiments, harvested blood was treated with 1 x erythrocyte lysis buffer (155 mM NH_4Cl, 10 mM $KHCO_3$ and 0.1 mM EDTA) for 5 min at 4 °C and centrifuged at 500 g for 10 min. The supernatant was discarded, and the harvested cells were used for either Western blot or DNA isolation immediately or stored at -80 °C until further use.

DNA isolation

Parasite pellet was re-suspended in 350 µl of TNE buffer (10 mM Tris HCl, pH 8.0, 0.5 mM EDTA and 100 mM NaCl). 10 µl of 10 mg/ml RNase A and 50 µl of 10 % SDS were added to a final volume of 0.5 ml. This was incubated at 37 °C for 10 min followed by pronase treatment for 1 h (10 µl of 10 mg/ml stock solution). 1 ml of Tris-saturated phenol was added to the sample and mixed gently by inverting. The sample was then centrifuged for 5 min at 10,000 g and the supernatant was carefully removed and treated

with 1 ml of 1:1 phenol-chloroform solution and centrifuged for 5 min at 10,000g. The supernatant was collected and treated with 1 ml of chloroform-isoamyl alcohol solution and centrifuged at 10,000 g for 5 min. The extracted supernatant was mixed with 1/10 vol of 3 M sodium acetate (pH 4.5) and 1 ml of absolute ethanol. The sample was mixed by inverting gently in order to precipitate DNA, centrifuged at 10,000 g for a min and the supernatant was discarded. DNA pellet was washed once with 70 % ethanol, air dried and re-suspended in 50 µl nuclease free water. PCR was performed using the cloning primers to confirm transfectants.

Protein extraction

Parasite pellet was re-suspended in 100 µl of parasite lysis buffer (10 mM Tris HCl, pH 8, 0.4 M NaCl, 1 mM EDTA and 1 % SDS) along with 0.5 volumes of acid treated glass beads and subjected to multiple rounds of freeze-thaw and vortexed intermittently. The lysate was centrifuged at 13,000g for 30 min, resolved on 12 % SDS-PAGE and electro-transferred onto PVDF membrane for detection using either anti-$(His)_6$ antibody or anti-PfIMPDH antibody.

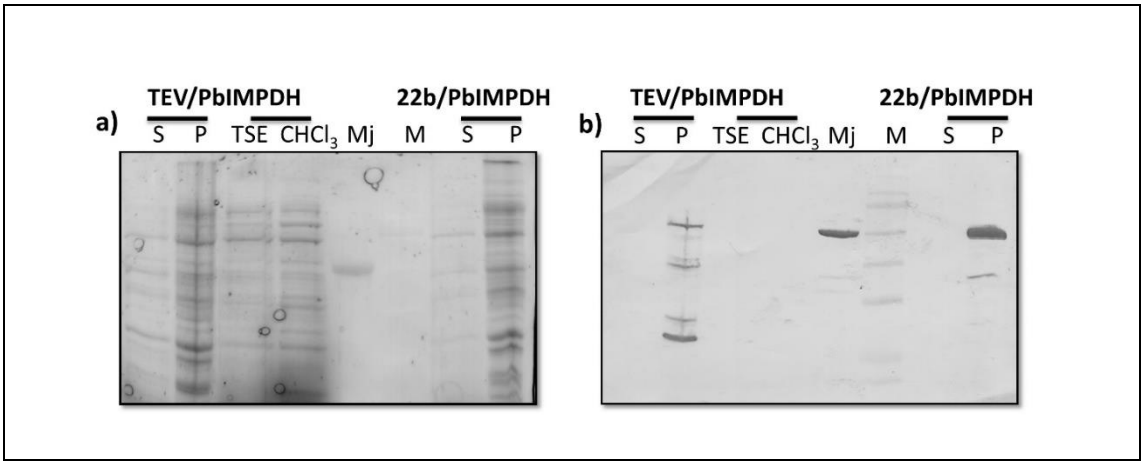

Figure D1. Expression and solubility analysis of PbIMPDH in ΔguaB^k(DE3) strain of E. coli. a) *Chloroform stained gel was visualized under UV light using the Bio-Rad gel doc system (Kazmin D et al., 2002). Lanes S and P correspond to the soluble and insoluble fractions collected after lysis; TSE was osmotic shock fluid extracted using 25 mM Tris HCl, 0.3 M Sucrose and 2.5 mM EDTA; $CHCl_3$ was the periplasmic fraction extracted with chloroform; Mj represents MjIMPDH (55 kDa) used as positive control for antibody detection, M- Pre-stained Prism Ultra protein ladder, Abcam, USA.* ***b)*** *Western detection and confirmation of PbIMPDH using anti-$(His)_6$ antibody used at 1.6000 dilutions. Goat secondary anti-mice antibody conjugated to HRP was used at 1.4500 and developed using AEC as substrate.*

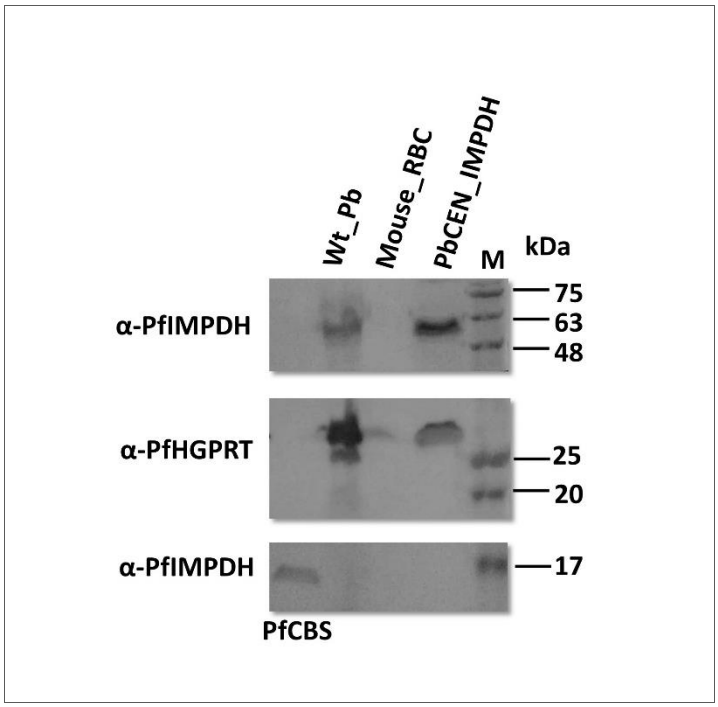

Figure D2. Episomal expression of PbIMPDH in P. berghei*. Wt_Pb represents wild type parasite lysate; M- Pre-stained Prism Ultra protein ladder, Abcam, USA; PbCEN_IMPDH corresponds to episomal expression of P. berghei IMPDH; anti-PfIMPDH antibody was used to probe PbIMPDH expression. PfCBS (14 kDa) served as a positive control for Western detection. Mouse RBC was used as a negative control. Presence of HGPRT was probed as an internal control using rabbit anti-PfHGPRT antibody. anti-P. falciparum antibodies cross-reacted with their respective P. berghei homologs. Western blot developed using AEC as a substrate for HRP conjugated to goat anti-rabbit secondary antibody.*

Conclusion

Recombinant PbIMPDH was found to be completely insoluble similar to that of *P. falciparum* IMPDH and thus unable to rescue the growth of *guaB* or *guaC* deletion strain of *E. coli* on M9 minimal medium (discussed in Chapter 2). Episomal expression of PbCEN5_PbIMPDH in mice infected with *P. berghei* was confirmed by Western blot**.**

Appendix E

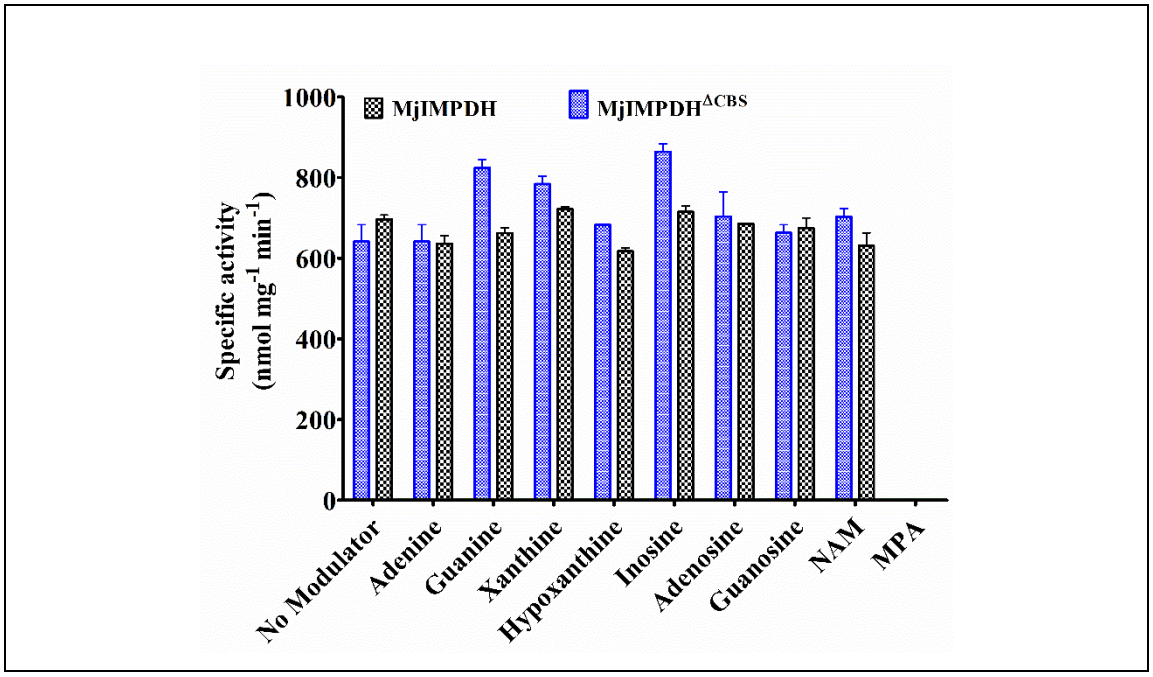

Figure E1. Effect of various nucleobases, nucleosides and MPA on the enzyme activity of MjIMPDH and MjIMPDH$^{\Delta CBS}$. *All the molecules were examined at a concentration of 0.5 mM with IMP and NAD$^+$ kept at sub-saturating levels. NAM refers to nicotinamide mononucleotide. No enzyme activity was observed in the presence of 0.5 mM mycophenolic acid (MPA) while purine nucelobases, and purine nucleosides displayed no effect.*

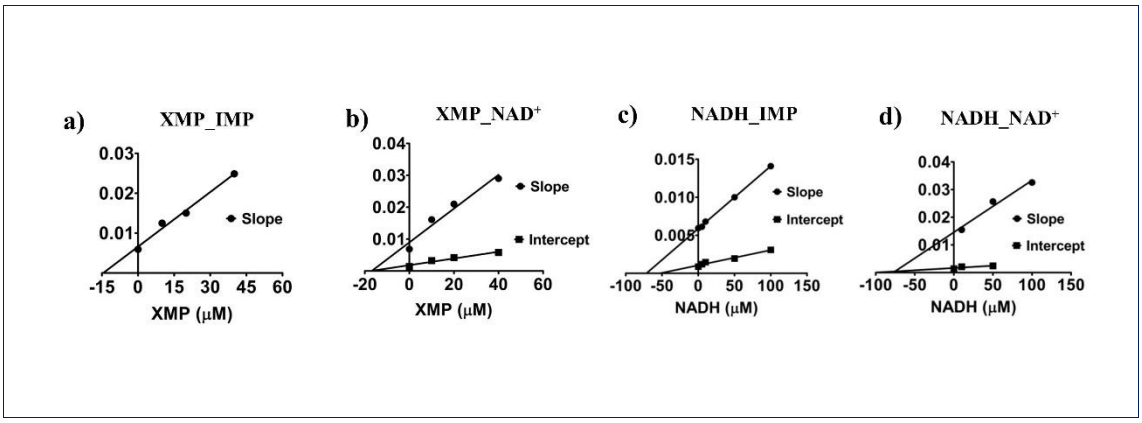

Figure E2. Slope and intercept replot of product inhibition on MjIMPDH. *a), and c) IMP as a variable. b), and d) NAD$^+$ as a variable.*

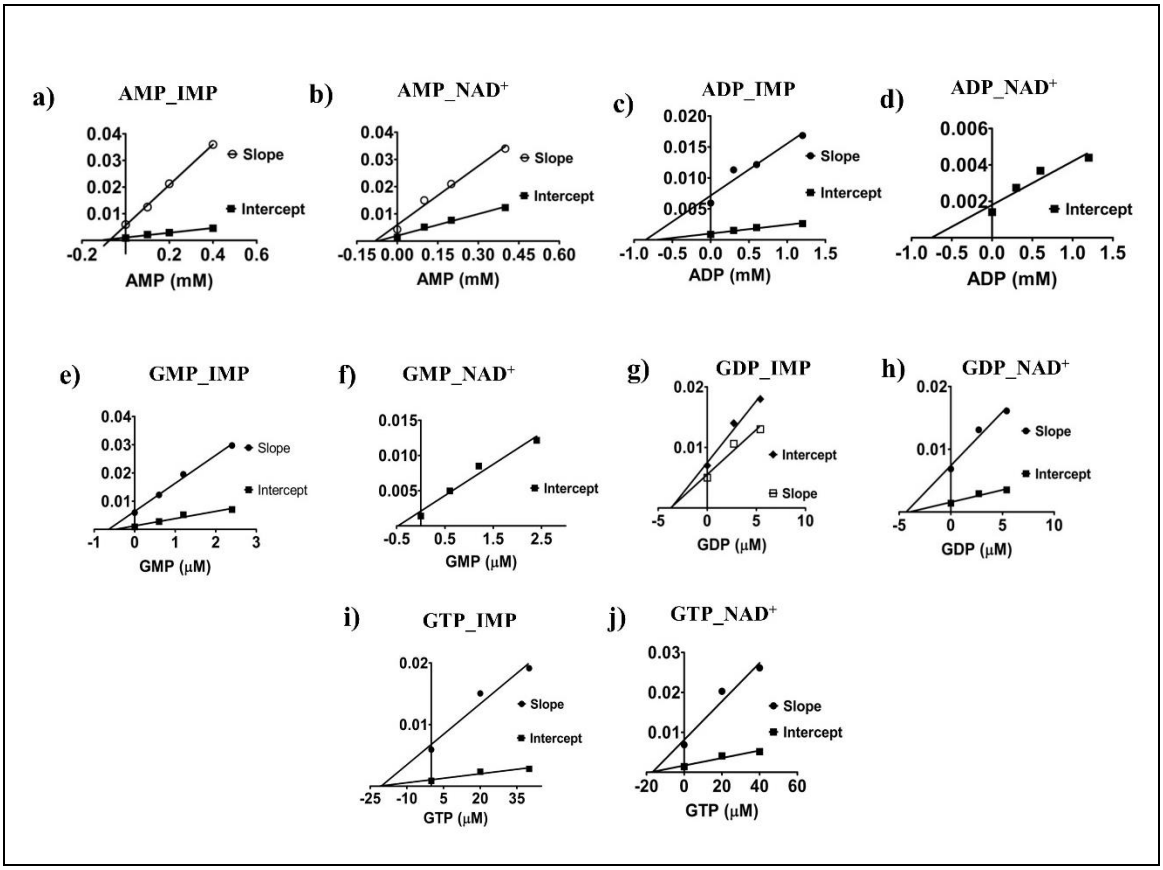

Figure E3. Slope and intercept replot of adenine and guanine nucleotide inhibition on MjIMPDH. *a), c), e), g), and i) IMP as a variable. b), d), f), h) and j) NAD^+ as a variable.*

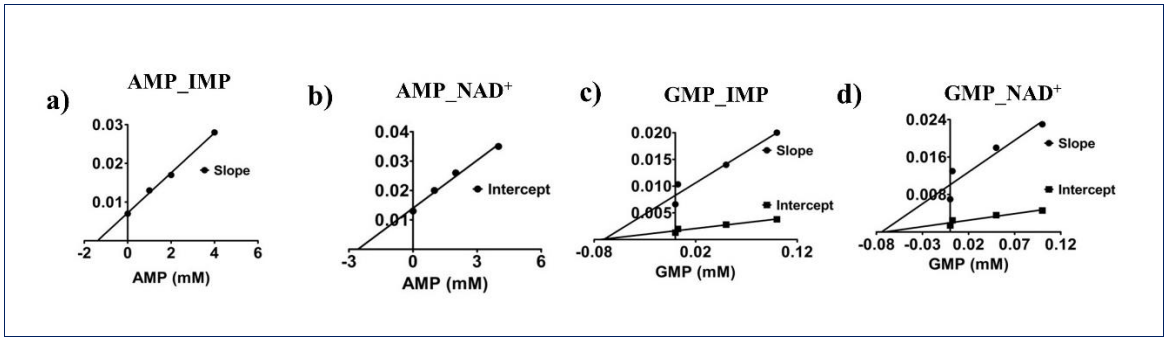

Figure E4. Slope and intercept replot of AMP and GMP inhibition on MjIMPDH$^{\Delta CBS}$. *a), and c) IMP as a variable. b), and d) NAD^+ as a variable.*

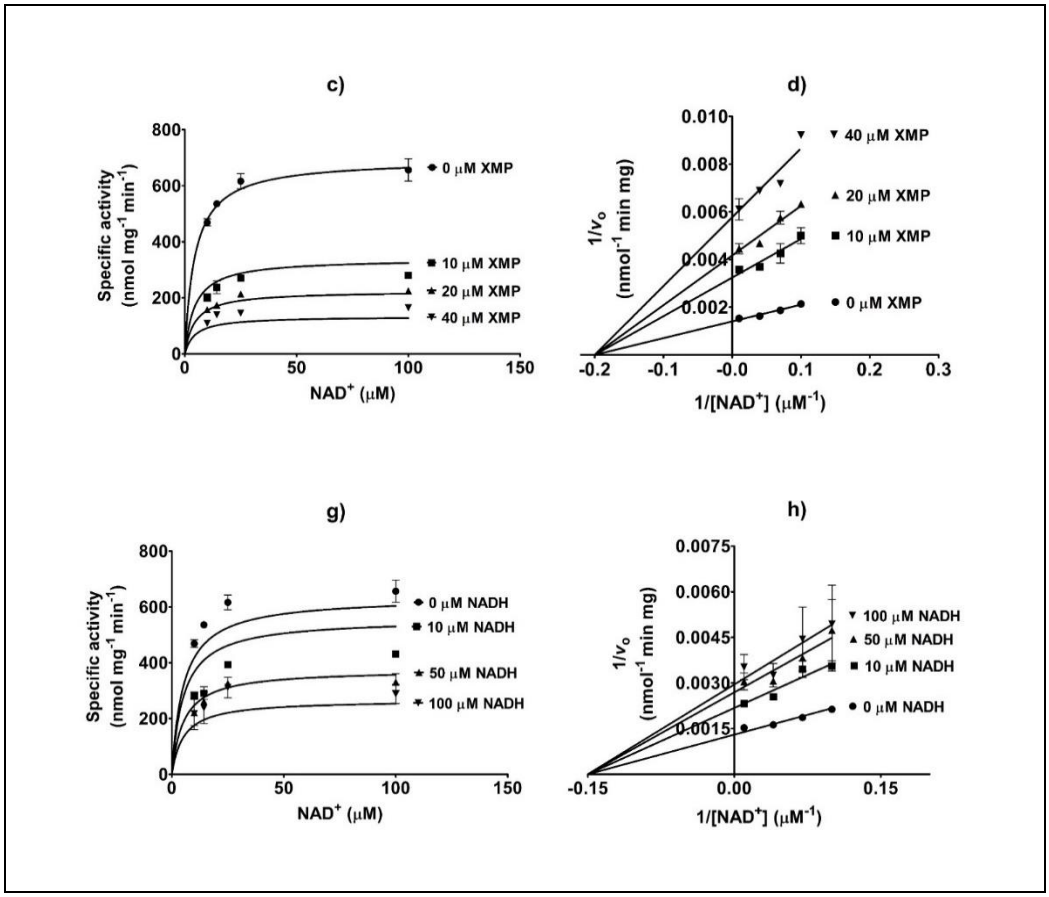

Figure E5. Product inhibition kinetics of MjIMPDH. c) *and* ***d) Inhibition plot for XMP*** *against NAD^+ as the variable substrate (noncompetitive).* ***g)*** *and* ***h) Inhibition plot for NADH*** *with respect to NAD^+ (noncompetitive inhibition).*

Table E1. Product inhibition constants of MjIMPDH determined from the global fit of the data and from the secondary plots of slope and intercept versus inhibitor concentration [I]. (refer to Appendix E for secondary plots). Reaction mix contained 100 mM KCl. Varied concentrations of IMP and NAD^+ were (2.5 µM, 3.57 µM, 6.25 µM) and (10 µM, 14.3 µM, 25 µM, and 100 µM), respectively. The standard deviation of the data is presented (n=2).

Inhibitor	Type of inhibition	K_i from global fit (µM)	K_i from the secondary plot of slope vs [I] (µM)	K_i from the secondary plot of intercept vs [I] (µM)
XMP_NAD^+	Noncompetitive	9.5 ± 0.7	11 ± 1.4	11.5 ± 0.7
NADH_NAD^+		60 ± 10	77 ± 30	74 ± 30

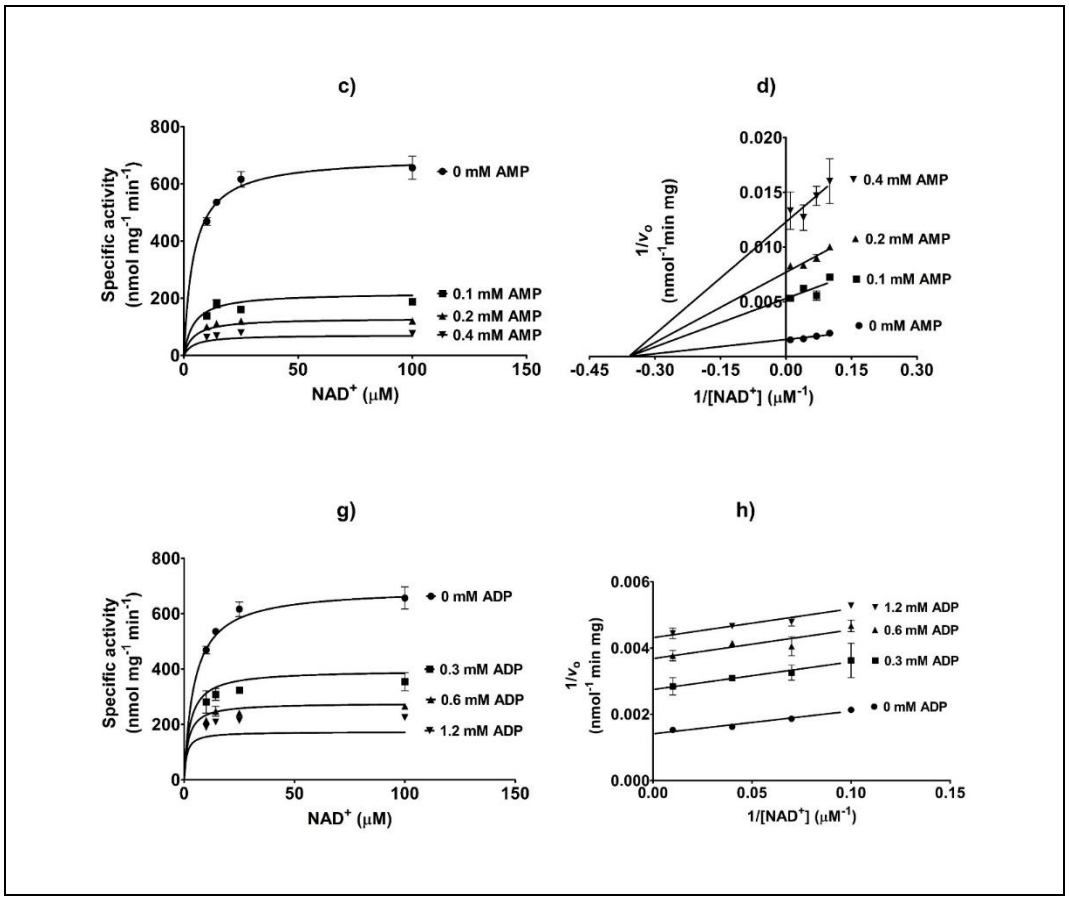

Figure E6. Effect of adenine nucleotides on dehydrogenase activity of MjIMPDH. c) and d) *Plots indicating AMP as a non-competitive inhibitor against NAD^+ binding.* ***g)*** *and* ***h)*** *Plots representing ADP as uncompetitive with respect to NAD^+.*

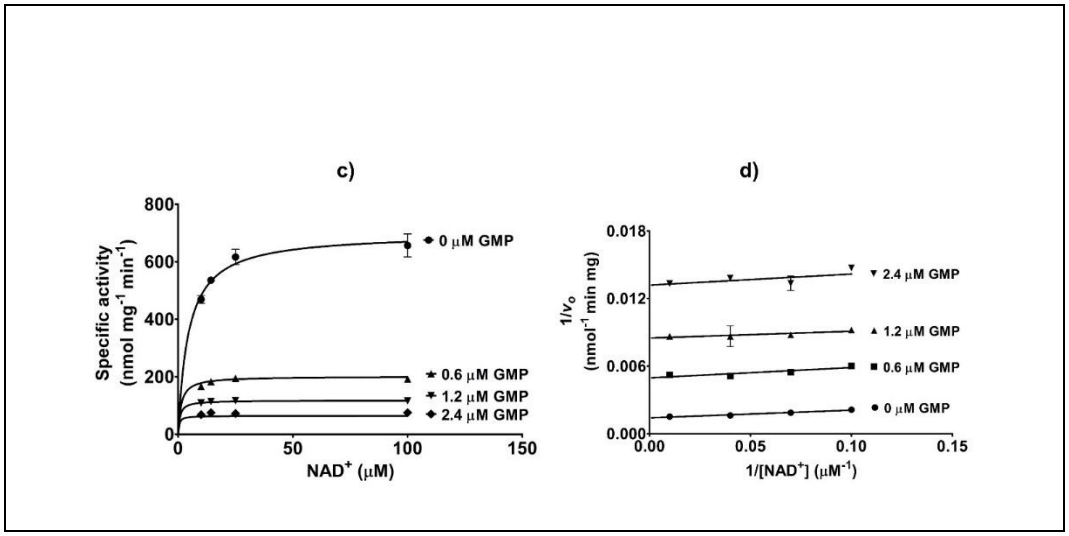

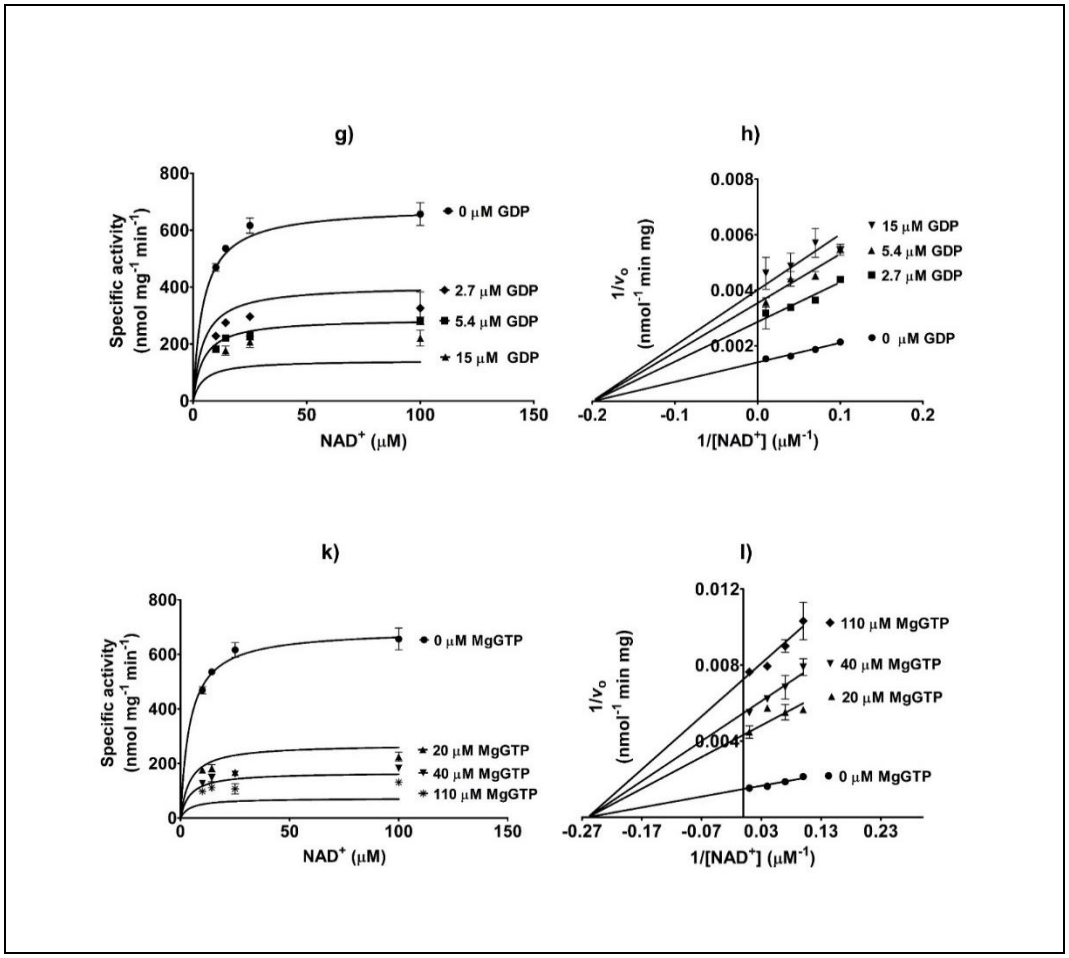

Figure E7. Effect of guanine nucleotides on dehydrogenase activity of MjIMPDH. g) *and* ***h)*** *Plots showing GDP as noncompetitive against NAD^+ binding.* ***k)*** *and* ***l)*** *Data showing Mg^{2+}-GTP as a non-competitive inhibitor against NAD^+.*

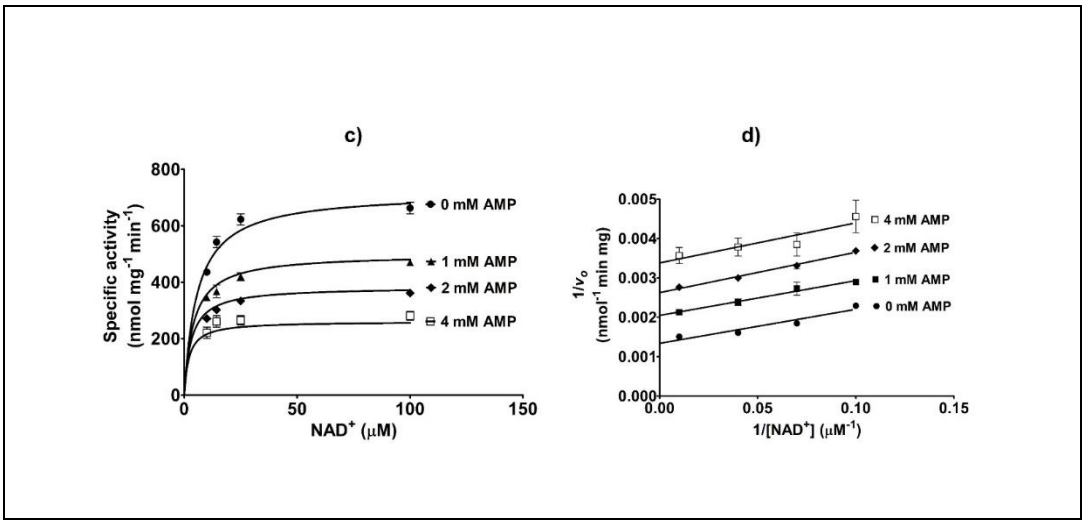

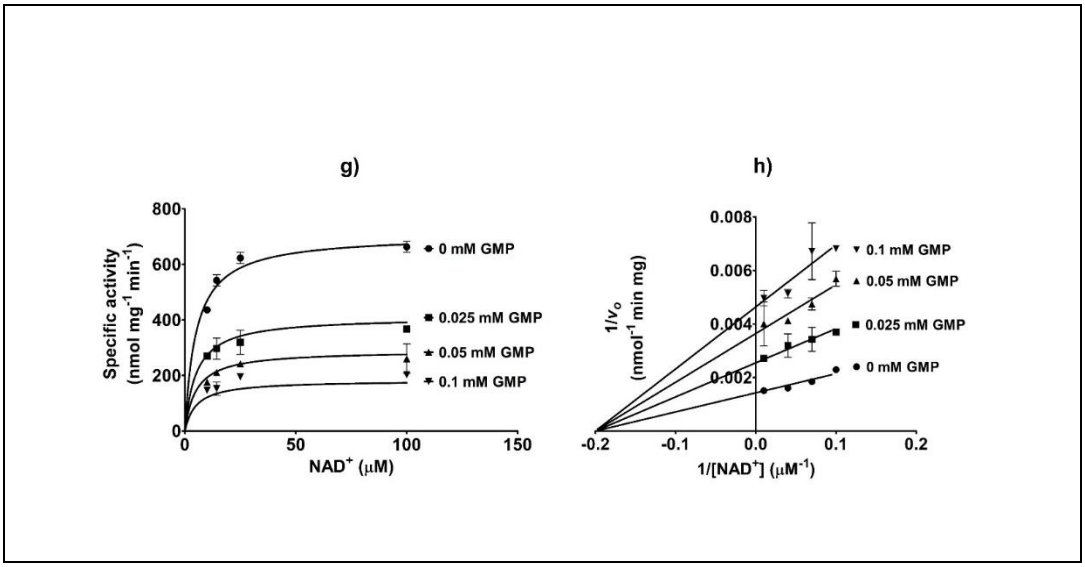

Figure E8. Modulation of IMP dehydrogenase activity by AMP and GMP- the effect of deletion of CBS domain. c) and d) *Plots indicating AMP as uncompetitive of NAD^+ which in the presence of CBS was found to be non-competitive with respect to both the substrates.* ***g)*** *and* ***h)*** *Plots representing GMP as non-competitive against NAD^+ binding which in the presence of CBS was found to be noncompetitive of IMP binding and uncompetitive against NAD^+.*

Table E2. Modulation of *M. jannaschii* IMP dehydrogenase activity by purine nucleotides as determined from the global fit of the data and from the secondary plots of slope and intercepts versus inhibitor concentration [I]. (refer to Appendix E for secondary plots). Varied concentrations of IMP and NAD^+ were (2.5 μM, 3.57 μM, 6.25 μM) and (10 μM, 14.3 μM, 25 μM, and 100 μM), respectively. The standard deviation of the data is presented (n=2).

MjIMPDH **Inhibitor_variable substrate**	**Type of inhibition**	**K_i from global fit (μM)**	**K_i from the secondary plot of slope vs [I] (μM)**	**K_i from the secondary plot of intercept vs [I] (μM)**
AMP_NAD^+	Noncompetitive	46 ± 3.5	112 ± 45	65 ± 18
ADP_NAD^+	Uncompetitive	*405 ± 64	-	376 ± 47
GMP_NAD^+	Uncompetitive	*0.25 ± 0.04	-	0.38 ± 0.05
GDP_NAD^+	Noncompetitive	4 ± 0.8	4.2 ± 0.5	4.1 ± 0.4
GTP_NAD^+		12.9 ± 1	18.4 ± 2	19 ± 2
MjIMPDH$^{\Delta CBS}$				
AMP_NAD^+	Uncompetitive	*2290 ± 226	-	2950 ± 353
GMP_NAD^+	Noncompetitive	34 ± 3	32 ± 8	32 ± 5

*refers to αK_i values for the uncompetitive mode of inhibition. Only the most potent inhibitor of MjIMPDH among adenine and guanine nucleotides was tested for its effect on MjIMPDH$^{\Delta CBS}$.